INNOVATIVE HYBRID TOOLS FOR URETER RECONSTRUCTION AND URINARY DIVERSION

Insights in Scaffold Design,
(Bio)mechanical Properties,
Tissue Remodeling and
Noninvasive Monitoring by MRI

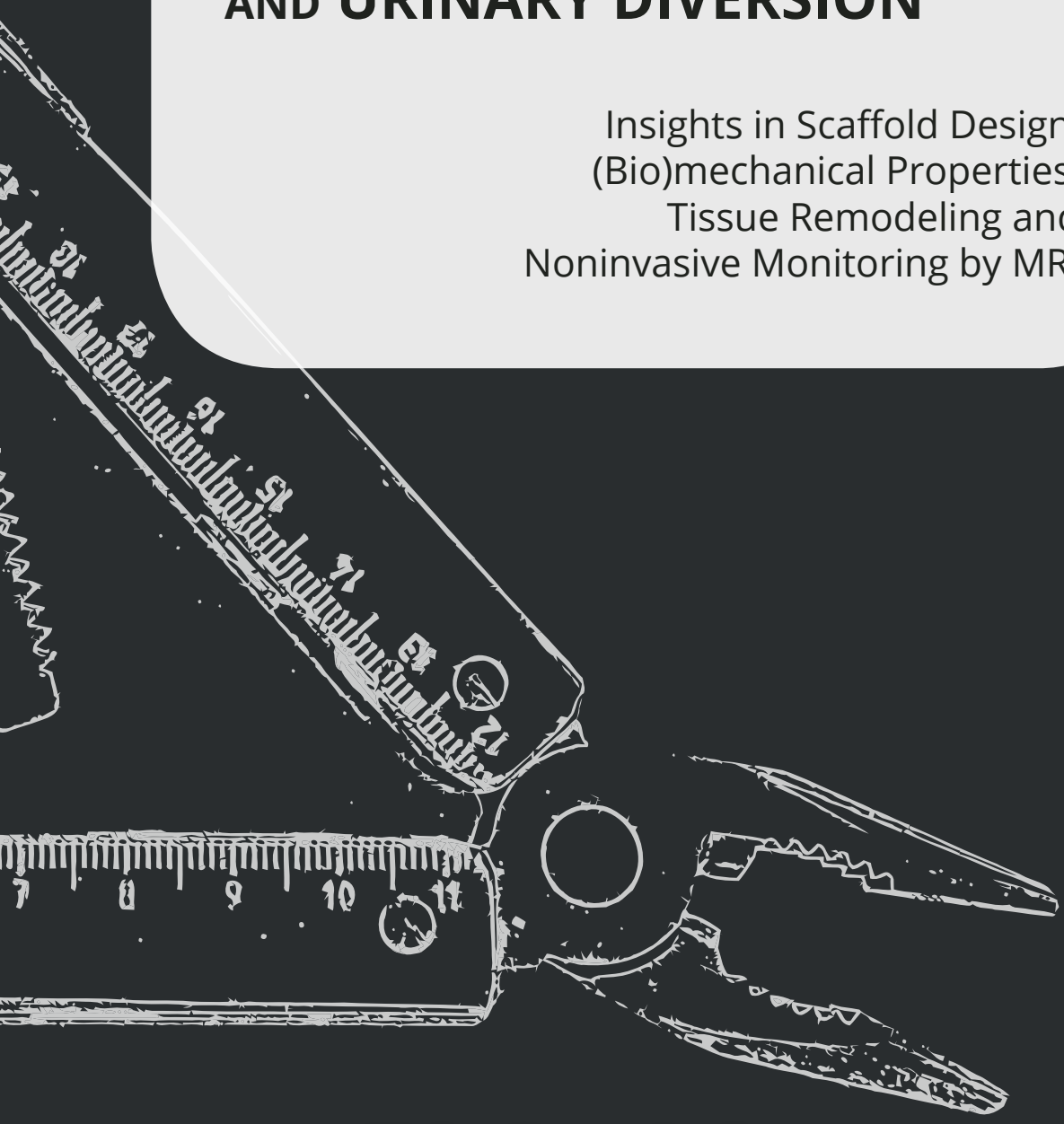

Heinz Peter Janke

Innovative Hybrid Tools for Ureter Reconstruction and Urinary Diversion

-

Insights in Scaffold Design, (Bio)mechanical Properties, Tissue Remodeling and Noninvasive Monitoring by MRI

Heinz Peter Janke

This research was performed at the Laboratory of Experimental Urology within the Department of Urology, Radboud Institute for Molecular Life Sciences (RIMLS), Radboud University Medical Center Nijmegen, under supervision of Dr. Egbert Oosterwijk and Prof. Dr. Wout F. J. Feitz.

The research leading to these results has received funding from the People Programme (Marie Curie Actions) of the European Union's Seventh Framework Programme FP7/2007-2013/ under REA grant agreement No. 607868 (iTERM).

The production and printing of this thesis was financially supported by the Radboud University and Radboud Institute for Molecular Life Sciences (RIMLS).

ISBN 978-94-028-1672-3

Cover by Patrick Körner and Sanne Kassenberg,
Layout and design by Sanne Kassenberg, persoonlijkproefschrift.nl.
Printing by Ipskamp Printing, proefschriften.net

Innovative Hybrid Tools for Ureter Reconstruction and Urinary Diversion

-

Insights in Scaffold Design, (Bio)mechanical Properties, Tissue Remodeling and Noninvasive Monitoring by MRI

Proefschrift

ter verkrijging van de graad van doctor
aan de Radboud Universiteit Nijmegen
op gezag van de rector magnificus prof. dr. J.H.J.M. van Krieken,
volgens besluit van het college van decanen
in het openbaar te verdedigen op

vrijdag 18 oktober 2019

om 12.30 uur precies

door

Heinz Peter Janke

geboren op 30 september 1984

te Neuss, Duitsland

Promotor:

Prof. dr. W.F.J. Feitz

Copromotor:

Dr. E. Oosterwijk

Manuscriptcommissie:

Prof. dr. ir. S.C.G. Leeuwenburgh	(Voorzitter)
Prof. dr. H. van Goor	
Prof. dr. M.C. Harmsen	(UMCG)

Paranimfen:

Dr. Marije Sloff

Dr. Paul de Jonge

Innovative Hybrid Tools for Ureter Reconstruction and Urinary Diversion

-

Insights in Scaffold Design, (Bio)mechanical Properties, Tissue Remodeling and Noninvasive Monitoring by MRI

Doctoral Thesis

to obtain the degree of doctor
from Radboud University Nijmegen
on the authority of the Rector Magnificus prof. dr. J.H.J.M. van Krieken,
according to the decision of the Council of Deans
to be defended in public on

Friday, October 18, 2019

at 12.30 hours

by

Heinz Peter Janke

born on September 30, 1984

in Neuss, Germany

Supervisor:

Prof. dr. W.F.J. Feitz

Co-supervisor:

Dr. E. Oosterwijk

Doctoral Thesis Committee:

Prof. dr. ir. S.C.G. Leeuwenburgh	(Chair)
Prof. dr. H. van Goor	
Prof. dr. M.C. Harmsen	(UMCG)

Paranymphs:

Dr. Marije Sloff

Dr. Paul de Jonge

Dedicated to Alena
and Mares

TABLE OF CONTENTS

CHAPTER 1

General Introduction
Thesis Objective & Outline

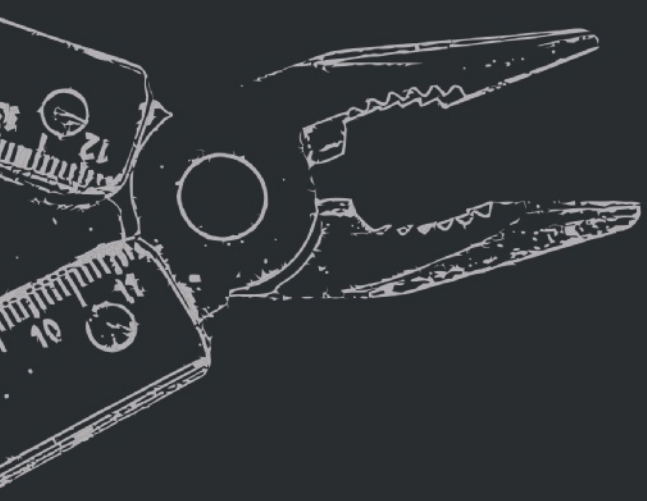

1 GENERAL INTRODUCTION

1.1 Ureter and Reconstruction Techniques

The ureter is a tubular organ responsible for the safe transport of urine from the kidney to the urinary bladder. The ureter consists of three compartments: i) The inner multi-layered lining of urothelial cells (UCs) has a barrier function preventing urine from leaking to adjacent tissue and preventing diffusion of toxic products and subsequent tissue damage. ii) A muscle layer composed of longitudinally- and circumferentially arranged smooth muscle cells (SMCs) organize urine transport by active contraction (peristalsis). iii) Connective tissue determines the overall tissue architecture and elasticity [1].

Ureter damage is mainly the consequence of trauma such as motor accidents, gun shots, or iatrogenic injuries incurred during surgical procedures [2]. Although ureteral injury is relatively uncommon, the failure to recognize the injury can lead to severe side effects, including sepsis or loss of renal function. Specific anatomical characteristics of the ureter, such as the segmental vascular supply, the site of ureteral injury (e.g. upper ureter, mid ureter, lower ureter or complete ureter) and the lack of native tissue for repair limits surgical ureteral reconstruction possibilities. Several surgical techniques are recommended to repair ureteral defects [3,4]: A uretero-ureterostomy is the most common repair performed albeit only preferred in small size defects of the upper and mid-ureter. Distal ureteral injuries are best managed by ureteral reimplantation which can be combined with a psoas hitch between the bladder and the ipsilateral psoas tendon. In extensive mid-lower ureteral injury, the large gap between ureter and bladder can be bridged with a tubularized L-shaped bladder flap (boari flap). Renal auto-transplantation and ileal interposition are options in reconstruction of the entire ureter. Especially, creation of neotissue using autologous harvested bowel tissue is associated with severe side effects and multiple unfavorable outcomes. For example, reconstructive surgery using tissue replacements created from tubularized intestine segments for ureter reconstruction often result in urinary tract infections, partial small bowel obstruction and metabolic imbalances [5,6]. In many cases multiple procedures are needed over time, mostly due to (re-)stenosis and (re-)strictures, and ultimately nephrectomy may be needed [7,8].

1.2 Urinary Bladder and Urinary Diversion

The urinary bladder is a flexible hollow organ which acts a temporary urine reservoir until the urine is actively evacuated by means of muscle contraction via the urethra to the exterior. The anatomy of the bladder wall is similar to that of the ureter and is composed of an multi-layered urothelium, a detrusor muscle composed of organized SMCs, and connective tissue [9].

Dysfunction of the urinary bladder are related to congenital defects (e.g. spina bifida), nerve damage (e.g. neuropathic bladder), inflammatory conditions (e.g. bladder pain syndrome) or tumors arising from bladder cancer. In all cases, surgical interventions are restricted to the use of bowel tissue for bladder reconstruction or radical cystectomy followed by urinary diversion may often be required. Here, the ileal conduit remains the gold standard procedure: Urine is drained from the ureters by a piece of small bowel tissue which is anastomosed to the abdominal skin surface [10]. However, the ileal conduit is associated with many post-operative complications: bowel obstruction, urinary flow obstruction, fistulas, stone formation, metabolic- or nutritional disorders are consequences of the bowel surgery and/or the urostomy transplantation [11–13].

1.3 Tissue Engineering (TE), Biomaterials and Scaffold Design

Taken together, alternative graft materials for ureter reconstruction and urinary diversion are highly desirable. The field of Tissue Engineering (TE) holds great potential to restore functionality of diseased organs and tissue and may circumvent gold standard related complications and graft shortage. In the "classical" TE paradigm autologous neotissue is created by using a so-called scaffold (aka template or matrix) [14]. The scaffold is the backbone of tissue-engineered grafts. The ideal scaffold should mimic the tissue of interest as much as possible as it needs to be able to keep its form to fill the defect and it needs to adapt to dynamic (bio)mechanical loads until its replaced by host tissue [15]. Hence, the scaffold design and its remodeling characteristics are pivotal to ensure functionality. Different biomaterials can be used to create tubular scaffolds for ureter reconstruction and urinary diversion, which can be of synthetic- or natural origin and each class of biomaterials have its specific advantages and disadvantages. Scaffolds designed from synthetic biomaterials are highly tunable and reproducible in overall architecture and strength but have a low bioactivity and biocompatibility. In contrary, scaffolds composed of natural biomaterials promote excellent cell adhesion and growth, but show limited design tunability and/or strength [16].

The main structural protein of most hard and soft tissues in mammals, collagen may be a promising naturally-derived biomaterial due to its biocompatibility, biodegradability, bioactivity and low antigenicity [16,17]. Due to the fact that collagen-based scaffolds can be tuned to highly porous tubular sponges of various diameter, length and pore architecture, they remain ideal candidates for customized tubular organ manufacture [18]. Unfortunately, highly porous collagen-based scaffolds have poor (bio)mechanical properties and they cannot comply with demands of native tissue. Chemical crosslinking by N-ethyl-3-(3-dimethylaminopropyl)-carbodiimide (EDC) / N-hydroxysuccinimide (NHS) is mostly performed to enhance overall strength and resistance against enzymatic degradation [19–22]. Furthermore, EDC/NHS -crosslinking can be used to actively bound growth factors to collagen to enhance graft remodeling and vascularization [23,24]. Although, crosslinking can enhance overall strength of collagen scaffolds, they remain fragile and their patency is strongly diminished during surgery as they can rupture easily [25,26]. Another strategy to induce overall strength to collagen-based scaffolds, reinforcement with e.g. (tubularized) meshes or electrospun synthetic biomaterials have been performed [27–29]. Such hybrid scaffolds may be proper templates for tubular organ reconstruction such as the ureter or urinary diversion. The supportive synthetic polymer acts as the backbone of the tubular graft providing sufficient strength and flexibility, while the collagen acts as the cellular stratum, guiding formation of neotissue.

1.4 Monitoring of TE Constructs

Traditionally, (immuno)histochemical techniques have been used to evaluate tissue-engineered constructs at pre-determined time points after implantation. However, these methods are destructive, and they do not allow for insights in graft integrity, remodeling up to resorption in real-time. Thus, the ability to monitor the fate of tissue-engineered constructs upon implantation is a critical need. Several imaging modalities are available for monitoring in a noninvasive, highly-sensitive manner including X-ray computed tomography (CT), optical coherence tomography (OCT), ultrasound (USI), positron emission tomography (PET), single-photon emission computed tomography (SPECT), and magnetic resonance imaging (MRI) [30]. Especially, MRI is an attractive multi-functional and non-invasive imaging modality which does not use ionizing radiation. However, tissue-engineered constructs such as collagen-based scaffolds usually give poor contrast as the selected materials have similar composition as that of the surrounding host tissue, and thus are

difficult to distinguish. In this context, collagen scaffolds have been labeled with contrast agents (CAs) such as superparamagnetic iron oxide nanoparticles (USPIOs) to enhance their MR visibility [31,32]. USPIOs generate a negative contrast, which however may be misinterpreted as other tissue components such as air inclusion may also cause negative contrast. Furthermore, the effect of USPIOs on the water signal may extend beyond its local presence (´blooming´ effect) and thus hamper their precise localization [31–33]. Since supportive polymers (e.g. electrospun material) give also a negative contrast in MR imaging [34–36], alternative CAs are desirable for MR imaging of hybrid collagen-based scaffolds.

1.5 Animal Models and Clinical Translation of TE Constructs

To allow translation to clinical settings, preclinical testing of new designed scaffolds upon *in vitro* characterization is required. Preclinical evaluation often starts with subcutaneous implantation of novel scaffolds in small animal models, to test their overall biocompatibility and tissue remodeling characteristics [37–40]. Subsequently, large animal models were used to reconstruct functional defects with tissue-engineered constructs as they may mimic more the human situation at clinically relevant sites with scaffolds of comparable size and surgical techniques [41]. Since different large animal models vary in their (cell) growth and regeneration kinetics (e.g. German Landrace and Göttingen Minipig) [42], different models for patients groups (e.g. young- and older patients) can be established.

Regardless, of the chosen animal model or type of scaffold, implementation of scaffolds to (pre)-clinical applications requires terminal sterilization. Therefore, it is a critically important task to choose an appropriate FDA/EMA- approved sterilization technique (e.g. gamma-irradiation, EtO-degassing) in order to effectively sterilize biodegradable scaffolds but at the same time to maintain their structural and biochemical integrity [43].

2 THESIS OBJECTIVE

The aim of this thesis was to develop innovative tools which can be used for ureteral reconstruction or creation of an artificial urostomy. Upon development of hybrid scaffolds, insights were given in scaffold design, (bio)mechanical properties, noninvasive MR imaging and tissue remodeling.

3 OUTLINE OF THIS THESIS

To indicate the "state-of-the-art" of ureter reconstruction and urinary diversion using TE approaches, a literature review was performed in **chapter 2** with emphasis on biomaterials, scaffold designs and reconstruction strategies.

Chapter 3 focuses on the development of new supportive structures composed of synthetic polymers. So-called coupled helical coils (CHCs) were manufactured to mimic collagen fiber orientation as found in tubular organs such as the ureter. Therefore, CHCs may be promising tools in tubular scaffold manufacture. CHCs of different polymer composition were tested to determine their mechanical properties and degradation profiles. In a final set of experiments, seamless and stable hybrid constructs consisting of CHCs and porous collagen type I were produced.

Subsequently, MR imaging was established as a noninvasive tool to monitor tissue-engineered hybrid constructs. In **chapter 4**, we used a naturally-derived hemin-L-lysine complex (HL) as a potential CA to label hybrid templates. In **chapter 5**, a fully synthetic injectable hydrogel was used in combination with a CA and cell binding motifs. This imageable 'artificial ECM' was monitored over time to access its properties as a template for tissue repair as well as a cell- and drug delivery vehicle.

Since the choice of sterilization may affect the overall performance of natural- and synthetic biomaterials, we studied the influence of γ-irradiation and EtO degassing on hybrid tubular scaffolds in **chapter 6**. The *in vitro* characteristics were extensively studied, including tensile strength analysis and degradation studies. For *in vivo* evaluation, constructs were subcutaneously implanted in a goat model to access tissue remodeling of biohybrid constructs.

Finally, **chapter 7** summarize the findings of this thesis and potential future directions are discussed.

4 REFERENCES

[1] R. Fröber, Surgical anatomy of the ureter, BJU Int. 100 (2007) 949-965. DOI:10.1111/j.1464-410X.2007.07207.x.

[2] F.N. Burks, R.A. Santucci, Management of iatrogenic ureteral injury., Ther. Adv. Urol. 6 (2014) 115–24. DOI:10.1177/1756287214526767.

[3] D.J. Summerton, N.D. Kitrey, N. Lumen, E. Serafetinidis, N. Djakovic, European Association of Urology, EAU Guidelines on Iatrogenic Trauma, Eur. Urol. 62 (2012) 628–639. DOI:10.1016/j.eururo.2012.05.058.

[4] D.J. Bryk, L.C. Zhao, Guideline of guidelines: a review of urological trauma guidelines, BJU Int. 117 (2016) 226–234. DOI:10.1111/bju.13040.

[5] S.A. Armatys, M.J. Mellon, S.D.W. Beck, M.O. Koch, R.S. Foster, R. Bihrle, Use of ileum as ureteral replacement in urological reconstruction., J. Urol. 181 (2009) 177–81. DOI:10.1016/j.juro.2008.09.019.

[6] A. Martini, D. Villari, G. Nicita, Long-term complications arising from bowel interposition in the urinary tract, Int. J. Surg. 44 (2017) 278–280. DOI:10.1016/j.ijsu.2017.07.030.

[7] B. Phillips, S. Holzmer, L. Turco, M. Mirzaie, E. Mause, A. Mause, A. Person, S.W. Leslie, D.L. Cornell, M. Wagner, R. Bertellotti, J.A. Asensio, Trauma to the bladder and ureter: a review of diagnosis, management, and prognosis, Eur. J. Trauma Emerg. Surg. 43 (2017) 763–773. DOI:10.1007/s00068-017-0817-3.

[8] T.W. Pike, S. Pandanaboyana, T. Hope-Johnson, L. Hostert, N. Ahmad, Ureteric reconstruction for the management of transplant ureteric stricture: a decade of experience from a single centre., Transpl. Int. 28 (2015) 529–534. DOI:10.1111/tri.12508.

[9] G.J Tortora, B. Derrickson, Principles of anatomy & physiology, 1st ed., Wiley-VCH Verlag GmbH & Co. KGaA, Weinheim, 2008. ISBN: 978-3527325108.

[10] O.M.S. El-Taji, A.Q. Khattak, S.A. Hussain, Bladder reconstruction: The past, present and future., Oncol. Lett. 10 (2015) 3–10. DOI:10.3892/ol.2015.3161.

[11] J.D. Roth, M.O. Koch, Metabolic and Nutritional Consequences of Urinary Diversion Using Intestinal Segments to Reconstruct the Urinary Tract, Urol. Clin. North Am. 45 (2018) 19–24. DOI:10.1016/j.ucl.2017.09.007.

[12] A. Prcic, E. Begic, Complications After Ileal Urinary Derivations, Med. Arch. 71 (2017) 320. DOI:10.5455/medarh.2017.71.320-324.

[13] R.E. Hautmann, S.H. Hautmann, O. Hautmann, Complications associated with urinary diversion, Nat. Rev. Urol. 8 (2011) 667–77. DOI:10.1038/nrurol.2011.147.

[14] J.P. Vacanti, R. Langer, Tissue engineering: the design and fabrication of living replacement devices for surgical reconstruction and transplantation., Lancet (London, England). 354 Suppl 1 (1999) SI32-4. DOI:10.1016/s0140-6736(99)90247-7.

[15] S.J. Hollister, Scaffold design and manufacturing: from concept to clinic., Adv. Mater. 21 (2009) 3330–42. DOI:10.1002/adma.200802977.

[16] F.J. O'Brien, Biomaterials & scaffolds for tissue engineering, Mater. Today. 14 (2011) 88–95. DOI:10.1016/S1369-7021(11)70058-X.

[17] C. Dong, Y. Lv, Application of Collagen Scaffold in Tissue Engineering: Recent Advances and New Perspectives, Polymers (Basel). 8 (2016) 42. DOI:10.3390/polym8020042.

[18] M.J.W. Koens, P.J. Geutjes, K.A. Faraj, J. Hilborn, W.F. Daamen, T.H. van Kuppevelt, Organ-specific tubular and collagen-based composite scaffolds., Tissue Eng. Part C. Methods. 17 (2011) 327–35. DOI:10.1089/ten.TEC.2010.0269.

[19] L.H. Olde Damink, P.J. Dijkstra, M.J. van Luyn, P.B. van Wachem, P. Nieuwenhuis, J. Feijen, Cross-linking of dermal sheep collagen using a water-soluble carbodiimide., Biomaterials. 17 (1996) 765–73. DOI: 10.1016/0142-9612(96)81413-X.

[20] L.H. Olde Damink, P.J. Dijkstra, M.J. van Luyn, P.B. van Wachem, P. Nieuwenhuis, J. Feijen, *In vitro* degradation of dermal sheep collagen cross-linked using a water-soluble carbodiimide., Biomaterials. 17 (1996) 679–84. DOI: 10.1016/0142-9612(96)86737-8.

[21] L.R. Versteegden, H.R. Hoogenkamp, R.M. Lomme, H. van Goor, D.M. Tiemessen, P.J. Geutjes, E. Oosterwijk, W.F. Feitz, T.G. Hafmans, N. Verdonschot, W.F. Daamen, T.H. van Kuppevelt, Design of an elasticized collagen scaffold: A method to induce elasticity in a rigid protein., Acta Biomater. 44 (2016) 277–85. DOI:10.1016/j.actbio.2016.08.038.

[22] J.S. Pieper, A. Oosterhof, P.J. Dijkstra, J.H. Veerkamp, T.H. van Kuppevelt, Preparation and characterization of porous crosslinked collagenous matrices containing bioavailable chondroitin sulphate., Biomaterials. 20 (1999) 847–58. 10.1016/S0142-9612(98)00240-3.

[23] J.S. Pieper, T. Hafmans, P.B. van Wachem, M.J.A. van Luyn, L.A. Brouwer, J.H. Veerkamp, T.H. van Kuppevelt, Loading of collagen-heparan sulfate matrices with bFGF promotes angiogenesis and tissue generation in rats, J. Biomed. Mater. Res. 62 (2002) 185–194. DOI:10.1002/jbm.10267.

[24] van Susante JLC, J. Pieper, P. Buma, T.H. van Kuppevelt, H. van Beuningen, P.M. van Der Kraan, J.H. Veerkamp, W.B. van den Berg, Veth RPH, Linkage of chondroitin-sulfate to type I collagen scaffolds stimulates the bioactivity of seeded chondrocytes *in vitro*., Biomaterials. 22 (2001) 2359–69. DOI: 10.1016/S0142-9612(00)00423-3.

[25] P.K.J.D. de Jonge, V. Simaioforidis, P.J. Geutjes, E. Oosterwijk, W.F.J. Feitz, Recent advances in ureteral tissue engineering., Curr. Urol. Rep. 16 (2015) 465. DOI:10.1007/s11934-014-0465-7.

[26] M. Sloff, V. Simaioforidis, P.J. Geutjes, H.R. Hoogenkamp, T.H. van Kuppevelt, W.F. Daamen, E. Oosterwijk, W.F. Feitz, Novel tubular constructs for urinary diversion: a biocompatibility study in pigs., J. Tissue Eng. Regen. Med. (2016). DOI:10.1002/term.2122.

[27] H.R. Hoogenkamp, M.J.W. Koens, P.J. Geutjes, H. Ainoedhofer, G. Wanten, D.M. Tiemessen, J. Hilborn, B. Gupta, W.F.J. Feitz, W.F. Daamen, A.K. Saxena, E. Oosterwijk, T.H. van Kuppevelt, Seamless vascularized large-diameter tubular collagen scaffolds reinforced with polymer knittings for esophageal regenerative medicine., Tissue Eng. Part C. Methods. 20 (2014) 423–30. DOI:10.1089/ten.TEC.2013.0485.

[28] S.J. Lee, J. Liu, S.H. Oh, S. Soker, A. Atala, J.J. Yoo, Development of a composite vascular scaffolding system that withstands physiological vascular conditions., Biomaterials. 29 (2008) 2891–8. DOI:10.1016/j.biomaterials.2008.03.032.

[29] E.M. Engelhardt, L. a Micol, S. Houis, F.M. Wurm, J. Hilborn, J. a Hubbell, P. Frey, A collagen-poly(lactic acid-co-e{open}-caprolactone) hybrid scaffold for bladder tissue regeneration, Biomaterials. 32 (2011) 3969–3976. DOI:10.1016/j.biomaterials.2011.02.012.

[30] A.A. Appel, M.A. Anastasio, J.C. Larson, E.M. Brey, Imaging challenges in biomaterials and tissue engineering., Biomaterials. 34 (2013) 6615–30. DOI:10.1016/j.biomaterials.2013.05.033.

[31] Y. Sun, P. Geutjes, E. Oosterwijk, A. Heerschap, *In vivo* magnetic resonance imaging of type I collagen scaffold in rat: improving visualization of bladder and subcutaneous implants., Tissue Eng. Part C. Methods. 20 (2014) 964–71. DOI:10.1089/ten.TEC.2014.0046.

[32] M.E. Mertens, A. Hermann, A. Buhren, L. Olde-Damink, D. Mockel, F. Gremse, J. Ehling, F. Kiessling, T. Lammers, Iron Oxide-labeled Collagen Scaffolds for Non-invasive MR Imaging in Tissue Engineering, Adv Funct Mater. 24 (2014) 754–762. DOI:10.1002/adfm.201301275.

[33] F. Kiessling, M.E. Mertens, J. Grimm, T. Lammers, Nanoparticles for imaging: top or flop?, Radiology. 273 (2014) 10–28. DOI:10.1148/radiol.14131520.

[34] N.L. Hansen, A. Barabasch, M. Distelmaier, A. Ciritsis, N. Kuehnert, J. Otto, J. Conze, U. Klinge, R.-D. Hilgers, C.K. Kuhl, N.A. Kraemer, First In-Human Magnetic Resonance Visualization of Surgical Mesh Implants for Inguinal Hernia Treatment, Invest. Radiol. 48 (2013) 770–778. DOI:10.1097/RLI.0b013e31829806ce.

[35] F.-L. Zhou, P.L. Hubbard, S.J. Eichhorn, G.J.M. Parker, Coaxially Electrospun Axon-Mimicking Fibers for Diffusion Magnetic Resonance Imaging, ACS Appl. Mater. Interfaces. 4 (2012) 6311–6316. DOI:10.1021/am301919s.

[36] J. Bouley, M. Fisher, N. Henninger, Comparison between coated vs. uncoated suture middle cerebral artery occlusion in the rat as assessed by perfusion/diffusion weighted imaging., Neurosci. Lett. 412 (2007) 185–90. DOI:10.1016/j.neulet.2006.11.003.

[37] J.-G. Shi, W.-J. Fu, X.-X. Wang, Y.-D. Xu, G. Li, B.-F. Hong, Y. Wang, Z.-Y. Du, X. Zhang, Tissue engineering of ureteral grafts by seeding urothelial differentiated hADSCs onto biodegradable ureteral scaffolds, J. Biomed. Mater. Res. Part A. 100A (2012) 2612–2622. DOI:10.1002/jbm.a.34182.

[38] S.-H. Kim, H.R. Lee, S.J. Yu, M.-E. Han, D.Y. Lee, S.Y. Kim, H.-J. Ahn, M.-J. Han, T.-I. Lee, T.-S. Kim, S.K. Kwon, S.G. Im, N.S. Hwang, Hydrogel-laden paper scaffold system for origami-based tissue engineering., Proc. Natl. Acad. Sci. U. S. A. 112 (2015) 15426–31. DOI:10.1073/pnas.1504745112.

[39] H. Koch, N. Hammer, S. Ossmann, K. Schierle, U. Sack, J. Hofmann, M. Wecks, A. Boldt, Tissue Engineering of Ureteral Grafts: Preparation of Biocompatible Crosslinked Ureteral Scaffolds of Porcine Origin., Front. Bioeng. Biotechnol. 3 (2015) 89. DOI:10.3389/fbioe.2015.00089.

[40] J.H. Park, J.M. Hong, Y.M. Ju, J.W. Jung, H.-W. Kang, S.J. Lee, J.J. Yoo, S.W. Kim, S.H. Kim, D.-W. Cho, A novel tissue-engineered trachea with a mechanical behavior similar to native trachea, Biomaterials. 62 (2015) 106–115. DOI:10.1016/j.biomaterials.2015.05.008.

[41] M. Sloff, R. de Vries, P. Geutjes, J. IntHout, M. Ritskes-Hoitinga, E. Oosterwijk, W. Feitz, Tissue Engineering in Animal Models for Urinary Diversion: A Systematic Review, PLoS One. 9 (2014) e98734. DOI:10.1371/journal.pone.0098734.

[42] D. Leonhäuser, M. Vogt, R.H. Tolba, J.O. Grosse, Potential in two types of collagen scaffolds for urological tissue engineering applications - Are there differences in growth behaviour of juvenile and adult vesical cells?, J. Biomater. Appl. 30 (2016) 961–73. DOI:10.1177/0885328215610824.

[43] Z. Dai, J. Ronholm, Y. Tian, B. Sethi, X. Cao, Sterilization techniques for biodegradable scaffolds in tissue engineering applications., J. Tissue Eng. 7 (2016) 2041731416648810. DOI:10.1177/2041731416648810.

CHAPTER 2

Reconstruction Strategies of the Ureter and Urinary Diversion using Tissue Engineering Approaches

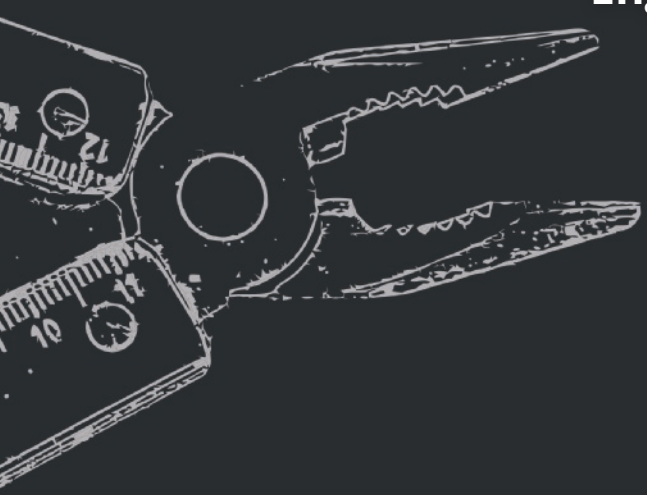

H.P. Janke[1], P.K.J.D. de Jonge[1], W.F.J. Feitz[1,2] and E. Oosterwijk[1]

[1]: Department of Urology, Radboud Institute for Molecular Life Science, Radboudumc, Geert Grooteplein 28; 6525 GE Nijmegen, The Netherlands
[2]: Radboudumc Amalia Children's Hospital, Geert Grooteplein-Zuid 10, 6525 GA Nijmegen, The Netherlands

Tissue Eng Part B Rev. 2019 Jun;25(3):237-248
DOI: 10.1089/ten.TEB.2018.0345

ABSTRACT

The standard for long-segment reconstruction of the ureter and urinary diversion is the creation of neo-tissue using autologous bowel tissue, albeit associated with multiple complications. Tissue-engineered (TE) constructs may provide alternative solutions. Here, we review ureter reconstruction and urinary diversion using Tissue Engineering approaches. A literature search strategy was applied in PubMed to identify available preclinical studies published up until September 2018. Subsequently, studies were screened for scaffolds used and relevance (e.g. reconstruction of full circumferential defects in preclinical settings) and further categorized based on whether grafts were directly implanted, seeded with cells prior to implantation, or preimplanted (with or without cells) before functional implantation. Future prospects are discussed with emphasis on scaffold design and functional tissue maturation of tissue engineered constructs to foster clinical translation.

1 INTRODUCTION

The main cause of ureter damage is trauma caused by e.g. motor accidents, gun shots, or iatrogenic injuries incurred during surgery [1]. While ureteral injury is relatively uncommon, the failure to recognize it can lead to severe side effects, including sepsis or loss of renal function. Surgical ureteral reconstruction possibilities are limited due to specific anatomical characteristics of the ureter (e.g. segmental vascular supply), site of ureteral injury, and the lack of native tissue for repair. Several surgical techniques are recommended to repair ureteral defects [2]. For long-segment reconstruction, the creation of neotissue using autologous harvested bowel tissue remains the gold standard. However, the use of this unrelated tissue source is associated with severe side effects and multiple unfavorable outcomes [3]. In many cases multiple procedures are needed over time, mostly due to (re-) stenosis and (re-)strictures, and ultimately nephrectomy may be needed [4].

For muscle-invasive bladder cancer (MIBC) and non-muscle invasive bladder cancer (NMIBC) with high risk of progression, the European guidelines recommend radical cystectomy followed by urinary diversion [5]. The most used form of urinary diversion is the ileal conduit using autologous intestine segments [6]. However -and very similar to ureteral reconstruction-, this is associated with many post-operative complications [7].

Thus, there is a clear need for alternative graft material and reconstruction techniques. The field of Tissue Engineering (TE) holds great potential to restore functionality of diseased organs and tissue and may circumvent gold standard-related complications and graft shortage [8]. Implementation of tissue-engineered grafts may prevent invasive bowel surgery, life-threatening complications and ultimately may improve quality of life (QoL) and reduce health costs significantly.

2 SEARCH STRATEGY AND AIM OF THIS REVIEW

Here, we review state-of-the art biomaterials, scaffold designs and reconstruction strategies in preclinical studies using TE approaches which may be used for ureter regeneration and urinary diversion. A predefined search strategy was applied in PubMed using customized search filters for ureter reconstruction, urinary diversion, scaffolds and tissue engineering synonyms [9]. These search filters were combined with the animal study filter developed by Hooijmanns, et al. [10] (see **Appendix**) resulting in 1290 studies (see **Figure 1**). After removal of studies which did not contain TE approaches (studies were considered to be about TE when processed tubular scaffolds composed of natural- and/or synthetic biomaterials were used) of full circumferential defects in original pre-clinical studies, studies were sub-divided according to their application (ureter reconstruction and urinary diversion) and reconstruction strategy (**Figure 2**): a) scaffolds directly implanted, b) scaffolds seeded with cells prior to implantation, or c) preimplanted (with or without cells) before functional implantation. Subsequently, basic information regarding animal model, scaffold (bio) material and defect length were extracted (see **Table 1** and **Table 2**). Furthermore, studies were analyzed in terms of functional outcomes such as urothelium formation, muscle ingrowth, vascularization and side-effects (e.g. graft shrinkage, strictures, obstruction/ occlusion, hydronephrosis). Additionally, we discuss a selection of recently published *in vitro* studies that describe novel scaffold designs and functional tissue maturation strategies which may ultimately foster clinical translation.

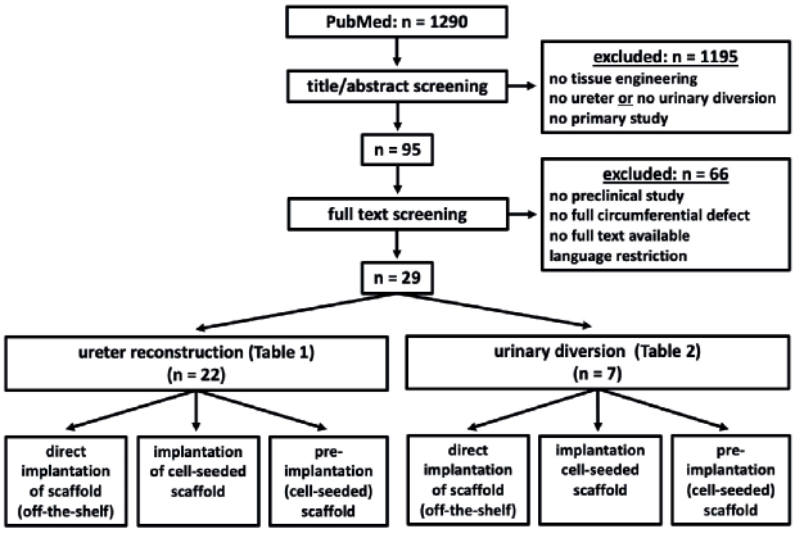

Figure 1: Flowchart of search- and screening process of preclinical studies including ureter reconstruction and urinary diversion using Tissue Engineering (TE) approaches.

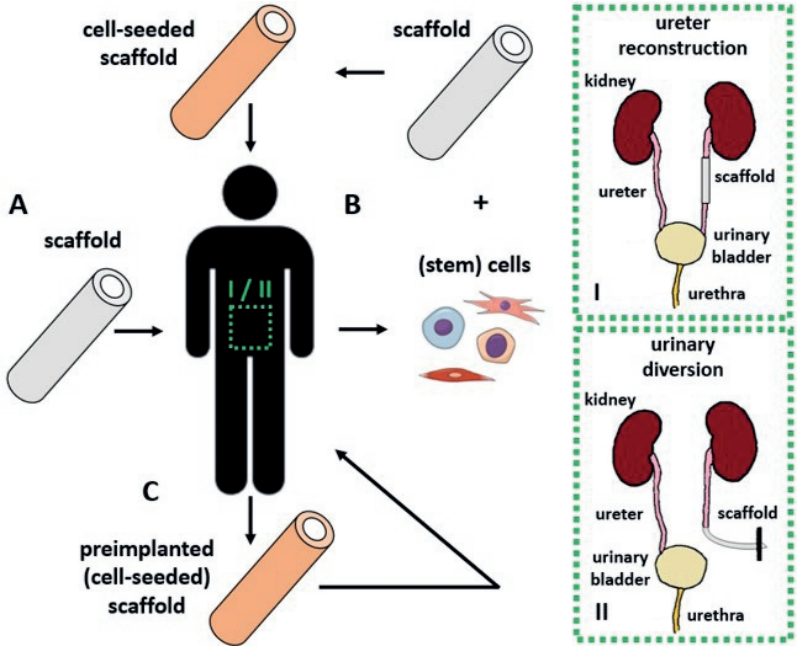

Figure 2: Implantation strategies of preclinical studies for full circumferential ureter reconstruction (I) and urinary diversion (II, black line marks the skin outlet) using Tissue Engineering (TE) approaches. A) Scaffolds directly implanted for reconstruction. B) (Stem) cells isolated from biopsies, expanded under cell culture conditions and seeded to a scaffold prior to functional implantation. C) Scaffolds or cells-seeded scaffolds are preimplanted before functional implantation.

Table 1: Preclinical studies of ureter reconstruction using Tissue Engineering (TE) approaches.

Authors / Year	Animal Model	Scaffold Type / Cell Source / Preimplantation Site (time in weeks)	Defect Length	Functional Outcome Positive / Negative	
A: Direct Implantation of Scaffolds to Full Circumferential Ureteral Defects					
1 Shalhav, et al.; 1999 [13]	(Mini) Pig	SIS (T*) and DU (T)	1.5-2.8 cm	U, M	H, F, I, Shr, Str, Ob
2 Xie, et al.; 2000 [14]	Pig	SIS (T*)	8 cm	U	Ur, F, H, Str
3 Jaffe, et al.; 2001 [15]	Rabbit	SIS (T*)	11 cm	U, M, V	D
4 Sofer, et al.; 2002 [16]	Pig	SIS (T*)	2 cm	U, M	F, I-2, H, Occ
5 Duchene, et al. 2004 [17]	Pig	SIS (T*)-halofuginone	2 cm	U, M, F	RA, H, I-2
6 El-Assmy, et al.; 2004 [19]	Dog	SIS (T*)	4 cm	U, M	F, I-2, H, Occ, Shr, D
7 Salehipour, et al.; 2013 [21]	Dog	AM (T*)	3.0 cm	-	L, H, F, I-2, D, Ob
8 Osman, et al.; 2004 [22]	Dog	DU (T)	3 cm	U, M	F, H, Obs, Shr
9 Dahms, et al.; 1997 [23]	Rat	DU (T)	0.3-0.8 cm	U, M, N, V	H
10 Tachibana, et al.;1985 [37]	Dog	COL (T)	5.0 cm	U, M	F, D, Str

Authors / Year	Animal Model	Scaffold Type / Cell Source / Preimplantation Site (time in weeks)	Defect Length	Functional Outcome Positive / Negative	
11 De Jonge, et al.; 2016 [51]	Pig	Collagen-Vicryl®-VEGF-bFGF (T)	5 cm	U, M	H, Ur, Str, Shr
12 Varady, et al.; 1982 [43]	Dog	PTFE (T)	5 cm	U	F, Obs
13 Sabanegh, et al.; 1996 [44]	Dog	PTFE (T)	10 cm	U, M	H, I-2, Obs
14 Peters, et al.; 1996 [45]	Dog	PTFE (T)	5 cm	V	F, Occ
15 Baltaci, et al.; 1998 [46]	Dog	PTFE (T)	5-8 cm	-	H, D, F, Str
16 Kloskowski, et. al.; 2015 [24]	Rat	AAM (T) and PLCL (T)	1.0 cm	U, M	H, I-1, Ob
B: Cell-Seeding of Scaffolds before Functional Implantation					
1 El-Hakim, et al.; 2005 [18]	Pig	SIS (T*) / UC+SMC	5.0 cm	-	F, H, Ob, Shr
2 Zhao, et al.; 2012 [25]	Rabbit	VECM (T*) / ADSCs -> SMCs	3.0 cm	U, M	-
C: Preimplantation of Scaffolds before Functional Implantation					
1 de Jonge et al.; 2017 [52]	Goat	COL-Vicryl® (T) / - / Subcutis (4)	5 cm	U, V	F
2 El-Hakim, et al.; 2005 [18]	Dog	DU (T) / UCs + SMCs / Omentum (ND)	3 cm	U, M, V	F, Ob, Shr
3 Zhao, et al.; 2016 [26]	Rabbit	VECM / ADSCs -> UCs + SMCs / Omentum (3)	ND	U, M, V	-
4 Liao, et al.; 2013 [27]	Rabbit	BAM (T*) / SMCs + MSCs / Omentum (2)	4 cm	U, M, V	-
5 Meng, et al.; 2015 [28]	Rabbit	BSM (T*) / SMCs + ADSCs / Omentum (2)	4 cm	U, M, V	-

Scaffold Abbreviations: COL, collagen; PTFE, polytetrafluorethylene (Dacron); SIS, small intestine submucosa; DU, decellularized ureter; AM, amniotic membrane; AAM, acellular aortic arch; PLCL, poly(L-lactide-co-caprolactone); VECM, vascular extracellular matrix; BAM, bladder acellular matrix; BSM, bladder submucosa matrix; VEGF, vascular endothelial growth factor; bFGF, basic fibroblast growth factor; T: Seamless tubular form; T*: Tubularized form;
Cell Source abbreviations: UCs, urothelial cells; SMCs, smooth muscle cells; MSCs, mesenchymal stem cells; ADSCs, adipose derived stem cells; ->, stem cell differentiation.
Functional outcome abbreviations: U, urothelial formation; M, muscle formation; N, nerve fibers; V, vascularization; F, fibrosis; Ur, urinoma; H, hydronephrosis; I, inflammation; I-1, mild inflammation; I-2, severe inflammation; RA, renal atrophy; Ob, obstruction; Str, stricture; D, dilatation; occlusion; Shr, (graft) shrinkage.
ND: not defined.

Table 2: Preclinical studies of creation of an artificial urostomy for urinary diversion using TE approaches.

Authors / Year	Animal Model	Scaffold / Cell Source / Preimplantation Site (time in weeks)	Urostoma Length	Functional Outcome Positive / Negative	
A: Creation of an Urostoma by using "off-the-shelf" Scaffolds					
1 Kloskowski, et. al.; 2015 [24]	Rat	AAM (T)	1.0 cm	U, M	H, Obs, Shr
	Rat	PLCL (T)	1.0 cm	U, M	H, Obs, Shr
B: Cell-Seeding of Scaffolds before Creation of an Urostoma					
1 Drewa, et al.; 2007 [20]	Rat	SIS (T*) / 3T3	3.0 cm		F, H, I-2, Occ
2 Geutjes, et al.; 2012 [53]	Pig	COL-Vypro®II (T) / UCs	12 cm	U	F, H, Occ
3 Basu, et al.; 2012 [50]	(Mini) Pig	PGA-PLGA (T*) /	ND		
		bladder SMCs		U, M, V	-
		adipose-derived SMCs		U, M, V	-
		peripheral blood-derived SMCs		U, M, V	-
C: Preimplantation of (cell-seeded) Scaffolds before Creation of an Urostoma					
1 Sloff, et al.; 2016 [55]	Pig	COL-Vicryl® (T) / - / Subcutis (4)	12 cm	U, M, V	H, Shr
2 Liao, et al.; 2013 [29]	Rabbit	BAM (T*) / UCs / Omentum (2)	4 cm	U, V	-
3 Meng, et al.; 2016 [30]	Rabbit	BAM (T*) / SMCs + ADSCs / Omentum (2)	4 cm	U, M, V	-

Scaffold abbreviations: COL, collagen; SIS, small intestine submucosa; AAM, acellular aortic arch; PLCL, poly(L-lactide-co-caprolactone); BAM, bladder acellular matrix; PGA, polyglycolic acid; PLGA, poly-dl-lactide-coglycolide; T, seamless tubular form; T*, tubularized form.
Cell source abbreviations: UCs, urothelial cells; SMCs, smooth muscle cells; ADSCs, adipose derived stem cells.
Functional outcome abbreviations: U, urothelial formation; M, muscle formation; V, vascularization; F, fibrosis; H, hydronephrosis; Ob, obstruction; Occ, occlusion; Shr, shrinkage; I-2, severe infammation.
ND: not defined.

3 BIOMATERIALS AND SCAFFOLD DESIGN IN PRECLINICAL SETTINGS

3.1 Natural Grafts

In TE applications, so-called scaffolds are the building blocks to create graft materials. The ideal scaffold should mimic the tissue of interest as much as possible, which guides material choice and mechanical design: it should be able to (i) keep its form to fill the defect, (ii) should be readily implantable, (iii) enhance tissue regeneration, and (iv) should be able to support tissue-specific functional demands, including (bio)mechanical loads until complete remodeling by the host tissue [11,12]. In most preclinical TE studies tubular scaffolds were produced from decellularized native tissue specimens such as small intestine submucosa [13–20], amniotic membrane [21], ureter [13,18,22,23], blood vessels [24–26] or bladder tissue [27–30]. Decellularized tissue resembles the native tissue the closest: it combines unique micro- and macro-architectural characteristics such as a regular, yet anisotropic network of extracellular matrix fibers, albeit that this architecture differs between organs and species [31,32]. Importantly, cell binding molecules and specific growth factors can be retained despite the decellularization process [33].

When designing a ureteral substitute, the (bio)mechanical properties should be considered. The ureter displays a "J"-shaped stress-strain behavior with a high elasticity zone giving rise to a stiffer zone at higher strain [34]. In general, the ureter is stiffer in longitudinal than in circumferential direction due to the collagen fiber density and its arrangement within the ECM of the ureter [35] and decellularized material such as a decellularized ureter can mimic this situation [36].

Alternatively, scaffolds have been produced from naturally-derived biomaterials such as collagen type I [37,38]. Besides being the main structural protein of most hard and soft tissues in mammals, collagen may a promising naturally-derived biomaterial due to its biocompatibility, biodegradability, bioactivity and low antigenicity [12,39]. However, this yields scaffolds of randomly oriented collagen fibers and collagen scaffolds need to be crosslinked to enhance strength and to slow down enzymatic degradation and thus the natural characteristics are chemically altered [40–42].

3.2 Synthetic Grafts

Besides natural derived biomaterials, fully synthetic scaffolds have been used for ureter reconstruction and urinary diversion. These can be categorized in degradable

or non-degradable scaffolds. Non-degradable polytetrafluoroethylene (PTFE) grafts were used for ureteral reconstruction in 4/16 studies [43–46]. This type of graft material has been used as an "off-the-shelf" graft for blood vessel reconstruction [47], and may also be applicable to genitourinary applications. Alternatively, (melt) electrospinning offers many opportunities in scaffold manufacture because scaffolds of different shape, porosity and fiber arrangement can be easily created [48] and electrospun scaffolds can be used as stents for treatment of ureteral strictures [49]. Despite of this flexibility, preclinical studies with electrospun material have been limited [24,50].

3.3 Hybrid Grafts

Alternatively, hybrid scaffolds have been produced combining natural and synthetic biomaterials aimed at improving handling ease and mechanical characteristics. Although chemical crosslinking provides increased strength to collagen scaffolds, these are still too weak to withstand the (bio)mechanical demands of native (ureteral) tissue. Hence collagen scaffolds have been reinforced with synthetic polymers to create stronger hybrid scaffolds [51–55]. Indeed, reinforcement with a mesh of synthetic polymers resulted in stronger hybrid scaffolds with a "J" shaped stress-strain behavior similar to the native ureter [52]. Furthermore, inclusion of these materials greatly improved the surgical handling which was much better compared to collagen-alone scaffolds examined in an earlier study [38,54]. Subsequently, full biodegradable collagen-based hybrid scaffolds showed superior tissue regeneration with respect to urothelium coverage, muscle pedicles and elastin formation when compared to semi-biodegradable hybrids [54]. Therefore such (biodegradable) collagen-based hybrid scaffolds appear to be promising candidates in genitourinary TE applications in view of the versatility of purified collagen type I to create tubular scaffolds of different diameter and pore size [56] that can easily be combined with enforcing materials.

4 RECONSTRUCTION STRATEGIES IN PRECLINICAL STUDIES USING TISSUE-ENGINEERED CONSTRUCTS

4.1 Direct Implantation of Grafts

4.1.1 Ureter

Because ureteral damage is usually acute it requires immediate reconstruction, emphasizing the need for a readily available 'off-the-shelf' product. Indeed, this approach was used in most preclinical studies (**Table 1A**). Direct implantation of decellularized tissue to fill a full ureteral defect (**Figure 2A**) showed limited tissue regeneration: urothelial cells covered the graft lumen, but smooth muscle cell (SMC) ingrowth remained mainly limited to the anastomosis side of the graft [13–17,19,21,22] regardless of the animal model used. As a result, most animals presented with (intense) fibrosis of the ureteral graft and graft shrinkage, strictures, obstruction as well as hydronephrosis occurred in almost all studies, an undesired outcome.

In other studies, scaffolds created from collagen-rich decellularized rat ureter showed enhanced epithelial lining and muscle formation throughout the transplanted scaffold in small defects < 0.8 cm in a rat model [23]. However, muscle ingrowth remained limited when larger defects were repaired in a large animal model (dog) using seamless tubular scaffolds composed of purified natural collagen. Fibrosis and dilatation of the ureter above the anastomosis side occurred, indicating progressive obstruction [37].

To enhance graft acceptance and graft remodeling growth factors (GFs) have been added to enhance tissue regeneration. In pig studies scaffolds were loaded with vascular endothelial growth factor (VEGF) and basic fibroblast growth factor (bFGF) through heparin binding meant to boost vascularization and tissue remodeling [51]. In all animals, graft shrinkage (approx. 24%) and constriction at the anastomosis site was observed as well as hydronephrosis. Post implantation the lumen of the neo-ureter was covered with a single layer of urothelium, regardless of whether GFs were added. Muscle ingrowth was limited and mainly occurred at the anastomosis site and in general, addition of GFs did not improve the outcome. Loading of SIS with the type I collagen inhibitor halofuginone meant to prevent stricture formation after grafting which was possibly caused by fast collagen degradation and tissue remodeling also did not improve outcome in porcine models [17].

Direct implantation of fully synthetic non-degradable grafts which would be easy to produce and kept as off-the-shelf grafts has met little success. Grafting resulted

in substantial complications such as fibrosis, acute and chronic inflammation around the implant, as well as obstruction/occlusion and stricture at the anastomosis site in a dog model [43–46].

Implantation of biodegradable electrospun PLCL scaffolds in wistar rats with a full ureteral defect resulted in a substantial size reduction of the graft (30%) and implantation of the PLCL template resulted in patent uretero-scaffold anastomosis in 4/6 animals studied, but ureter outcome and kidney function and its integration with native ureter was generally worse compared to decellularized scaffold [24].

Regardless of the graft (bio)material and animal model used, direct implantation of bare scaffolds to bridge full circumferential ureteral defects has been consistently associated with severe side effects such as fibrosis, graft shrinkage, strictures, dilatation and/or hydronephrosis. Albeit that urothelium regeneration was possible in most cases, formation of functional muscle tissue has remained limited. Therefore, direct implantation of current cell-free grafts may not advisable.

4.1.2 Urinary Diversion

When an urostoma is created, graft material is anastomosed to the ureter and as such, a urinary conduit used for urinary diversion can be viewed as an extended ureter (**Figure 2, II**). Thus, the requirements for scaffolds used for urinary diversion are similar to the requirements of ureteral scaffolds. Unlike ureteral reconstruction where immediate repair is mostly imperative, clinical management of muscle-invasive bladder cancer provides a time-window for TE approaches: cystectomy, requiring the formation of an urinary diversion, should be performed within 3 months of diagnosis to have a significant survival benefit [5].

Studies examining whether direct implantation of scaffolds could be used to form a urinary diversion have been very limited (**Table 2A**). Implantation of synthetic and biodegradable conduits showed poor integration with the ureter, and a patent conduit-to-skin anastomosis with good functional results was only formed in 1 out of 5 cases [24] in a rat model. Grafting of decellularized material led to occlusion at the conduit-to-skin anastomosis and graft shrinkage, hydronephrosis and ureter dilatation [24] in the same model.

4.2 Cell-Seeding of Scaffolds before Functional Implantation

4.2.1 Ureter

Despite the difficulties encountered with current cell-free scaffolds and in view of the possibility that cell seeding might enhance tissue regeneration, very few

preclinical studies have been performed examining the effect of cell seeding before implantation (**Table 1B** and **Figure 2B**). It is important to realize that grafts for ureter repair and urinary diversion will be exposed to and saturated with urine, and that this will probably hamper tissue regeneration. A cellular lining might mitigate the detrimental effects of urine exposure on tissue regeneration. An early strategy was to seed a SIS scaffold with autologous porcine bladder UCs and SMCs, followed by conditioning under static cell culture conditions to bridge a 5 cm full circumferential ureteral defect in a pig model [18]. The cell-seeding and conditioning did not improve the functional outcome when compared to the implanted non-seeded SIS: In all grafts contraction and stenosis occurred, with complete obstruction of the ipsilateral renal unit. Severe hydroureteronephrosis was evident proximal to the graft as well as total renal obstruction. In one study autologous adipose derived stem cells (ADSCs) were seeded [25]. This cell type could be differentiated into SMCs and seeding of these cells to scaffolds upon implantation improved the outcome in a rabbit model: post implantation, a stratified urothelium and organized muscle bundles were observed in the implants and ureteral strictures or hydroureteronephrosis were absent. Thus, whether the addition of autologous cells to scaffolds is beneficial remains unclear.

4.2.2 Urinary Diversion

In one of the first TERM studies for urinary diversion an artificial urinary conduit was formed by seeding 3T3 fibroblasts to SIS scaffolds and transplanted in a rat model. Based on the inflammatory reaction within the peritoneal cavity and the occurrence of hydronephrosis in all transplanted animals it was concluded that 3T3 fibroblasts are not useful as a "feeder layer" for ureteral augmentation [20].

Implantation of tubular semi-biodegradable hybrid collagen-Vypro® scaffolds seeded with primary UCs as an incontinent urostomy revealed the formation of a retroperitoneal tunnel functioning as a urostomy in 50% of cases in pigs. However, complications still occurred and included a hydroureter and hydronephrosis in all animals without major differences between cellular and acellular constructs [53].

In another study, synthetic scaffolds were combined with cells followed by bioreactor conditioning demonstrating that the addition of SMCs was essential: after grafting of tissue engineered tubular constructs seeded with autologous SMCs in a mini pig model, a patent urinary diversion for post cystectomy management of urine elimination was created [50].

4.3 Preimplantation of Scaffolds before Functional Implantation

4.3.1 Ureter

Preimplantation of scaffolds at non-functional implantation sites (**Figure 2C**) aims at scaffold remodeling and the development of a vascularized scaffold outside of the functional defect. Transposition, preferably with the vascular trunk intact might enhance tissue regeneration because an adequate blood supply is important for the viability of the graft. Tubular scaffolds have been preimplanted at the omentum or subcutis to induce angiogenesis and to form neotissue in large animal models within 2-4 weeks (**Table 1C**). Subcutaneous implantation of cell-free collagen-based scaffolds in adult goats, mimicking the elderly human target population, produced a remodeled and well-vascularized scaffold which showed (bio)mechanical characteristics comparable to the native goat ureter [52]. After functional implantation these preimplants showed significantly better outcomes compared to directly implanted collagen-Vicryl® hybrid scaffolds. However, muscle ingrowth was not improved, and functional muscle tissue was only formed at the anastomosis site.

Preimplantation has also been used in combination with cell seeding: autologous bladder cells were seeded on decellularized ureters of porcine origin and these constructs were preimplanted in the omentum and subsequently used to replace a 3 cm segment of the ureter in a dog model. Despite better vascularity caused by the omental implantation, similar clinical results were observed when compared to non-seeded or cell-seeded scaffolds in a pig model [18].

The combination of preimplantation and cell seeding with stem cells has shown promising results: Co-culture of ADSC-differentiated UCs and SMCs [26], primary SMCs with MSCs [27] and primary SMCs with ADSCs [28] on scaffolds followed by pre-implantation in the omentum resulted in urothelium and muscle formation and vascularization over the entire scaffold in a rabbit model. The functional outcome was very promising as strictures and hydronephrosis were absent.

Thus far, preimplantation of cell-seeded scaffolds appears to be the most promising strategy as it is associated with good functional outcomes when compared to other implantation strategies. However, this approach remains very time consuming (approximately 4-7 weeks), complex and clinical translation is not readily foreseen.

4.3.2 Urinary Diversion

In several studies scaffolds were pre-implanted before functional implantation for urinary diversion (**Figure 2C** and **Table 2C**). When different strategies were compared in landrace pigs, transplantation of a pre-implanted hybrid tubular collagen-Vicryl® scaffold showed a favorable outcome compared to non-preimplantation strategies (better urinary drainage, limited hydroureteronephrosis, improved tissue regeneration) albeit that severe construct shrinkage and skin contraction occurred [55].

Better functional outcomes were also observed when cells were added before preimplantation: in rabbits functional urostoma were created with multilayered urothelium on the luminal side and organized smooth muscle tissue on the other side, without leakage, stricture, or obstructions when a urostoma was engineered from pre-implanted decellularized tissue seeded with bladder epithelial cells [29] or co-culture of ADSCs and SMCs [30]. Similar to ureter reconstruction, the complexity of this procedure may limit clinical translation.

5 FUTURE DIRECTIONS

5.1 Regulatory Affairs

In Europe, tissue engineering products fall under the European regulation on Advanced therapy medicinal products (ATMPs). In the US tissue engineered products (TEMPs) are regulated as drugs, biologics, devices, or combination products by the US Food and Drug Administration (FDA). Whether the product can be viewed as a regenerative medicine advances therapy (RMAT) in the US is governed by Section 3033 of the 21st Centuries Cures Act of the FDA regulations [57]. Other regulations may apply, depending on homologous use of cells [58]. Regulations for ATMPs/RMAT are complex and this has lead to the establishment of the Committee for Advanced Therapies (CAT) in Europe [59]. The (hybrid) scaffolds without/with cells that have been studied thus far are clear examples of ATMPs/RMAT products that fall under the CAT directory. CAT and FDA accept that rigorous control of the manufacturing process has limitations inherent to the complex character of ATMPs. Nevertheless, in view of the regulations it is certainly advisable to think about regulatory requirements before initiating studies. For instance, can the production of the chosen components be controlled, what is the influence of sterilization on the final product. Thus far, this issue was not addressed in the reviewed studies, but is of utmost importance when clinical translation is desired. It is undesirable to study scaffolds that will never pass regulatory hurdles. Future studies should take regulatory issues into account, particularly with respect to material choice, sterilization and complexity. This “bedside to bench and back” approach for developing TEMPs for clinical applications was recently reviewed [60].

5.2 Scaffold Design

Although engraftment of tubularized intestine segments remains the standard procedure for long-segment ureter reconstruction and urinary diversion in the clinic, their complication rates are relatively high. For TE approaches to be a viable alternative the functional outcome must at least be similar: safe and active transport of urine must be ensured. At the same time complications must be minimal. In particular stricture formation, occlusion, dilatation and hydronephrosis must be circumvented. The collective evidence of the animal studies showed that cell-free functional implantation of scaffolds –regardless of the biomaterial of choice- appears to be problematic: it leads to fibrosis, graft-shrinkage, stricture formation,

occlusion and ultimately hydronephrosis despite the generation of a urothelial lining. Thus, there is a need of novel smart graft (bio)materials.

Natural biomaterials such as decellularized tissue have been hypotized as ideal candidates for grafting as they are biocompatible and may closely resemble the tissue of interest. However, despite the similarity of decellularized tissues to native tissue, the functional outcome of ureter reconstruction and urinary diversion has been disappointing. It is possible that the decellularization processes can alter its (bio) mechanical functionality [33,36,61,62], potentially impairing its use as ureteral graft and ultimately graft failure may relate to these alterations. Reinforcement of decellularized tissue has been performed to improve their biomechanical performance [63,64].

Other graft materials such as PTFE scaffolds showed a structural stiffness and low radial compliance which are known to cause poor long-term patency [47]. Therefore, this type of graft material may not suitable for ureteral reconstruction. To mimic the general (bio)mechanical behavior of soft tubular tissues such as the ureter, Rapoport et al. engineered a hybrid synthetic scaffold of electrospun elastic polyurethane reinforced with a poly-glycolic acid (PGA) woven mesh [65]. The *in vivo* functionality as a tubular genitourinary scaffold remains to be established.

Similar, biodegradable collagen-based hybrid scaffolds have been prepared to improve their overall strength and tissue regeneration [54], but despite these improvements the functional outcome was poor in preclinical studies [51,52,55]. Thus, other design parameters such as fiber arrangement, thickness and degradation profile of the reinforcement may be of importance. Coupled helical coils (CHCs) may be a promising reinforcement design. Through incorporation of “stent-like” CHCs within collagen type I sponges, hybrid scaffolds can be prepared with a ”J”-shaped stress-strain behavior similar to the ureter [66]. Additionally, the hybrid scaffold can resist compressive loads to maintain its tubular form. This may ultimately be beneficial to prevent graft shrinkage, stricture formation and occlusion.

Equally important is the cellular stratum that guides tissue regeneration. The collagen component of hybrid scaffolds can be further tuned with radial oriented pores [67] or an alternating multilayered arrangement of condensed- and porous layers [68]. Both strategies may guide cell alignment and ECM deposition. Alternatively, collagen can also be used in electrospinning to produce smart mixtures: Electrospun spiral poly-L-lactic acid (PLLA) in combination with electrospun collagen was used *in vivo*, showing improved cell attachment and regeneration [69,70].

Regardless of the biomaterial of choice, clinical implementation of grafts requires sterilization with EMA- and FDA- approved techniques. A recent study showed that

the effect of final sterilization of hybrid scaffolds is considerable: Sterilization affects tissue remodeling upon implantation [71]. Thus, the method of sterilization should be carefully considered when designing novel scaffolds.

In summary, combinations of natural- and synthetic biomaterials to form smart hybrid scaffolds combing defined (bio)mechanical properties and a biocompatibility may improve graft patency. However, it is important to realize that grafts will be heavily exposed to urine leading to saturation of scaffolds with urine which contains waste material and its composition is non-physiologic and detrimental to cells. This may explain the poor outcome that has been observed when scaffolds were implanted without cell seeding or bioreactor conditioning. Possibly, luminal coating with biocompatible but urine impenetrable materials may solve part of the complications that are observed leading to satisfactory functional outcome, but this remains to be established. Such luminal coating should still provide a proper surface area to permit urothelium formation acting as a "starter" submucosa guiding urothelial formation preferably at the luminal side.

5.3 Generation of Functionalized Tissue

Seeding of e.g. collagen-based scaffolds with SMCs cells and culturing in a conventional incubator at 37 °C and 5% CO_2 exposure (static conditions) lead to an unorganized SMC alignment within the scaffold architecture which is atypical for native tissue [72]. Improved seeding techniques and culture conditions may be needed to overcome limited SMC ingrowth which is generally observed but is necessary to generate functional neotissue. Culturing of cell-seeded tubular constructs in bioreactor systems may overcome these problems as they provide mechanical cues by means of continuous flow and/or axial stretching (dynamic culturing). In several bioreactor studies implants were created that resembled complex tubular structures consisting of multiple cell types (**Table 3**): bioreactor culture of tubularized cell sheets of dermal fibroblasts seeded with urothelial cells in the lumen resulted in a tubular graft with urothelium lining the luminal surface. The burst pressure of this construct was three times as high as that of porcine urethras and suturing was accomplished without difficulty [73]. Furthermore, a mature stratified- and multilayered urothelium could be generated which ultimately improved barrier function [74]. When primary porcine SMC were embedded in a fibrin gel with a stabilizing PVDF (poly(vinylidene fluoride)) mesh and cultured under dynamic conditions, histological evaluation revealed a native-like cellular alignment in the fibrin gel: smooth muscle cells were circumferentially aligned inside the matrix and longitudinally aligned on the outer surface of the tubular structure

[75]. When cell-laden (primary human SMCs and UCs) compressed tubular collagen scaffolds were stimulated in a flow bioreactor mimicking the physiological pressure, peristalsis, and flow conditions of the human ureter [72] the differentiation of both cell types into their mature forms was observed. Furthermore, smooth muscle cells aligned predominantly perpendicular to the flow direction, comparable to the cell orientation in native ureteral tissue [72]. Wang et al. used ADSCs seeded tubularized PGA scaffolds and differentiated these into SMCs and further conditioned the construct by mechanical extension in a bioreactor [76]. The investigators were able to form neo-muscular tubes and after the addition of primary oral mucosal epithelial and additional stimulation in a bioreactor an epithelial lining similar to native tissue was observed [77]. When these mechanically stimulated constructs were tested in a dog model to treat a full circumferential urethral defect, development into relatively normal architectures resembling nearby autologous urethral tissue was observed.

Additionally, alternative cell sources and bacterial cellulose (BC) as scaffold material has been studied to tissue-engineer a urinary diversion [78]. These scaffolds were seeded with human urine-derived stem cells (UDSC) that were differentiated into UCs and SMCs. After culturing under dynamic conditions (rotary orbital shaker at 10 or 40 rpm) for 1 week, the scaffold surface was covered with multiple layers of SMCs and UCs, and some cells infiltrated into the scaffold. After subcutaneous implantation of the cell-seeded scaffolds in mice, the cells appeared to differentiate and expressed urothelial and SMC markers. Based on these initial promising results, cell-seeded BC scaffolds may hold promise for use as urinary conduits for urinary diversion. Moreover, cell coverage of scaffolds will prevent saturation with passing urine which may alleviate complications.

Buccal mucosa may be another potential source of tissue for reconstruction purposes. Buccal mucosa graft ureteroplasty has been used successfully and this has become a gold standard for urethral reconstruction when feasible, owing to its excellent tissue characteristics for grafting into the urinary tract [79]. However, harvesting of oral mucosa may lead to donor-site morbidity [80]. To overcome this, tissue-engineered oral mucosa grafts have been produced from small buccal mucosa biopsies and found to be safe and efficient in urethroplasty [81]. Thus, tissue-engineered oral mucosa grafts may have a high potential for future long-defect ureter reconstruction and urinary diversion purposes.

It is clear that addition of cells, mechanical stimulation and/or preimplantation of cell-seeded scaffolds are promising strategies for genitourinary TE, but such procedures are very challenging and time-consuming: time that is not available when acute ureteral

defects need to be repaired. However, a percutaneous nephrostomy catheter may be used to drain urine [82] and may allow for a time window until (functional) neotissue is generated. Nevertheless, generation of neotissue should be as fast as possible.

Table 3*:* Studies using dynamic culturing (mechanical stimulation) in a bioreactor system to generate functional tissue for tubular genitourinary tissue reconstruction.

Authors / Year	Scaffold Type	Cell Source	Dynamic Culturing Procedure (Mechanical Stimulation Protocol) / Culturing Time	Cell Orientation	Functional Outcome[1]
1 Magnan, et al.; 2008 [73]	gelatine coating (cell sheet) (T*)	DF + UCs	intraluminal perfusion (continuous flow) / 1 week	ND	BP →, UC-GE ↑
2 Cattan, et al.; 2011 [74]	cell sheets (T*)	DF + UCs	intraluminal perfusion (flow rate: 15 mL/min; shear stress: 0.1 dynes/cm^2 + hydrostatic pressure: 15 cmH_2O) / 2 weeks	stratified-, multilayered U	ECM ↑, BF ↑*, UC-GE ↑*
3 Seifarth, et al.; 2015 [75]	fibrin gel + PVDF mesh (T)	SMCs	mimicking urine bolus via kyphoplasty catheter (1st: inflation of catheter tip, 2nd: pulling through scaffold lumen at a constant unidirectional speed of 2.5 mm/s; 3rd: deflation of catheter tip; 4th: repetition at a frequency of 0.015 Hz) / 2 weeks	scaffold lumen: circumferential + outer scaffold layer: axial	BP ↑, BF →,
4 Vardar, et al.; 2015 [72]	compressed collagen (T)	UCs + SMCs	intraluminal flow mimicking ureter peristalsis (5±1 peristaltic contractions/minute; luminal pressure: ~ 22 cmH_2O; shear stress: ~ 4 dynes/cm^2; R: < 2000) / 2 weeks	SMCs perpendicular to the flow + U lining similar to native	P →, ECM ↑, UC-GE ↑*, SMC-GE ↑*
5 Fu, et al.; 2014 [77]	PGA (T*)	ADSCs -> SMCs + #OMEC/ECs	intraluminal flow (mechanical extension stimulation by peristaltic pump; 75 times/minute; luminal pressure: 0.02 MPa) / 7 weeks	scaffold lumen: ECs scaffold center: SMCs	ECM ↑*, PGA ↓*, SMC-GE ↑*

Scaffold abbreviations: T, seamless tubular form; T*, tubularized form; PVDF, poly vinylidene fluoride; PGA, poly-glycolic acid.
Cell source abbreviations: UCs, urothelial cells; SMCs, smooth muscle cells; DF, dermal fibroblasts; #OMECs, oral mucosa epithelial cells were sorted by flow cytometry to yield ECs, epithelial cells; ->, stem cell differentiation.
Functional outcome ([1]compared to static culturing in a conventional incubator without any mechanical stimulation): ↑, enhancement/increase; ↑*, significant enhancement/increase; ↓*, significant decrease; →, no difference; U, urothelium formation; M, muscle formation; ECM, production/formation of extracellular matrix *de novo*; BP, burst pressure; P, proliferation; BF, barrier function, UC-GE, gene expression of urothelial cells; SMC-GE, gene expression of smooth muscle cells.
ND, not defined; R, Reynolds number; rpm, rounds per minute.

5.4 3D Bioprinting

3D Bioprinting has emerged as a new key technology in TE approaches and may be valuable for ureter reconstruction and urinary diversion. This technology enables the simultaneous printing of cells and biomaterials in precise locations within defined

patient specific dimensions [83,84]. In a recent *in vitro* study, primary UCs and SMCs isolated from a bladder biopsy were printed with fibrin-based hydrogels and with synthetic PCL/PLCL blends as scaffolding (bio)material to form a 3D bioprinted urethra [85]. This study provides a basis to produce tubular constructs with proper mechanical properties and bioactivity within a reasonable time frame. In future studies, 3D bioprinting may be used to create patient (animal model) specific grafts which can be subsequently used for dynamic stimulation, preimplantation and/or direct implantation for genitourinary reconstruction purposes.

5.5 Study Design

In most studies, cell-seeded and/or preimplanted constructs were compared with non-seeded constructs. Remarkably, except in one animal [18], none of the preclinical studies included repair of a defect with the clinical standard - reconstruction with bowel tissue - as control. Thus, it is difficult to assess the value of the tissue-engineered constructs. It would be advisable to implement such controls in preclinical studies to justify the scaffold biomaterial and reconstruction strategy. Moreover, different animal models have been used hampering a solid conclusion. Importantly, the composition of urine differs between species and this may influence the outcome between different animal models as well. In view of the former, the study design of future studies needs to improve to be able to adequately judge the value of a particular TE approach.

In the majority of preclinical studies large animal were studied. A recent systematic review suggested that this appears to allow a better translation to the human situation, within respect to surgical techniques, scaffold dimensions and anatomy [9]. Nevertheless, remodeling kinetics of tissue-engineered constructs may vary: for example, Göttingen minipigs and juvenile German Landrace pigs differ in (cell) growth, and show different regeneration kinetics [86]. Moreover, further research should focus on larger numbers of patients / animals and study endpoints of > 12 months need to be included to confirm the long-term safety of TE approaches.

Finally, in future studies a special focus is needed on the stoma region and skin interaction in relation with the external urinary collecting bag and adhesive materials, an aspect that has received little attention. This may ultimately aid the translation of TE approaches to the clinic as alternative reconstruction procedures.

6 ACKNOWLEDGMENTS

The research leading to these results has received funding from the People Programme (Marie Curie Actions) of the European Union's Seventh Framework Programme FP7/2007-2013/ under REA grant agreement No. 607868 (iTERM).

7 REFERENCES

[1] F.N. Burks, R.A. Santucci, Management of iatrogenic ureteral injury., Ther. Adv. Urol. 6 (2014) 115–24. DOI:10.1177/1756287214526767.

[2] D.J. Summerton, N.D. Kitrey, N. Lumen, E. Serafetinidis, N. Djakovic, European Association of Urology, EAU Guidelines on Iatrogenic Trauma, Eur. Urol. 62 (2012) 628–639. DOI:10.1016/j.eururo.2012.05.058.

[3] A. Martini, D. Villari, G. Nicita, Long-term complications arising from bowel interposition in the urinary tract, Int. J. Surg. 44 (2017) 278–280. DOI:10.1016/j.ijsu.2017.07.030.

[4] T.W. Pike, S. Pandanaboyana, T. Hope-Johnson, L. Hostert, N. Ahmad, Ureteric reconstruction for the management of transplant ureteric stricture: a decade of experience from a single centre., Transpl. Int. 28 (2015) 529–534. DOI:10.1111/tri.12508.

[5] J. Alfred Witjes, T. Lebret, E.M. Compérat, N.C. Cowan, M. De Santis, H.M. Bruins, V. Hernández, E.L. Espinós, J. Dunn, M. Rouanne, Y. Neuzillet, E. Veskimäe, A.G. van der Heijden, G. Gakis, M.J. Ribal, Updated 2016 EAU Guidelines on Muscle-invasive and Metastatic Bladder Cancer, Eur. Urol. 71 (2017) 462–475. DOI:10.1016/j.eururo.2016.06.020.

[6] N.J. Farber, I. Faiena, V. Dombrovskiy, A.L. Tabakin, B. Shinder, R. Patel, S.E. Elsamra, T.L. Jang, E.A. Singer, R.E. Weiss, Disparities in the Use of Continent Urinary Diversions after Radical Cystectomy for Bladder Cancer, Bl. Cancer. 4 (2018) 113–120. DOI:10.3233/BLC-170162.

[7] R.E. Hautmann, S.H. Hautmann, O. Hautmann, Complications associated with urinary diversion, Nat. Rev. Urol. 8 (2011) 667–77. DOI:10.1038/nrurol.2011.147.

[8] R. Langer, J.P. Vacanti, Tissue engineering., Science. 260 (1993) 920–6. DOI: 10.1126/science.8493529.

[9] M. Sloff, R. de Vries, P. Geutjes, J. IntHout, M. Ritskes-Hoitinga, E. Oosterwijk, W. Feitz, Tissue Engineering in Animal Models for Urinary Diversion: A Systematic Review, PLoS One. 9 (2014) e98734. DOI:10.1371/journal.pone.0098734.

[10] C.R. Hooijmans, A. Tillema, M. Leenaars, M. Ritskes-Hoitinga, Enhancing search efficiency by means of a search filter for finding all studies on animal experimentation in PubMed, Lab. Anim. 44 (2010) 170–175. DOI:10.1258/la.2010.009117.

[11] S.J. Hollister, Scaffold design and manufacturing: from concept to clinic., Adv. Mater. 21 (2009) 3330–42. DOI:10.1002/adma.200802977.

[12] F.J. O'Brien, Biomaterials & scaffolds for tissue engineering, Mater. Today. 14 (2011) 88–95. DOI:10.1016/S1369-7021(11)70058-X.

[13] A.L. Shalhav, A.M. Elbahnasy, E. Bercowsky, G. Kovacs, A. Brewer, K.L. Maxwell, E.M. McDougall, R.V. Clayman, Laparoscopic Replacement of Urinary Tract Segments Using Biodegradable Materials in a Large-Animal Model, J. Endourol. 13 (1999) 241–244. DOI:10.1089/end.1999.13.241.

[14] H. Xie, B.S. Shaffer, Y. Wadia, K.W. Gregory, Use of reconstructed small intestine submucosa for urinary tract replacement., ASAIO J. 46 (2000) 268–272. DOI: 10.1097/00002480-200005000-00005

[15] J.S. Jaffe, P.C. Ginsberg, S.J. Yanoshak, L.E.J. Costa, F.N. Ogbolu, C.P. Moyer, C.H. Greene, L.H. Finkelstein, R.C. Harkaway, Ureteral segment replacement using a circumferential small-intestinal submucosa xenogenic graft., J. Invest. Surg. 14 (2001) 259–265. DOI: 10.1080/089419301753170039

[16] M. Sofer, E. Rowe, D.M. Forder, J.D. Denstedt, Ureteral segmental replacement using multilayer porcine small-intestinal submucosa., J. Endourol. 16 (2002) 27–31. DOI:10.1089/089277902753483682.

[17] D.A. Duchene, L. Jacomides, K. Ogan, G. Lindberg, B.D. Johnson, M.S. Pearle, J.A. Cadeddu, Ureteral replacement using small-intestinal submucosa and a collagen inhibitor in a porcine model., J. Endourol. 18 (2004) 507–11. DOI:10.1089/0892779041271472.

[18] A. El-Hakim, R. Marcovich, K.-Y. Chiu, B.R. Lee, A.D. Smith, First prize: ureteral segmental replacement revisited., J. Endourol. 19 (2005) 1069–74. DOI:10.1089/end.2005.19.1069.

[19] A. El-Assmy, A.T. Hafez, M.T. El-Sherbiny, M.A. El-Hamid, T. Mohsen, E.M. Nour, M. Bazeed, Use of Single Layer Small Intestinal Submucosa for Long Segment Ureteral Replacement: A Pilot Study., J. Urol. 171 (2004) 1939–1942. DOI:10.1097/01.ju.0000121437.94629.ef.

[20] T. Drewa, The Artificial Conduit for Urinary Diversion in Rats: A Preliminary Study, Transplant. Proc. 39 (2007) 1647–1651. DOI:10.1016/j.transproceed.2007.02.092.

[21] M. Salehipour, R. Mohammadian, S. Jahanbini, V. Emadmarvasti, B. Geramizadeh, N. Tanideh, Is amniotic membrane a suitable biomaterial for reconstruction of long ureteral defects?, Saudi J. Kidney Dis. Transpl. 24 (2013) 135–8. DOI: 10.4103/1319-2442.106311.

[22] Y. Osman, A. Shokeir, M. Gaber, N. El-Tabey, T. Mohsen, M. El-Baz, Canine ureteral replacement with long acellular matrix tube: is it clinically applicable?, J. Urol. 172 (2004) 1151–1154. DOI:10.1097/01.ju.0000134886.44065.00.

[23] S.E. Dahms, H.J. Piechota, L. Nunes, R. Dahiya, T.F. Lue, E.A. Tanagho, Free ureteral replacement in rats: regeneration of ureteral wall components in the acellular matrix graft., Urology. 50 (1997) 818–825. DOI:10.1016/S0090-4295(97)00391-9.

[24] T. Kloskowski, A. Jundzill, T. Kowalczyk, M. Nowacki, M. Bodnar, A. Marszalek, M. Pokrywczynska, M. Frontczak-Baniewicz, T.A. Kowalewski, P. Chlosta, T. Drewa, Ureter regeneration-the proper scaffold has to be defined., PLoS One. 9 (2014) e106023. DOI:10.1371/journal.pone.0106023.

[25] Z. Zhao, H. Yu, F. Xiao, X. Wang, S. Yang, S. Li, Differentiation of adipose-derived stem cells promotes regeneration of smooth muscle for ureteral tissue engineering, J. Surg. Res. 178 (2012) 55–62. DOI:10.1016/j.jss.2012.01.047.

[26] Z. Zhao, H. Yu, C. Fan, Q. Kong, D. Liu, L. Meng, Differentiate into urothelium and smooth muscle cells from adipose tissue-derived stem cells for ureter reconstruction in a rabbit model., Am. J. Transl. Res. 8 (2016) 3757–3768. ISSN: 1943-8141/AJTR0033794

[27] W. Liao, S. Yang, C. Song, X. Li, Y. Li, Y. Xiong, Construction of Ureteral Grafts by Seeding Bone Marrow Mesenchymal Stem Cells and Smooth Muscle Cells Into Bladder Acellular Matrix, Transplant. Proc. 45 (2013) 730–734. DOI:10.1016/j.transproceed.2012.08.023.

[28] L.-C. Meng, W.-B. Liao, S.-X. Yang, Y.-H. Xiong, C. Song, L.-Q. Liu, Seeding Homologous Adipose-Derived Stem Cells and Bladder Smooth Muscle Cells Into Bladder Submucosa Matrix for Reconstructing the Ureter in a Rabbit Model., Transplant. Proc. 47 (2015) 3002–11. DOI:10.1016/j.transproceed.2015.10.035.

[29] W. Liao, S. Yang, C. Song, Y. Li, L. Meng, X. Li, Y. Xiong, Tissue-engineered tubular graft for urinary diversion after radical cystectomy in rabbits, J. Surg. Res. 182 (2013) 185–191. DOI:10.1016/j.jss.2012.10.024.

[30] L. Meng, W. Liao, S. Yang, Y. Xiong, C. Song, L. Liu, Tissue-engineered tubular substitutions for urinary diversion in a rabbit model., Exp. Biol. Med. (Maywood). 241 (2016) 147–156. DOI:10.1177/1535370215600101.

[31] T. Gilbert, T. Sellaro, S. Badylak, Decellularization of tissues and organs, Biomaterials. 27 (2006) 3675–83. DOI:10.1016/j.biomaterials.2006.02.014.

[32] D.A. Taylor, L.C. Sampaio, Z. Ferdous, A.S. Gobin, L.J. Taite, Decellularized matrices in regenerative medicine, Acta Biomater. 74 (2018) 74–89. DOI:10.1016/j.actbio.2018.04.044.

[33] O. Syed, N.J. Walters, R.M. Day, H.-W. Kim, J.C. Knowles, Evaluation of decellularization protocols for production of tubular small intestine submucosa scaffolds for use in oesophageal tissue engineering, Acta Biomater. 10 (2014) 5043–5054. DOI:10.1016/j.actbio.2014.08.024.

[34] F.C. Yin, Y.C. Fung, Mechanical properties of isolated mammalian ureteral segments., Am. J. Physiol. 221 (1971) 1484–93. DOI: 10.1152/ajplegacy.1971.221.5.1484.

[35] A. Rassoli, M. Shafigh, A. Seddighi, A. Seddighi, H. Daneshparvar, N. Fatouraee, Biaxial mechanical properties of human ureter under tension., Urol. J. 11 (2014) 1678–86. http:// DOI: http://dx.DOI.org/10.22037/uj.v11i3.2472.

[36] C. Derham, H. Yow, J. Ingram, J. Fisher, E. Ingham, S. a Korrosis, S. Homer-Vanniasinkam, Tissue engineering small-diameter vascular grafts: preparation of a biocompatible porcine ureteric scaffold., Tissue Eng. Part A. 14 (2008) 1871–82. DOI:10.1089/ten.tea.2007.0103.

[37] M. Tachibana, G.R. Nagamatsu, J.C. Addonizio, Ureteral replacement using collagen sponge tube grafts., J. Urol. 133 (1985) 866–869. DOI: 10.1016/s0022-5347(17)49268-8.

[38] P.K. de Jonge, V. Simaioforidis, P.J. Geutjes, E. Oosterwijk, W.F. Feitz, Recent advances in ureteral tissue engineering, Curr Urol Rep. 16 (2015) 465. DOI:10.1007/s11934-014-0465-7.

[39] C. Dong, Y. Lv, Application of Collagen Scaffold in Tissue Engineering: Recent Advances and New Perspectives, Polymers (Basel). 8 (2016) 42. DOI:10.3390/polym8020042.

[40] L.H. Olde Damink, P.J. Dijkstra, M.J. van Luyn, P.B. van Wachem, P. Nieuwenhuis, J. Feijen, *In vitro* degradation of dermal sheep collagen cross-linked using a water-soluble carbodiimide., Biomaterials. 17 (1996) 679–84. DOI: https://DOI.org/10.1016/0142-9612(96)86737-8.

[41] L.H. Olde Damink, P.J. Dijkstra, M.J. van Luyn, P.B. van Wachem, P. Nieuwenhuis, J. Feijen, Cross-linking of dermal sheep collagen using a water-soluble carbodiimide., Biomaterials. 17 (1996) 765–73. DOI: https://DOI.org/10.1016/0142-9612(96)81413-X.

[42] M.G. Haugh, C.M. Murphy, R.C. McKiernan, C. Altenbuchner, F.J. O'Brien, Crosslinking and Mechanical Properties Significantly Influence Cell Attachment, Proliferation, and Migration Within Collagen Glycosaminoglycan Scaffolds, Tissue Eng. Part A. 17 (2011) 1201–1208. DOI:10.1089/ten.tea.2010.0590.

[43] S. Varady, E. Friedman, W.T. Yap, A. Lage, J.P. Richie, Ureteral replacement with a new synthetic material: Gore-Tex., J. Urol. 128 (1982) 171–175. DOI: 10.1016/S0022-5347(17)52812-8

[44] E.S. Sabanegh, J.R. Downey, A.L. Sago, Long-segment ureteral replacement with expanded polytetrafluoroethylene grafts., Urology. 48 (1996) 312–6. DOI:10.1016/S0090-4295(96)00185-9.

[45] J.J. Peters, W.B. Shingleton, D. Morgan, B. Allen, J.E.J. Fowler, Neointimized Gore-Tex graft for ureteral prosthesis in the dog., Urology. 48 (1996) 379–382. DOI: 10.1016/s0090-4295(96)00163-x.

[46] S. Baltaci, G. Ozer, E. Ozer, T. Soygür, O. Beşalti, K. Anafarta, Failure of ureteral replacement with Gore-Tex tube grafts., Urology. 51 (1998) 400–3. DOI: 10.1016/S0090-4295(97)00632-8.

[47] C. Singh, C. Wong, X. Wang, Medical Textiles as Vascular Implants and Their Success to Mimic Natural Arteries, J. Funct. Biomater. 6 (2015) 500–525. DOI:10.3390/jfb6030500.

[48] M.L. Muerza-Cascante, D. Haylock, D.W. Hutmacher, P.D. Dalton, Melt electrospinning and its technologization in tissue engineering., Tissue Eng. Part B. Rev. 21 (2015) 187–202. DOI:10.1089/ten.TEB.2014.0347.

[49] X. Wang, L. Zhang, Q. Chen, Y. Hou, Y. Hao, C. Wang, H. Shan, A Nanostructured Degradable Ureteral Stent Fabricated by Electrospinning for Upper Urinary Tract Reconstruction., J. Nanosci. Nanotechnol. 15 (2015) 9899–904. DOI: 10.1166/jnn.2015.10747.

[50] J. Basu, M.J. Jayo, R.M. Ilagan, K.I. Guthrie, N. Sangha, C.W. Genheimer, S.F. Quinlan, R. Payne, T. Knight, E. Rivera, D. Jain, T.A. Bertram, J.W. Ludlow, Regeneration of native-like neo-urinary tissue from nonbladder cell sources., Tissue Eng. Part A. 18 (2012) 1025–34. DOI:10.1089/ten.TEA.2011.0569.

[51] P. de Jonge, V. Simaioforidis, P. Geutjes, E. Oosterwijk, W. Feitz, Ureteral reconstruction with reinforced collagen scaffolds in a porcine model., J. Tissue Eng. Regen. Med. (2016). DOI:10.1002/term.2366.

[52] P.K.J.D. de Jonge, M. Sloff, H.-P. Janke, L.R.M. Versteegden, B.B.M. Kortmann, R.P.E. de Gier, P.J. Geutjes, E. Oosterwijk, W.F.J. Feitz, Ureteral Reconstruction in Goats Using Tissue-Engineered Templates and Subcutaneous Preimplantation., Tissue Eng. Part A. (2017). DOI:10.1089/ten.TEA.2017.0347.

[53] P. Geutjes, L. Roelofs, H. Hoogenkamp, M. Walraven, B. Kortmann, R. de Gier, F. Farag, D. Tiemessen, M. Sloff, E. Oosterwijk, T. van Kuppevelt, W. Daamen, W. Feitz, Tissue engineered tubular construct for urinary diversion in a preclinical porcine model, J Urol. 188 (2012) 653–660. DOI:10.1016/j.juro.2012.03.119.

[54] M. Sloff, V. Simaioforidis, P.J. Geutjes, H.R. Hoogenkamp, T.H. van Kuppevelt, W.F. Daamen, E. Oosterwijk, W.F. Feitz, Novel tubular constructs for urinary diversion: a biocompatibility study in pigs., J. Tissue Eng. Regen. Med. (2016). DOI:10.1002/term.2122.

[55] M. Sloff, V. Simaioforidis, D.M. Tiemessen, H.P. Janke, B.B.M. Kortmann, L.A.J. Roelofs, P.J. Geutjes, E. Oosterwijk, W.F.J. Feitz Prof, Tubular constructs as artificial urinary conduits., J. Urol. (2016). DOI:10.1016/j.juro.2016.04.092.

[56] M.J.W. Koens, P.J. Geutjes, K.A. Faraj, J. Hilborn, W.F. Daamen, T.H. van Kuppevelt, Organ-specific tubular and collagen-based composite scaffolds., Tissue Eng. Part C. Methods. 17 (2011) 327–35. DOI:10.1089/ten.TEC.2010.0269.

[57] 21st Century Cures Act. H.R. 34, 114th Congress. 2016. https://www.gpo.gov/fdsys/pkg/BILLS-114hr34enr/pdf/BILLS-114hr34enr.pdf. Accessed 4th of April 2019.

[58] US Food and Drug Administration - Regulatory Considerations for Human Cells, Tissues, and Cellular and Tissue-Based Products: Minimal Manipulation and Homologous Use. Guidance for Industry and Food and Drug Administration Staff, (n.d.). https://www.fda.gov/downloads/biologicsbloodvaccines/guidancecomplianceregulatoryinformation/guidances/cellularandgenetherapy/ucm585403.pdf. Accessed 4th of April 2019.

[59] Committee for Advanced Therapies (CAT), CAT Scientific Secretariat, C.K. Schneider, P. Salmikangas, B. Jilma, B. Flamion, L.R. Todorova, A. Paphitou, I. Haunerova, T. Maimets, J.-H. Trouvin, E. Flory, A. Tsiftsoglou, B. Sarkadi, K. Gudmundsson, M. O'Donovan, G. Migliaccio, J. Ancāns, R. Maciulaitis, J.-L. Robert, A. Samuel, J.H. Ovelgönne, M. Hystad, A.M. Fal, B.S. Lima, A.S. Moraru, P. Turcáni, R. Zorec, S. Ruiz, L. Akerblom, G. Narayanan, A. Kent, F. Bignami, J.G. Dickson, D. Niederwieser, M.-A. Figuerola-Santos, I.G. Reischl, C. Beuneu, R. Georgiev, M. Vassiliou, A. Pychova, M. Clausen, T. Methuen, S. Lucas, M. Schüssler-Lenz, V. Kokkas, Z. Buzás, N. MacAleenan, M.C. Galli, A. Linē, J. Gulbinovic, G. Berchem, M. Fraczek, M. Menezes-Ferreira, N. Vilceanu, M. Hrubisko, P. Marinko, M. Timón, W. Cheng, G.A. Crosbie, N. Meade, M.L. di Paola, T. VandenDriessche, P. Ljungman, L. D'Apote, O. Oliver-Diaz, I. Büttel, P. Celis, Challenges with advanced therapy medicinal products and how to meet them, Nat. Rev. Drug Discov. 9 (2010) 195–201. DOI:10.1038/nrd3052.

[60] L. Lu, H.M. Arbit, J.L. Herrick, S.G. Segovis, A. Maran, M.J. Yaszemski, Tissue Engineered Constructs: Perspectives on Clinical Translation, Ann. Biomed. Eng. 43 (2015) 796–804. DOI:10.1007/s10439-015-1280-0.

[61] S. Schleifenbaum, T. Prietzel, G. Aust, A. Boldt, S. Fritsch, I. Keil, H. Koch, R. Möbius, H.A. Scheidt, M.F.X. Wagner, N. Hammer, Acellularization-Induced Changes in Tensile Properties Are Organ Specific - An In-Vitro Mechanical and Structural Analysis of Porcine Soft Tissues, PLoS One. 11 (2016) e0151223. DOI:10.1371/journal.pone.0151223.

[62] A. SINGH, D. Lee, H. Jeong, C. Yu, J. Li, C. Fang, P. Sabnekar, X. Liu, T. Yoshida, N. Sopko, T. Bivalacqua, Tissue-engineered Neo-Urinary Conduit from Decellularized Trachea, Tissue Eng. Part A. (2018) ten.TEA.2017.0436. DOI:10.1089/ten.TEA.2017.0436.

[63] W. Gong, D. Lei, S. Li, P. Huang, Q. Qi, Y. Sun, Y. Zhang, Z. Wang, Z. You, X. Ye, Q. Zhao, Hybrid small-diameter vascular grafts: Anti-expansion effect of electrospun poly ε-caprolactone on heparin-coated decellularized matrices., Biomaterials. 76 (2016) 359–70. DOI:10.1016/j.biomaterials.2015.10.066.

[64] C. Johnson, P. Sheshadri, J.M. Ketchum, L.K. Narayanan, P.M. Weinberger, R.A. Shirwaiker, *In vitro* characterization of design and compressive properties of 3D-biofabricated/decellularized hybrid grafts for tracheal tissue engineering, J. Mech. Behav. Biomed. Mater. 59 (2016) 572–585. DOI:10.1016/j.jmbbm.2016.03.024.

[65] H.S. Rapoport, J. Fish, J. Basu, J. Campbell, C. Genheimer, R. Payne, D. Jain, Construction of a tubular scaffold that mimics J-shaped stress/strain mechanics using an innovative electrospinning technique., Tissue Eng. Part C. Methods. 18 (2012) 567–74. DOI:10.1089/ten.TEC.2011.0286.

[66] H.P. Janke, J. Bohlin, R.M.L.M. Lomme, S.M. Mihaila, J. Hilborn, W.F.J. Feitz, E. Oosterwijk, Bioinspired coupled helical coils for soft tissue engineering of tubular structures – Improved mechanical behavior of tubular collagen type I templates, Acta Biomater. 59 (2017) 234–242. DOI:10.1016/j.actbio.2017.06.038.

[67] H.R. Hoogenkamp, M.W. Pot, T.G. Hafmans, D.M. Tiemessen, Y. Sun, E. Oosterwijk, W.F. Feitz, W.F. Daamen, T.H. van Kuppevelt, Scaffolds for whole organ tissue engineering: Construction and *in vitro* evaluation of a seamless, spherical and hollow collagen bladder construct with appendices, Acta Biomater. (2016). DOI:10.1016/j.actbio.2016.07.022.

[68] A. Singh, D. Lee, N. Sopko, H. Matsui, P. Sabnekar, X. Liu, J. Elisseeff, M.P. Schoenberg, K. Pienta, T.J. Bivalacqua, Biomanufacturing Seamless Tubular and Hollow Collagen Scaffolds with Unique Design Features and Biomechanical Properties., Adv. Healthc. Mater. 6 (2017). DOI:10.1002/adhm.201601136.

[69] J.-G. Shi, W.-J. Fu, X.-X. Wang, Y.-D. Xu, G. Li, B.-F. Hong, Y. Wang, Z.-Y. Du, X. Zhang, Tissue engineering of ureteral grafts by seeding urothelial differentiated hADSCs onto biodegradable ureteral scaffolds, J. Biomed. Mater. Res. Part A. 100A (2012) 2612–2622. DOI:10.1002/jbm.a.34182.

[70] W.-J. Fu, Y.-D. Xu, Z.-X. Wang, G. Li, J.-G. Shi, F.-Z. Cui, Y. Zhang, X. Zhang, New ureteral scaffold constructed with composite poly(L-lactic acid)-collagen and urothelial cells by new centrifugal seeding system, J. Biomed. Mater. Res. Part A. 100A (2012) 1725–1733. DOI:10.1002/jbm.a.34134.

[71] M. Sloff, H.P. Janke, P.K.J.D. de Jonge, D.M. Tiemessen, B.B.M. Kortmann, S.M. Mihaila, P.J. Geutjes, W.F.J. Feitz, E. Oosterwijk, The Impact of γ-Irradiation and EtO Degassing on Tissue Remodeling of Collagen-based Hybrid Tubular Templates, ACS Biomater. Sci. Eng. (2018) acsbiomaterials.8b00369. DOI:10.1021/acsbiomaterials.8b00369.

[72] E. Vardar, E.-M. Engelhardt, H.M. Larsson, E. Mouloungui, K. Pinnagoda, J.A. Hubbell, P. Frey, Tubular Compressed Collagen Scaffolds for Ureteral Tissue Engineering in a Flow Bioreactor System., Tissue Eng. Part A. 21 (2015) 2334–45. DOI:10.1089/ten.TEA.2015.0048.

[73] M. Magnan, P. Lévesque, R. Gauvin, J. Dubé, D. Barrieras, A. El-Hakim, S. Bolduc, Tissue Engineering of a Genitourinary Tubular Tissue Graft Resistant to Suturing and High Internal Pressures, Tissue Eng. Part A. 15 (2009) 197–202. DOI:10.1089/ten.tea.2007.0303.

[74] V. Cattan, G. Bernard, A. Rousseau, S. Bouhout, S. Chabaud, F.A. Auger, S. Bolduc, Mechanical Stimuli-induced Urothelial Differentiation in a Human Tissue-engineered Tubular Genitourinary Graft, Eur. Urol. 60 (2011) 1291–1298. DOI:10.1016/j.eururo.2011.05.051.

[75] V. Seifarth, J.O. Grosse, M. Gossmann, H.P. Janke, P. Arndt, S. Koch, M. Epple, G.M. Artmann, A.T. Artmann, Mechanical induction of bi-directional orientation of primary porcine bladder smooth muscle cells in tubular fibrin-poly(vinylidene fluoride) scaffolds for ureteral and urethral repair using cyclic and focal balloon catheter stimulation, J. Biomater. Appl. 32 (2017) 321–330. DOI:10.1177/0885328217723178.

[76] Y. Wang, Q. Fu, R.-Y. Zhao, C.-L. Deng, Muscular tubes of urethra engineered from adipose-derived stem cells and polyglycolic acid mesh in a bioreactor., Biotechnol. Lett. 36 (2014) 1909–1916. DOI:10.1007/s10529-014-1554-x.

[77] Q. Fu, C.-L. Deng, R.-Y. Zhao, Y. Wang, Y. Cao, The effect of mechanical extension stimulation combined with epithelial cell sorting on outcomes of implanted tissue-engineered muscular urethras., Biomaterials. 35 (2014) 105–12. DOI:10.1016/j.biomaterials.2013.09.067.

[78] A. Bodin, S. Bharadwaj, S. Wu, P. Gatenholm, A. Atala, Y. Zhang, Tissue-engineered conduit using urine-derived stem cells seeded bacterial cellulose polymer in urinary reconstruction and diversion, Biomaterials. 31 (2010) 8889–8901. DOI:10.1016/j.biomaterials.2010.07.108.

[79] L.C. Zhao, A.C. Weinberg, Z. Lee, M.J. Ferretti, H.P. Koo, M.J. Metro, D.D. Eun, M.D. Stifelman, Robotic Ureteral Reconstruction Using Buccal Mucosa Grafts: A Multi-institutional Experience, Eur. Urol. 73 (2018) 419–426. DOI:10.1016/j.eururo.2017.11.015.

[80] M.R. Markiewicz, J.L. DeSantis, J.E. Margarone, M.A. Pogrel, S.-K. Chuang, Morbidity associated with oral mucosa harvest for urological reconstruction: an overview., J. Oral Maxillofac. Surg. 66 (2008) 739–44. DOI:10.1016/j.joms.2007.11.023.

[81] G. Ram-Liebig, G. Barbagli, A. Heidenreich, D. Fahlenkamp, G. Romano, U. Rebmann, D. Standhaft, H. van Ahlen, S. Schakaki, U. Balsmeyer, M. Spiegler, H. Knispel, Results of Use of Tissue-Engineered Autologous Oral Mucosa Graft for Urethral Reconstruction: A Multicenter, Prospective, Observational Trial., EBioMedicine. 23 (2017) 185–192. DOI:10.1016/j.ebiom.2017.08.014.

[82] C.S. Ogg, H.M. Saxton, J.S. Cameron, Percutaneous needle nephrostomy., Br. Med. J. 4 (1969) 657–60. DOI: 10.1136/bmj.4.5684.657.

[83] T. Xu, K.W. Binder, M.Z. Albanna, D. Dice, W. Zhao, J.J. Yoo, A. Atala, Hybrid printing of mechanically and biologically improved constructs for cartilage tissue engineering applications, Biofabrication. 5 (2012) 015001. DOI:10.1088/1758-5082/5/1/015001.

[84] H.-W. Kang, S.J. Lee, I.K. Ko, C. Kengla, J.J. Yoo, A. Atala, A 3D bioprinting system to produce human-scale tissue constructs with structural integrity, Nat. Biotechnol. 34 (2016) 312–319. DOI:10.1038/nbt.3413.

[85] K. Zhang, Q. Fu, J. Yoo, X. Chen, P. Chandra, X. Mo, L. Song, A. Atala, W. Zhao, 3D bioprinting of urethra with PCL/PLCL blend and dual autologous cells in fibrin hydrogel: An *in vitro* evaluation of biomimetic mechanical property and cell growth environment, Acta Biomater. 50 (2017) 154–164. DOI:10.1016/j.actbio.2016.12.008.

[86] D. Leonhauser, M. Vogt, R.H. Tolba, J.O. Grosse, Potential in two types of collagen scaffolds for urological tissue engineering applications - Are there differences in growth behaviour of juvenile and adult vesical cells?, J Biomater Appl. 30 (2016) 961–973. DOI:10.1177/0885328215610824.

APPENDIX

Search Strategy PubMed

Search Component 1: Urology (Ureter and Urinary Diversion)

(ureter[MeSH] OR urinary diversion[MeSH] OR ureterostomy[Mesh] OR genitourinary[tiab] OR ureter[tiab] OR ureters[tiab] OR (urinary[tiab] AND diversions[tiab]) OR (urinary[tiab] AND diversion[tiab]) OR (ileal[tiab] AND conduit[tiab]) OR ureterostomy[tiab] OR ureterostomies[tiab] OR ureteral[tiab] OR ureteral reconstruction[tiab] OR ureterotomy[tiab] OR ureterotomies[tiab])

Search Component 2: Scaffold and Tissue Engineering

(tissue scaffolds [MeSH] OR biocompatible materials [MeSH] OR decellularized [tiab] OR acellular [tiab] OR autograft [tiab] OR autografts [tiab] OR graft [tiab] OR grafts [tiab] OR matrix [tiab] OR matrices [tiab] OR biomatrix [tiab] OR biomatrices [tiab] or biomaterial [tiab] OR biomaterials [tiab] OR scaffold [tiab] OR scaffolds [tiab] OR scaffolding [tiab] OR bioengineered substitutes [tiab] OR cell-free [tiab] OR extracellular matrix [tiab] OR conduit [tiab] OR cell constructs [tiab] OR tissue engineering [MeSH] OR tissue culture techniques [MeSH] OR organ culture techniques [MeSH] OR organoids [MeSH] OR guided tissue regeneration [MeSH] OR regenerative medicine [MeSH] OR artificial organs [MeSH] OR biocompatible materials [MeSH] OR (regenerative [tiab] AND (medicine [tiab] OR medicines [tiab])) OR regeneration [tiab] OR regenerated [tiab] OR regenerating [tiab] OR reconstruction [tiab] OR reconstructed [tiab] OR reconstructing [tiab] OR tissue-engineered [tiab] OR (tissue [tiab] AND (engineered [tiab] OR engineering [tiab])) OR bio-engineering [tiab] OR bioengineering [tiab] OR bioengineered [tiab] OR bio-engineered [tiab] OR organoids [tiab] OR organoid [tiab] OR bioartificial [tiab] OR bio-artificial [tiab] OR artificial [tiab])

Search Component 3 ('Animal Filter'):

(adapted from: C.R. Hooijmans, A. Tillema, M. Leenaars, M. Ritskes-Hoitinga, Enhancing search efficiency by means of a search filter for finding all studies on animal experimentation in PubMed, Lab. Anim. 44 (2010) 170–175. DOI:10.1258/la.2010.009117)

("animal experimentation"[MeSH Terms] OR "models, animal"[MeSH Terms] OR "invertebrates"[MeSH Terms] OR "Animals"[Mesh:noexp] OR "animal population groups"[MeSH Terms] OR "chordata"[MeSH Terms:noexp] OR

"chordata, nonvertebrate"[MeSH Terms] OR "vertebrates"[MeSH Terms:noexp] OR "amphibians"[MeSH Terms] OR "birds"[MeSH Terms] OR "fishes"[MeSH Terms] OR "reptiles"[MeSH Terms] OR "mammals"[MeSH Terms:noexp] OR "primates"[MeSH Terms:noexp] OR "artiodactyla"[MeSH Terms] OR "carnivora"[MeSH Terms] OR "cetacea"[MeSH Terms] OR "chiroptera"[MeSH Terms] OR "elephants"[MeSH Terms] OR "hyraxes"[MeSH Terms] OR "insectivora"[MeSH Terms] OR "lagomorpha"[MeSH Terms] OR "marsupialia"[MeSH Terms] OR "monotremata"[MeSH Terms] OR "perissodactyla"[MeSH Terms] OR "rodentia"[MeSH Terms] OR "scandentia"[MeSH Terms] OR "sirenia"[MeSH Terms] OR "xenarthra"[MeSH Terms] OR "haplorhini"[MeSH Terms:noexp] OR "strepsirhini"[MeSH Terms] OR "platyrrhini"[MeSH Terms] OR "tarsii"[MeSH Terms] OR "catarrhini"[MeSH Terms:noexp] OR "cercopithecidae"[MeSH Terms] OR "hylobatidae"[MeSH Terms] OR "hominidae"[MeSH Terms:noexp] OR "gorilla gorilla"[MeSH Terms] OR "pan paniscus"[MeSH Terms] OR "pan troglodytes"[MeSH Terms] OR "pongo pygmaeus"[MeSH Terms]) OR ((animals[tiab] OR animal[tiab] OR mice[Tiab] OR mus[Tiab] OR mouse[Tiab] OR murine[Tiab] OR woodmouse[tiab] OR rats[Tiab] OR rat[Tiab] OR murinae[Tiab] OR muridae[Tiab] OR cottonrat[tiab] OR cottonrats[tiab] OR hamster[tiab] OR hamsters[tiab] OR cricetinae[tiab] OR rodentia[Tiab] OR rodent[Tiab] OR rodents[Tiab] OR pigs[Tiab] OR pig[Tiab] OR swine[tiab] OR swines[tiab] OR piglets[tiab] OR piglet[tiab] OR boar[tiab] OR boars[tiab] OR "sus scrofa"[tiab] OR

ferrets[tiab] OR ferret[tiab] OR polecat[tiab] OR polecats[tiab] OR "mustela putorius"[tiab] OR "guinea pigs"[Tiab] OR "guinea pig"[Tiab] OR cavia[Tiab] OR callithrix[Tiab] OR marmoset[Tiab] OR marmosets[Tiab] OR cebuella[Tiab] OR hapale[Tiab] OR octodon[Tiab] OR chinchilla[Tiab] OR chinchillas[Tiab] OR gerbillinae[Tiab] OR gerbil[Tiab] OR gerbils[Tiab] OR jird[Tiab] OR jirds[Tiab] OR merione[Tiab] OR meriones[Tiab] OR rabbits[Tiab] OR rabbit[Tiab] OR hares[Tiab] OR hare[Tiab] OR diptera[Tiab] OR flies[Tiab] OR fly[Tiab] OR dipteral[Tiab] OR drosophila[Tiab] OR drosophilidae[Tiab] OR cats[Tiab] OR cat[Tiab] OR carus[Tiab] OR felis[Tiab] OR nematoda[Tiab] OR nematode[Tiab] OR nematodes[Tiab] OR sipunculida[Tiab] OR dogs[Tiab] OR dog[Tiab] OR canine[Tiab] OR canines[Tiab] OR canis[Tiab] OR sheep[Tiab] OR sheeps[Tiab] OR mouflon[Tiab] OR mouflons[Tiab] OR ovis[Tiab] OR goats[Tiab] OR goat[Tiab] OR capra[Tiab] OR capras[Tiab] OR rupicapra[Tiab] OR rupicapras[Tiab] OR chamois[Tiab] OR haplorhini[Tiab] OR monkey[Tiab] OR monkeys[Tiab] OR anthropoidea[Tiab] OR anthropoids[Tiab] OR saguinus[Tiab] OR tamarin[Tiab] OR tamarins[Tiab] OR leontopithecus[Tiab] OR hominidae[Tiab] OR ape[Tiab] OR apes[Tiab] OR "pan paniscus"[Tiab] OR

bonobo[Tiab] OR bonobos[Tiab] OR "pan troglodytes"[Tiab] OR gibbon[Tiab] OR gibbons[Tiab] OR siamang[Tiab] OR siamangs[Tiab] OR nomascus[Tiab] OR symphalangus[Tiab] OR chimpanzee[Tiab] OR chimpanzees[Tiab] OR prosimian[Tiab] OR prosimians[Tiab] OR "bush baby"[Tiab] OR bush babies[Tiab] OR galagos[Tiab] OR galago[Tiab] OR pongidae[Tiab] OR gorilla[Tiab] OR gorillas[Tiab] OR "pongo pygmaeus"[Tiab] OR orangutan[Tiab] OR orangutans[Tiab] OR lemur[Tiab] OR lemurs[Tiab] OR lemuridae[Tiab] OR horse[Tiab] OR horses[Tiab] OR equus[Tiab] OR cow[Tiab] OR calf[Tiab] OR bull[Tiab] OR chicken[Tiab] OR chickens[Tiab] OR gallus[Tiab] OR quail[Tiab] OR bird[Tiab] OR birds[Tiab] OR quails[Tiab] OR poultry[Tiab] OR poultries[Tiab] OR fowl[Tiab] OR fowls[Tiab] OR reptile[Tiab] OR reptilia[Tiab] OR reptiles[Tiab] OR snakes[Tiab] OR snake[Tiab] OR lizard[Tiab] OR lizards[Tiab] OR alligator[Tiab] OR alligators[Tiab] OR crocodile[Tiab] OR crocodiles[Tiab] OR turtle[Tiab] OR turtles[Tiab] OR amphibian[Tiab] OR amphibians[Tiab] OR amphibia[Tiab] OR frog[Tiab] OR frogs[Tiab] OR bombina[Tiab] OR salientia[Tiab] OR toad[Tiab] OR toads[Tiab] OR "epidalea calamita"[Tiab] OR salamander[Tiab] OR salamanders[Tiab] OR eel[Tiab] OR eels[Tiab] OR fish[Tiab] OR fishes[Tiab] OR pisces[Tiab] OR catfish[Tiab] OR catfishes[Tiab] OR siluriformes[Tiab] OR arius[Tiab] OR heteropneustes[Tiab] OR sheatfish[Tiab] OR perch[Tiab] OR perches[Tiab] OR percidae[Tiab] OR perca[Tiab] OR trout[Tiab] OR trouts[Tiab] OR char[Tiab] OR chars[Tiab] OR salvelinus[Tiab] OR minnow[Tiab] OR cyprinidae[Tiab] OR carps[Tiab] OR carp[Tiab] OR zebrafish[Tiab] OR zebrafishes[Tiab] OR goldfish[Tiab] OR goldfishes[Tiab] OR guppy[Tiab] OR guppies[Tiab] OR chub[Tiab] OR chubs[Tiab] OR tinca[Tiab] OR barbels[Tiab] OR barbus[Tiab] OR pimephales[Tiab] OR promelas[Tiab] OR "poecilia reticulata"[Tiab] OR mullet[Tiab] OR mullets[Tiab] OR eel[Tiab] OR eels[Tiab] OR seahorse[Tiab] OR seahorses[Tiab] OR mugil curema[Tiab] OR atlantic cod[Tiab] OR shark[Tiab] OR sharks[Tiab] OR catshark[Tiab] OR anguilla[Tiab] OR salmonid[Tiab] OR salmonids[Tiab] OR whitefish[Tiab] OR whitefishes[Tiab] OR salmon[Tiab] OR salmons[Tiab] OR sole[Tiab] OR solea[Tiab] OR lamprey[Tiab] OR lampreys[Tiab] OR pumpkinseed[Tiab] OR sunfish[Tiab] OR sunfishes[Tiab] OR tilapia[Tiab] OR tilapias[Tiab] OR turbot[Tiab] OR turbots[Tiab] OR flatfish[Tiab] OR flatfishes[Tiab] OR sciuridae[Tiab] OR squirrel[Tiab] OR squirrels[Tiab] OR chipmunk[Tiab] OR chipmunks[Tiab] OR suslik[Tiab] OR susliks[Tiab] OR vole[Tiab] OR voles[Tiab] OR lemming[Tiab] OR lemmings[Tiab] OR muskrat[Tiab] OR muskrats[Tiab] OR lemmus[Tiab] OR otter[Tiab] OR otters[Tiab] OR

marten[Tiab] OR martens[Tiab] OR martes[Tiab] OR weasel[Tiab] OR badger[Tiab] OR badgers[Tiab] OR ermine[Tiab] OR mink[Tiab] OR minks[Tiab] OR sable[Tiab] OR sables[Tiab] OR gulo[Tiab] OR gulos[Tiab] OR wolverine[Tiab] OR wolverines[Tiab] OR mustela[Tiab] OR llama[Tiab] OR llamas[Tiab] OR alpaca[Tiab] OR alpacas[Tiab] OR camelid[Tiab] OR camelids[Tiab] OR guanaco[Tiab] OR guanacos[Tiab] OR chiroptera[Tiab] OR chiropteras[Tiab] OR bat[Tiab] OR bats[Tiab] OR fox[Tiab] OR foxes[Tiab] OR iguana[Tiab] OR iguanas[Tiab] OR xenopus laevis[Tiab] OR parakeet[Tiab] OR parakeets[Tiab] OR parrot[Tiab] OR parrots[Tiab] OR donkey[Tiab] OR donkeys[Tiab] OR mule[Tiab] OR mules[Tiab] OR zebra[Tiab] OR zebras[Tiab] OR shrew[Tiab] OR shrews[Tiab] OR bison[Tiab] OR bisons[Tiab] OR buffalo[Tiab] OR buffaloes[Tiab] OR deer[Tiab] OR deers[Tiab] OR bear[Tiab] OR bears[Tiab] OR panda[Tiab] OR pandas[Tiab] OR “wild hog”[Tiab] OR “wild boar”[Tiab] OR fitchew[Tiab] OR fitch[Tiab] OR beaver[Tiab] OR beavers[Tiab] OR jerboa[Tiab] OR jerboas[Tiab] OR capybara[Tiab] OR capybaras[Tiab] OR canine [tiab] OR bovine [tiab] OR porcine [tiab] OR hog [tiab] OR hogs [tiab]) NOT medline[sb])

SC1 + SC2 + SC3= 1290 hits (12th of September 2018)

CHAPTER 3

Bioinspired Coupled Helical Coils for Soft Tissue Engineering of Tubular Structures - Improved Mechanical Behavior of Tubular Collagen Type I Templates

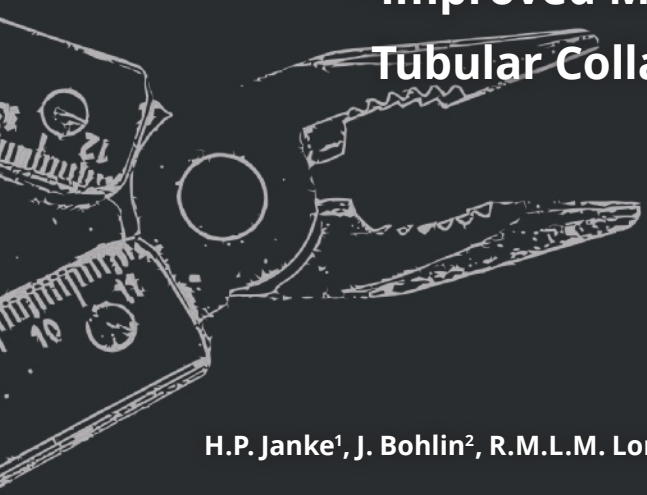

H.P. Janke[1], J. Bohlin[2], R.M.L.M. Lomme[3], S.M. Mihaila[1], J. Hilborn[2], W.F.J. Feitz[1,4] and E. Oosterwijk[1]

[1]: Department of Urology – Experimental Urology, Radboud Institute for Molecular Life Science Radboud University Medical Center, Geert Grooteplein 28, 6525 GE Nijmegen, The Netherlands
[2]: Department of Chemistry - Division of Polymer Chemistry, Ångström Laboratory, A Science for Life, Laboratory Uppsala University, Lägerhyddsvägen 1, 751 21 Uppsala, Sweden
[3]: Department of Surgery, Radboud Institute for Health Science, Radboud University Medical Center, Geert Grooteplein 26, 6525 GE Nijmegen, The Netherlands
[4]: Radboudumc Amalia Children's Hospital, Geert Grooteplein-Zuid 10, 6525GA Nijmegen, The Netherlands

Acta Biomater. 2017 Sep 1;59:234-242
DOI:10.1016/j.actbio.2017.06.038

ABSTRACT

The design of constructs for tubular tissue engineering is challenging. Most biomaterials need to be reinforced with supporting structures such as knittings, meshes or electrospun material to comply with the mechanical demands of native tissues. In this study, coupled helical coils (CHCs) were manufactured to mimic collagen fiber orientation as found in nature. Monofilaments of different commercially available biodegradable polymers were wound and subsequently fused, resulting in right-handed and left-handed polymer helices fused together in joints where the filaments cross. CHCs of different polymer composition were tested to determine the tensile strength, strain recovery, hysteresis, compressive strength and degradation of CHCs of different composition. Subsequently, seamless and stable hybrid constructs consisting of PDSII® USP 2-0 CHCs embedded in porous collagen type I were produced. Compared to collagen alone, this hybrid showed superior strain recovery (93.5 ± 0.9% vs 71.1 ± 12.6% in longitudinal direction; 87.1 ± 6.6% vs 57.2 ± 4.6% in circumferential direction) and hysteresis (18.9 ± 2.7% vs 51.1 ± 12.0% in longitudinal direction; 11.5 ± 4.6% vs 46.3 ± 6.3% in circumferential direction). Furthermore, this hybrid construct showed an improved Young's Modulus in both longitudinal 0.5 ± 0.1 MPa vs 0.2 ± 0.1 MPa; 2.5-fold) and circumferential 1.65 ± 0.07 MPa vs (2.9 ± 0.3) x 10^{-2} MPa; 57-fold) direction, respectively, compared to templates created from collagen alone. Moreover, hybrid template characteristics could be modified by changing the CHC composition and CHCs were produced showing a mechanical behavior similar to the native ureter. CHC-enforced templates, which are easily tunable to meet different demands may be promising for tubular tissue engineering.

1 INTRODUCTION

The design of an ideal template in Tissue Engineering and Regenerative Medicine (TERM) is defined to be able to keep its form to fill the defect, should be readily implantable, enhance tissue regeneration, and should be able to support tissue-specific functional demands including (bio)mechanical loads [1]. Especially in tubular Tissue Engineering (TE), construct strength as well as elasticity are pivotal parameters to guarantee functionality of a construct to avoid compliance mismatch, which can result in failure of the graft [2,3]. Additionally, the template should be able to withstand external mechanical loads initially as well as degrade and resorb progressively as it is being replaced by new tissue [4,5]. Tubular templates have been produced by (melt) electrospinning [6], casting of extracellular matrix-based biomaterials [7], cell sheets [8] or decellularized tissues [9]. In general, the mechanical strength of these templates may be limited and reinforcement with e.g. tubularized woven or non-woven meshes, knittings or electrospun material is needed to provide sufficient strength and, ideally, comply with the (bio)mechanical requirements of native tissue [10–14].

The stress-strain behavior of native soft tubular tissue is reported as a "J-shaped" curve beginning with an initial high elasticity followed by sharp strain-induced stiffening prior rupture [15]. The amount and orientation of structural extracellular matrix proteins such as elastin and collagen significantly impact the mechanical behavior [16]. Thus, an engineered template with a fiber arrangement like native tissue may be a valuable approach as previously suggested [17].

Within the intimal- and adventitial layer of the aorta and healthy arteries, collagen fibers are helically arranged to coupled helical coils (CHCs) -also known as a cross-ply structure-. Such collagen fiber arrangement is also observed within the submucosa of tubular organs like the ureter, the esophagus and small intestine [18–21]. To comply with (bio)mechanical demands of various tubular organs, incorporation of tunable synthetic CHCs may be a beneficial design for tubular template engineering [22].

In this research report, we created bioinspired CHCs prepared of different commercially available, resorbable surgical suture monofilaments and studied their mechanical properties. Porcine ureteral tissue was used as an example of native tubular tissue for comparison, to evaluate their potential for tubular TE purposes. The most promising CHC was incorporated in a tubular collagen type I sponge to test the mechanical performance of this biocompatible, but structurally weak, template.

2 MATERIALS AND METHODS

2.1 Materials

Resorbable surgical suture monofilaments used were: Monocryl® (poly(glycolide-co-ε-caprolactone) (PGCL), Ethicon, LLC, Sommerville, NJ, USA), PDSII® (poly(p-dioxanone) (PDS), Ethicon, LLC, Sommerville, NJ, USA) and Caprolon® (poly(L-lactide-co-ε-caprolactone) (PLCL), Resorba Medical GmbH, Nuremberg, Germany). Filament size was USP 2-0 (0.255 – 0.299 mm) and USP 1 (0.400 – 0.499 mm). Unless otherwise indicated, reagents were purchased from Sigma-Aldrich (St. Louis, MO, USA). Ureteral tissue from Landrace pigs (100 kg; 6 months old) was obtained from the local slaughterhouse < 4 h after slaughter.

2.2 Preparation of Coupled Helical Coils

Figure 1A-B shows the manufacturing procedure of coupled helical coils (CHCs). Monofilaments were wound on a custom-made steel mandrel with a diameter of 8 mm connected to a rotator (Labinco, Breda, The Netherlands). Filaments were wrapped around the mandrel in a clockwise- and anticlockwise helix (approximately 11 rpm), resulting in tubular structures with a defined rhombus pattern (**Figure 1C**; distance between filaments = 5 mm). Filament intersection points were fused in a laboratory oven (UT6, Thermo, Langenselbold, Germany) at defined temperature for 5 min. Temperatures used were 120 °C for PDSII® CHCs, 175 °C for Caprolon® CHCs and 200 °C for Monocryl CHCs, respectively. The filament thickness and the thickness at the filament intersection points in longitudinal (LONG) and circular (CIRC) direction were measured with a digital caliper (Kraftfixx, Stuhr, Germany). Mesh pore size, mesh angle in LONG and CIRC direction, as well as the surface area at the filament intersection points, were examined using ImageJ (U.S. National Institutes of Health, Bethesda, Maryland, USA).

2.3 Preparation of a Collagen Template Reinforced with a Coupled Helical Coil

Tubular collagen type I templates were prepared as previous described with slight modifications [11,23]. Highly purified collagen type I from bovine Achilles tendon (Collagen Solutions, Glasgow, Scotland, United Kingdom) was swollen in 0.25 M acetic acid overnight followed by homogenization using a Silverson L5M-A laboratory mixer (Silverson, Chesham, United Kingdom) and de-airing by centrifugation (800 rpm for 30 min) to obtain a 0.7% (w/v) solution. The collagen solution was poured in a polystyrene

mold and a steel mandrel (6 mm in diameter) was placed in the middle of the mold to form a tubular template made of a collagen alone (COL). To form a hybrid tubular template (hybrid), a CHC of PDSII® USP 2-0 was placed between the steel mandrel and polystyrene wall (Figure 1E). Samples were frozen down at -20 °C for at least 24 h. After the freezing procedure, samples were lyophilized (Zirbus Sublimator 500II, Bad Grund, Germany) and subsequently chemically crosslinked with 33 mM N-ethyl-3-(3-dimethylaminopropyl)-carbodiimide (EDC) and 6 mM N-hydroxysuccinimide (NHS) to enhance strength and resistance against degradation of collagen [24–26]. In brief, templates were transferred to 50 mM 2-morpholineoethane sulphonic acid (MES buffer; pH 5.0) containing 40% (v/v) ethanol. Templates were incubated for a total of 4 h to EDC/NHS dissolved in MES buffer. Crosslinking reaction was stopped by 2 times washing with 0.1 M Na_2HPO_4 for 1 h. Subsequently, templates were washed using 1M NaCl, 2M NaCl and demineralized water. Finally, templates were stored in 70% (v/v) ethanol at -20 °C until further use.

2.4 Scanning Electron Microscopy (SEM)

SEM was used to analyze filament structure, filament intersection points after production and during degradation and integration of CHC in tubular collagen type I sponges. Examination was performed with a JEOL SEM 6310 apparatus (JEOL Ltd., Japan) operating at an accelerating voltage of 15 kV. Prior SEM analyses, samples were fixed on a stub with double-sided carbon tape and sputtered with gold for 60 seconds (1.5 kV; 20 mA) by a Scancoat Six SEM Sputter Coater (Temescal/Edwards, Crawley, United Kingdom) to achieve an ultrathin gold layer (approximately 20.4 nm) before being analyzed.

2.5 Mechanical Properties

2.5.1 Tensile Tests

To investigate the mechanical properties of suture monofilaments and various tubular templates, test specimen of l = 25 mm of suture monofilaments (n = 3), CHCs alone (n = 5), COL (n = 3), hybrid (n = 5) and porcine ureter (n = 5) were mounted to a tensile tester (Z2.5 TN, Zwick/Roell, Ulm, Germany) via plastic hose clamps. Load cells used were 20 N (CHCs; COL; hybrid) and 2.5 kN (suture monofilaments; porcine ureter), respectively. All ring specimen were hydrated in phosphate buffered saline (PBS; 0.01 M; pH 7.4) prior mounting. With a crosshead speed of 50 mm/min, a uniaxial load was applied in a longitudinal direction until rupture of the construct (gauge length constructs = 10 mm). Construct testing were valid when the

sample broke in the middle. Force-displacement data were normalized to the test specimen dimensions to compute a stress-strain curve. The stress was expressed as the recorded force F [N] which reacted on the cross-sectional area A [mm2] of the test specimen, while the strain was expressed as the change in length delta L [mm] divided by its original length L0 [mm]. Material parameters were derived as previously described [12,27]: (1) Initial modulus (E1) was calculated from the first slope (toe region) of the computed stress-strain curve. (2) Upswing (Young´s) modulus (E2) was calculated from the slope (upswing region) of the computed stress-strain curve. (3) Ultimate tensile strength (UTS) and (4) failure strain were defined as the maximum stress and maximum strain, respectively in the stress-strain curve before failure of the construct.

Subsequently, ring specimen (l = 10 mm; n = 3) of COL and hybrid templates were also stretched in the circumferential direction. Therefore, test specimen were mounted between custom-made hooks (hook-to-hook distance = 6 mm) and stretched until total failure of the construct. Test machine and material parameter were derived and used as described above.

2.5.2 Cyclic Stretching

To investigate strain recovery and energy loss, CHCs (l = 65 mm; diameter = 8 mm; n = 5) were loaded in the tensile tester as described above (load cell = 20 N; cross head speed = 50 mm/min) and stretched longitudinally to identify the most appropriate CHC. Constructs were stretched ten times up to 15% of their original length. Strain recovery was calculated as previously described [28,29]. In brief, Strain recovery was defined as the difference in applied strain and the resulting strain after 10 cycles divided by the applied strain. Materials´ loss in energy uptake during unloading (hysteresis) was expressed as the percentage area under the loaded- and unloaded curve divided by the area under the loading curve using ImageJ.

Subsequently, measurements were also performed on COL and hybrid in longitudinal (stretching 10 times up to 15% of their original length) and circumferential (stretching ten times up to 50% of their original length) direction, respectively. Measurements were performed in triplicate.

2.5.3 Compression Test

To study the behavior of CHCs under compressive loads, 20 mm long specimens (n = 5) were placed between 2 plates. A strain rate of 50 mm/min was applied until the test specimen was compressed to 50% of the constructs' original diameter.

A compressive load was retained for 15 sec and released until the construct had regained the original diameter. Recorded compressive loads (load cell = 2.5 kN) were normalized and expressed in megapascal [MPa]. Compressive stress over time and compressive stress-strain curves were recorded and the compressive modulus was determined from the slope of the compressive stress-strain curve. The percentage remaining compressive strength was calculated as the difference in peak compressive stress at 50% strain and stress after retention for 15 sec.

Subsequently, the hybrid (l = 10 mm; n = 4) were compressed to 50% of the constructs' original diameter. Compressive modulus for the hybrid template was derived from the slope between 25% and 45% strain to neglect initial compressive strength caused by collagen (**Appendix A4**).

2.6 Degradation Test

To test long-term stability of all produced CHCs, ring specimen (l = 20 mm; n= 5) of CHCs were incubated in an enzymatic degradation solution as previous described with modifications [30]. In brief, to phosphate buffered saline (PBS; 0.01 M; pH 7.4), 244 U/L α-amylase from Bacillus sp., 24 ng/mL collagenase, 13 mg/L lysozyme, 190 U/mL lipase, 2.6 U/mL hyaluronidase, 10.8 mg/L phospholipase A2 and 0.2 g/L sodium azide were added. Samples were immersed in this solution (10 mL per CHC) and kept in a cell culture incubator under standard cell culture conditions (37 °C; 5% CO_2). Samples were collected at day 0, 3, 6, 10 and 18 for weight measurement (dry weight) and compression test as described above. Calculated strength degradation curve was expressed as the peak compressive stress over time. Calculated mass loss of CHCs was expressed as relative loss of samples initial dry weight over time (weight loss % = (initial dry weight before degradation – dry weight after degradation) / initial dry weight before degradation x 100%).

2.7 Statistics

All values are expressed as means ± standard deviation. Minimum requirement for independent assays was n = 3. One-way ANOVA with Bonferroni post-hoc test was performed for statistical analysis of differences between different CHCs and CHCs compared with native porcine ureteral tissue. If COL templates were compared with hybrid templates, unpaired two-tailed Student's t-tests were performed. $P < 0.05$ was considered statistically significant. All statistical calculations were performed using GraphPad Prism software (version 5.03 and 7.04 respectively, GraphPad Software Inc, La Jolla, CA, USA).

3 RESULTS

3.1 Coupled Helical Coil- and Hybrid Dimensions

The diameters of the resorbable surgical suture monofilaments were 0.29 ± 0.01 mm and 0.47 ± 0.01 mm for USP 2-0 and USP 1 filaments, respectively. The distance from one intersection point to the next in longitudinal (LONG) direction after fusing was approximately 5 mm, while the distance in circular (CIRC) direction was approximately 8 mm. The mesh pore sizes of CHC were as follows: PDSII® USP 2-0: 19.2 ± 2.2 mm^2; PDSII® USP 1: 19.3 ± 1.2 mm^2, Monocryl® USP 2-0: 18.6 ± 2.4 mm^2; Monocryl® USP 1: 18.6 ± 1.3 mm^2; Caprolon® USP 2-0: 18.3 ± 3.4 mm^2 and Caprolon® USP 1: 20.8 ± 1.8 mm^2 respectively. The difference in the pore size between CHC was not significant ($p > 0.999$). The LONG angle and CIRC angle of different constructs were similar ($p > 0.999$) underscoring the control of CHC manufacture.

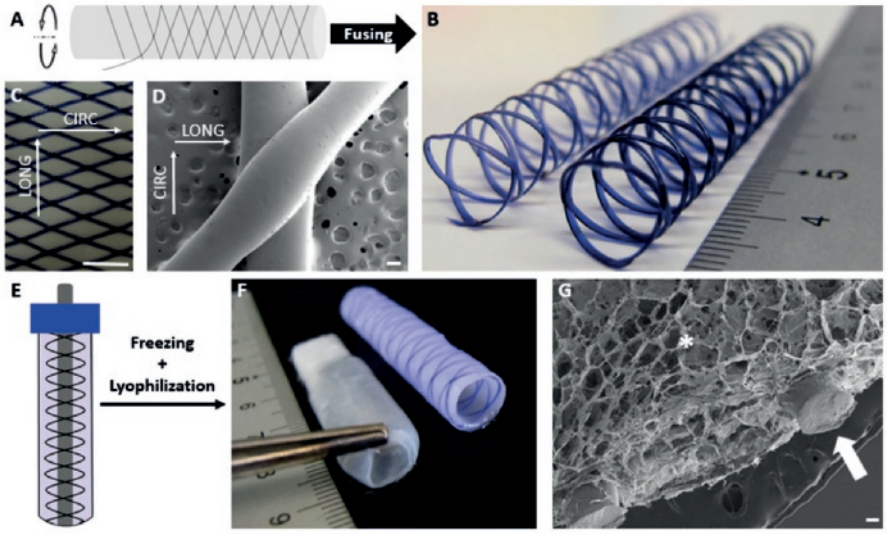

Figure 1: Preparation of coupled helical coils (CHCs) and production of a hybrid tubular template. (A) Schematic illustration of the production procedure. CHCs are manufactured by winding suture monofilaments around a steel mandrel in a clockwise- and anticlockwise helix and fusing in a laboratory oven. (B) CHCs with a crosswise/rhombus pattern. Left coil: Monocryl® USP 2-0 CHC. Right coil: Monocryl® USP 1 CHC. (C) Macroscopic image of the crosswise/rhombus pattern (scale bar = 5 mm. (D) Scanning electron microscopy (SEM) image of the filament intersection points fused together in joints (scale bar = 100 micron). (E) Production of a hybrid tubular template. Casting of collagen type I suspension in a polystyrene mold containing a steel mandrel (diameter = 6 mm) and CHC. After freezing and subsequent lyophilization, a hybrid tubular template is formed. (F) Tubular collagen type I template (COL, left) and hybrid tubular template (hybrid, right). The hybrid maintained its tubular structure with an open lumen, while COL collapsed when wetted. (G) SEM image of the hybrid. The CHC was well integrated in the collagen template (see white arrow) without influencing the luminal site (indicated by the asterisks; scale bar = 100 micron).

Fusing of CHCs resulted in a decrease of the filament's original diameter (**Appendix A1**). The filaments were flattened, and the filament thickness decreased to approximately 50% of the original diameter. Filament thickness outside the intersection points differed substantially from the thickness at the intersection points in all constructs. Intersections of USP 2-0 CHCs and Monocryl® USP 1 CHC (**Figure 1D**) showed joint-like structures with a smaller surface area, and consequently showed a more flexible behavior (more compliant) in the axial direction as compared to PDSII® USP 1- and Caprolon® USP 1 CHC. Overall, CHC production process resulted in seamless tubular structured with structural anisotropy.

Collagen type I (0.7%(w/v)) reinforced with a PDSII® USP 2-0 CHC (hybrid) resulted in a stable tubular template (**Figure 1F**). The CHC was well integrated in the typical porous honeycomb-like collagen scaffold structure (**Figure 1G**).

3.2 Mechanical Properties

3.2.1 Tensile Tests

For suture monofilaments, a linear stress-strain curve was obtained until the filaments ruptured. Young's modulus of suture monofilaments was as follows: PDSII® USP 2-0: (1.26 ± 0.08) x 10^3 MPa; PDSII® USP 1: (1.4 ± 0.4) x 10^3 MPa; Monocryl® USP 2-0: (1.1 ± 0.6) x 10^3 MPa; Monocryl® USP 1: (0.9 ± 0.4) x 10^3 MPa; Caprolon® USP 2-0: (1.4 ± 0.6) x 10^3 MPa and Caprolon® USP 1: (1.2 ± 0.3) x 10^3 MPa, respectively. Differences in Young's modulus between all suture monofilaments were not significant ($p > 0.05$).

The results of the tensile tests of coupled helical coils (CHCs) and porcine ureter along the longitudinal axis are shown in **Figure 2**. Porcine ureter and CHCs made of USP 2-0 fibers showed a typical ''J'' shaped stress-strain curve with an initial high elasticity (toe region) followed by an uprising slope indicative of a significant ($p < 0.05$) stiffness before total failure, while Monocryl® USP 2-0 underwent plastic deformation prior rupture (see plateau phase of Monocryl® CHCs in **Figure 2A**). In all Caprolon® constructs, also plastic deformation beyond the initial toe region was observed indicating strain hardening of the material. Consequently, Caprolon® constructs showed a limited strain range in reversible elasticity compared to all other constructs. For PDSII® USP 1- and Monocryl® USP 1 CHC, a linear curve was obtained until the construct ruptured. Regardless of CHC composition, all constructs ruptured at their filament intersection points. Furthermore, the upswing (Young`s) modulus E2 in both constructs differed from native tissue. Ultimate tensile strength (UTS), failure strain was highest for Monocryl® USP 2-0 CHCs. No significant differences (p

= 0.1810 for E1; p = 0.1230 for E2; p = 0.0568 for UTS; p > 0.9999 for failure strain) of PDSII® USP 2-0 CHCs were found when compared with porcine ureter.

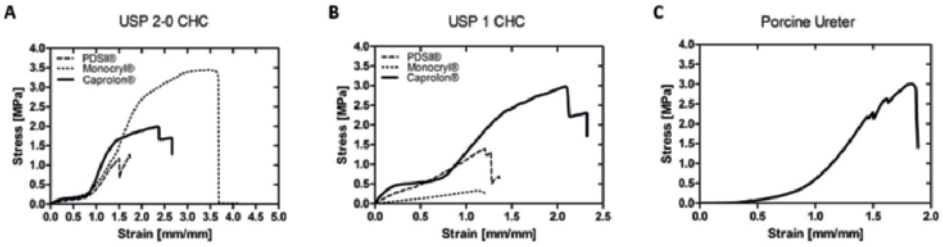

D

	Initial Modulus E1; (MPa)	*Upswing (Young`s) Modulus E2; (MPa)*	*Ultimate Tensile Strength UTS; (MPa)*	*Failure Strain (mm/mm)*
USP2-0 CHCs				
PDSII® CHC	0.3 ± 0.2	2.4 ± 0.9	1.19 ± 0.08	1.1 ± 0.3
Monocryl® CHC	0.35 ± 0.07	2.6 ± 0.4	4.3 ± 0.7**	7.1 ± 3.2***
Caprolon® CHC	0.5 ± 0.2	2.2 ± 0.7	1.6 ± 0.4	2.2 ± 0.5*
USP1 CHCs				
PDSII® CHC	-	1.1 ± 0.4**	1.1 ± 0.3	0.9 ± 0.3
Monocryl® CHC	-	0.34 ± 0.08***	0.5 ± 0.3**	1.02 ± 0.06
Caprolon® CHC	-	2.6 ± 0.6	3.0 ± 0.3	2.1 ± 0.3*
Porcine Ureter	0.6 ± 0.4	4.8 ± 3.0	2.3 ± 1.4	1.1 ± 0.6

Figure 2: Mechanical analysis of CHCs and porcine ureter in longitudinal direction. (A) Representative stress-strain curves of CHCs prepared from USP 2-0 suture monofilaments. (B) Representative stress-strain curves of CHCs prepared from USP 1 suture monofilaments. (C) Representative stress-strain curves of porcine ureteral tissue. (D) Mechanical properties derived from stress-strain curves in longitudinal direction of CHCs and native porcine ureteral tissue. Data represent mean ± standard deviation. One-way ANOVA with Bonferroni post-hoc test, *= $p < 0.05$ compared to ureteral tissue, **= $p < 0.01$ compared to ureteral tissue, ***= $p < 0.0001$ compared to ureteral tissue.

The results of the tensile tests of COL- and hybrid template along both, longitudinal and circumferential axis are shown in **Figure 3**. Like native tissue, stress-strain behavior of COL templates and hybrids were "J"-shaped in longitudinal- and circumferential direction, respectively (**Appendix A2A** and **Appendix A2B**). In the longitudinal direction, the collagen reinforced with a CHC made of PDSII® USP 2-0 showed a significant improvement ($p < 0.05$) in strength compared to the COL template. Initial modulus E1 were (1.8 ± 0.6) x 10^{-2} MPa and 0.12 ± 0.06 MPa for the COL template and the hybrid template, respectively. The upswing (Young`s) modulus E2 were 0.2 ± 0.1 MPa and 0.5 ± 0.1 MPa for the COL template and the hybrid template, respectively. Ultimate tensile strength and corresponding failure strain of the hybrid were dictated by the collagen component of the hybrid; the CHC remained intact. No significant differences of failure in ultimate tensile strength ($p = 0.4947$) and failure strain ($p = 0.1049$) of the hybrid were observed compared to COL (**Figure 3B**).

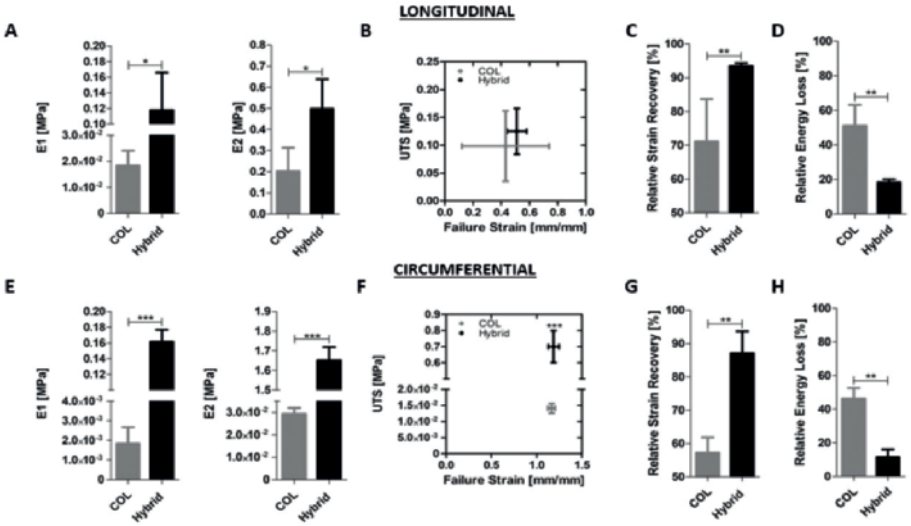

Figure 3: Mechanical properties and subsequent analysis under cyclic loads of collagen type I templates (COL) and collagen type I templates reinforced with a PDSII® 2-0 CHC (hybrid). (A) Analysis of initial elastic modulus (E1) and upswing (Young's) modulus (E2) of COL and hybrid in longitudinal direction. (B) Analysis of ultimate tensile strength (UTS) and failure strain of COL and hybrid in longitudinal direction. (C) Relative strain recovery of COL and hybrid after 10 loading cycles in longitudinal direction. (D) Relative energy loss after unloading of COL and hybrid after 10 loading cycles in longitudinal direction. (E) Initial modulus (E1) and upswing (Young's) modulus (E2) of COL and hybrid in circumferential direction. (F) Analysis of ultimate tensile strength (UTS) and failure strain of COL and hybrid in circumferential direction. (G) Relative strain recovery of COL and hybrid after 10 loading cycles in circumferential direction. (H) Relative energy loss after unloading of COL and hybrid after 10 loading cycles in circumferential direction. Data represent mean ± standard deviation. Two-tailed Student's t-test, *= $p < 0.05$, **= $p < 0.01$, ***= $p < 0.0001$.

Furthermore, the formed hybrid showed a significantly ($p < 0.0001$) superior strength in the circumferential direction as compared to the COL template. In the circumferential direction, Initial modulus E1 were (1.8 ± 0.8) x 10^{-3} MPa and 0.16 ± 0.02 MPa for the COL template and the hybrid template, respectively. The upswing (Young`s) modulus E2 were (2.9 ± 0.3) x 10^{-2} MPa and 1.65 ± 0.07 MPa for the collagen template and the hybrid template, respectively. The ultimate tensile strength (UTS) and corresponding failure strain of the hybrid were dictated by the CHC. The hybrid ruptured at the CHC component of the construct. No distortion of the collagen before rupture of CHC was observed. Additionally, the UTS of hybrid templates was significantly higher ($p < 0.0001$) than COL. No significant differences ($p = 0.6103$) in failure strain of the hybrid were observed compared to COL (**Figure 3F**).

3.2.2 Cyclic Stretching

Strain recovery of Monocryl®- and PDSII® CHCs from longitudinal cyclic loading was significantly ($p < 0.0001$) better than the recovery of CHCs produced from Caprolon® (**Appendix A3A**). Subsequently, analysis of construct energy loss during unloading/relaxation showed the smallest hysteresis loop for PDSII® USP 2-0 CHC, and thus lowest loss of energy during relaxation compared to other constructs (8.3 ± 1.0% loss of energy; **Appendix A3B**). As can be seen in **Figure 3C** and **Figure 3G**, strain recovery (93.5 ± 0.9% in the longitudinal direction; 87.1 ± 6.6% in the circumferential direction) of the hybrid were significantly ($p < 0.01$) improved as compared to COL (71.1 ± 12.6% in the longitudinal direction; 57.2 ± 4.6% in the circumferential direction). Additionally, reinforcement of collagen with PDSII® USP 2-0 CHC resulted in a significantly ($p < 0.01$) smaller hysteresis (18.9 ± 2.7% and 11.5 ± 4.6%) as compared with COL (51.1 ± 12.0% and 46.3 ± 6.3%) in longitudinal- and circumferential direction, respectively (**Figure 3D** and **Figure 3H**).

3.2.3 Compression Tests

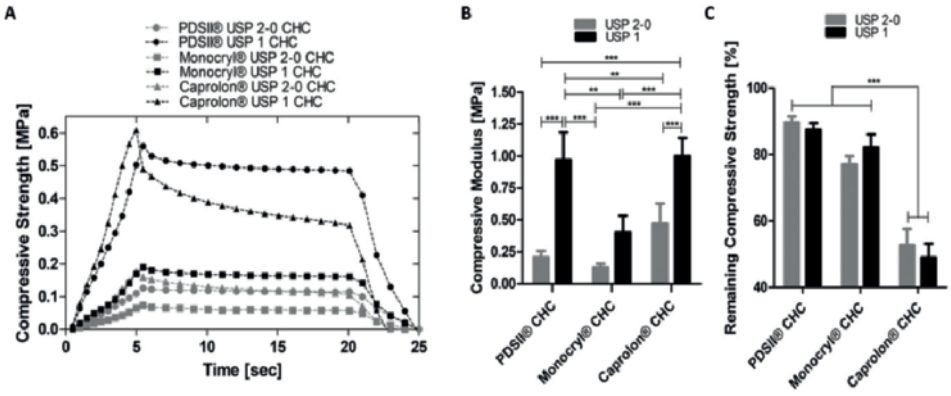

Figure 4: Analysis of the behavior of coupled helical coils (CHCs) under compressive loads. (A) Representative graph of resulting compressive strength over time of different CHCs. (B) Quantitative evaluation of the compressive modulus of different CHCs. (C) Quantitative evaluation of the remaining compressive strength after holding the compressive load for 15 seconds. Data represent mean ± standard deviation. One-way ANOVA with Bonferroni post-hoc test, **= $p < 0.01$, ***= $p < 0.0001$.

Compression tests demonstrated that all prepared CHCs resisted compressive loads (**Figure 4A**). Individual compressive moduli are shown in **Figure 4B**. The compressive modulus increased with increased filament dimensions. PDSII® and Caprolon® in the dimension USP 1 showed the highest compressive strength compared to other

constructs. When the applied pressure was maintained for 15 seconds, a decrease of the peak compressive stress was observed for all constructs (see plateau phase or drop of strength, respectively in **Figure 4A**). The remaining compressive load normalized to the initial compressive load for PDSII® was 89.7 ± 1.8% and 87.5 ± 2.0% for USP 2-0 and USP 1 constructs, respectively. The loss of compressive strength of PDSII®- and Monocryl® CHCs were lower expressed compared with Caprolon® CHCs (**Figure 4C**).

The hybrid template of collagen type I and CHC resulted in a seamless tubular structure in which an open lumen was maintained, while tubular structures made from collagen type I only collapsed when wetted (**Figure 1F**). Hybrid templates kept an open lumen when compressed up to 50% of the original diameter (**Appendix A4A**). The hybrid structure remained intact when compressed. When unloaded, the hybrid structure resumed its original dimensions (**Appendix A4B**). Compressive stress-strain behavior was also "J"-shaped indicating that the initial compressive load was carried by the collagen type I only. After approximately 10% strain, the compressive load was carried by the CHC. The compressive modulus of the hybrid was $(3.8 \pm 0.7) \times 10^{-2}$ MPa.

3.2.4 Degradation

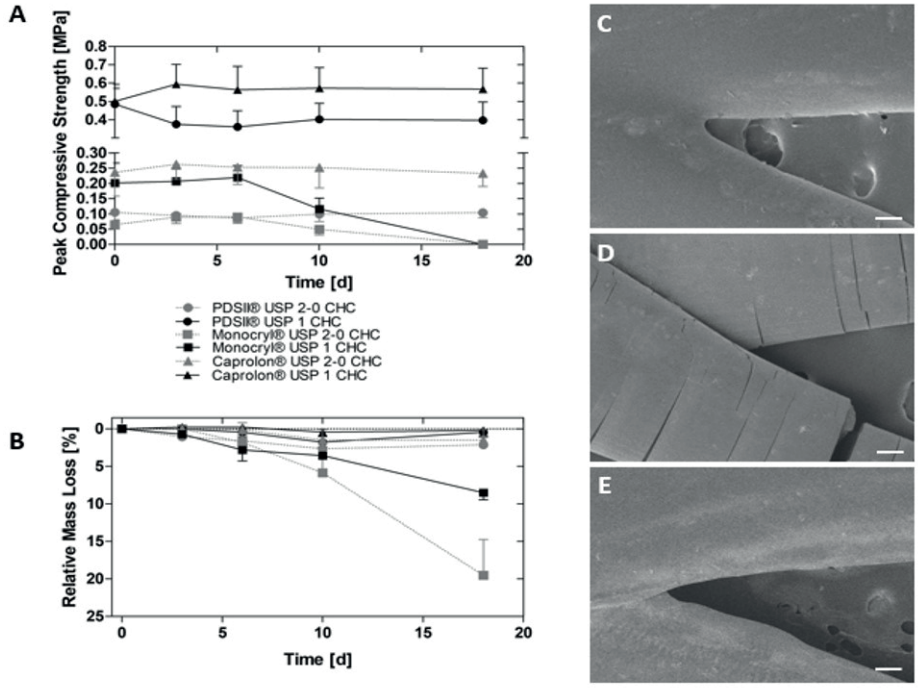

Figure 5: Degradation study of prepared coupled helical coils (CHCs). (A) Peak compressive strength of CHCs over time. (B) Relative mass loss of CHCs over time. Representative scanning electron microscopy (SEM) images at the intersection points of (B) PDSII® USP 1 CHC, (C) Monocryl® USP 1 CHC and (D) Caprolon® USP 1 CHC at day 12. Scale bar = 100 micron.

The degradation of CHCs was investigated concerning the loss of peak compressive strength (**Figure 5A**) and relative mass loss (**Figure 5B**) at different time points. Monocryl® constructs lost their original strength and became fragile at day 10 (residual compressive strength of 55.0 ± 20.6% and 52.9 ± 16.4% for USP 2-0 CHCs and USP 1 CHCs, respectively) while other constructs remained their original strength and structural integrity much longer (**Figure 5A**). Beyond day 10, any mechanical load that could be born (e.g. compression, tensile or cyclic) was very low on Monocryl® CHCs. These CHCs almost immediately collapsed once any mechanical load was applied. Additionally, Monocryl® constructs showed a mass loss of 5.9 ± 2.0% and 3.6 ± 0.4% for USP 2-0 CHCs and USP 1 CHCs respectively at day 10 (**Figure 5B**). At Day 18, mass loss was determined as 19.5 ± 4.8% and 8.5 ± 0.9% for USP 2-0 CHCs and USP 1 CHCs respectively. Other constructs remained their original mass.

Furthermore, incubation of PDSII®- and Caprolon® CHCs showed no impact on the microstructure as determined by SEM analysis (**Figure 5C, Figure 5E**). In contrast, the initially smooth surface of Monocryl® CHCs was fractured along the circumferential axis (**Figure 5D**), resulting in a total collapse of the CHC when compressed after degradation.

4 DISCUSSION

Development of bioinspired materials and constructs as tubular templates for soft tissue engineering has been hampered by their poor (bio)mechanical performance once implanted. We hypothesized that tubular templates with a CHC would be superior to other designs such as tubularized meshes or electrospun materials. Through the incorporation of CHCs produced from polymers that have received FDA approvals as suture threads, seamless and stable, yet compliant, tubular structures that showed similar mechanical behavior to native tissue were produced.

In the current study, we specifically focused on the development of a template useful for a urological indication, i.e. the ureter, where there is need for new templates which guide ureteral regeneration [31]. In tubular organs, such as the ureter, collagen fibers are arranged as coupled helical coils (CHCs) combining strength and flexibility needed to pass urine [18].

CHC were manually produced from PDSII®, Monocryl® and Caprolon® of different filament diameter. Because fusing changed the original dimensions and the original mechanical properties of the suture filaments was altered. Thus, comparison between the cured CHC and the filament was deemed less relevant. More important, overall mechanical properties of produced CHCs are based on 3 parameter: (i) Winding of CHCs (pitches and pitch size): We have produced multiple CHC with different pitches in pilot experiments (data not shown). At a higher density, the coils became like meshes, at higher pitch sizes the coils became extraordinary flexible and showed little mechanical resistance. The pitch size (mesh pores) also influenced the outcome of the final hybrid template as collagen were less integrated at higher pitch sizes. (ii) Surface area at the fiber intersection points: CHCs produced from Monocryl® USP 1 and PDSII® USP 1 showed a linear stress-strain behavior until failure, very dissimilar from native tissue elasticity. While the rigidity of the PDSII® USP 1 might be caused by the large surface area at the intersection points, resulting in a limited elasticity and hence increased strength, the weakness of Monocryl® USP 1 CHC, might be caused by the limited intersection surface area. (iii) filament diameter: By changing the filament diameter to 0.29 mm (PDSII® USP 2-0 and Monocryl® USP 2-0) the longitudinal stress-strain behavior of CHCs were very similar to native tubular tissue such as the ureter, which was used as reference tissue. In these CHCs designs, the intersections act as a joint, providing high initial elasticity associated with a lower tensile strength to increased tensile strength at higher strain, a mechanical characteristic similar to the extracellular matrix of native tissue [16]. Because the surface area of an intersection

point can be tailored by adapting the fusion time and temperature, upswing strength, UTS and failure strain can be modified. Additionally, diameter of CHCs can be easily adjusted by changing the steel mandrel. This provides the opportunity to customize the mechanical properties of CHC to match the requirements of different tissues.

While overall elasticity/strength is important, strain recovery and hysteresis (energy transmission) of templates are equally important for templates that undergo continuous or repetitive movements due to peristalsis or lateral extensions: strain recovery should be high with minimal energy loss. CHCs from PDSII® USP 2-0 showed a high strain recovery and the lowest energy loss during cyclic tensile loads. Collectively these results demonstrate that CHCs from PDSII® USP 2-0 may be superior to CHC from other tested materials to reinforce relatively weak biomaterials for tubular tissue engineering.

It is clear that CHCs alone cannot function as a template and that they have to be incorporated in other biomaterials to provide a cellular stratum. Collagen type I-based sponges are used abundantly in soft tissue engineering. Despite their excellent biocompatibility, these templates are relatively weak and reinforcement with supporting materials are needed to enhance its (bio)mechanical performance [3,11,23]. Incorporation of CHCs into 0.7% (w/v) collagen type I templates resulted in seamless hybrid tubular templates with adequate mechanical performance and native-like anisotropy. Many tissues, including those with a tubular architecture (ureter, blood vessels, trachea, esophagus), are characterized by anisotropy, that is an asymmetric mechanical performance when the load is applied in different directions. Therefore, collagen type I templates (COL) and hybrid templates were also exposed to various loads. In agreement with earlier work [32], pressure build-up in porous structures such as the hybrid and COL described here, was minimal in burst pressure measurements as fluids extravasated before a pressure build-up could occur (data not shown). In tubular tissues such as the ureter, build-up of high pressures are unlikely [31,33]. Nevertheless, to prevent potential e.g. urine leakage of the hybrid after transplantation, fibrin glue may be used as a sealant [23]. However, *in vivo* experiments are needed to investigate this issue.

COL templates are very weak in both longitudinal- and circumferential direction respectively if compared with the hybrid. At biologically relevant physiological stress-strain of native tubular tissues such as the ureter [31,33], the CHCs remained fully incorporated within the template, without any visible exfoliation or rupture/displacement of the collagen from the CHC. Based on the longitudinal- and circumferential tensile tests, the produced hybrid template has superior suture retention strength compared to the COL template.

Next to longitudinal- and circumferential tensile loads, CHC were exposed to compressive loads. All produced CHCs and the hybrid counterpart were dimensionally stable and resisted repetitive compressive loads, while templates made of collagen alone collapsed. We hypothesized that constructs serving as substitutes for tubular tissues should to be able to resist compressive loads caused from the surrounding tissue (e.g. due to wound healing) to prevent collapse, which will result in obstruction and formation of strictures [34,35]. Indeed, strictures still remain the biggest problem in tubular organ TERM. Our manufactured CHCs and the formed hybrid may be a useful approach to avoid strictures and guarantee the maintenance of an open lumen once implanted [4]. However, the CHCs described here are manufactured from biodegradable polymers, i.e. structural and mechanical support will be temporary only. Since the template degrades and is resorbed progressively as it is being replaced by new tissue [36], the degradation rate of CHCs should be tuned carefully to match the regenerative behavior of the intended organ and species of interest. A moderate degradation rate is suggested to be optimal [4], Therefore, fast degrading materials such as Monocryl® with CHC physically collapsing after 10 days may not be adequate. Slowly degrading materials such as PDSII® that retained their strength and mass over 48 days (data not shown) may be more beneficial. Nevertheless, the rate of degradation and remodeling will be highly dependent on the area of implantation: ureter, esophagus, vascular, or urethra replacement are likely to show very different outcomes. We have previously shown that implantation at different tissues results in very different remodeling [37], Moreover, the *in vivo* outcome will be highly dependent on retained mechanical properties, which differ between different organs. Indeed, *in vivo* experiments are going to be crucial to show the ultimate value of CHC/collagen hybrid templates. In previous studies, we have analyzed constructs similar to the ones described here [23], These were prepared from collagen type I and either (a) a semi-biodegradable Vypro® II polymer (COL-Vypro®), (b) a rapidly biodegradable Vicryl® polymer (COL-Vicryl®) or (c) an additional collagenous layer (COL-DUAL). After implantation as a bladder appendix COL-DUAL and COL-Vicryl® showed better biocompatibility and only small remnants of these constructs were found 1 month post-implantation. Based on this information we assume that the hybrid CHC that we describe here will have very similar characteristics, although this must be shown *in vivo*.

Various approaches have been described for the production of tubular templates, albeit almost exclusively for vascular grafts. Textile fabrics (e.g. knitted- and woven meshes), and polymer windings/springs have been used to provide mechanical support to tubular structures, and tubular structures were created

by electrospinning [17,38], However, these approaches have shown functional limitations such as isotropy, low kinking resistance and compliance mismatch [17], For instance, the implantation of a vascular construct (diameter approximately 6 mm) with mismatched (bio)mechanical behavior created local tissue stiffening. The compliance of the tubular wall was dissimilar, while the disturbed flow might cause thrombus formation and hyperplasia [2,3,12,39], It is likely that mechanical compatibility and compliance mismatch also play a role for tubular templates of larger diameter. To the best of our knowledge, the importance of mechanical match on tissue remodeling of implanted tubular scaffolds of large diameter it is currently unclear. However, native-like compliance of flat structures such as heart valves is of utmost importance to guarantee pliability of tissue-engineered leaflets [40], It is likely that the same holds true for tubular templates. While the mechanical characteristics of textile fabrics and electrospun materials do not match native tissues, reinforcement with macro fibers, arranged in a native-like manner, were shown to improve graft patency [40], Similarly, the reinforcement of tubular scaffolds with CHCs is expected to lead to a better functional outcome with less fibrosis, less construct shrinkage, and maintenance of desired structural dimensions.

Other approaches to engineering various tubular templates have been based on the use of decellularized tubular tissues e.g. arteries and trachea. However, decellularization processes can result in reduced mechanical functionality and, therefore, the reinforcement with other tubular materials may be advantageous to ensure compliance like native (cellularized) tissue as well as structural integrity [13,41], Besides collagen and decellularized tissue, tubular templates were also prepared from tubularized cell sheets. Highly organized cell sheets have been investigated as an excellent template [8,42], Some cell-sheet fabrics displayed adequate physiological compliance and strength [43,44], However, very similar to collagen templates, these templates are structurally weak and reinforcement with the e.g. electrospun material may be required [14]. Albeit that cell-sheet fabrics have been used to engineer small diameter vascular grafts, large engineered constructs combining cell sheet techniques remains to be demonstrated.

Finally, the hybrid architecture described here shows also a similar physiological stress-strain behavior of larger native tissues such as the trachea [45,46]. Furthermore, paired with the versatility of the production process, mainly by simply changing molding- and casting tools [7], hybrid collagen type I templates of various tube diameter, wall thickness and tube length can be prepared for a wide variety of purposes.

5 CONCLUSION

CHCs are promising bioinspired materials and constructs as support structures to produce tubular templates. The production procedure is relatively easy, reproducible and mechanical features can be controlled. We created a hybrid tubular template composed of collagen type I reinforced with a CHC showing similar mechanical behavior as native tubular soft tissue. These CHC-enforced templates which are easily tunable to meet different demands are promising for tubular tissue engineering.

6 ACKNOWLEDGEMENTS

The authors would like to thank Mr. Bastian Schreiber and Henk R. Hoogenkamp, PhD for their support in establishing the production process of CHCs.

The research leading to these results has received funding from the People Programme (Marie Curie Actions) of the European Union's Seventh Framework Programme FP7/2007-2013/ under REA grant agreement No. 607868 (iTERM).

7 REFERENCES

[1] S.J. Hollister, Scaffold design and manufacturing: from concept to clinic., Adv. Mater. 21 (2009) 3330–42. DOI:10.1002/adma.200802977.

[2] P.M. Crapo, Y. Wang, Physiologic compliance in engineered small-diameter arterial constructs based on an elastomeric substrate., Biomaterials. 31 (2010) 1626–35. DOI:10.1016/j.biomaterials.2009.11.035.

[3] S.J. Lee, J. Liu, S.H. Oh, S. Soker, A. Atala, J.J. Yoo, Development of a composite vascular scaffolding system that withstands physiological vascular conditions., Biomaterials. 29 (2008) 2891–8. DOI:10.1016/j.biomaterials.2008.03.032.

[4] Y. Ikada, Challenges in tissue engineering, J. R. Soc. Interface. 3 (2006). DOI: 10.1098/rsif.2006.0124.

[5] F.J. O'Brien, Biomaterials & scaffolds for tissue engineering, Mater. Today. 14 (2011) 88–95. DOI:10.1016/S1369-7021(11)70058-X.

[6] M.L. Muerza-Cascante, D. Haylock, D.W. Hutmacher, P.D. Dalton, Melt electrospinning and its technologization in tissue engineering., Tissue Eng. Part B. Rev. 21 (2015) 187–202. DOI:10.1089/ten.TEB.2014.0347.

[7] M.J.W. Koens, P.J. Geutjes, K.A. Faraj, J. Hilborn, W.F. Daamen, T.H. van Kuppevelt, Organ-specific tubular and collagen-based composite scaffolds., Tissue Eng. Part C. Methods. 17 (2011) 327–35. DOI:10.1089/ten.TEC.2010.0269.

[8] H. Takahashi, T. Okano, Cell Sheet-Based Tissue Engineering for Organizing Anisotropic Tissue Constructs Produced Using Microfabricated Thermoresponsive Substrates., Adv. Healthc. Mater. 4 (2015) 2388–407. DOI:10.1002/adhm.201500194.

[9] F. Boccafoschi, M. Botta, L. Fusaro, F. Copes, M. Ramella, M. Cannas, Decellularized biological matrices: an interesting approach for cardiovascular tissue repair and regeneration., J. Tissue Eng. Regen. Med. (2015). DOI:10.1002/term.2103.

[10] M. Sloff, V. Simaioforidis, D.M. Tiemessen, H.P. Janke, B.B.M. Kortmann, L.A.J. Roelofs, P.J. Geutjes, E. Oosterwijk, W.F.J. Feitz Prof, Tubular constructs as artificial urinary conduits., J. Urol. (2016). DOI:10.1016/j.juro.2016.04.092.

[11] H.R. Hoogenkamp, M.J.W. Koens, P.J. Geutjes, H. Ainoedhofer, G. Wanten, D.M. Tiemessen, J. Hilborn, B. Gupta, W.F.J. Feitz, W.F. Daamen, A.K. Saxena, E. Oosterwijk, T.H. van Kuppevelt, Seamless vascularized large-diameter tubular collagen scaffolds reinforced with polymer knittings for esophageal regenerative medicine., Tissue Eng. Part C. Methods. 20 (2014) 423–30. DOI:10.1089/ten.TEC.2013.0485.

[12] H.S. Rapoport, J. Fish, J. Basu, J. Campbell, C. Genheimer, R. Payne, D. Jain, Construction of a tubular scaffold that mimics J-shaped stress/strain mechanics using an innovative electrospinning technique., Tissue Eng. Part C. Methods. 18 (2012) 567–74. DOI:10.1089/ten.TEC.2011.0286.

[13] W. Gong, D. Lei, S. Li, P. Huang, Q. Qi, Y. Sun, Y. Zhang, Z. Wang, Z. You, X. Ye, Q. Zhao, Hybrid small-diameter vascular grafts: Anti-expansion effect of electrospun poly ε-caprolactone on heparin-coated decellularized matrices., Biomaterials. 76 (2016) 359–70. DOI:10.1016/j.biomaterials.2015.10.066.

[14] H. Ahn, Y.M. Ju, H. Takahashi, D.F. Williams, J.J. Yoo, S.J. Lee, T. Okano, A. Atala, Engineered small diameter vascular grafts by combining cell sheet engineering and electrospinning technology., Acta Biomater. 16 (2015) 14–22. DOI:10.1016/j.actbio.2015.01.030.

[15] Y.C. (Yuan-cheng) Fung, Biomechanics : mechanical properties of living tissues, Springer-Verlag, 1993. DOI: 10.1007/978-1-4757-2257-4

[16] G.A. Holzapfel, S. Tissue, Announcement: Biomechanics of Soft Tissue, J. Biomech. 34 (2001) 1105. DOI:10.1016/S0021-9290(01)00091-4.

[17] C. Singh, C. Wong, X. Wang, Medical Textiles as Vascular Implants and Their Success to Mimic Natural Arteries, J. Funct. Biomater. 6 (2015) 500–525. DOI:10.3390/jfb6030500.

[18] P. Dorrell, R. Wilkinson, S.D. Gorham, M. Aitchison, R. Scott, Collagen arrangements in ureter., Urol. Res. 21 (1993) 325–8. DOI: 10.1007/BF00296829.

[19] A.N. Natali, E.L. Carniel, H. Gregersen, Biomechanical behaviour of oesophageal tissues: material and structural configuration, experimental data and constitutive analysis., Med. Eng. Phys. 31 (2009) 1056–62. DOI:10.1016/j.medengphy.2009.07.003.

[20] G. Gabella, The cross-ply arrangement of collagen fibres in the submucosa of the mammalian small intestine., Cell Tissue Res. 248 (1987) 491–7. DOI: 10.1007/bf00216474.

[21] T.C. Gasser, R.W. Ogden, G.A. Holzapfel, Hyperelastic modelling of arterial layers with distributed collagen fibre orientations., J. R. Soc. Interface. 3 (2006) 15–35. DOI:10.1098/rsif.2005.0073.

[22] J. Huo, R. Rojas, J. Bohlin, J. Hilborn, E.K. Gamstedt, Parametric elastic analysis of coupled helical coils for tubular implant applications: experimental characterization and numerical analysis., J. Mech. Behav. Biomed. Mater. 29 (2014) 462–9. DOI:10.1016/j.jmbbm.2013.09.026.

[23] M. Sloff, V. Simaioforidis, P.J. Geutjes, H.R. Hoogenkamp, T.H. van Kuppevelt, W.F. Daamen, E. Oosterwijk, W.F. Feitz, Novel tubular constructs for urinary diversion: a biocompatibility study in pigs., J. Tissue Eng. Regen. Med. (2016). DOI:10.1002/term.2122.

[24] L.H. Olde Damink, P.J. Dijkstra, M.J. van Luyn, P.B. van Wachem, P. Nieuwenhuis, J. Feijen, Cross-linking of dermal sheep collagen using a water-soluble carbodiimide., Biomaterials. 17 (1996) 765–73. DOI: 10.1016/0142-9612(96)81413-X.

[25] L.H. Olde Damink, P.J. Dijkstra, M.J. van Luyn, P.B. van Wachem, P. Nieuwenhuis, J. Feijen, *In vitro* degradation of dermal sheep collagen cross-linked using a water-soluble carbodiimide., Biomaterials. 17 (1996) 679–84. DOI: 10.1016/0142-9612(96)86737-8.

[26] P.J. Geutjes, K.A. Faraj, W.F. Daamen, T.H. van Kuppevelt, Preparation of differently sized injectable collagen micro-scaffolds, J. Tissue Eng. Regen. Med. 5 (2011) 665–667. DOI:10.1002/term.360.

[27] S.A. Korossis, C. Booth, H.E. Wilcox, K.G. Watterson, J.N. Kearney, J. Fisher, E. Ingham, Tissue engineering of cardiac valve prostheses II: biomechanical characterization of decellularized porcine aortic heart valves., J. Heart Valve Dis. 11 (2002) 463–71. PMID:12150291.

[28] A. Lendlein, A.M. Schmidt, R. Langer, AB-polymer networks based on oligo(epsilon-caprolactone) segments showing shape-memory properties., Proc. Natl. Acad. Sci. U. S. A. 98 (2001) 842–7. DOI:10.1073/pnas.031571398.

[29] A.J. Ryan, F.J. O'Brien, Insoluble elastin reduces collagen scaffold stiffness, improves viscoelastic properties, and induces a contractile phenotype in smooth muscle cells., Biomaterials. 73 (2015) 296–307. DOI:10.1016/j.biomaterials.2015.09.003.

[30] M.E. Gomes, H.S. Azevedo, A.R. Moreira, V. Ellä, M. Kellomäki, R.L. Reis, Starch-poly(epsilon-caprolactone) and starch-poly(lactic acid) fibre-mesh scaffolds for bone tissue engineering applications: structure, mechanical properties and degradation behaviour., J. Tissue Eng. Regen. Med. 2 (2008) 243–52. DOI:10.1002/term.89.

[31] D.P. Sokolis, Multiaxial mechanical behaviour of the passive ureteral wall: experimental study and mathematical characterisation., Comput. Methods Biomech. Biomed. Engin. 15 (2012) 1145–56. DOI:10.1080/10255842.2011.581237.

[32] M.J.W. Koens, K.A. Faraj, R.G. Wismans, J.A. van der Vliet, A.G. Krasznai, V.M.J.I. Cuijpers, J.A. Jansen, W.F. Daamen, T.H. van Kuppevelt, Controlled fabrication of triple layered and molecularly defined collagen/elastin vascular grafts resembling the native blood vessel., Acta Biomater. 6 (2010) 4666–74. DOI:10.1016/j.actbio.2010.06.038.

[33] D.P. Sokolis, Identification and characterisation of regional variations in the material properties of ureter according to microstructure., Comput. Methods Biomech. Biomed. Engin. 17 (2014) 1653–70. DOI:10.1080/10255842.2012.761692.

[34] T. Zou, L. Wang, W. Li, W. Wang, F. Chen, M.W. King, A resorbable bicomponent braided ureteral stent with improved mechanical performance., J. Mech. Behav. Biomed. Mater. 38 (2014) 17–25. DOI:10.1016/j.jmbbm.2014.06.004.

[35] Q. Fu, C.-L. Deng, R.-Y. Zhao, Y. Wang, Y. Cao, The effect of mechanical extension stimulation combined with epithelial cell sorting on outcomes of implanted tissue-engineered muscular urethras., Biomaterials. 35 (2014) 105–12. DOI:10.1016/j.biomaterials.2013.09.067.

[36] I. Engelberg, J. Kohn, Physico-mechanical properties of degradable polymers used in medical applications: a comparative study., Biomaterials. 12 (1991) 292–304. DOI:10.1016/0142-9612(91)90037-B.

[37] Y. Sun, P. Geutjes, E. Oosterwijk, A. Heerschap, *In vivo* magnetic resonance imaging of type I collagen scaffold in rat: improving visualization of bladder and subcutaneous implants., Tissue Eng. Part C. Methods. 20 (2014) 964–71. DOI:10.1089/ten.TEC.2014.0046.

[38] E. Zakhem, K.N. Bitar, Development of Chitosan Scaffolds with Enhanced Mechanical Properties for Intestinal Tissue Engineering Applications., J. Funct. Biomater. 6 (2015) 999–1011. DOI:10.3390/jfb6040999.

[39] S. Brugaletta, B.D. Gogas, H.M. Garcia-Garcia, V. Farooq, C. Girasis, J.H. Heo, R.J. van Geuns, B. de Bruyne, D. Dudek, J. Koolen, P. Smits, S. Veldhof, R. Rapoza, Y. Onuma, J. Ormiston, P.W. Serruys, Vascular compliance changes of the coronary vessel wall after bioresorbable vascular scaffold implantation in the treated and adjacent segments., Circ. J. 76 (2012) 1616–23. DOI: 10.1253/circj.CJ-11-1416.

[40] R. Moreira, C. Neusser, M. Kruse, S. Mulderrig, F. Wolf, J. Spillner, T. Schmitz-Rode, S. Jockenhoevel, P. Mela, Tissue-Engineered Fibrin-Based Heart Valve with Bio-Inspired Textile Reinforcement, Adv. Healthc. Mater. 5 (2016) 2113–2121. DOI:10.1002/adhm.201600300.

[41] C. Johnson, P. Sheshadri, J.M. Ketchum, L.K. Narayanan, P.M. Weinberger, R.A. Shirwaiker, *In vitro* characterization of design and compressive properties of 3D-biofabricated/decellularized hybrid grafts for tracheal tissue engineering, J. Mech. Behav. Biomed. Mater. 59 (2016) 572–585. DOI:10.1016/j.jmbbm.2016.03.024.

[42] Y. Haraguchi, T. Shimizu, K. Matsuura, H. Sekine, N. Tanaka, K. Tadakuma, M. Yamato, M. Kaneko, T. Okano, Cell Sheet Technology for Cardiac Tissue Engineering, in: 2014: pp. 139–155. DOI:10.1007/978-1-4939-1047-2_13.

[43] M. Magnan, P. Lévesque, R. Gauvin, J. Dubé, D. Barrieras, A. El-Hakim, S. Bolduc, Tissue Engineering of a Genitourinary Tubular Tissue Graft Resistant to Suturing and High Internal Pressures, Tissue Eng. Part A. 15 (2009) 197–202. DOI:10.1089/ten.tea.2007.0303.

[44] R. Gauvin, R. Parenteau-Bareil, D. Larouche, H. Marcoux, F. Bisson, A. Bonnet, F.A. Auger, S. Bolduc, L. Germain, Dynamic mechanical stimulations induce anisotropy and improve the tensile properties of engineered tissues produced without exogenous scaffolding, Acta Biomater. 7 (2011) 3294–3301. DOI:10.1016/j.actbio.2011.05.034.

[45] E.G. Mansfield, V.K. Greene, D.T. Auguste, Patterned, tubular scaffolds mimic longitudinal and radial mechanics of the neonatal trachea., Acta Biomater. 33 (2016) 176–82. DOI:10.1016/j.actbio.2016.01.034.

[46] L. Zhao, S. Sundaram, A. V Le, A.H. Huang, J. Zhang, G. Hatachi, A. Beloiartsev, M.G. Caty, T. Yi, K. Leiby, A. Gard, M.H. Kural, L. Gui, K.A. Rocco, A. Sivarapatna, E. Calle, A. Greaney, L. Urbani, P. Maghsoudlou, A. Burns, P. DeCoppi, L.E. Niklason, Engineered Tissue-Stent Biocomposites as Tracheal Replacements., Tissue Eng. Part A. 22 (2016) 1086–97. DOI:10.1089/ten.TEA.2016.0132.

APPENDIX

	Thickness Filament (mm)	*Width Filament (mm)*	*Thickness Filament Intersections (mm)*	*Surface Area Filament Intersections (mm^2)*	*Mesh Angle LONG (degree)*	*Mesh Angle CIRC (degree)*	*Mesh Pores (mm^2)*	*CHC Density (mg/mm^3)*
USP2-0	**0.29 ± 0.01**	**0.29 ± 0.01**	-	-	-	-	-	-
PDSII® CHC	0.16 ± 0.03	0.5 ± 0.2	0.22 ± 0.05	1.0 ± 0.3	129.6 ± 3.1	57.4 ± 4.8	19.2 ± 2.2	0.46 ± 0.09
Monocryl® CHC	0.12 ± 0.03	0.6 ± 0.1	0.19 ± 0.01	0.9 ± 0.2	126.7 ± 2.7	55.4 ± 5.9	18.6 ± 2.4	0.61 ± 0.04
Caprolon® CHC	0.19 ± 0.01	0.7 ± 0.1	0.29 ± 0.03	1.2 ± 0.3	122.6 ± 4.8	53.7 ± 8.7	18.3 ± 3.4	0.39 ± 0.06
USP1	**0.47 ± 0.01**	**0.47 ± 0.01**	-	-	-	-	-	-
PDSII® CHC	0.31 ± 0.08	1.4 ± 0.1	0.40 ± 0.06	4.8 ± 1.0	126.3 ± 8.7	54.6 ± 3.5	19.3 ± 1.2	0.80 ± 0.08
Monocryl® CHC	0.28 ± 0.03	0.70 ± 0.08	0.43 ± 0.06	1.4 ± 0.2	125.4 ± 3.5	50.4 ± 3.1	18.3 ± 1.3	0.7 ± 0.1
Caprolon® CHC	0.24 ± 0.02	1.2 ± 0.2	0.43 ± 0.04	2.4 ± 0.4	123.4 ± 4.2	56.6 ± 4.2	20.8 ± 1.8	0.67 ± 0.08

A1: Dimensions of coupled helical coils (CHCs) produced from different commercially available, resorbable surgical suture monofilaments.

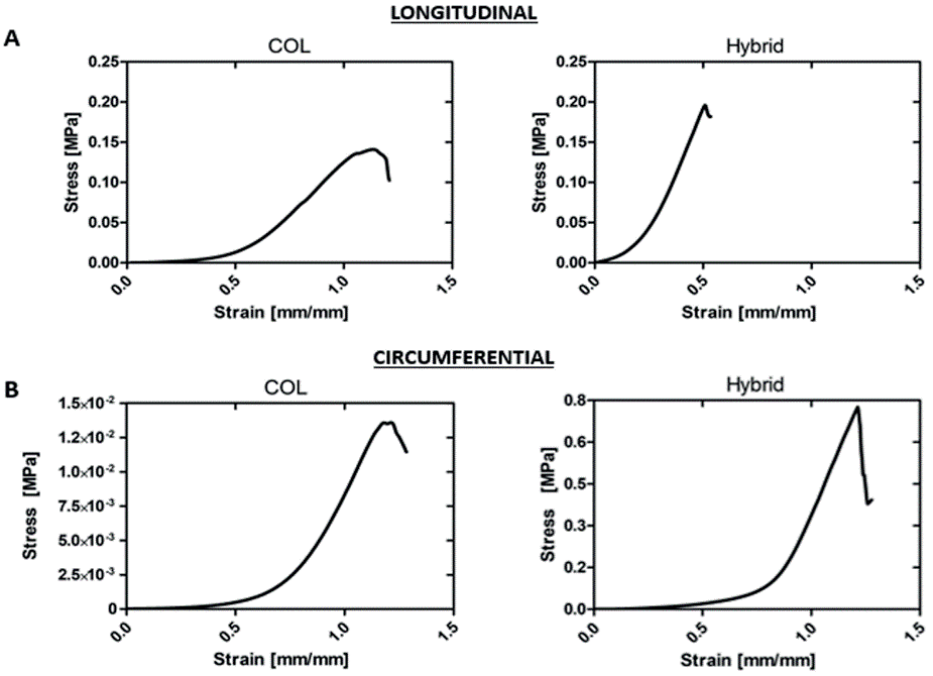

A2: Mechanical properties of collagen type I templates (COL) and collagen type I templates reinforced with a PDSII® USP 2-0 coupled helical coil (hybrid). (A) Representative stress-strain curves of COL and hybrid in longitudinal direction. (B) Representative stress-strain curves of COL and hybrid in circumferential direction.

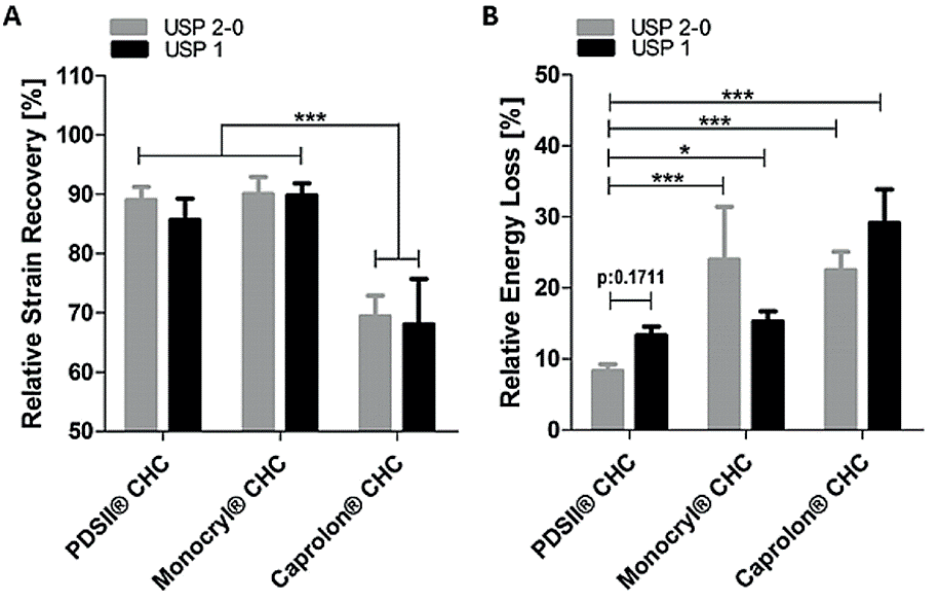

A3: Analysis of coupled helical coil (CHCs) under cyclic mechanical loads. (A) Relative strain recovery of CHCs after 10 loading cycles. (B) relative energy loss after unloading of CHCs after 10 loading cycles. Data represent mean ± standard deviation. One-way ANOVA with Bonferroni post-hoc test, *= $p < 0.05$, ***= $p < 0.0001$.

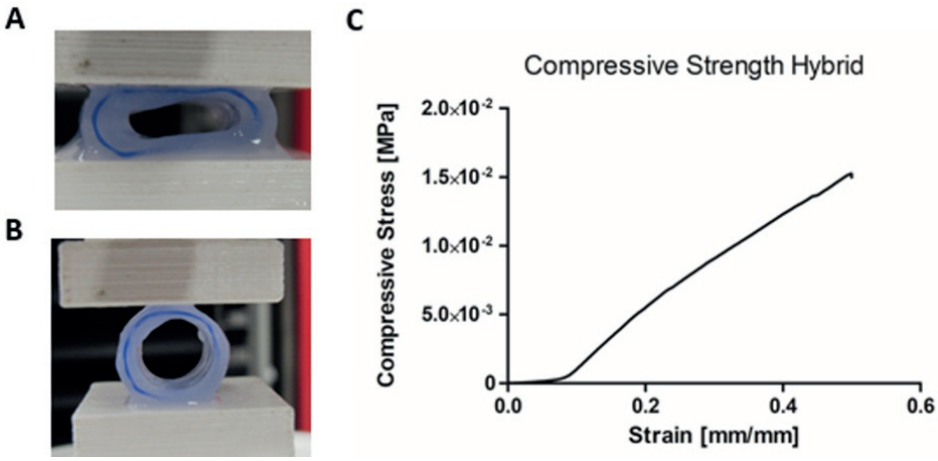

A4: Analysis of collagen type I template reinforced with a PDSII® USP 2-0 coupled helical coil (hybrid) under compressive loads. (A) Compression of the hybrid. No distortion of the hybrid was observed during compression and after release of the load (B). (C) Corresponding stress-strain curve of the hybrid under compressive loads.

CHAPTER 4

Labeling of Collagen Type I Templates with a Naturally Derived Contrast Agent for Noninvasive MR Imaging in Soft Tissue Engineering

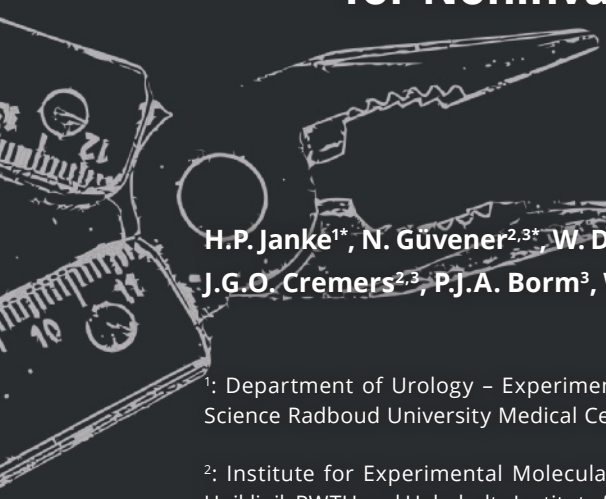

H.P. Janke[1*], N. Güvener[2,3*], W. Dou[4,5], D.M. Tiemessen[1], A. YantiSetiasti[1,6], J.G.O. Cremers[2,3], P.J.A. Borm[3], W.F.J. Feitz[1,7], A. Heerschap[4], F. Kiessling[2] and E. Oosterwijk[1]

[1]: Department of Urology – Experimental Urology, Radboud Institute for Molecular Life Science Radboud University Medical Center, Geert Grooteplein 28, 6525 GE Nijmegen, The Netherlands

[2]: Institute for Experimental Molecular Imaging, Center for Biohybrid Medical Systems, Uniklinik RWTH and Helmholtz Institute for Biomedical Engineering, RWTH Aachen University, Forckenbeckstr. 55, 52074 Aachen, Germany

[3]: Nano4Imaging GmbH Zentrum für Biomedizintechnik (ZBMT), Pauwelsstrasse 17, 52074 Aachen, Germany

[4]: Department of Radiology and Nuclear Medicine, Radboud University Medical Center, PO Box 9101, 6500 HB, Nijmegen, The Netherlands

[5]: GE Healthcare MR Research China, Beijing 100176, China

[6]: Department of Anatomical Pathology, Faculty of Medicine, University of Padjadjaran, Jalan Professor Eyckman No. 38, Bandung 4016, Indonesia

[7]: Radboudumc Amalia Children's Hospital, Geert Grooteplein-Zuid 10, 6525GA Nijmegen, The Netherlands

*: contributed equally

Adv Healthc Mater. 2018 Sep;7(18):e1800605

DOI: 10.1002/adhm.201800605

ABSTRACT

In vivo monitoring of tissue-engineered constructs is important to assess their integrity, remodeling, and degradation. However, this is challenging when the contrast with neighboring tissues is low, necessitating labeling with contrast agents (CAs), but current CAs have limitations (i.e., toxicity, negative contrast, label instability, and/or inappropriate size). Therefore, a naturally derived hemin-L-lysine (HL) complex is used as a potential CA to label collagen-based templates for magnetic resonance imaging (MRI). Labeling does not change the basic characteristics of the collagen templates. When hybrid templates composed of collagen type I reinforced with degradable polymers are subcutaneously implanted in mice, longitudinal visualization by MRI is possible with good contrast and in correlation with template remodeling. In contrast, unlabeled collagen templates are hardly detectable, and the fate of these templates cannot be monitored by MRI. Interestingly, tissue remodeling and vascularization are enhanced within HL-labeled templates. Thus, HL labeling is presented as a promising universal imaging marker to label tissue-engineered implants for MRI, which additionally seems to accelerate tissue regeneration.

1 INTRODUCTION

Tissue engineering (TE) aims at the development of templates that repair, regenerate, or replace damaged tissues and/or organs [1]. The ideal TE template should keep its form to fill the defect, be readily implantable, enhance tissue regeneration, and be able to support tissue-specific functional demands until the template is remodeled completely and replaced by native host tissue [2,3]. Transplantation of tissue-engineered templates often leads to shrinkage or graft failure (e.g., stricture formation and obstruction) and graft failure is often recognized too late or, in experimental settings, when templates are harvested [4–6]. Therefore, monitoring the fate of templates upon implantation is of utmost importance. Several imaging modalities are available to provide information of template integrity, remodeling, and resorption in a noninvasive, highly sensitive manner [7], albeit imaging of implanted grafts has been limited.

Magnetic resonance imaging (MRI) is an attractive multifunctional and noninvasive imaging modality that does not use ionizing radiation. Various templates used in TE have been monitored using MRI. For example, good image contrast was achieved *in vivo* for bone TE, particularly after modifications of the filling material (e.g., calcium phosphate cement) with contrast agents (CAs) [8–10]. Indeed, templates used for TE usually give poor contrast as the selected materials have similar composition to that of the surrounding host tissue, and thus difficult to distinguish. For instance, porous collagen type I templates show excellent biocompatibility and have been used for various applications extensively [11], but the imaging contrast to surrounding tissues is poor, and the evaluation of its remodeling after transplantation *in vivo* commonly relies on histological examinations. Incorporation of CAs such as ultrasmall superparamagnetic iron oxide nanoparticles (USPIOs) in collagen templates can enhance MR visibility [12,13]. USPIOs decrease the signal of water by T_2 or T_2* relaxation and thus generate a negative contrast, which however may be misinterpreted as other tissue components such as air inclusion may also cause negative contrast. Furthermore, the effect of USPIOs on the water signal may extend beyond its local presence (“blooming” effect) and thus hamper their precise localization. Finally, USPIOs may be washed out of the collagen independent of its remodeling and thus images may not accurately represent the engineered template [12–14].

Another limitation associated with collagen type I templates is their poor mechanical strength. Incorporation of polymers or surgical meshes can enhance overall strength and ensure the stability of collagen templates [15–17]. An additional

advantage is that these supportive polymers give a negative contrast in MR images, which can assist as an anatomical guide within the hybrid structure [18–20]. However, USPIO-labeled collagen templates cannot be distinguished from these polymers via MR anymore since both generate a negative contrast.

Low molecular weight gadolinium (Gd) complexes are widely used for MRI, generating a positive MR signal. Gd labeling of collagen templates might enhance MRI visibility and allow longitudinal follow-up. However, Gd has been linked to adverse effects such as local or systemic fibrosis, especially in patients with renal insufficiency as well as brain accumulation in patients with normal renal function [21]. Additionally, areas of long-term deposition of Gd-based CAs appeared to be the bone and spleen in healthy subjects [22]. Alternatively, (metallo)porphyrins may be considered as an alternative class of MR CAs, because they form stable chelate complexes with paramagnetic metal ions [23,24]. Hemin, one of the (metallo) porphyrins, is a natural Fe^{3+}-containing constituent of oxygen-carrying hemoglobin [25] and may be suited as an MR CA since it is a high spin complex. However, hemin is virtually insoluble under physiological conditions. Here, we synthesized a water-soluble hemin-L-lysine (HL) complex to label various collagen type I based templates via covalent conjugation and physical adsorption. The MRI properties of the labeled templates, their labeling efficiency, and their biocompatibility were examined *in vitro*. Furthermore, HL-labeled templates were implanted subcutaneously *in vivo* to assess their visibility by MRI and to longitudinally study their remodeling.

2 MATERIALS AND METHODS

2.1 Materials

Hemin, L-lysine, N-ethyl-3-(3-dimethylaminopropyl)-carbodiimide (EDC), N-hydroxysuccinimide (NHS) and 2-morpholineoethane sulphonic acid (MES) were purchased from Sigma-Aldrich (St. Louis MO, USA). Acetone, NaCl and Na_2HPO_4 and phosphate buffered saline (PBS) were purchased from Merck (Darmstadt, Germany). Trinitrobenzene sulfonic acid (TNBS) was purchased from Fluka Chemie AG (Buchs, Switzerland). Dry and highly purified collagen type I derived from bovine achilles tendon was purchased from Collagen Solutions (Glasgow, Scotland, United Kingdom). USP2-0 Maxon® resorbable suture monofilaments were purchased from Covidien / Medtronic (Neustadt/Donau, Germany).

2.2 Hemin-L-Lysine Complex (HL) Conjugation

Hemin-L-lysine conjugation was performed as described by Ingberg et al. [26]. In brief, Hemin and L-lysine (molar ratio 1:3) were suspended in a solvent mixture of demineralized water and acetone (1:15 (v/v)). The sample was rotated overnight and the solid formed was filtered, washed with acetone and lyophilized resulting as a water-soluble dark powder (hemin-L-lysine complex (HL)).

2.3 Collagen Type I Template Production

Templates made of collagen type I were prepared as previously described [17,27] with slight modifications. A 0.5 % (w/v) collagen solution was prepared by swelling highly purified collagen type I from bovine achilles tendon in 0.25 M acetic acid overnight followed by homogenization using a Silverson L5M-A laboratory mixer (Silverson, Chesham, United Kingdom) and de-airing by centrifugation (800 rpm for 30 min). To create a standard collagen type I template (COL), homogenized and de-aired collagen suspensions of 2 mL were poured into 24-well plates. To create a hybrid tubular template (COL-CHC), homogenized and de-aired collagen type I suspensions (7 mL) were poured into a polystyrene mold. A steel mandrel (d = 6 mm) was fixed to the middle of the polystyrene mold. To reinforce the collagen and to strengthen the construct, a coupled helical coil made of Maxon® USP2-0 was placed between the steel mandrel and polystyrene wall. Afterwards, the mold was stored in a metal block. Filled molds were frozen at -20 °C for at least 24 hours. Samples were subsequently lyophilized (Zirbus Sublimator 500II, Bad Grund, Germany). After

lyophilization, 10 mm disc-shaped hybrid patches (COL-CHC patches) were prepared from hybrid tubular templates by using a tissue punch (Punchy, Erlangen, Germany).

2.4 Labeling of HL to Collagen Type I Templates

HL of different concentration was dissolved in 0.1 M phosphate buffered saline (PBS; 7.4 pH; range 0 - 1.25 mM). Dry collagen type I templates were pre-wetted in 70% (v/v) ethanol to preserve the porous structure [28]. For covalent conjugation: collagen type I templates were soaked in 25 mL HL solution at different concentrations, de-gassed under vacuum and incubated until a homogenous distribution of HL within the collagen template was achieved (approx. 4 h) as judged by visual inspection. Afterwards, crosslinking / covalent conjugation of HL-soaked templates was performed with 33 mM EDC and 6 mM NHS [28–30]. In detail, templates were transferred to 50 mM MES buffer (pH 5.0) containing 40% (v/v) ethanol. Next, the templates were incubated for 4 h in EDC / NHS / MES buffer solution. Crosslinking / labeling reaction was stopped by 2 times washing with 0.1 M Na_2HPO_4 for 1 h. Subsequently, templates were washed twice with 1.0 M NaCl, 2.0 M NaCl (3x) and demineralized water (6x). Alternatively, collagen templates were labeled with HL by physical adsorption. Here, collagen templates were crosslinked as described above, incubated in 70% (v/v) ethanol, de-gassed and soaked in 25 mL of various HL solutions (approx. 4h until the appearance of the template was homogeneous) followed by washing with PBS (11x) (similar to washings for actively-labeled templates). For *in vitro* studies, all templates were washed in 70% (v/v) ethanol (4 x for 1 h and 1 x overnight) and sterile NaCl (4x for 1 h and 1x overnight) followed by an overnight incubation in culture medium if cell seeding studies were performed. For *in vivo* evaluation, all templates were frozen again at -20 °C and lyophilized. Dry scaffolds were sterilized by 25 kGray of gamma (γ)-irradiation (Staris, Etten-Leur, The Netherlands).

2.5 Template Characterization

Produced templates were subsequently analyzed in terms of pore architecture via scaning electron microscopy (SEM). SEM was performed with a Zeiss Sigma 300 (Carl Zeiss, Jena, Germany) operating at an accelerating voltage of 15 kV. Samples were sputtered with gold for 60 seconds by a Scancoat Six SEM Sputter Coater (Temescal/ Ferrotec, Unterensingen, Germany) before being analyzed. Degree of Crosslinking was performed via 2,4,6-trinitrobenzenesulfonic acid (TNBS) assay [29] and the iron content of each template was determined by inductively coupled plasma optical

emission spectrometry (ICP-OES). In brief, samples were dissolved in 65% nitric acid (HNO_2) and diluted to 4% HNO_2 with milliQ water. The obtained values were expressed in micro grams of iron per mg collagen template material.

2.6 Mechanical Properties

To investigate the mechanical properties of the hybrid templates, compression and tensile ring tests were performed. For compression tests, COL- and COL-HL cylinders with different HL amounts (n = 9; diameter = 13 mm; height = 8 mm) were placed in a petri dish filled with PBS (0.1 M; pH 7.4). A compressive load was applied via a tensile tester (Z2.5 TN, Zwick/Roell, Ulm, Germany) equipped with a load cell of 20 N. With a test speed of 50 mm/min, test specimen were compressed up to 80% of its original length and the resulting load in Newton [N] were subsequently recorded to indicate compressive strength. To indicate the mechanical behavior of COL-CHC and COL-HL-CHC, a tensile ring test was performed on ring specimen (l = 5 mm; n = 5) mounted between customized hooks (hook-to-hook distance = 6 mm). With a crosshead speed of 50 mm/min, all test specimens were pre-conditioned radially by stretching 10 times up to 50% of constructs' strain. Afterwards, the uniaxial load was applied in radial direction until rupture of the construct. Mechanical properties of the templates were derived as previously described [17].

2.7 Cytocompatibility

NIH 3T3 fibroblasts were cultured in standard culture medium composed of DMEM (Gibco, Invitrogen, Germany) supplemented with 10% fetal calf serum (FCS; Invitrogen, Germany) including 1% Pen/Strep (10,000 U/mL penicillin; 10,000 U/mL streptomycin, Invitrogen, Germany). For cytotoxicity studies, equal amounts (length: 10 mm; weight: 30 mg) of the COL-CHC and COL-HL-CHC templates and latex material (positive control) were incubated in standard culture medium for 72 h. Subsequently, the conditioned culture media were added to NIH 3T3 cells (cell density: 4,000 cells / 96-well) and incubated for 24 h. Cell viability was measured using the WST-1 assay (Roche) according to manufacturer's protocol.

In a subsequent set of experiments, NIH 3T3 cells (2×10^6 cells/mL) were seeded on COL and COL-HL (diameter = 13 mm; height = 8 mm) as follows: 1 mL of cell suspension was added to each pre-wetted template and incubated for 6 h on a rollerbank in a humidified incubator (5% CO_2) at 37 °C to allow cell adhesion. Subsequently, specimen were placed in tissue culture dishes and harvested after cell adhesion (day 0; n = 6) and day 7 (n = 6) post-seeding to determine double

stranded DNA (dsDNA) content. In brief, a biopsy of the cell-seeded template was minced, transferred to milliQ water and frozen down to -20 °C. Subsequently, the supernatant was collected and diluted in Tris-EDTA (TE) buffer (10 mM Tris-HCl, 1 mM EDTA, pH 8). dsDNA content was measured in an opaque white, 96-wells plate using a Quant-iT™ PicoGreen® kit (Invitrogen, Carlsbad, USA) according to manufactures protocol. Fluorescence was measured with a Victor3 multilabel plate reader (Perkin Elmer, Waltham, USA) at an excitation of 485 nm and emission of 528 nm. A DNA quantification curve was made using a Lambda DNA standard (Promega, Madison, USA).

2.8 *In vitro* Magnetic Resonance Imaging

MRI experiments were performed on an 11.7 Tesla preclinical MR system (BioSpec, Bruker, Germany) equipped with a ^{1}H volume coil with an inner diameter of 40 mm. Templates were embedded in 10% (w/v) agarose phantoms prior to scanning. A rapid acquisition with relaxation enhancement (RARE) sequence was employed for acquiring T_1- weighted MR imaging, with the following parameters: echo time (T_E) = 6 ms, repetition time (T_R) = 600ms, excitation angle = 90°, refocusing angle = 180°, number of slices = 20, slice thickness = 0.5 mm, RARE factor = 4, field of view (FOV) = 50 × 50 mm, matrix size = 256 × 256 and 8 averages. The scan time was 3 mins 5 secs. The T_1- and T_2 relaxation properties of hemin–L-lysine and the hemin conjugate incorporated in collagen templates were estimated with a multi-T_R and multi-T_E RARE sequence. For T_1 estimation, images were recorded at 8 T_Rs (i.e., 200, 500, 1000, 2000, 3000, 5000, 7000, 10000 ms) and T_1 values were estimated by fitting the signal intensity (M_z) as a function of T_R to the model:

$$M_z(T_R)=M_0(1-e^{-T_R/T_1})$$

The scan time was 7 minutes and 39 seconds. For T_2 estimation, the image signal intensity at 30 T_Es from 10 to 300 ms with an increment of 10 ms were recorded with a total scan time of 3 mins 12 seconds. The image signal intensity (M) at different T_Es were fitted with a mono-exponential model to determine T_2 values:

$$M(T_E)=M_0e^{-T_E/T_2}+C$$

The reciprocals of T_1- and T_2 relaxation times, defined as R_1- and R_2 relaxation rates, were calculated, respectively. Subsequently, R_1- and R_2 relaxation rate were plotted as a function of the HL concentration to determine the overall relaxivity (slope of the curve; see **Appendix A1**).

Image contrast between the applied template and the background were assessed using the contrast to noise ratio (CNR), which was defined as the difference in the

two contrast giving tissues divided by the standard deviation of the background noise. A region of interest (ROI) of 0.15 cm^2 was drawn within the area of contrast giving tissues (template and tissue phantom, respectively) and background. Mean image intensities as well as the standard deviations were obtained using imageJ (U.S. National Institutes of Health, Bethesda, Maryland, USA).

2.9 *In vivo* Evaluation

HL-modified and plain COL-CHC patches were grafted subcutaneously in 18 immune-competent female BALB/cByJ mice (age: 7-8 weeks; weight: ± 20 g) to follow the fate of the implant *in vivo*. The animal experiment was conducted in accordance with standards and protocols of the Radboudumc, Nijmegen, The Netherlands. National guidelines for care and use of laboratory animals were obeyed and the experiment was approved by the Ethical Committee on Animal Research of the Radboud University Medical Center, Nijmegen, The Netherlands (DEC 2017-0013-005). Mice were randomly divided into 3 groups. Prior to surgery, the mice were pre-medicated by intraperitoneal injection of Rimadyl (Pfizer, USA; 5 mg carprofen/kg). Anesthesia was induced by inhalation of 5% Isoflurane FiO_2/N_2O 1:2 (maintenance dose of 2-3% Isoflurane FiO_2/N_2O 1:2) and the skin of the graft area was disinfected with Iodine (Eurovet animal health, the Netherlands). An incision of ± 1.5 cm was made on the back of the mice in line with the spine and two subcutaneous pockets were created on the left and right side of the back of the mouse (viewed from the prone position). HL-labeled hybrid patches were placed in the right pocket and unlabeled (control) hybrid patches were placed in the left pocket. The incision was closed with metal clips that were removed after wound closure (± 3 days). For day 0 evaluation, the incision of each randomly chosen mouse (n = 6) was closed with an absorbable 6-0 coated Vicryl Plus suture (Ethicon, USA). For MRI, animals were anesthetized with 2-3% Isoflurane FiO_2/N_2O 1:2, and heartbeat and body temperature were monitored during scanning.

In vivo MRI experiments were also performed at 11.7T using the same ^1H volume coil as used for the *in vitro* studies. High resolution T_1 weighted MR images were acquired with a RARE sequence to visualize the implanted template in mice at weeks 2, 4 and 12. The following sequence parameters values were used: T_E = 10ms, T_R = 560 ms, RARE factor = 2, number of slices = 20, slice thickness = 0.5 mm, FOV = 50 × 50 mm, matrix size = 512 × 512 and 16 averages. The scan time was 28 minutes and 40 seconds. In addition, the same protocol as used for the *in vitro* study was applied to determine T_1 relaxation times of the implanted templates at each time point. In

addition, image contrast of implanted templates in mice was estimated using the CNR. For both, T_1 and CNR calculations, a 0.6 mm2 ROI was set within the collagen-labeled structure of the scaffold. Volumes of implanted COL-HL-CHC templates were determined as previously described by using ImageJ. [12] In brief, the template volume was measured by manually outlining the template area in each MR image slice and multiplication by slice thickness (0.5 mm). At pre-determined endpoints (2, 4, and 12 weeks post transplantation), animals were sacrificed by carbon dioxide asphyxiation, imaged and tissues harvested for analysis.

2.10 (Immuno)histochemical Analysis

Harvested implants were split and fixed in 4% paraformaldehyde (PFA) followed by paraffin embedding, or immediately embedded in Tissue Tek (Sakura, Torrance, USA) and snap-frozen in a dry ice cooled isopentane and stored at -85°C. Morphology, cellular content of implanted materials and extracellular matrix deposition were analyzed by Hematoxyline and Eosin (HE), Masson Trichrome / Verhoeff stain and immuno(fluorescence) staining.

2.10.1 Vessel formation

To visualize vessel formation, excised implants were stained for collagen type I, alfa-smooth muscle actin (α-SMA) and Cluster of Differentiation 31 (CD31). Cryostat sections were fixed in ice-cold aceton, washed with PBS and incubated with rabbit anti-mouse collagen I (NB600-408, Novus Biologicals, Cambridge, United Kingdom, 1:100), rat anti-mouse CD31 (553370, BD Biosciences, Heidelberg, Germany, 1:100) or Biotin anti-mouse smooth muscle actin (BK61501.0.5, Progen, Heidelberg, Germany, 1:500) in 12% BSA/PBS at 4°C overnight. After washing sections were incubated with Goat anti-rabbit IgG (111-155-003, Dianova, Hamburg, Germany, 1:50), Donkey-anti-Rat IgG (712-546-153, Dianova, Hamburg Germany, 1:350) or Streptavidin anti-biotin (ab134348, Abcam, Cambridge, United Kingdom, 1:100) in 12% BSA/PBS for 45 min at room temperature. After washing sections were embedded in Mowiol® and analyzed.

To quantify blood vessel formation, sections were stained for alfa-smooth muscle actin with Bright-3,3'Diaminobenzidine (Bright-DAB). Paraffin sections (5 micron) were deparaffinized using xylene, followed by graded series of ethanol and re-hydrated in PBS. Subsequently, sections were immersed in 1% (v/v) H_2O_2/PBS for 10 minutes at room temperature to block endogenous peroxidase followed by mouse-on-mouse blocking with MOM kit (Sigma Aldrich, St. Louis MO, USA).

Afterwards, sections were incubated with anti-alfa-smooth muscle actin (Sigma Aldrich, St. Louis MO, USA), washed and incubated with biotinylated anti-mouse IgG (Immunologic, Duiven, The Netherlands) for 10 minutes at room temperature. Next, the sections were washed in PBS and incubated for 45 minutes with ABC-PO (Avidin 1:100 and Biotin 1:100 in PBS; 30' pre-incubation at room temperature (Sigma Aldrich, St. Louis MO, USA). All sections were stained with Bright-DAB (Immunologic) for 5 minutes and counterstained with hematoxylin. For blood vessel quantification, the number of blood vessels were counted and normalized to the cross-sectional area of the region of interest using ImageJ.

2.10.2 Immune Response

The excised implants were stained for F4/80 and Dihydrochloride (DAPI) for immune response evaluation. Sections were first stained with rat anti-mouse F4/80 (MCA497GA, AbD Serotec (Bio-Rad), Düsseldorf, Germany, 1:50) in 12% BSA/PBS and were incubated at 4 °C overnight. Following to washing step, sections were incubated with donkey anti-rabbit IgG (711-546-152, Dianova, Hamburg, Germany, 1:500) and donkey anti-rat IgG (712-166-153, Dianova, Hamburg, Germany, 1:500) in 12% BSA/PBS for 45 min at room temperature. As a final step, sections were counterstained with 4',6-Diamidino-2-Phenylindole, Dihydrochloride (DAPI, Life Technologies, Carlsbad, USA, 1:500) in 12% BSA/PBS for 45 min at room temperature and mounted. To quantify F4/80 positive cells, the ratio of F4/80 positive cells (nuclei) over total nuclei content was calculated using 3 micrographs (magnification: 200x) from n = 3 mice per time point and template with ImageJ micrographs. Furthermore, brightfield images were scored to indicate cellular content (lymphocytes, polynuclear morphocytes, giant cells and (myo)fibroblasts), extracellular matrix and vascularity. Scoring was performed by 2 independent observers (HPJ, AYS). If the observers were discordant, samples were re-analyzed until concordance was reached. Infiltrating cells were scored as – = not present, +/- = sporadically present, + = moderately present or ++ = abundantly present.

2.11 Statistical Analysis

Data regarding the pore perimeter of COL and COL-HL were obtained directly from each measurement, without any pre-processing. Results are presented as mean ± standard deviation. Per template type, 10 randomly chosen pores were measured and each template type was measured n = 3 independently. A Student's t-test (two-tailed) was applied to determine statistical differences between COL and COL-HL.

DNA content of cell seeded templates were obtained from raw absorbance data and normalized to the weight of individual templates. Data are expressed as mean ± standard deviation. Sample size was n = 6 for each group. A two-tailed Student's t-test was performed to determine statistical differences between COL and COL-HL.

Load-displacement data from tensile ring tests were normalized to dimensions and gauge lengths of COL-CHC and COL-HL-CHC to obtain initial modulus (E1), upswing (Young's) modulus (E2), ultimate tensile strength (UTS and failure strain from a computed stress-strain curve. Data are expressed as mean ± standard deviation with a sample size of n = 5 for each group. A Student's t-test (two-tailed) was applied to indicate statistical differences between COL-CHC and COL-HL-CHC.

Iron content data (ppm) were normalized to µg iron per mg of template material. Results are expressed as mean ± standard deviation. Sample size was n = 9 for each condition.

Data regarding compressive strength were directly obtained from measurements without any pre-processing. Data are expressed as mean ± standard deviation. Sample size was n = 9 for each group from independent measurements. Regression, Pearson correlation coefficient r and p value (two-tailed) were determined to describe the correlation between iron concentration and strength of different templates.

Data from the TNBS assay (free NH_2-groups) were obtained from raw absorbance data and normalized to the weight of individual templates. To obtain the degree of crosslinking, crosslinked templates were normalized to non-crosslinked templates. Results correspond to mean ± standard deviation of a sample size of n = 3. A two-tailed Student's t-test was performed to determine statistical differences between crosslinked and non-crosslinked templates. In addition, regression, Pearson correlation coefficient r and p value (two-tailed) were determined to describe the correlation between iron concentration and NH_2-groups.

Relaxation rate (R_1) data were calculated from relaxation time (T_1) measurements and data on contrast-to-noise ratio (CNR) data were calculated from raw imaging data (image intensities). All data sets are expressed as mean ± standard deviation. Sample size for each group was n = 6 for each group. When COL-CHC templates were compared with COL-HL-CHC templates, a two-tailed Student's t-test was performed to determine statistical differences. Regression, Pearson correlation coefficient r and p value (two-tailed) were determined to describe the correlation between iron concentration and strength of different templates.

To determine the number of blood vessels, blood vessels were counted and normalized to the cross-sectional area of the ROI. Data represent mean ± standard deviation with a sample size of n = 6 for each group. COL-CHC were compared with COL-HL-CHC. A two-tailed Student's t-test was performed to determine statistical differences.

For all analysis, $p < 0.05$ was considered statistically significant. GraphPad Prism (version 5.03, GraphPad Software Inc, La Jolla, CA, USA) was used for all statistical analysis.

3 RESULTS AND DISCUSSION

3.1 Template Production and HL Incorporation

Prior to labeling with the hemin-L-lysine complex (HL, F**igure 1A**), various collagen type I-based templates were produced as prototypic template materials: i) simple disc-shaped collagen type I templates (COL; **Figure 1B-i**), ii) hybrid tubular templates composed of collagen type I reinforced with a coupled helical coil (COL-CHC; **Figure 1B-ii)** and iii) COL-CHC patches derived from hybrid tubular templates (**Figure 1B-iii**). All produced templates showed a typical honeycomb-like porous structure as evaluated by scanning electron microscopy (SEM) (see **Figure 1B-iv** for COL and **Figure 1B-v** for COL-CHC).

To increase the solubility of hemin in aqueous media, three mole of L-lysine / mole hemin was needed to dissolve the hemin [26]. This yielded in a soluble hemin-L-lysine (HL) complex: no precipitate was observed after 20 min of centrifugation at 10000g. HL solutions of different concentrations ranging from 0.0 mM to 1.25 mM were prepared in phosphate buffered saline (PBS; 0.1 M; pH 7.4) in glass vials.

Subsequently, collagen type I templates were incubated in these HL concentrations. To achieve a homogeneous distribution of HL throughout the templates pre-incubation of dry collagen type I templates in 70% (v/v) ethanol and subsequent de-airing / degassing under vacuum was essential to preserve the honeycomb-like porous structure: dry COL soaked directly in HL collapsed immediately resulting in an inhomogeneous distribution of HL mainly at the outer margin of the templates. Subsequently, HL was covalently conjugated to amine- (NH_2) and / or carboxylic (COOH) groups of collagen type I via N-ethyl-3-(3-dimethylaminopropyl)-carbodiimide (EDC) / N-hydroxysuccinimide (NHS) during crosslinking to form stable amide bonds (**Figure 1C**). In addition to collagen crosslinking, this method has been well established to covalently conjugate molecules to collagen templates (e.g., chondroitin-sulfate and heparan sulfate) [31,32].

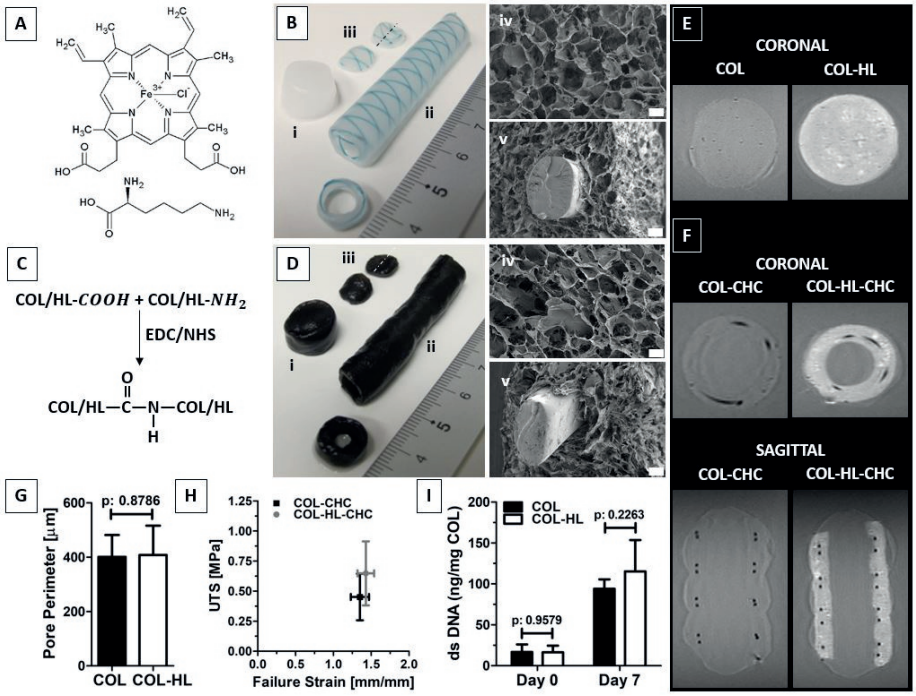

Figure 1: A) Chemical structure of the hemin-L-lysine (HL) complex. B) Various collagen type I templates. Macroscopic image of (i) a disc-shaped COL template, (ii) hybrid tubular COL-CHC template, and (iii) COL-CHC patches derived from tubular hybrid templates. Cross-sectional scanning electron microscopy (SEM) images of COL (iv) and COL-CHC (v) (scale bar SEM = 100 µm). C) Covalent conjugation of HL to COL via N-ethyl-3-(3-dimethylaminopropyl)-carbodiimide (EDC)/N-hydroxysuccinimide (NHS) during crosslinking procedure. D) Various collagen type I templates covalently conjugated with HL. Macroscopic image of (i) a disc-shaped COL-HL template, (ii) tubular COL-HL-CHC, and (iii) COL-HL-CHC patches. SEM of COL-HL (iv) and COL-HL-CHC (v) (scale bar: 100 µm). E) *In vitro* T_1-weighted magnetic resonance images (T_1w-MRI) of disc-shaped COL and COL-HL templates. F) *In vitro* T_1w-MRI of tubular COL-CHC and COL-HL-CHC. G) Pore perimeter of honeycomb template structure of COL and COL-HL. Data represent mean ± standard deviation with a sample size of n = 3 for each group. Two-tailed Student's t-test was performed to determine statistical differences. H) $p < 0.05$ was considered statistically significant ultimate tensile strength (UTS) and failure strain of COL-CHC and COL-HL-CHC. Data represent mean ± standard deviation with a sample size of n = 5. I) Cell attachment (day 0) and cell proliferation (day 7) of seeded NIH 3T3 fibroblasts to COL and COL-HL templates. Data represent mean ± standard deviation with a sample size of n = 3 for each group. Two-tailed Student's t-test was performed to determine statistical differences. $p < 0.05$ was considered statistically significant.

After stopping the crosslinking process, HL loss during subsequent washing procedures was limited and only observed when collagen templates were incubated in HL concentrations of 1 mM and higher, suggesting that available conjugation sites were saturated. Covalently conjugated templates appeared in dark brown color (COL alone (COL-HL; **Figure 1D-i**), hybrid templates with coupled helical coil (COL-HL-

CHC; **Figure 1D-ii** and **1D-iii**). Alternatively, COL templates were physically adsorbed through incubation in HL of various concentration after crosslinking. This procedure of physical adsorption has been described as a strategy to bind growth factors such as bone morphogenetic protein-2 [33,34]. Substantial HL-loss was observed during washing steps. These templates appeared light brown with increasing intensity in an HL concentration-dependent trend (see **Appendix A2**).

Crosslinking of collagen type I templates was successful as evidenced by the 2,4,6-Trinitrobenzenesulfonic acid (TNBS) assay. Non-crosslinked collagen templates showed an average of 260 ± 114 nmol of free amine groups per mg collagen. Free amine groups of crosslinked collagen templates significantly decreased ($p < 0.0001$) to 99 ± 27 nmol per mg collagen (38.2 ± 10.2% reduction). COL-HL templates used for covalent conjugation had an amount of 496 ± 52 nmol of free amine groups per mg prior to crosslinking / conjugation. After crosslinking / conjugation, free amine groups were significantly ($p < 0.0001$) reduced to 267 ± 48 nmol per mg (53.9 ± 9.7% reduction). Overall, covalent conjugation of HL to collagen resulted in significantly ($p < 0.0001$) higher free amine groups after crosslinking when compared to collagen alone.

The iron content of covalently conjugated- and physically adsorbed templates after subsequent washings are presented in **Appendix A7** and was found higher for covalently conjugated templates. The iron content of covalently conjugated templates used for *in vitro* and *in vivo* studies was 6.8 ± 2.7 µg Fe / mg collagen. Collectively, covalent conjugation of HL was successful and preferable over physical adsorption as loss of HL is expected to be directly related to collagen remodeling whereas with physical adsorption HL loss is not necessarily a reflection of collagen remodeling.

3.2 *In Vitro* MRI

To assess the applicability of HL as a CA, the relaxivity of HL dissolved in PBS was measured on an 11.7T pre-clinical MR system. Using a rapid acquisition with relaxation enhancement (RARE) sequence with variations of repetition time (T_R) or echo time (T_E), the T_1-relaxivity (r_1) was assessed as 0.42 ± 0.02 $mM^{-1}s^{-1}$ and the T_2-relaxivity (r_2) was assessed as 4.3 ± 0.7 $mM^{-1}s^{-1}$ (**Appendix A1**). These relaxivities are common for metalloporphyrins such as HL [24]. However, bright MRI signal indicates HL as a T_1-weighted MR CA similar to other Fe^{3+}-chelated CAs which may be an alternative to gadolinium-based CAs for T_1-weighted magnetic resonance imaging (T_1w-MRI) [35]. It is clear that a full characterization of the relaxivity properties

of HL at different field strengths (e.g. at 3T) is required to better understand the contrast properties observed and to be able to optimize these properties for future applications.

Subsequently, T_1w-MR images of labeled collagen type I templates were acquired. Both covalently conjugated- and physically adsorbed collagen templates, were better visualized by MRI compared to unlabeled collagen templates. The best visualization in T_1w-MR images (**Appendix A2**) and largest T_1w-MR relaxation rate (R_1) difference between HL-labeled and control templates changes (**Appendix A7**) were achieved for the covalently conjugated collagen type I templates. R_1 significantly correlated with iron concentration ($r = 0.9582$; $p = 0.0026$; $R^2 = 0.9182$), whereas no significant correlation was found for physically adsorbed HL ($r = 0.7493$; $p = 0.0864$; $R^2 = 0.5614$), most likely because HL washout was faster at the highest HL concentrations due to a steeper concentration gradient. Furthermore, the contrast-to-noise ratio (CNR) of both covalently conjugated and physically adsorbed HL reached a plateau at 1.0 mM HL (**Appendix A7**), resulting in a clear visualization when compared to COL alone (**Figure 1E**).

The T_1 effect on the water signal may be variable for physically adsorbed collagen templates due to diffusion of HL out of the complex and thus unrelated to collagen remodeling and / or degradation. Therefore, physical adsorption was deemed unreliable, as the intention was to develop an MR imageable template where MR signal and collagen content were strongly correlated. The covalent conjugation of HL to collagen resulted in higher labeling efficacies as well as higher relaxation rates and contrast-to noise ratios of the templates compared to physical adsorption. HL labeling efficiency was concentration-dependent, but contrast-to-noise ratios did not improve when templates were incubated in HL levels beyond 1 mM. Thus, subsequent experiments were performed with collagen templates which were covalently conjugated with 1 mM HL via EDC / NHS.

Following to the identification of the best labeling strategy and the most efficient HL / iron concentration, hybrid templates covalently conjugated with 1 mM HL (COL-HL-CHC) showed a strong contrast in T_1-weighted MR images (**Figure 1F**). The collagen component of the hybrid templates was clearly distinguishable from the surrounding tissue phantom and allowed the visualization of the integrated CHC (the negative contrast of CHC shown in MR images). In the unlabeled hybrid templates (COL-CHC), only the CHC was visible, while the collagen component could not be distinguished from the surrounding tissue phantom (**Figure 1F**). R_1 and CNR values

of the labeled hybrid templates were significantly higher compared to unlabeled templates ($p < 0.0001$; see **Table 1**, Day 0).

To the best of our knowledge, this is the first time that an MRI examination of a hybrid template, for Tissue Engineering and Regenerative Medicine (TERM) purposes, enabled to visualize both collagen type I (the cellular stratum) labeled with a naturally-derived CA giving positive contrast and the CHC (the supportive polymer) giving negative contrast with respect to surrounding tissue. Similar to our approach, Gd has been used to monitor tissue-engineered templates, albeit very limited [36,37]. However, Gd is associated with a risk of nephrogenic systemic fibrosis, and there have also been concerns about the deposition of Gd in the body after repetitive use [22,38]. The degradation of heavily Gd labeled collagen scaffolds might lead to systemic Gd exposure. On the contrary, hemin and L-lysine are both natural compounds, and thus the corresponding degradation products are not anticipated to have adverse effects.

3.3 Template Porosity, (Bio)mechanical Properties and Cytocompatibility

HL-labeled templates showed the same porous honeycomb collagen architecture with no changes in pore perimeter (**Figure 1G**) when compared to COL-alone templates (compare **Figures 1B-iv,v** with **Figures 1D-iv,v**). A porous structure is essential and plays a key-role in cellular/tissue ingrowth into the template as well is crucial for vascularization, diffusion of nutrients, metabolites and waste products [39,40].

When (bio)mechanical properties were evaluated, a significant increase in compressive strength was observed for covalently conjugated collagen templates (**Appendix A7**, Pearson correlation coefficient $r = 0.9591$, $p = 0.0025$) when compared to physically adsorbed collagen templates (Pearson correlation coefficient $r = 0.7164$, $p = 0.19092$). This significant enhancement in the stiffness of covalently conjugated COL-HL might be related to the conjugation of an increased amount of material (HL) compared to COL alone and physically adsorbed COL-HL. Template stiffness is known to have an effect on cell behavior as mechanical cues play a role in cell fate [41]. However, whether the increase in collagen stiffness is of importance in hybrid templates is questionable, because overall strength and structural integrity are dictated by this supportive structure [17]. For labeled- (COL-HL-CHC) and unlabeled- (COL-CHC) hybrid templates, a 'J'-shaped stress-strain behavior (**Appendix A3A**) was observed, which is typical for soft tissues. Initial moduli E1 were $26 \pm 3 \times 10^{-3}$ MPa

for the unlabeled and 44 ± 22 x 10^{-3} MPa for the labeled template, respectively. The upswing (Young`s) moduli E2 were 1.0 ± 0.2 MPa and 1.2 ± 0.3 MPa for the unlabeled collagen templates and the labeled templates, respectively (**Appendix A3B**). Consequently, no significant differences in overall strength were found between COL-HL-CHC and COL-CHC hybrids (E1: p = 0.0930; E2: p = 0.3015). Furthermore, ultimate tensile strength (COL-CHC: 0.5 ± 0.2 MPa; COL-HL-CHC: 0.7 ± 0.3 MPa) and failure strain (COL-CHC: 1.35 ± 0.12 mm/mm; COL-HL-CHC: 1.43 ± 0.11 mm/mm) were similar between labeled- and unlabeled templates (**Figure 1H**). Thus, active labeling of COL-CHC with HL did not change the basic characteristics of the hybrid templates.

In a final set of *in vitro* experiments, cytocompatibility and cellular outgrowth were evaluated. Supernatants from unlabeled and labeled templates incubated in culture media did not show any cytotoxic effects on NIH 3T3 fibroblasts (**Appendix A4**). Furthermore, these cells attached and proliferated when seeded on COL and COL-HL templates with no significant differences between both groups (**Figure 1I**). Initial values (Day 0) for nanogram double-stranded DNA (ds-DNA) per mg template were 16.8 ± 9.3 and 15.3 ± 8.1 for COL and COL-HL, respectively. At day 7 post seeding, the DNA content increased significantly when compared with day 0 ($P < 0.0001$). The DNA contents were 94.0 ± 10.5 nanogram ds DNA per mg for COL and 99.4. ± 38.5 nanogram ds DNA per mg for COL-HL (not significant). Thus, active HL-labeling did not influence cell adhesion and proliferation *in vitro*.

3.4 *In vivo* MRI of Hybrid Templates

Table 1. Relaxation rate R_1 (n = 6), contrast-to-noise-ratio CNR (n= 6) and volume measurement (n = 6) of implanted hybrid collagen type I templates covalently conjugated (COL-HL-CHC) or unlabeled (COL-CHC) with hemin-L-lysine over time. Data are expressed as mean ± standard deviation. Two-tailed Student's t-test was performed to determine statistical differences. $P < 0.05$ was considered statistically significant. * = $p < 0.05$ compared to COL-CHC; ** = $p < 0.01$ compared to COL-CHC. *** = $p < 0.0001$ compared to COL-CHC.

		Day 0	Week 2	Week 4	Week 12
R_1 [s^{-1}]					
	COL-CHC	0.36 ± 0.04	0.41 ± 0.03	0.41 ± 0.07	0.51 ± 0.07
	COL-HL-CHC	0.62 ± 0.07***	0.57 ± 0.08**	0.57 ± 0.05**	0.64 ± 0.09*
CNR [-]					
	COL-CHC	5.1 ± 3.9	9.9 ± 5.3	3.4 ± 2.2	7.1 ± 3.7
	COL-HL-CHC	49.6 ± 6.5***	37.0 ± 11.5**	31.0 ± 9.1**	25.9 ± 14.1*
Template Volume [mm^3]					
	COL-HL-CHC	57.0 ± 7.5	32.6 ± 7.5	27.3 ± 8.5	30.2 ± 7.4

To study whether covalently conjugated collagen templates could be visualized *in vivo*, COL-CHC and COL-HL-CHC patches were subcutaneously implanted in immune competent BALB/c mice. Immediately after transplantation MRI revealed a strong signal / contrast of the labeled hybrid (COL-HL-CHC) patch which could easily be delineated from the surrounding tissue. Within the hybrid structure, the labeled collagen component could be distinguished with its bright contrast from the polymeric coupled helical coil (CHC) structure with negative contrast. In contrast, the collagen component of the unlabeled hybrid (COL-CHC) patch could not be identified by MRI, and only the CHC polymer was visible as an anatomical guide (**Figure 2**). At all evaluation points, T_1 relaxation rate (R_1) values of COL-HL-CHC were significantly higher than those for COL-CHC (**Table 1**). Also, the CNR was significantly higher for COL-HL-CHC. Identical ROI were selected for the T_1 and CNR values and the hyperintense area of the T_1 weighted MRI was selected. The average volume of the implanted COL-HL-CHC templates was 57.0 ± 7.5 mm^3 at day 0 as determined visually on the T_1 weighted images. This volume decreased to approximately 55% of its initial value at 2 weeks post-implantation. No further decrease in template volume was observed until the end of the experiment. The MRI contrast in close vicinity to the embedded polymer was decreasing, suggesting remodeling and/or loss of COL-HL-CHC material. For COL-CHC, accurate volume measurements were not feasible due to lack of contrast, which demonstrates that the covalent conjugation of HL to collagen templates is essential for their longitudinal assessment by MRI.

Whereas the template volume decreased over time, MR signal and gross morphology of the implanted templates were stable over time. This correlated very well with the histological evaluation of the implants: the template was still intact with no macroscopic signs of resorption, suggesting that the molecular modification permitted adequate monitoring of the template. In similar studies, USPIOs were passively entrapped within collagen templates and subcutaneously implanted or implanted on the bladder wall to monitor template integrity and remodeling [12,13]. Passive entrapment of USPIOs correlated well with template remodeling in early time points (e.g. 22 days) [13]. However, ultimately MR images did not correlate with the template anymore because the entrapped USPIO were washed out. Also, USPIO washout is heavily dependent on the site of implantation [12]. This site dependency is less likely to play a dominant role here on the COL-HL templates, as the density-generating contrast agent HL is covalently conjugated to the collagen template.

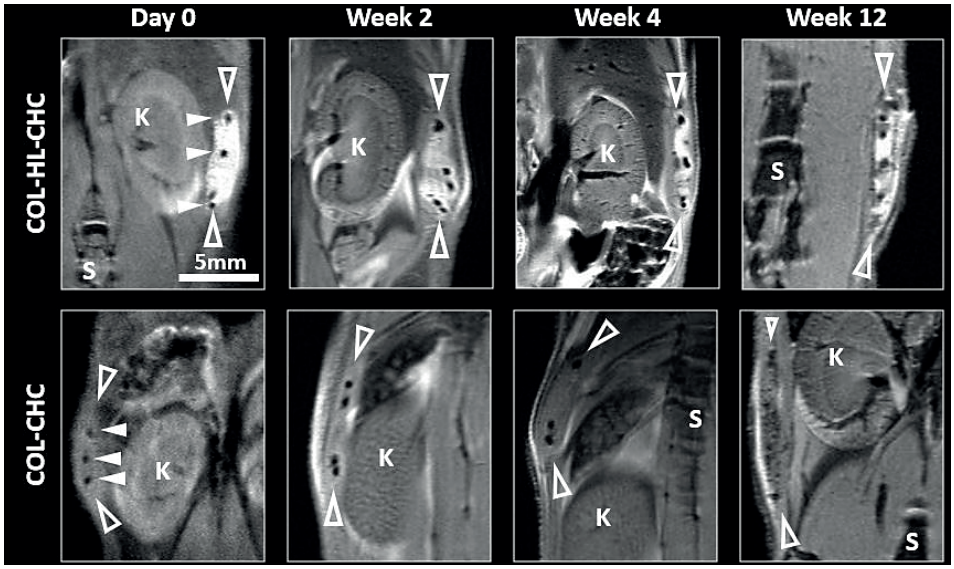

Figure 2. Coronal T_1-weighted MR images of subcutaneously implanted COL-CHC and COL-HL-CHC templates obtained by a 11.7T preclinical MRI system (BioSpec, Bruker, Germany) with ^1H volume coil (ID = 40mm) via T_1 RARE sequence (T_E = 10 ms, T_R = 560 ms, RARE factor = 2, number of slices = 20, slice thickness = 0.5 mm, FOV = 50 × 50 mm, matrix size = 512 × 512 and 16 averages). Scale bar = 5 mm. Transparent arrows indicate the subcutaneously implanted template. Please note the similar MR image intensities of unmodified collagen template. Filled arrows indicate the CHC component within COL at day 0, Week 2, 4 and 12 respectively. K = Kidney. S = Spine.

3.5 Phenotypic Analysis of Excised Templates

Representative images and the scoring of inflammatory cells in excised implants are presented in **Figures 3-5** and **Table 2**, respectively. At 2 weeks post-implantation (**Figure 3**), lymphocytes, polymorphonuclear lymphocytes (PMNs) and fibroblasts were observed within all templates, regardless of whether HL was incorporated or not. Additionally, giant cells appeared in COL-HL-CHC. At this time point, no major differences in template remodeling and deposition of new extracellular matrix (ECM) within the template architecture were observed in both groups. (**Appendix A5, Figure 3A-i** and **Figure 3B-i**). Furthermore, the amount of F4/80 positive macrophages for labeled- and unlabeled- templates were similar (**Figure 3A-ii** for COL-CHC and **Figure 3B-ii** for COL-HL-CHC). COL-CHC and COL-HL-CHC were surrounded by a fibrous, well-vascularized capsule (**Figure 3A-iii** and **Figure 3B-iii**). Mature blood vessels as judged by Cluster of Differentiation 31 (CD31) and alpha smooth muscle actin (α-SMA) were found mainly at the template periphery (see **Appendix A6** and **Figure 3A-iv, Figure 3B-iv**).

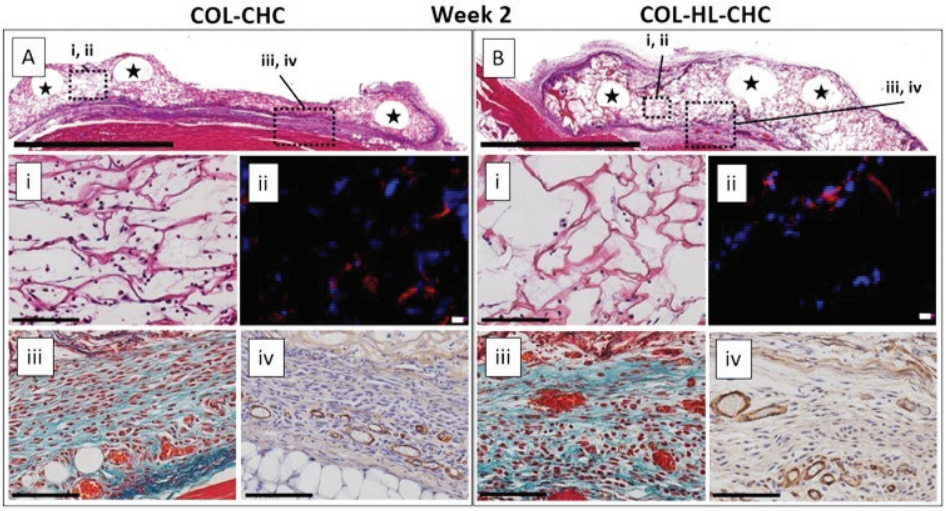

Figure 3. (Immuno-)histochemistry of excised subcutaneously implanted COL-CHC (A, i-iv) and COL-HL-CHC (B, i-iv) 2 weeks after implantation. A,B) Template overview, Hematoxyline / Eosine staining (scale bar = 2 mm). Boxes correspond to areas shown in A,B i-iv, stars indicate the CHC polymer within the collagen template architecture. A,B-i) HE staining of the template center (scale bar = 200 micron). A,B-ii) Macrophage staining (F4/80) in red, cell nuclei in blue (scale bar = 10 micron). A,B-iii) Masson Trichrome / Verhoeff staining in template periphery (scale bar = 200 micron). A,B-iv) Alpha-smooth muscle actin staining, to indicate blood vessels, in template periphery (scale bar = 200 micron).

At 4 weeks post-implantation (**Figure 4**), cell ingrowth (**Appendix A5**), template remodeling and deposition of extracellular matrix appeared to be more pronounced for the COL-HL-CHC template as evaluated by Masson Trichrome / Verhoeff staining (**Figure 4A-i, 4B-i**). Additionally, more α-SMA positive cells were observed within COL-HL-CHC templates (compare **Figure 4A-ii** with **Figure 4B-ii**). Despite this enhanced remodeling, the templates' scaffold structures remained intact, and the thickness of the fibrous tissue capsule at the periphery of both templates decreased (**Figure 4A-iii** for COL-CHC and **Figure 4B-iii** for COL-HL-CHC). No difference in vascularization between COL-CHC and COL-HL-CHC was detected (**Figure 4A-iv, 4B-iv**) and similar macrophage infiltration was observed in both templates as indicated by F4/80 positive cells (**Figure 4A-v** and **4B-v**). Moreover, no signs of structural degradation of the CHC in both templates were noticed (**Figure 4A-vi** and **4B-vi**).

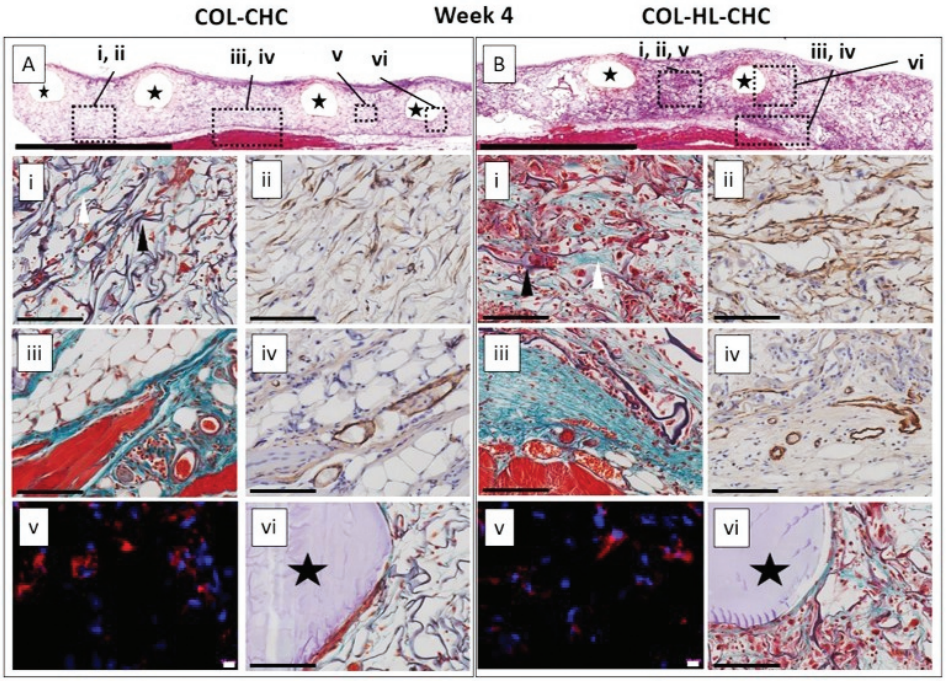

Figure 4. (Immuno-)histochemistry of excised subcutaneously implanted COL-CHC (A, A-i-vi) and COL-HL-CHC (B, B-i-vi) 4 weeks after implantation. A,B) Template overview, Hematoxyline / Eosine staining (scale bar 2 mm). Boxes correspond to areas shown in A,B-i-vi, stars indicate the CHC polymer within the collagen template architecture. A,B-i) Masson Trichrome / Verhoeff staining. Black arrow heads indicate template architecture. White arrow heads indicate newly formed collagen fibrils within the template architecture (scale bar = 200 micron). A,B-ii) Alpha-smooth muscle actin staining of the template center (scale bar = 200 micron). A,B-iii) Masson Trichrome / Verhoeff staining of the template periphery (scale bar = 200 micron). A,B-iv) Alpha-smooth muscle actin staining, to indicate blood vessels, of the template periphery (scale bar = 200 micron). A,B-v) Macrophage staining (F4/80) in red, cell nuclei in blue (scale bar = 10 micron). A,B-vi) Masson Trichrome / Verhoeff staining of the CHC imbedded in collagen (scale bar = 200 micron).

At 12 weeks post-implantation (**Figure 5**), Masson Trichrome / Verhoeff staining revealed the presence of more ECM in the COL-HL-CHC group (**Figure 5A-i** for COL-CHC; **Figure 5B-i** for COL-HL-CHC). More newly formed mature blood vessels (**Appendix A6**) appeared to be present in and around the COL-HL-CHC templates (COL-CHC: 4 ± 2 blood vessels /mm^2; COL-HL-CHC: 7 ± 3 blood vessels /mm^2, **Figure 5A-ii,iv, 5B-ii,iv**), albeit this difference was not significant (P=0.11). In addition, the fibrous capsule surrounding the template was further diminished compared to earlier time points. Only a thin ECM-rich layer was observed between the musculature and the template (**Figure 5: A-iii** and **B-iii**). Also, no difference in

macrophage infiltration was observed between COL-CHC and COL-HL-CHC (**Figure 5A-v** and **5B-v**). Structural degradation of the CHC in both templates started to occur (**Figure 5A-vi** and **5B-vi**).

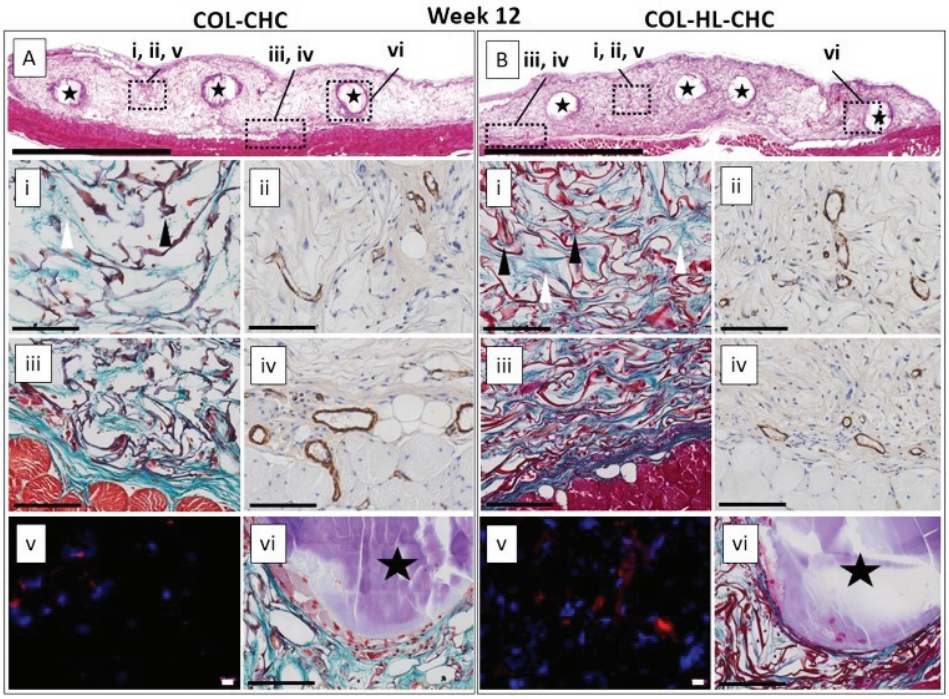

Figure 5. (Immuno-)histochemistry of excised subcutaneously implanted COL-CHC (A, A-i-vi) and COL-HL-CHC (B, B-i-vi) 12 weeks after implantation. A,B) Template overview, Hematoxyline / Eosine staining (scale bar 2 mm). Boxes correspond to areas shown in A,B-i-vi, stars indicate the CHC polymer within the collagen template architecture. A,B-i) Masson Trichrome / Verhoeff staining. Black arrow heads indicate template architecture. White arrow heads indicate newly formed collagen fibrils within the template architecture (scale bar 200 miron). A,B-ii) Alpha-smooth muscle actin staining of the template center to indicate blood vessel formation (scale bar = 200 micron). A,B-iii) Masson Trichrome / Verhoeff staining of the template periphery (scale bar = 200 micron). A,B-iv) Alpha-smooth muscle actin staining, to indicate blood vessels, of the template periphery (scale bar = 200 micron). A,B-v) Macrophage staining (F4/80) in red, cell nuclei in blue (scale bar = 10 micron). A,B-vi) Masson Trichrome / Verhoeff staining of the CHC imbedded in collagen (scale bar = 200 micron).

Collectively, at the last time point of evaluation (12 weeks) cell density in COL-HL-CHC templates was higher and cells produced more ECM, and vascularization appeared to be more pronounced compared to unlabeled hybrids. This may be because more inflammatory cells were present within the COL-HL-CHC as a consequence of more foreign (bio)material (e.g. iron) that was implanted [12,42].

Subsequently, more myofibroblast formation was observed within COL-HL-CHC 4 weeks after implantation as evidenced by the expression of smooth muscle actin. Myofibroblasts play a crucial role in ECM production as well as they guide and mediate neo-vascularization [43,44]. It is possible that myofibroblasts were activated by the inflammatory signals provided by the inflammatory cells [45]. Since oxygen affinity is driven by hemin [46], enhanced oxygenation may have occured within COL-HL-CHC templates. This may also have contributed to enhanced ECM production and vascularization. In general, the faster template remodeling may ultimately be beneficial since both ECM production and vascularization within templates are pivotal in TERM to guarantee functionality and ultimately prevent template failure [47–49].

Table 2. Cellular content and remodelling of harvested templates after subcutaneous implantation in a mouse model. Scoring was performed based on Hematoxyline / Eosine (HE) and Masson Trichrome / Verhoeff slides of implanted COL-HL-CHC and COL-CHC templates. – (not present), +/- (sporadically present), + (moderately present) or ++ (abundantly present).

		COL-CHC	COL-HL-CHC
Macrophages	Week 2	+/-	+/-
	Week 4	+	+
	Week 12	+/-	+/-
Giant cells	Week 2	-	+
	Week 4	+/-	+
	Week 12	+/-	+/-
PMN	Week 2	+	+/-
	Week 4	-	+
	Week 12	-	-
Lymphocytes	Week 2	+	+
	Week 4	+/-	+
	Week 12	+/-	+/-
Vascularity	Week 2	-	+/-
	Week 4	+/-	+/-
	Week 12	+/-	+
(Myo)fibroblasts	Week 2	+/-	+/-
	Week 4	+	++
	Week 12	-	+/-
ECM deposition	Week 2	+/-	+/-
	Week 4	+	++
	Week 12	+	++

4 CONCLUSION

In conclusion, we show that collagen type I hybrid templates can easily and covalently conjugated with the hemin-L-lysine complex (HL). This allows the non-invasive monitoring of the localization and remodeling of the template *in vivo*. For future applications full characterisation of the relaxivity properties at different field strengths for both, HL and template conjugates, may required to optimise these properties and better understand the contrast properties observed.

We found a close correlation between the acquired MR images and the histological findings. The covalent conjugation of HL did not alter the main structural properties in the hybrid templates, and initial cell attachment *in vitro* and *in vivo* was unaffected. Furthermore, the observed improvements in the cell penetration and colonization of HL-labeled templates indicate that the HL content may also support the template remodeling *in vivo*. Hence, the presence of HL can assist the visibility and integration performance of tissue-engineered constructs.

5 ACKNOWLEDGEMENTS

The authors would like to thank Dr. Simone Mastrogiacomo, Andor Veltien, Bianca Lemmers–van den Weem, and Dr. Larissa Y. Rizzo for technical support.

The research leading to these results received funding from the People Programme (Marie Curie Actions) of the European Union's Seventh Framework Programme FP7/2007-2013/ under REA grant agreement No. 607868 (iTERM).

N.G., P.J.A.B., F.K., and J.G.O.C. filed patent EP3295962A1, WO2018050450A1 for the use of tetrapyrroles conjugates as MRI contrast agent.

6 REFERENCES

[1] R. Langer, J.P. Vacanti, Tissue engineering., Science. 260 (1993) 920–6. DOI: 10.1126/science.8493529.

[2] S.J. Hollister, Scaffold design and manufacturing: from concept to clinic., Adv. Mater. 21 (2009) 3330–42. DOI:10.1002/adma.200802977.

[3] F.J. O'Brien, Biomaterials & scaffolds for tissue engineering, Mater. Today. 14 (2011) 88–95. DOI:10.1016/S1369-7021(11)70058-X.

[4] T. Kloskowski, A. Jundzill, T. Kowalczyk, M. Nowacki, M. Bodnar, A. Marszalek, M. Pokrywczynska, M. Frontczak-Baniewicz, T.A. Kowalewski, P. Chlosta, T. Drewa, Ureter regeneration-the proper scaffold has to be defined., PLoS One. 9 (2014) e106023. DOI:10.1371/journal.pone.0106023.

[5] M. Sloff, V. Simaioforidis, D.M. Tiemessen, H.P. Janke, B.B.M. Kortmann, L.A.J. Roelofs, P.J. Geutjes, E. Oosterwijk, W.F.J. Feitz Prof, Tubular constructs as artificial urinary conduits., J. Urol. (2016). DOI:10.1016/j.juro.2016.04.092.

[6] J.C. Chan, K. Burugapalli, Y.-S. Huang, J.L. Kelly, A. Pandit, A clinically relevant *in vivo* model for the assessment of scaffold efficacy in abdominal wall reconstruction, J. Tissue Eng. 8 (2017) 204173141668653. DOI:10.1177/2041731416686532.

[7] M. Ventura, O.C. Boerman, C. de Korte, M. Rijpkema, A. Heerschap, E. Oosterwijk, J.A. Jansen, X.F. Walboomers, Preclinical imaging in bone tissue engineering., Tissue Eng. Part B. Rev. 20 (2014) 578–95. DOI:10.1089/ten.TEB.2013.0635.

[8] M. Ventura, Y. Sun, V. Rusu, P. Laverman, P. Borm, A. Heerschap, E. Oosterwijk, O.C. Boerman, J.A. Jansen, X.F. Walboomers, Dual contrast agent for computed tomography and magnetic resonance hard tissue imaging., Tissue Eng. Part C. Methods. 19 (2013) 405–16. DOI:10.1089/ten.tec.2012.0007.

[9] S. Mastrogiacomo, N. Güvener, W. Dou, H.S. Alghamdi, W.A. Camargo, J.G.O. Cremers, P.J.A. Borm, A. Heerschap, E. Oosterwijk, J.A. Jansen, X.F. Walboomers, A theranostic dental pulp capping agent with improved MRI and CT contrast and biological properties, Acta Biomater. 62 (2017) 340–351. DOI:10.1016/j.actbio.2017.08.018.

[10] S. Mastrogiacomo, W. Dou, O. Koshkina, O.C. Boerman, J.A. Jansen, A. Heerschap, M. Srinivas, X.F. Walboomers, Perfluorocarbon/Gold Loading for Noninvasive *in Vivo* Assessment of Bone Fillers Using 19F Magnetic Resonance Imaging and Computed Tomography., ACS Appl. Mater. Interfaces. 9 (2017) 22149–22159. DOI:10.1021/acsami.7b04075.

[11] A.B. Shekhter, A.L. Fayzullin, M.N. Vukolova, T.G. Rudenko, V.D. Osipycheva, P.F. Litvitsky, Medical applications of collagen and collagen-based materials, Curr. Med. Chem. 25 (2017). DOI:10.2174/0929867325666171205170339.

[12] Y. Sun, P. Geutjes, E. Oosterwijk, A. Heerschap, *In vivo* magnetic resonance imaging of type I collagen scaffold in rat: improving visualization of bladder and subcutaneous implants., Tissue Eng. Part C. Methods. 20 (2014) 964–71. DOI:10.1089/ten.TEC.2014.0046.

[13] M.E. Mertens, A. Hermann, A. Buhren, L. Olde-Damink, D. Mockel, F. Gremse, J. Ehling, F. Kiessling, T. Lammers, Iron Oxide-labeled Collagen Scaffolds for Non-invasive MR Imaging in Tissue Engineering, Adv Funct Mater. 24 (2014) 754–762. DOI:10.1002/adfm.201301275.

[14] F. Kiessling, M.E. Mertens, J. Grimm, T. Lammers, Nanoparticles for imaging: top or flop?, Radiology. 273 (2014) 10–28. DOI:10.1148/radiol.14131520.

[15] S.J. Lee, J. Liu, S.H. Oh, S. Soker, A. Atala, J.J. Yoo, Development of a composite vascular scaffolding system that withstands physiological vascular conditions., Biomaterials. 29 (2008) 2891–8. DOI:10.1016/j.biomaterials.2008.03.032.

[16] K.M. Brouwer, W.F. Daamen, H.R. Hoogenkamp, P.J. Geutjes, I. de Blaauw, W. Janssen-Kessels, W. de Boode, E. Versteeg, R.M. Wijnen, W.F. Feitz, M. Wijnen, T.H. van Kuppevelt, Collagen-Vicryl scaffolds for reconstruction of the diaphragm in a large animal model., J. Biomed. Mater. Res. B. Appl. Biomater. 102 (2014) 756–63. DOI: 10.1002/jbm.b.33056.

[17] H.P. Janke, J. Bohlin, R.M.L.M. Lomme, S.M. Mihaila, J. Hilborn, W.F.J. Feitz, E. Oosterwijk, Bioinspired coupled helical coils for soft tissue engineering of tubular structures – Improved mechanical behavior of tubular collagen type I templates, Acta Biomater. 59 (2017) 234–242. DOI:10.1016/j.actbio.2017.06.038.

[18] N.L. Hansen, A. Barabasch, M. Distelmaier, A. Ciritsis, N. Kuehnert, J. Otto, J. Conze, U. Klinge, R.-D. Hilgers, C.K. Kuhl, N.A. Kraemer, First In-Human Magnetic Resonance Visualization of Surgical Mesh Implants for Inguinal Hernia Treatment, Invest. Radiol. 48 (2013) 770–778. DOI:10.1097/RLI.0b013e31829806ce.

[19] F.-L. Zhou, P.L. Hubbard, S.J. Eichhorn, G.J.M. Parker, Coaxially Electrospun Axon-Mimicking Fibers for Diffusion Magnetic Resonance Imaging, ACS Appl. Mater. Interfaces. 4 (2012) 6311–6316. DOI:10.1021/am301919s.

[20] J. Bouley, M. Fisher, N. Henninger, Comparison between coated vs. uncoated suture middle cerebral artery occlusion in the rat as assessed by perfusion/diffusion weighted imaging., Neurosci. Lett. 412 (2007) 185–90. DOI:10.1016/j.neulet.2006.11.003.

[21] L. Pasquini, A. Napolitano, E. Visconti, D. Longo, A. Romano, P. Tomà, M.C.R. Espagnet, Gadolinium-Based Contrast Agent-Related Toxicities, CNS Drugs. 32 (2018) 229-240. DOI:10.1007/s40263-018-0500-1.

[22] E. Di Gregorio, R. Iani, G. Ferrauto, R. Nuzzi, S. Aime, E. Gianolio, Gd accumulation in tissues of healthy mice upon repeated administrations of Gadodiamide and Gadoteridol, J. Trace Elem. Med. Biol. 48 (2018) 239–245. DOI:10.1016/j.jtemb.2018.04.018.

[23] H.-L.M. Cheng, I.E. Haedicke, W. Cheng, J. Tchouala Nofiele, X. Zhang, Gadolinium-free T1 contrast agents for MRI: tunable pharmacokinetics of a new class of manganese porphyrins., J. Magn. Reson. Imaging. 40 (2014) 1474–80. DOI:10.1002/jmri.24483.

[24] F. Bryden, R.W. Boyle, Metalloporphyrins for Medical Imaging Applications, in: 2016: pp. 141–221. DOI:10.1016/bs.adioch.2015.09.003.

[25] C. Rimington, Porphyrins and Their Relation to the Metabolism of Blood Pigments: (Section of Therapeutics and Pharmacology)., Proc. R. Soc. Med. 32 (1939) 1268–75. PMID: 19992067.

[26] G.D. Ingberg, R.L.A. Penttila, R.O. Tokola, R. Tenhunen, Process for preparation of a new hemin complex, (1991). https://patents.google.com/patent/US5008388A/en. Accessed: 4th of April, 2019.

[27] D. Tiemessen, P. de Jonge, W. Daamen, W. Feitz, P. Geutjes, E. Oosterwijk, The effect of a cyclic uniaxial strain on urinary bladder cells, World J. Urol. 35 (2017) 1531–1539. DOI:10.1007/s00345-017-2013-9.

[28] J.S. Pieper, A. Oosterhof, P.J. Dijkstra, J.H. Veerkamp, T.H. van Kuppevelt, Preparation and characterization of porous crosslinked collagenous matrices containing bioavailable chondroitin sulphate., Biomaterials. 20 (1999) 847–58. DOI: 10.1016/S0142-9612(98)00240-3.

[29] L.H. Olde Damink, P.J. Dijkstra, M.J. van Luyn, P.B. van Wachem, P. Nieuwenhuis, J. Feijen, Cross-linking of dermal sheep collagen using a water-soluble carbodiimide, Biomaterials. 17 (1996) 765–773. DOI: 10.1016/0142-9612(96)81413-X.

[30] L.R. Versteegden, H.R. Hoogenkamp, R.M. Lomme, H. van Goor, D.M. Tiemessen, P.J. Geutjes, E. Oosterwijk, W.F. Feitz, T.G. Hafmans, N. Verdonschot, W.F. Daamen, T.H. van Kuppevelt, Design of an elasticized collagen scaffold: A method to induce elasticity in a rigid protein., Acta Biomater. 44 (2016) 277–85. DOI:10.1016/j.actbio.2016.08.038.

[31] van Susante JLC, J. Pieper, P. Buma, T.H. van Kuppevelt, H. van Beuningen, P.M. van Der Kraan, J.H. Veerkamp, W.B. van den Berg, Veth RPH, Linkage of chondroitin-sulfate to type I collagen scaffolds stimulates the bioactivity of seeded chondrocytes *in vitro*., Biomaterials. 22 (2001) 2359–69. DOI: 10.1016/S0142-9612(00)00423-3.

[32] J.S. Pieper, T. Hafmans, P.B. van Wachem, M.J.A. van Luyn, L.A. Brouwer, J.H. Veerkamp, T.H. van Kuppevelt, Loading of collagen-heparan sulfate matrices with bFGF promotes angiogenesis and tissue generation in rats, J. Biomed. Mater. Res. 62 (2002) 185–194. DOI:10.1002/jbm.10267.

[33] J.D. Boerckel, Y.M. Kolambkar, K.M. Dupont, B.A. Uhrig, E.A. Phelps, H.Y. Stevens, A.J. García, R.E. Guldberg, Effects of protein dose and delivery system on BMP-mediated bone regeneration, Biomaterials. 32 (2011) 5241–5251. DOI:10.1016/j.biomaterials.2011.03.063.

[34] H. SUN, J. WANG, F. DENG, Y. LIU, X. ZHUANG, J. XU, L. LI, Co-delivery and controlled release of stromal cell-derived factor-1α chemically conjugated on collagen scaffolds enhances bone morphogenetic protein-2-driven osteogenesis in rats, Mol. Med. Rep. 14 (2016) 737–745. DOI:10.3892/mmr.2016.5339.

[35] P. Boehm-Sturm, A. Haeckel, R. Hauptmann, S. Mueller, C.K. Kuhl, E.A. Schellenberger, Low-Molecular-Weight Iron Chelates May Be an Alternative to Gadolinium-based Contrast Agents for T1-weighted Contrast-enhanced MR Imaging, Radiology. 286 (2018) 537–546. DOI:10.1148/radiol.2017170116.

[36] C.P. Neu, H.F. Arastu, S. Curtiss, A.H. Reddi, Characterization of engineered tissue construct mechanical function by magnetic resonance imaging., J. Tissue Eng. Regen. Med. 3 (2009) 477–85. DOI:10.1002/term.188.

[37] W. Sun, Y. Sun, A.S. Klar, P. Geutjes, E. Reichmann, A. Heerschap, E. Oosterwijk, Functional Analysis of Vascularized Collagen/Fibrin Templates by MRI *In Vivo*., Tissue Eng. Part C. Methods. 22 (2016) 747–55. DOI:10.1089/ten.TEC.2016.0035.

[38] H. Malikova, M. Holesta, Gadolinium contrast agents – are they really safe?, J. Vasc. Access. 18 (2017) 1–7. DOI:10.5301/jva.5000713.

[39] J. Rnjak-Kovacina, A.S. Weiss, Increasing the Pore Size of Electrospun Scaffolds, Tissue Eng. Part B Rev. 17 (2011) 365–372. DOI:10.1089/ten.teb.2011.0235.

[40] F. Kunz, C. Bergemann, E.-D. Klinkenberg, A. Weidmann, R. Lange, U. Beck, J.B. Nebe, A novel modular device for 3-D bone cell culture and non-destructive cell analysis, Acta Biomater. 6 (2010) 3798–3807. DOI:10.1016/J.ACTBIO.2010.03.015.

[41] S.J. Mousavi, M. Hamdy Doweidar, Role of Mechanical Cues in Cell Differentiation and Proliferation: A 3D Numerical Model, PLoS One. 10 (2015) e0124529. DOI:10.1371/journal.pone.0124529.

[42] J.D. Brain, S.B. Bloom, P.A. Valberg, P. Gehr, Correlation between the behavior of magnetic iron oxide particles in the lungs of rabbits and phagocytosis., Exp. Lung Res. 6 (1984) 115–31. PMID: 6745211.

[43] B. Hinz, S.H. Phan, V.J. Thannickal, A. Galli, M.-L. Bochaton-Piallat, G. Gabbiani, The myofibroblast: one function, multiple origins., Am. J. Pathol. 170 (2007) 1807–16. DOI:10.2353/ajpath.2007.070112.

[44] W.W. Kilarski, B. Samolov, L. Petersson, A. Kvanta, P. Gerwins, Biomechanical regulation of blood vessel growth during tissue vascularization, Nat. Med. 15 (2009) 657–664. DOI:10.1038/nm.1985.

[45] T.A. Wynn, T.R. Ramalingam, Mechanisms of fibrosis: therapeutic translation for fibrotic disease, Nat. Med. 18 (2012) 1028–1040. DOI:10.1038/nm.2807.

[46] Y. Wu, A. Dean, W. Egan, A.N. Schechter, Control of oxygen affinity of hemoglobin in K562 cells induced by hemin., Blood. 63 (1984) 1447–52. PMID: 6202345.

[47] J.P. Vacanti, R. Langer, Tissue engineering: the design and fabrication of living replacement devices for surgical reconstruction and transplantation., Lancet (London, England). 354 Suppl 1 (1999) SI32-4. DOI: 10.1016/s0140-6736(99)90247-7.

[48] J. Rouwkema, N.C. Rivron, C.A. van Blitterswijk, Vascularization in tissue engineering, Trends Biotechnol. 26 (2008) 434–441. DOI:10.1016/j.tibtech.2008.04.009.

[49] N.C. Rivron, C.C. Raiss, J. Liu, A. Nandakumar, C. Sticht, N. Gretz, R. Truckenmüller, J. Rouwkema, C.A. van Blitterswijk, Sonic Hedgehog-activated engineered blood vessels enhance bone tissue formation., Proc. Natl. Acad. Sci. U. S. A. 109 (2012) 4413–8. DOI:10.1073/pnas.1117627109.

APPENDIX

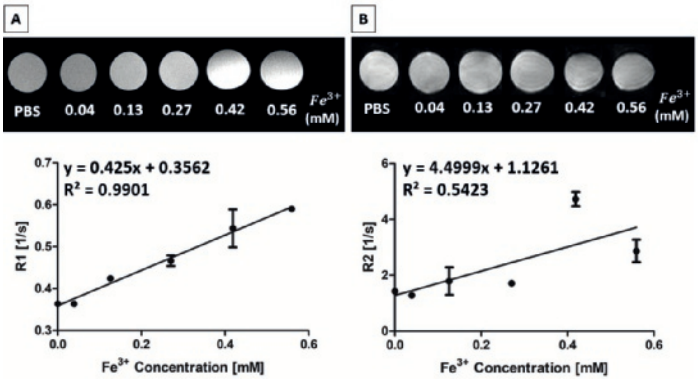

A1. Hemin-L-lysine complex (HL) and its relaxation properties in 11.7T magnetic resonance imaging (MRI). A: Qualitative T_1-weighted MRI and R_1 relaxometry analysis of HL at different (iron) concentrations in phosphate buffered saline (PBS). Data represent mean ± standard deviation (sample size n = 3). The relaxivity r_1 was derived from the slope and of the relaxation-iron concentration curve. B: Qualitative T_2-weighted MRI and R_2 relaxometry analysis of HL at different (iron) concentrations in PBS. Data represent mean ± standard deviation (sample size n = 3). The relaxivity r_2 was derived from the slope and of the relaxation-iron concentration curve.

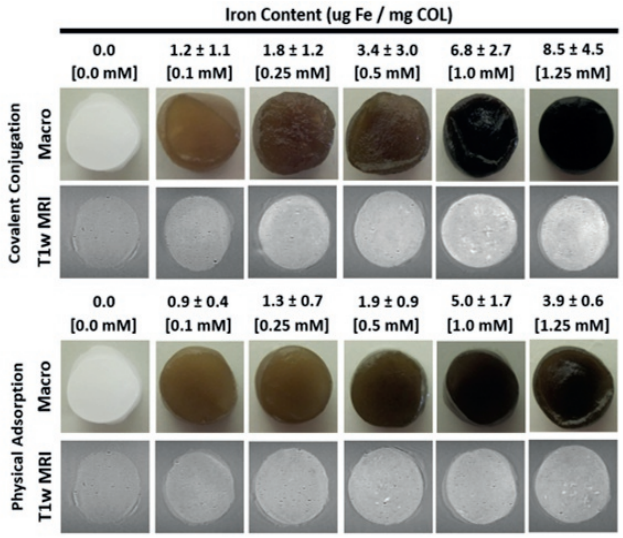

A2. Visual depiction and T_1-weigthed MRI of standard collagen type I cylinders (COL) which were covalently conjugated or physically adsorbed with hemin-L-lysine complex (HL) (initial HL concentrations are given in brackets). For covalent conjugation: incubation of collagen sponges in HL -> crosslinking / covalent conjugation via EDC/NHS -> subsequent washings; for physical adsorption: crosslinked collagen sponges -> incubation in HL -> subsequent washings. Template diameter = 14 mm. Iron content data represent mean ± standard deviation with a sample size of n = 9 of each group.

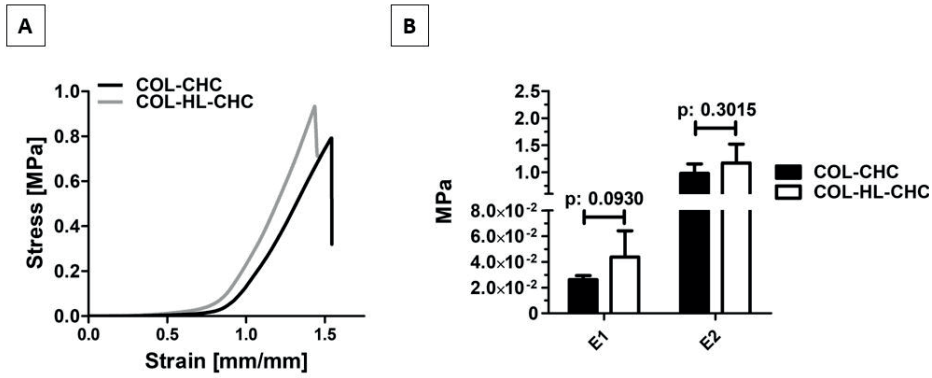

A3. Mechanical Properties of COL-HL-CHC and COL-CHC. A: Stress-strain curve of COL-CHC and COL-HL-CHC. B: Initial modulus (E1) and Upswing (Young's) modulus (E2) of COL-CHC and COL-HL-CHC derived from stress-strain curve. E1 was derived from the initial slope and E2 was derived from the 2nd slope of the stress-strain curve, respectively. Data represent mean ± standard deviation with a sample size of n = 5 of each group. Two-tailed Student's t-test was performed to determine statistical differences. $P < 0.05$ was considered statistically significant.

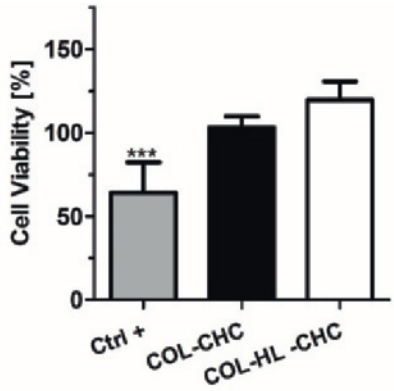

A4. Cytotoxicity / cell viability study of COL-HL-CHC and COL-CHC. Equal amounts of COL-CHC and COL-HL-CHC templates were incubated in standard culture medium for 72 h. Latex was used as positive control (Ctrl +). Subsequently, the conditioned culture media were added to NIH 3T3 cells and incubated for 24 h in these extractions. Data of cytotoxicity analysis were obtained from raw absorbance data and normalized to negative control (3T3 cells in standard culture medium). Data are expressed as mean ± standard deviation and the sample size was n = 3 for positive control (Latex), COL-CHC and COL-HL-CHC, respectively. One-way ANOVA with Bonferroni post-hoc test was performed for comparison of these 3 groups. $P < 0.05$ was considered statistically significant. *** = $p<0.0001$ compared to all other conditions.

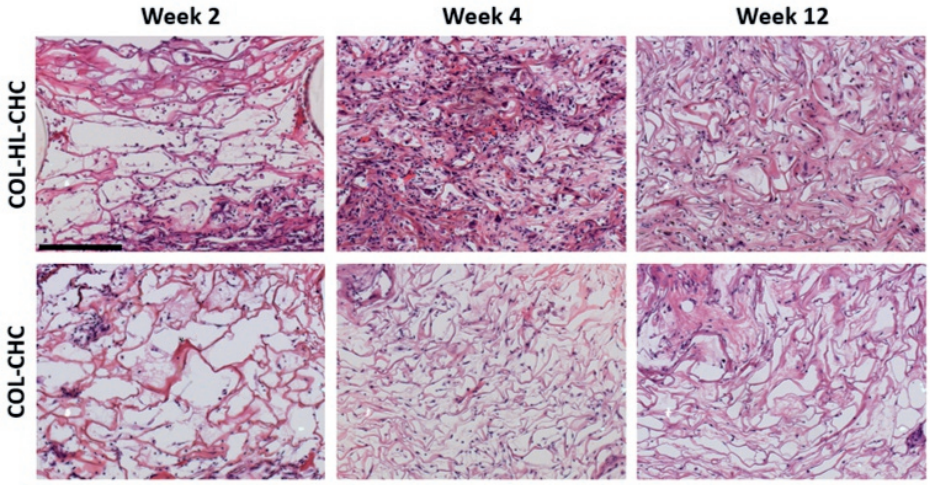

A5. Hematoxyline and Eosin (HE) staining of the template center of excised templates. Scale bar = 200 micron.

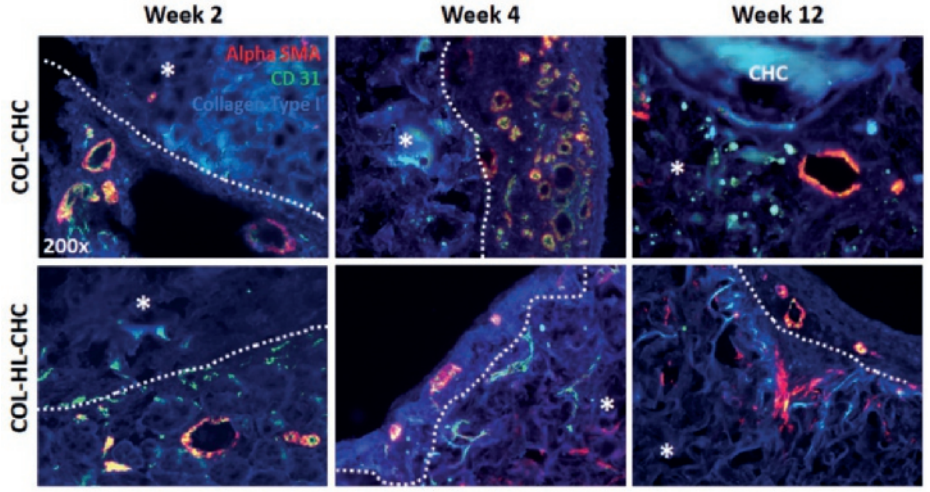

A6. (Immuno)Fluorescence histochemistry of vasculature of excised templates (200x magnification). White dotted line marks border of template and native tissue. White star marks the template center.

A7. Iron content (n = 9), free NH_2 groups (n = 3), compressive strength (n = 9), relaxation rate R_1 (n = 4) and contrast-to-noise ratio CNR (n = 4) of simple disc-shaped collagen type I templates (COL) covalently conjugated or physically adsorbed with hemin-L-lysine complex (HL). Data are expressed as mean ± standard deviation. Regression R^2, Pearson correlation coefficient r and p value (two-tailed) were determined to describe the correlation between iron concentration and free NH_2 groups / compressive strength / relaxation rate R_1 / contrast-to-noise ratio CNR of different templates. $P < 0.05$ was considered statistically significant.

0.5 % (w/v) COL Incubated in HL [mM]	Iron Content [ug Fe / mg COL]	Free NH_2 [nmol / mg COL] (% free NH_2)	Compressive Strength [N]	R_1 [s^{-1}]	CNR [-]
0.0 (Ctrl)	-	99 ± 27 (38.2±10.2%)	0.11 ± 0.04	0.34 ± 0.03	6.0 ± 3.9
Covalent Conjugation					
0.1	1.2 ± 1.1	281 ± 39 (75.1±10.3%)	0.12 ± 0.06	0.49 ± 0.07	17.7 ± 7.1
0.25	1.8 ± 1.2	304 ± 74 (74.9±18.2%)	0.13 ± 0.08	0.53 ± 0.13	27.8 ± 10.6
0.5	3.4 ± 3.0	263 ± 51 (64.7±12.6%)	0.17 ± 0.13	0.65 ± 0.18	31.0 ± 15.2
1.0	6.8 ± 2.7	267 ± 48 (53.9±9.7%)	0.18 ± 0.05	0.73 ± 0.16	49.9 ± 6.1
1.25	8.5 ± 4.5	178 ± 77 (69.7±30.2%)	0.24 ± 0.09	0.81 ± 0.11	40.0 ± 12.3
P value	-	0.9165	0.0025	0.0026	0.0182
R^2	-	0.003102	0.9200	0.9182	0.7880
Pearson (r)	-	0.05569	0.9591	0.9582	0.8877
Physical Adsorption					
0.1	0.9 ± 0.4	138 ± 47 (36.7±12.4%)	0.09 ± 0.02	0.39 ± 0.02	9.2 ± 7.9
0.25	1.3 ± 0.7	175 ± 37 (43.1±9.2%)	0.13 ± 0.04	0.43 ± 0.08	14.6 ± 15.1
0.5	1.9 ± 0.9	171 ± 42 (39.7±9.7%)	0.09 ± 0.03	0.73 ± 0.11	17.5 ± 10.4
1.0	5.0 ± 1.7	198 ± 61 (40.0±12.2%)	0.19 ± 0.11	0.63 ± 0.14	24.8± 18.0
1.25	3.9 ± 0.6	236 ± 46(92.8±18.0%)	0.15 ± 0.08	0.76 ± 0.16	23.7 ± 19.7
P value	-	0.0323	0.19092	0.0864	0.0023
R^2	-	0.7215	0.5132	0.5614	0.9232
Pearson (r)	-	0.8494	0.7164	0.7493	0.9608

CHAPTER 5

Noninvasive Magnetic Resonance Imaging Demonstrates Structural Changes of Gd-functionalized Polyisocyanopeptide Hydrogels upon Injection

H.P. Janke[1,*], J. Simo Padial[2,*], W. Dou[3,4], D.M. Tiemessen[1], K. Liu[1,2], W.F.J. Feitz[1,5], A. Rowan[2,6], A. Heerschap[3], P.H.J. Kouwer[2] and E. Oosterwijk[1]

[1]: Department of Urology – Experimental Urology, Radboud Institute for Molecular Life Science Radboud University Medical Center, Geert Grooteplein 28, 6525 GE Nijmegen, The Netherlands.
[2]: Radboud University, Institute for Molecules and Materials, Heyendaalseweg 135, 6525 AJ Nijmegen, The Netherlands.
[3]: Department of Radiology and Nuclear Medicine, Radboud University Medical Center, PO Box 9101, 6500 HB Nijmegen, The Netherlands.
[4]: GE Healthcare, MR Research China, Beijing Shi Daxing Quo 100176, China.
[5]: Radboudumc Amalia Children's Hospital, Radboud University Medical Center, Geert Grooteplein 28, 6525 GA Nijmegen, The Netherlands.
[6]: The University of Queensland, Australian Institute for Bioengineering and Nanotechnology, Brisbane, QLD 4072, Australia.
[*]: Contributed equally

Submitted

ABSTRACT

Injectable hydrogels have become valuable tools in various (bio)medical applications such as cell-, drug delivery or Tissue Engineering and Regenerative Medicine (TERM) purposes. In this context, novel synthetic thermosensitive hydrogels such as polyisocyanopeptide (PIC) have gained interest as they provide unique properties: They form a stable 3D network at room temperature closely resembling the native extracellular matrix including stiffening response at high strains. Furthermore, PIC hydrogels can be decorated with cell binding motifs and/or growth factors to increase overall biocompatibility and tissue remodeling. Monitoring of hydrogels upon their injection *in vivo* may give valuable information of their integrity and degradation. However, direct monitoring of hydrogels with non-invasive imaging modalities such as magnetic resonance imaging (MRI) remains challenging due to similar contrast characteristics when compared to surrounding tissue. In this study, we functionalized PICs hydrogels with a gadolinium-based contrast agent (PIC-GdDO3A) to enhance their MR visibility. Mixtures of functionalized PIC hydrogels containing cell binding motifs (PIC-GRGDS) were used to form hybrid gels allowing both imaging and increased biocompatibility (PIC hybrid). Upon injection *in vivo*, PIC-GdDO3A- and PIC hybrids could be monitored via MRI. Longitudinal follow up demonstrated changes in volume and consistency of the gel scaffold over time and conventional histology correlated well with the MRI results. Longitudinal, non-invasive monitoring by MRI may help to further develop smart PIC hydrogels which can be used for a wide variety of purposes.

1 INTRODUCTION

Injectable hydrogels have become valuable tools in various medical procedures. They can be applied in a minimally invasive manner and once injected, they can form stable 3D environments which can mimic the extracellular matrix of native tissues. Hence, hydrogels are ideal candidates not only for cell delivery and tissue repair, but also for bulking procedures. In addition, they are frequently used for drug delivery [1,2]. Hydrogels can be created from natural- or synthetic materials: naturally-derived hydrogels provide biomimetic features such as cell-adhesive integrin-binding domains and biomechanical cues, but these features are hard to control. Hydrogels created from synthetic polymers provide the possibility to tune overall mechanical properties, molecular structure, and other physical attributes of the material [3], but many have dense architecture that render them unsuitable in 3D cell culture applications.

Polyisocyanopeptides (PICs) are fully synthetic and water-soluble polymers that spontaneously form a hydrogel when warmed above a critical temperature, even at a super-low concentration (0.1% w/w). In contrast to most other synthetic hydrogels, PIC hydrogels closely mimic the architecture and mechanical properties of the cytoskeleton or extracellular matrix mimetic, including strain-stiffening at low stresses [4]. Furthermore, conjugation of integrin binding peptides (GRGDS, Gly-Arg-Gly-Asp-Ser) to compensate for the absence of cell binding sites induces bioactivity [5,6]. Because the thermosensitivity, strain-stiffening and ligand coverage can be tuned, PIC hydrogels are a promising class of new injectables.

Despite the increased use of injectable hydrogels follow-up procedures and longitudinal *in vivo* monitoring of hydrogels has been limited [7] because the contrast characteristics are similar to adjacent tissue. Magnetic resonance imaging (MRI) is a noninvasive tool which allows good soft tissue contrast at high resolution [7]. Due to their high water content, however, hydrogels are difficult to distinguish from surrounding tissue by MRI. To achieve sufficient contrast, contrast agents (CAs) such as low molecular weight gadolinium (Gd) complexes have been physically entrapped or chemically conjugated to hydrogels to enhance their MR visualization [8–12]. Chemical conjugation of CAs may be the preferred strategy for hydrogel labeling as images are likely to directly reflect morphology and location of the hydrogel after injection. In addition, conjugation prevents leaking of the CA in the surrounding tissue, allowing for long-term imaging.

In this research report, we describe conjugation of a Gd-based CA to the PIC polymer and created injectable hydrogel mixtures allowing to assess both bioactivity and visualization via MR imaging. Upon injection *in vivo*, we obtained fundamental insights in hydrogel properties in real-time.

2 MATERIALS AND METHODS

2.1 Synthesis of Polyisocyanopeptide (PIC) Polymers

PIC polymers were synthesized as previously described [4,13]. In brief, 200 mg of a mixture of isocyanide monomers **M1** (non-functional) and **M2** (azide-functionalized) was dissolved in freshly distilled toluene (4 mL) The molar ratio between **M1** and **M2** was varied between 30:1 and 400:1. A solution of initiator nickel perchlorate hexahydrate (in 1:10 absolute ethanol:toluene, concentration 0.096 mg/mL) was added in a monomer:catalyst ratio 4000:1. After 24 hrs stirring at room temperatures, the polymers were precipitated in diisopropyl ether. Two more precipitations from dichloromethane in diisopropyl ether provided pure polymers. The molecular weight of all polymers, as measured by viscometry was ~500 kg/mol [14].

2.2 Functionalization of PIC Polymers

PIC polymers were conjugated with a gadolinium(III) complex. To this end, gadolinium(III) 1,4,7,10-tetraazacyclododecane-1,4,7-tris(acetic acid)-10-(4-aminobutyl)acetamide (**Gd-DO3A**-butylamine) was reacted with dibenzocyclooctyne-*N*-hydroxysuccinimidyl ester (**DBCO-NHS** ester) (**Figure 1A**). Then, the complex **DBCO-GdDO3A** was reacted to **PIC-N3** polymers via the strain-promoted azide-alkyne cycloaddition reaction (copper-free click chemistry, **Figure 1B**). Finally, polymers were purified by precipitation in diisopropyl ether and air-dried. Hydrogel solutions were prepared by dissolving **PIC-GdDO3A** polymers at a concentration of 2 mg/mL in MilliQ water for *in vitro* MR studies. For other *in vitro* and for *in vivo* studies PIC samples were dissolved in medium as described below. Solutions were gently stirred at 4 °C over 12 h in order to ensure complete dissolution of the material. The gadolinium (Gd) concentration of prepared hydrogels was determined by inductively coupled plasma mass spectrometry (ICP-MS).

To enable cell attachment, cell spreading and to enhance biocompatibility of PIC hydrogels, GRGDS (Gly-Arg-Gly-Asp-Ser peptides)-functionalized PICs with a GRGDS concentration of 100 μM/mg polymer [5,6]. In this work, PIC-GRGDS (75%) hydrogels were mixed with PIC-GdDO3A (25%) to form hybrid gels with enhanced cell-PIC interactions that allows MRI visualization.

All PIC polymers used for cell culture and *in vivo* studies, were disinfected via UV light exposure (4 x 5 min) prior to dissolving. Afterwards, disinfected materials were dissolved in minimum essential medium (MEM, Gibco/Life Technologies, Carlsbad, CA, USA) supplemented with 100 IU/mL penicillin and 100 microgram/mL streptomycin

(both Gibco/Life Technologies, Carlsbad, CA, USA) and incubated at 4 °C overnight. The final concentration of all PIC polymers used in this study was 2 mg/mL.

Rheology measurements of prepared PIC hydrogels were performed with a stress-controlled rheometer (DHR-1 / DHR-2 TA-Instruments) as previously described [4,14] and used to determine the storage modulus *G'* and gelation temperature T_{gel} of the polymer solutions.

2.3 Cytocompatibility and Cell Culture in PIC Hydrogels

For cell-hydrogel studies, human adipose derived stem cells (hADSCs) were isolated from healthy donors undergoing reconstructive surgery (Radboudumc Nijmegen, The Netherlands) and cultured as previous described [15]. For cytotoxicity studies, equal amounts of PIC-GdDO3A, PIC-GRGDS, hybrid gels and latex material (negative control) were incubated in standard culture medium (MEM supplemented with 100U/mL penicillin/100µg/mL streptomycin and 10% fetal calf serum (FCS)) for 72h. Subsequently, the conditioned culture media were added to hADSCs (passage 2-4; cell density: 4,000 cells / 96-well) and incubated for 24 h. Cell viability was measured using the WST-1 assay (Roche) according to the manufacturer's protocol. NIH 3T3 cells incubated in standard cell culture medium were used as positive control. The measured absorbance was normalized against the positive control to indicate cell viability.

For 3D studies hADSCs (100,000 cells) at passage 2-4 were resuspended in the cold PIC solution (0.3 mL) at approximately 8 °C and seeded into insert rings (0.4 µm polyester membranes, Costar, NY, USA). Immediately after seeding, the PIC/cell mixtures were warmed up to allow the formation of the 3D hydrogel and the samples were incubated at standard cell culture conditions (37 °C and 5% CO_2). Culture media was refreshed every 2-3 days and monitored via light microscope (Leica DC200, Wetzlar, Germany).

2.4 *In vitro* MRI

PIC hydrogels conjugated with various GdDO3A densities, PIC-GRGDS and hybrid PIC hydrogels (all 0.1 mL) were stored in Eppendorf tubes (0.5 mL) and transferred to an 11.7 Tesla preclinical MR system (BioSpec, Bruker, Germany) equipped with a ^{1}H volume coil with an inner diameter of 40 mm. Scanning was performed as previously described [16]. In detail, a rapid acquisition with relaxation enhancement (RARE) sequence was employed for acquiring T_1-weighted MR imaging, with the following parameters: echo time (T_E) = 6 ms, repetition time (T_R) = 600 ms, excitation

angle = 90°, refocusing angle = 180°, number of slices = 20, slice thickness = 0.5 mm, RARE factor = 4, field of view (FOV) = 50 × 50 mm matrix size = 256 × 256 and 8 averages. The scan time was 3 minutes and 5 seconds. In addition, this RARE sequence was also used for T_2-weighted MR image acquisition but with some parameter modifications, including T_E = 60 ms, T_R = 2000 ms, number of slices = 10, RARE factor = 1 and 1 average. The scan time was thus 4 minutes 16 seconds. The T_1- and T_2 relaxation properties of various PIC hydrogels were also respectively estimated with a multi-T_R and multi-T_E RARE sequence. For T_1 estimation, the images at 8 T_Rs (i.e., 200, 500, 1000, 2000, 3000, 5000, 7000, 10000 ms) were applied and the T_1 values were estimated by fitting signal intensities (M_z) to the following equation:

$$M_z(T_R)=M_0(1-e^{-T_R/T_1})$$

The scan time was 7 minutes 39 seconds. For T_2 estimation, the image signal intensity at 30 T_Es from 10 to 300 ms with an increment of 10 ms were recorded with a total scan time of 3 minutes and 12 seconds. The image signal intensities (M) at different TEs were fitted with a mono-exponential model to determine T_2 values:

$$M(T_E)=M_0e^{-T_E/T_2}+C$$

The reciprocals of T_1- and T_2 relaxation times, defined as R_1- and R_2 relaxation rates, were calculated, respectively. Subsequently, R_1- and R_2 relaxation rate were plotted as a function of the Gd concentration to determine the overall relaxivity (slope of the curve) of GdDO3A-functionalized PIC hydrogels.

Subsequently, T_1-weighted MR images were processed with ImageJ (U.S. National Institutes of Health, Bethesda, Maryland, USA). Image contrast between the applied hydrogel and the background were assessed using a pseudo-color function.

2.5 PIC as *in vivo* Injectables

Hydrogels (unmodified PIC, PIC-GRGDS, PIC-GdDO3A, and PIC hybrids) were injected in immune-competent female, inbred, Balb/cByJ mice (Charles River, L'Arbresle, France; age: 7-8 weeks; weight: approx. 20 gram). Animal experiments were performed after approval by the Animal Welfare Body of the Radboudumc (DEC 2016-0013), conducted in accordance with institutional and national guidelines. In detail, 18 mice were randomly divided into three groups of different time points (day 7; day 14; day 28). PIC aliquots were placed on ice. Prior to injection, the mice were pre-medicated by the intravenous injection of the analgesic Rimaldyl (Pfizer, USA; 5 mg carprofen/kg). Anesthesia was induced by inhalation of 5% Isoflurane FiO2/N2O 1:2 (maintenance dose of 2-3% Isoflurane FiO_2/N_2O 1:2) and the skin of the intervention area was shaved followed by disinfection with Jodium (Eurovet

animal health, the Netherlands). Subsequently, 100 µL of hydrogels were injected subcutaneously, on the left- (PIC alone or PIC-GRGDS) or right (PIC-GdDO3A or PIC-GdDO3A/PIC-GRGDS hybrid mixture) side of the back, respectively. Injection was carried out via a pre-cooled 18G needle (BD, Oxford, United Kingdom). Injection areas were marked with a waterproof marker. Subsequently, mice were placed in a heating chamber at 37°C for a minimum of 10-15 min to ameliorate hydrogel solidification. Subsequently, n = 3 randomly chosen animals were used for MR imaging (day 0 evaluation) under prolonged anaesthesia. Body temperature and breathing were monitored. *In vivo* MRI experiments were also performed at 11.7T using the ^{1}H volume coil as described before [16]: High resolution T_1-weighted images were acquired with a RARE sequence to visualize the injected hydrogels in mice at day 7, 14 and 28 post injection. The corresponding scanning parameters were of T_E = 10ms, T_R = 560 ms, RARE factor = 2, number of slices = 20, slice thickness = 0.5 mm, FOV = 50 × 50 mm, matrix = 512 × 512 and 16 averages. The scan time was 28 mins 40 secs.

In addition, the same protocol as used for the *in vitro* study was applied to determine R_1 relaxation rates of injected hydrogels at each time point. In addition, image contrast of the injected hydrogels in mice was estimated as described above.

At pre-determined endpoints (7, 14, and 28 days post injection), animals were sacrificed by carbon dioxide asphyxiation, scanned via MRI, and hydrogels and surrounding tissues were harvested from the animals and fixated in 4% formaldehyde prior to dehydration and embedding in paraffin. Subsequently, paraffin samples were cut at 5 µm and stained with hematoxylin and eosin (HE) and Masson trichrome / Verhoeff staining.

2.6 Statistics

Unless otherwise indicated, data sets are expressed as mean ± standard deviation. Regression, Pearson correlation coefficient r and p value (two-tailed) were determined to describe the correlation between Gd concentration and $r_{1,2}$-relaxivity of GdDO3A-functionalized PIC hydrogels. A one-way ANOVA test with post-hoc Bonferroni correction was performed for statistical analysis of differences between PIC-GdDO3A, PIC-GRGDS, PIC hybrids and control. For all analysis, $p < 0.05$ was considered statistically significant. GraphPad Prism (version 5.03, GraphPad Software Inc, La Jolla, CA, USA) was used for all statistical analysis.

3 RESULTS AND DISCUSSION

3.1 Functionalization of PIC Polymers

PIC polymers with different degrees of azide functionalization were prepared by copolymerization of the isocyanide monomers **M1** and **M2**. The molar ratios between the two monomers ranged from 1:30 to 1:400, which gives a statistical spacing of functional groups along the PIC backbone of 3 nm to 40 nm. The **DBCO-GdDO3A** complex (**Figure 1A**) was reacted to the **PIC-N3** polymers via the strain-promoted azide-alkyne cycloaddition reaction (copper-free click chemistry, **Figure 1B**). Since this click reaction shows nearly quantitative conversion [17], the azide density in **PIC-N3** directly determines the Gd loading in the polymers. Indeed, quantitative analysis of polymer-bound Gd via coupled plasma mass spectrometry (ICP-MS) confirms that hydrogels with increasing **M2** contain increasing amounts of Gd (**Figure 2A**). This conjugation approach allows for precise control over the degree of functionalization of the hydrogel and ultimately fosters reproducibility [3]. All prepared PIC polymers remained a liquid at 4-8 °C and formed a hydrogel beyond 16 °C (**Figure 2**). Prepared hydrogels are relatively soft materials with similar storage moduli (G´) between 150-250 Pa at 37 °C.

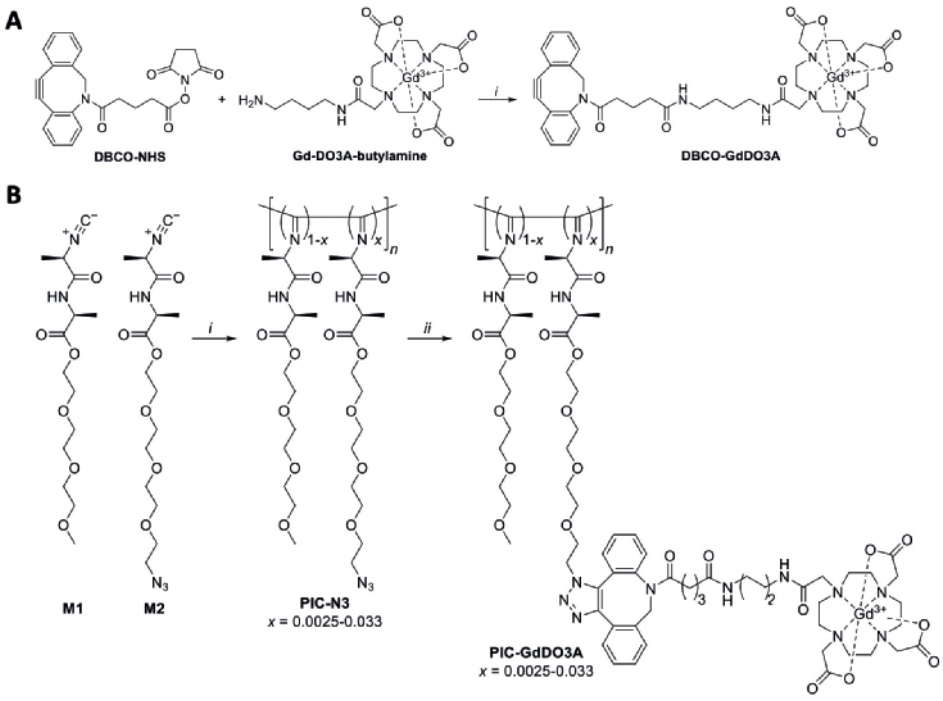

Figure 1: Gadolinium-decorated polyisocyanopeptide (PIC) gels. A: GdDO3A was equipped with a DBCO group suitable for copper-free click chemistry. Key: borate buffer, pH = 8.5, overnight, room temperature. B: Azide-functionalized PICs were obtained by copolymerization of monomers M1 and M2 and subsequently reacted with DBCO-GdDO3A. Key: (*i*) $Ni(ClO_4)_2$ in ethanol/toluene, overnight, room temperature; (*ii*) acetonitrile, overnight, room temperature.

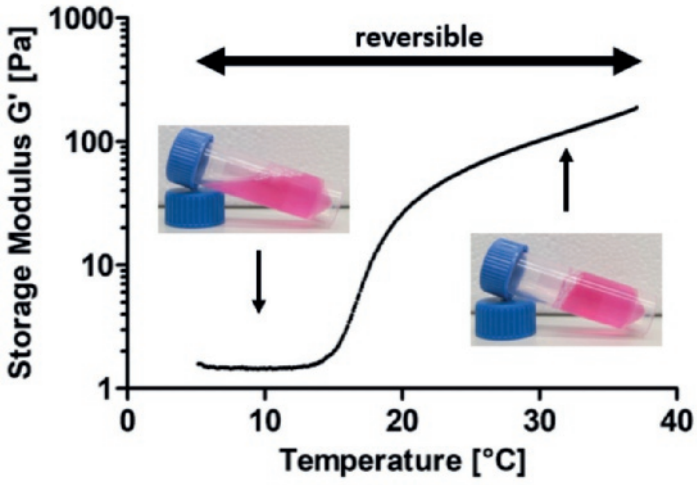

Figure 2: Stiffness of PIC-GdDO3A in culture medium as a function of temperature *T*. A gel is formed at *T* > 16 °C and dissolved again on cooling.

3.2 *In vitro* MRI and Cytocompatibility of Functionalized PIC Hydrogels

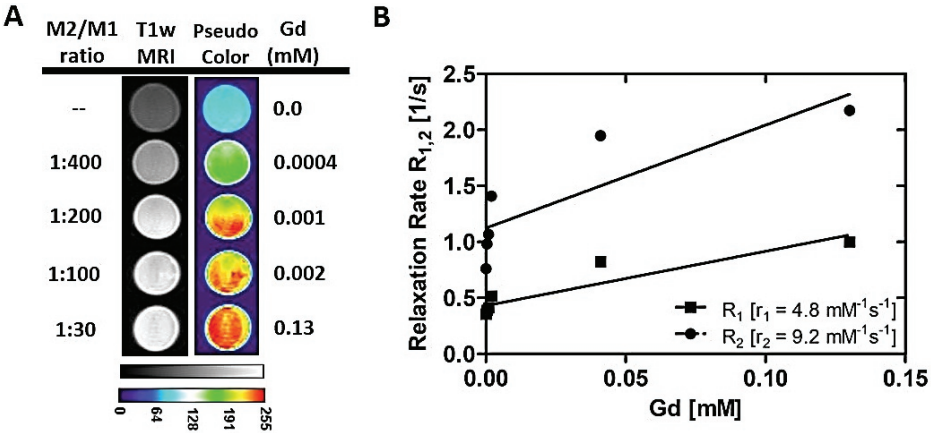

Figure 3: MRI characteristics of PIC hydrogels conjugated with the MRI contrast agent Gd-DO3A. A: M2/M1 ratio, T_1-weighted MRI images at 11.7T, corresponding pseudo-color images, and concentration of Gd of PIC hydrogels conjugated with various amounts of GdDO3A. B: r_1- and r_2 relaxivity assessment of PIC hydrogels conjugated with various amounts of GdDO3A.

MR imaging of the GdDO3A-conjugated PIC hydrogels at room temperature was performed to determine their MRI properties. The contrast of these hydrogels increased with increasing GdDO3A content in T_1-weighted MR images (**Figure 3A**). The corresponding r_1-relaxivity of PIC-GdDO3A hydrogels, as assessed by a RARE sequence with variable T_R's, was 4.8 ± 0.9 $mM^{-1}s^{-1}$, which is in line with values obtained in similar studies at 11.7 T using Gd-based CAs to label injectables [8,18]. Using variable T_E's a r_2-relaxivity of 9.2 ± 2.9 $mM^{-1}s^{-1}$ was obtained, which is remarkably smaller than we previously obtained for other Gd labeled injectables at 11.7 T [8,18]. However, with an r_2/r_1 ratio of 1.9 the PIC-GdDO3A hydrogels can still be adequately imaged by T_1-weighted MR imaging [19,20]. Furthermore, both the R_1- and R_2 relaxation rates strongly correlated with the Gd-content (**Figure 3B**; r = 0.9208 and p = 0.0092 for R_1; r = 0.8473 and p = 0.0332 for R_2). The highest R_1 relaxation rate (1.0 ± 0.2 s^{-1}) and highest contrast in T_1-weighted MR images was achieved with PIC-GdDO3A at a ratio of 1:30, and thus this material was used in mixing experiments.

Although PIC-GdDO3A hydrogels were clearly visible *in vitro* in MR imaging, further modification of the hydrogel is necessary for use in e.g. a 3D matrix for cell culture, injectable and functional organ regeneration. We used GRGDS (Gly-Arg-Gly-Asp-Ser)-modified PICs (PIC-GRGDS) to enable cell attachment, cell spreading and to enhance bioactivity of PIC hydrogels [5,6] and prepared hybrids of PIC-GRGDS

(75%) with PIC-GdDO3A (25%) at 2 mg/mL total concentration. Despite the lower CA density, this hydrogel mixture was still clearly visible in MRI as indicated by enhancement of the relaxation rate and contrast when compared to non-labeled Gd hydrogels (**Figure 4A** and **Figure 4B**).

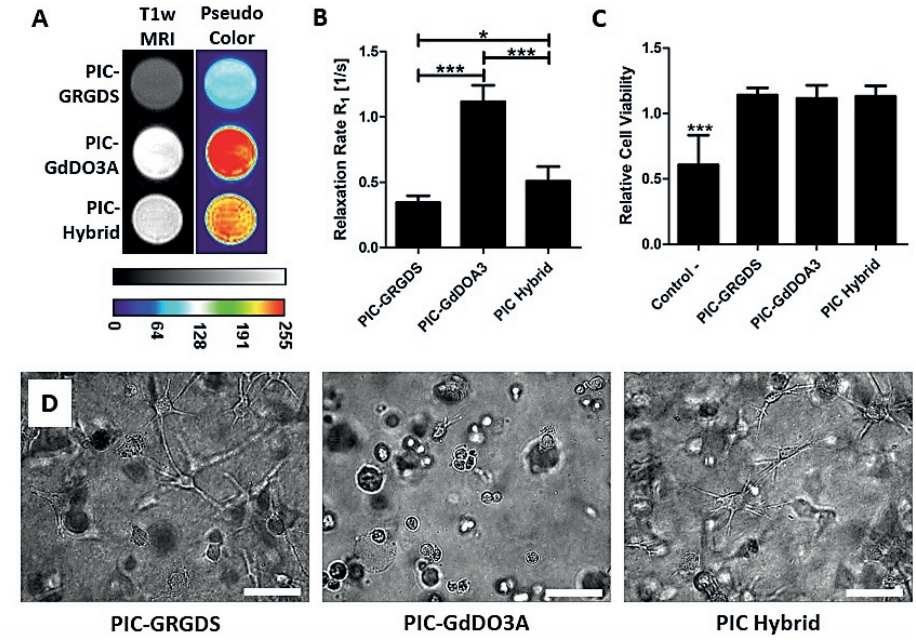

Figure 4: MRI imaging and cytocompatibility of PIC hydrogels conjugated with GRGDS peptides (PIC-GRGDS), PIC hydrogels conjugated with the MR contrast agent GdDO3A (PIC-GdDO3A) and a mixture (75 % PIC-GRGDS + 25% PIC-GdDO3A) of both hydrogels (PIC Hybrid). A: T_1-weighted MRI- and corresponding pseudo-color images. B: R_1 relaxation rate. C: cell viability assay with adipose derived stem cells (ADSCs) cultured for 48h with hydrogel extractions (control -: Latex). D: Brightfield images of ADSCs cultured within PIC hydrogels (scale bar = 50 micron). A one-way ANOVA with Bonferroni post hoc test was performed for statistical analysis of differences between PIC-GdDO3A, PIC-GRGDS, and PIC Hybrid. ***: $p < 0.0001$, *: $p < 0.05$.

Cell viability assays with adipose derived stem cells (ADSCs) confirmed the absence of cytotoxicity of unmodified PIC hydrogels and PIC hydrogels functionalized with GdDO3A (**Figure 4C**). This suggests that Gd is stably chelated after covalent conjugation to the backbone of the PIC polymer and that mixing of different gels and solidifying at low concentrations does not influence the Gd content. 3D culture of ADSCs in modified PIC hydrogels showed extensive cell spreading and cell-cell contact (**Figure 4D**) suggesting cell attachment and interaction with this 'artificial extracellular matrix'. In contrast, when ADSC were cultured in unmodified PIC hydrogels or PIC-GdDO3A conjugates cell-matrix interactions were impaired:

ADSCs remained round-shaped suggesting no spreading or interaction with the PIC polymers. Consequently, this may be an unfavorable environment for cells and may hamper functional tissue formation for regeneration purposes when used *in vivo*.

The PIC-GdDO3A/PIC-GRGDS hybrid showed a gelation temperature at approximately 16 °C and a stiffness G' = 188 Pa at 37 °C (**Figure 2**). Thus, this mixture has similar physical properties as the other (functionalized) PIC gels described in other studies [17,21]. Especially the stiffness of our prepared hybrid injectable mixture should be carefully considered when the intended use is a (cell-containing) substitute for tissue repair (injectable) since the stiffness of scaffolds is known to have an effect on cell behavior as mechanical cues play a role in (stem) cell fate [17,22]. Taken together, the prepared PIC hydrogels may offer a favorable microenvironment, which closely resembles the natural microenvironment as far as mechanical characteristics go.

3.3 *In vivo* MRI of Functionalized PIC Hydrogels

In a final set of experiments, we tested various PIC hydrogels *in vivo* to follow their fate upon injection. Subcutaneous injection of PIC-GdDO3A and hybrid hydrogels resulted in a 'bleb-like' polymer deposit which could easily be identified via T_1-weighted MR imaging (**Figure 5A**). The signals in T_1-weighted MR images were bright in contrast to surrounding tissue (**Figure 5B**), whilst PIC hydrogels containing no CA (unmodified PIC and PIC-GRGDS) could not be detected. Indeed, through coupling of a contrast agent to the PIC polymer, MR imaging may be an adequate tool to assess the hydrogel patency and degradation / remodeling upon injection. PIC-GdDO3A might be useful to also follow this hydrogel when used as dressing, particularly because loss of material can be caused by cleaning and rubbing. In a recent study, PIC hydrogels (PIC alone and PIC-GRGDS) were used as wound dressings [21]. Unfortunately, not unexpected, these hydrogels could not be localized after application and assessment of their patency and effects remained unclear.

The volume of injected hydrogels decreased from its initial value 7 days after injection as judged by MRI (**Figure 5C**; 35.7 ± 7.0% for PIC-GdDO3A and 43.0 ± 13.6% for PIC Hybrid). The loss of volume in this early phase of monitoring can be explained by fluid loss and / or polymer loss resulting from hysteresis when forming a gel in situ [11]. The contrast increased, hence the T_1 value of the hydrogels decreased (**Figure 5A, Figure 5B** and **Table 1**) indicating densification of the injected material and the loss of volume is therefore most likely caused by fluid loss. Densification of the hydrogel may decrease molecular tumbling and this may ultimately enhance the relaxation rate, and subsequently improve MR contrast [12,20,23].

Table 1: T_1- relaxation times of PIC hydrogels upon injection *in vivo* over time. Data represent mean ± standard deviation (day 0: n = 3; other time points: n = 6).

T_1 Hydrogel [ms]	Day 0	Day 7	Day 14	Day 28
PIC-GdDO3A	1011.3 ± 235.7	527.8 ± 181.2	691.2 ± 180.8	578.2 ± 139.8
PIC Hybrid	1919.5 ± 196.4	939.4 ± 118.9	995.2 ± 291.9	911.8 ± 155.6

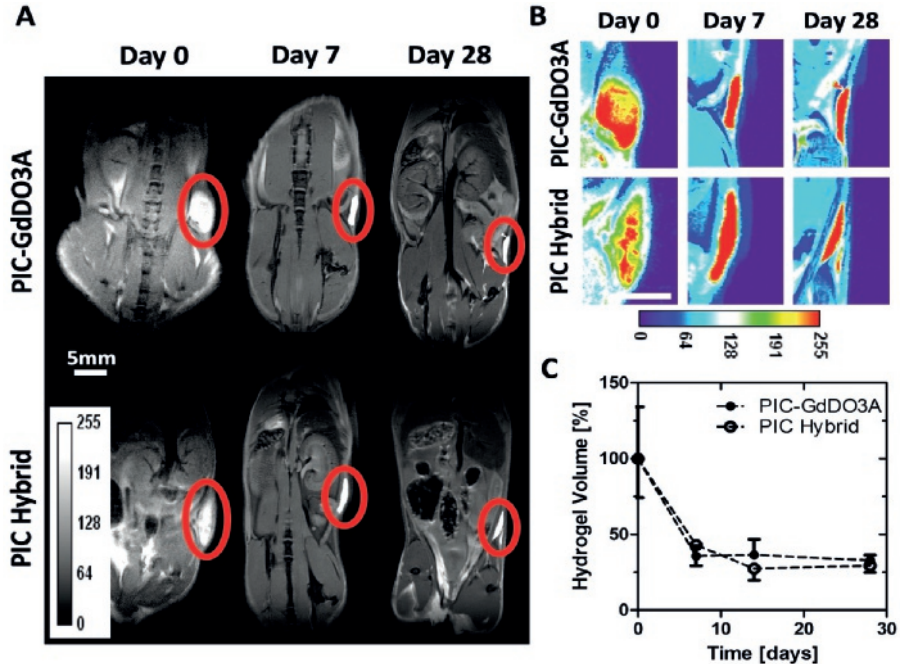

Figure 5: *In vivo* MRI imaging and analysis of PIC hydrogels with GRGDS peptides (PIC-GRGDS), PIC hydrogels conjugated with the MR contrast agent GdDO3A (PIC-GdDO3A) and a mixture (75 % PIC-GRGDS + 25% PIC-GdDO3A) of both hydrogels (PIC Hybrid). A: Representative T_1-weighted MR images of different PIC hydrogels subcutaneously injected in a mouse model. The red circle indicates the injected hydrogel. B: Representative pseudo-color T_1-weighted MR images of different PIC hydrogels. Scale bar = 5mm. C: Residual volume upon injection over time. Data represent mean ± standard deviation (day 0: n = 3; other time points: n = 6).

The loss of volume in the early phase upon injection is particularly relevant when the hydrogel is used as an injectable, for instance as drug delivery vehicle. Simple physical entrapment of e.g. growth factors or therapeutic drugs will lead to an immediate burst release into the surrounding tissue caused by the fluid loss. Straightforward chemical conjugation as performed in this study may prolong the exposure of cells to therapeutics or growth factors within the gels and release would occur due to degradation of the hydrogel. When used for cell delivery, cells may be released immediately into the surrounding and, more importantly, the physical characteristics

of the gel will be altered as densification leads to higher polymer concentrations and higher strain-stiffening values. Hence, when aiming for particular strain-stiffening values *in vivo* either the polymer concentration needs to be adjusted or the initial strain-stiffening values as measured *in vitro* may need to be lowered to ultimately reach the desired strain-stiffening values *in vivo*. Polymer volume, contrast, and relaxation time of Gd-loaded PIC hydrogels remained stable from day 7 onwards until the end of the experiment, whereas bulk- or surface degradation was anticipated during the time of monitoring. Thus, the polymer is remarkably stable and resistant to *in vivo* degradation. This can partly be explained by the polymer composition which does not contain biologically degradable chemical bonds. The MRI image observations correlated well to the histological analysis (**Figure 6**): hydrogels remained structurally intact over time. PIC hydrogels deposits harvested 7 days post injection were encapsulated by host tissue and no or very limited cell influx was observed regardless of the hydrogel composition. A collagenous fibrous network, host immune cells (lymphocytes), and capillaries surrounded the injected hydrogels without any influx of cells into the gel in the early observation period. At day 28 post injection, invasion of host cells into the gels was observed and these cells deposited extracellular matrix components within the PIC hydrogel, albeit that the gross morphology of the gels stayed intact (**Figure 6**). Overall, the immune reaction of PIC hydrogels was assessed to be mild to moderate very similar when compared to well-established standard hydrogels such as Matrigel® [21].

Interestingly, cell invasion and remodeling within PIC alone, PIC-GRGDS, PIC-GdDO3A and the hybrid mixture deposits were similar. The *in vivo* influx of cells in PIC alone and PIC-GdDO3A hydrogels was somewhat unanticipated as in *in vitro* studies cell spreading and migration was much more apparent in 3D PIC-GRGDS constructs. Apparently, the dynamic tissue microenvironment permitted cell in-growth, a situation which is dissimilar from the passive cell encapsulation in the *in vitro* studies. This suggests that although GRGDS conjugation to PIC polymers is necessary *in vitro*, its benefit *in vivo* may be limited.

The high visibility in MR imaging that we achieved through conjugation of GdDO3A to the backbone of the PIC polymer may be of clinical relevance for the use of these hydrogels. Safety concerns in using Gd-based CAs upon injection have been considered [24], but the molar amount of Gd in the polymer deposits is very limited and orders of magnitude lower than Gd-based agents used for MRI examinations such as heart and vessels imaging. It is therefore unlikely that this may pose a safety concern. Alternatives such as naturally-derived CAs are available, albeit that their overall T_1-relaxivity is lower when compared to gadolinium [16,25]. However, such CA

alternatives may be potentially considered for PIC labelling as their relaxivity may be further increased due to densification upon injection. Overall, the data obtained in this study provides important clues for further development of PIC-based hydrogels which can be used for a wide variety of purposes.

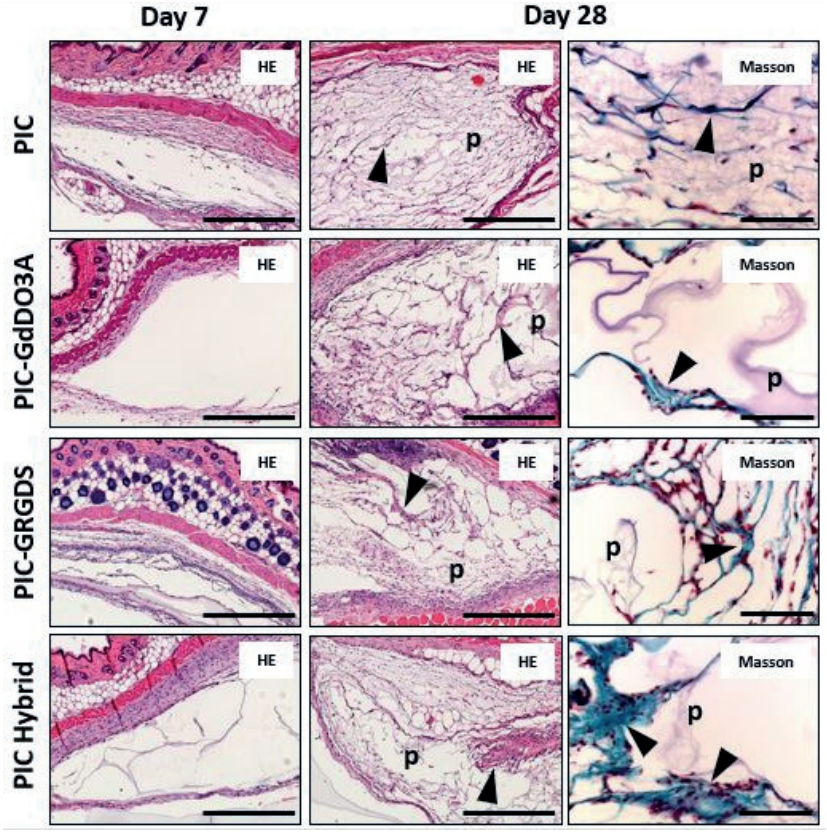

Figure 6: Representative histological images of injected hydrogels at day 7 and day 28 post injection. Left images (Hematoxyline/Eosine HE) give an overview on the injected hydrogels (scale bar = 500 micron). Right images (Masson Trichrome / Verhoeff staining) display the center of the injected hydrogels at higher magnification (scale bar = 100 micron; Pic polymer = purple/transparent (p); de novo extracellular matrix deposit by invaded cells = green (arrow); cell nuclei = red/brown).

4 CONCLUSION

Through chemical conjugation of contrast agents and cell-binding sides to PIC polymers, functional and highly reproducible smart hydrogel mixtures can be created that can be monitored by MR imaging. Conjugation of contrast agents did not impair basic PIC hydrogel characteristics. The MRI and histological analysis of these hydrogels after injection gave fundamental insights into their fate *in vivo* and provide a proper basis for further development of PIC-based hydrogels which can be used for a wide variety of purposes.

5 ACKNOWLEDGEMENTS

The authors would like to thank Bianca Lemmers - van de Weem, Andor Veltien and Kees Jansen for assistance during *in vivo* experiments.

The research leading to these results has received funding from the People Programme (Marie Curie Actions) of the European Union's Seventh Framework Programme FP7/2007-2013/ under REA grant agreement No. 607868 (iTERM).

6 REFERENCES

[1] A. Sivashanmugam, R. Arun Kumar, M. Vishnu Priya, S. V. Nair, R. Jayakumar, An overview of injectable polymeric hydrogels for tissue engineering, Eur. Polym. J. 72 (2015) 543–565. DOI:10.1016/J.EURPOLYMJ.2015.05.014.

[2] M. Norouzi, B. Nazari, D.W. Miller, Injectable hydrogel-based drug delivery systems for local cancer therapy, Drug Discov. Today. 21 (2016) 1835–1849. DOI:10.1016/J.DRUDIS.2016.07.006.

[3] D. Seliktar, Designing Cell-Compatible Hydrogels for Biomedical Applications, Science (80-.). 336 (2012) 1124–1128. DOI:10.1126/science.1214804.

[4] P.H.J. Kouwer, M. Koepf, V.A.A. Le Sage, M. Jaspers, A.M. van Buul, Z.H. Eksteen-Akeroyd, T. Woltinge, E. Schwartz, H.J. Kitto, R. Hoogenboom, S.J. Picken, R.J.M. Nolte, E. Mendes, A.E. Rowan, Responsive biomimetic networks from polyisocyanopeptide hydrogels., Nature. 493 (2013) 651–5. DOI:10.1038/nature11839.

[5] J. Zimoch, J.S. Padial, A.S. Klar, Q. Vallmajo-Martin, M. Meuli, T. Biedermann, C.J. Wilson, A. Rowan, E. Reichmann, Polyisocyanopeptide hydrogels: A novel thermo-responsive hydrogel supporting pre-vascularization and the development of organotypic structures, Acta Biomater. 70 (2018) 129–139. DOI:10.1016/j.actbio.2018.01.042.

[6] K. Liu, S.M. Mihaila, A. Rowan, E. Oosterwijk, P. Kouwer, Synthetic extracellular matrices with nonlinear elasticity regulate cellular organization, Biomacromolecules. (2019). DOI:10.1021/ACS.BIOMAC.8B01445.

[7] A.A. Appel, M.A. Anastasio, J.C. Larson, E.M. Brey, Imaging challenges in biomaterials and tissue engineering., Biomaterials. 34 (2013) 6615–30. DOI:10.1016/j.biomaterials.2013.05.033.

[8] D. Bermejo-Velasco, W. Dou, A. Heerschap, D. Ossipov, J. Hilborn, Injectable hyaluronic acid hydrogels with the capacity for magnetic resonance imaging, Carbohydr. Polym. 197 (2018) 641–648. DOI:10.1016/j.carbpol.2018.06.028.

[9] A. Berdichevski, H. Simaan Yameen, H. Dafni, M. Neeman, D. Seliktar, Using bimodal MRI/fluorescence imaging to identify host angiogenic response to implants, Proc. Natl. Acad. Sci. 112 (2015) 5147–5152. DOI:10.1073/pnas.1502232112.

[10] A. Berdichevski, Y. Shachaf, R. Wechsler, D. Seliktar, Protein composition alters in vivo resorption of PEG-based hydrogels as monitored by contrast-enhanced MRI, Biomaterials. 42 (2015) 1–10. DOI:10.1016/j.biomaterials.2014.11.015.

[11] J. Liu, K. Wang, J. Luan, Z. Wen, L. Wang, Z. Liu, G. Wu, R. Zhuo, Visualization of in situ hydrogels by MRI *in vivo*, J. Mater. Chem. B. 4 (2016) 1343–1353. DOI:10.1039/C5TB02459E.

[12] M.H. Bakker, C.C.S. Tseng, H.M. Keizer, P.R. Seevinck, H.M. Janssen, F.J. Van Slochteren, S.A.J. Chamuleau, P.Y.W. Dankers, MRI Visualization of Injectable Ureidopyrimidinone Hydrogelators by Supramolecular Contrast Agent Labeling, Adv. Healthc. Mater. 7 (2018) 1701139. DOI:10.1002/adhm.201701139.

[13] S. Mandal, Z.H. Eksteen-Akeroyd, M.J. Jacobs, R. Hammink, M. Koepf, A.J.A. Lambeck, J.C.M. van Hest, C.J. Wilson, K. Blank, C.G. Figdor, A.E. Rowan, Therapeutic nanoworms: towards novel synthetic dendritic cells for immunotherapy, Chem. Sci. 4 (2013) 4168. DOI:10.1039/c3sc51399h.

[14] M. Jaspers, M. Dennison, M.F.J. Mabesoone, F.C. MacKintosh, A.E. Rowan, P.H.J. Kouwer, Ultra-responsive soft matter from strain-stiffening hydrogels, Nat. Commun. 5 (2014) 5808. DOI:10.1038/ncomms6808.

[15] S.M. Mihaila, A.M. Frias, R.P. Pirraco, T. Rada, R.L. Reis, M.E. Gomes, A.P. Marques, Human adipose tissue-derived SSEA-4 subpopulation multi-differentiation potential towards the endothelial and osteogenic lineages., Tissue Eng. Part A. 19 (2013) 235–46. DOI:10.1089/ten.TEA.2012.0092.

[16] H.P. Janke, N. Güvener, W. Dou, D.M. Tiemessen, A. YantiSetiasti, J.G.O. Cremers, P.J.A. Borm, W.F.J. Feitz, A. Heerschap, F. Kiessling, E. Oosterwijk, Labeling of Collagen Type I Templates with a Naturally Derived Contrast Agent for Noninvasive MR Imaging in Soft Tissue Engineering, Adv. Healthc. Mater. (2018) 1800605. DOI:10.1002/adhm.201800605.

[17] R.K. Das, V. Gocheva, R. Hammink, O.F. Zouani, A.E. Rowan, Stress-stiffening-mediated stem-cell commitment switch in soft responsive hydrogels, Nat. Mater. 15 (2016) 318–325. DOI:10.1038/nmat4483.

[18] S. Mastrogiacomo, A.E. Kownacka, W. Dou, B.P. Burke, R.T.M. de Rosales, A. Heerschap, J.A. Jansen, S.J. Archibald, X.F. Walboomers, Bisphosphonate Functionalized Gadolinium Oxide Nanoparticles Allow Long-Term MRI/CT Multimodal Imaging of Calcium Phosphate Bone Cement, Adv. Healthc. Mater. 7 (2018) 1800202. DOI:10.1002/adhm.201800202.

[19] E.-K. Lim, B. Kang, Y. Choi, E. Jang, S. Han, K. Lee, J.-S. Suh, S. Haam, Y.-M. Huh, Gadolinium-based nanoparticles for highly efficient T1-weighted magnetic resonance imaging., Nanotechnology. 25 (2014) 245103. DOI:10.1088/0957-4484/25/24/245103.

[20] P. Fries, J.N. Morelli, F. Lux, O. Tillement, G. Schneider, A. Buecker, The issues and tentative solutions for contrast-enhanced magnetic resonance imaging at ultra-high field strength., Wiley Interdiscip. Rev. Nanomed. Nanobiotechnol. 6 (2014) 559–73. DOI:10.1002/wnan.1291.

[21] R.C. op 't Veld, O.I. van den Boomen, D.M.S. Lundvig, E.M. Bronkhorst, P.H.J. Kouwer, J.A. Jansen, E. Middelkoop, J.W. Von den Hoff, A.E. Rowan, F.A.D.T.G. Wagener, Thermosensitive biomimetic polyisocyanopeptide hydrogels may facilitate wound repair, Biomaterials. 181 (2018) 392–401. DOI:10.1016/j.biomaterials.2018.07.038.

[22] S.J. Mousavi, M. Hamdy Doweidar, Role of Mechanical Cues in Cell Differentiation and Proliferation: A 3D Numerical Model, PLoS One. 10 (2015) e0124529. DOI:10.1371/journal.pone.0124529.

[23] E.J. Werner, A. Datta, C.J. Jocher, K.N. Raymond, High-Relaxivity MRI Contrast Agents: Where Coordination Chemistry Meets Medical Imaging, Angew. Chemie Int. Ed. 47 (2008) 8568–8580. DOI:10.1002/anie.200800212.

[24] H. Malikova, M. Holesta, Gadolinium contrast agents – are they really safe?, J. Vasc. Access. 18 (2017) 1–7. DOI:10.5301/jva.5000713.

[25] E.M. Gale, I.P. Atanasova, F. Blasi, I. Ay, P. Caravan, A Manganese Alternative to Gadolinium for MRI Contrast., J. Am. Chem. Soc. 137 (2015) 15548–57. DOI:10.1021/jacs.5b10748.

CHAPTER 6

The Impact of γ-irradiation and EtO Degassing on Tissue Remodeling of Collagen-based Hybrid Tubular Templates

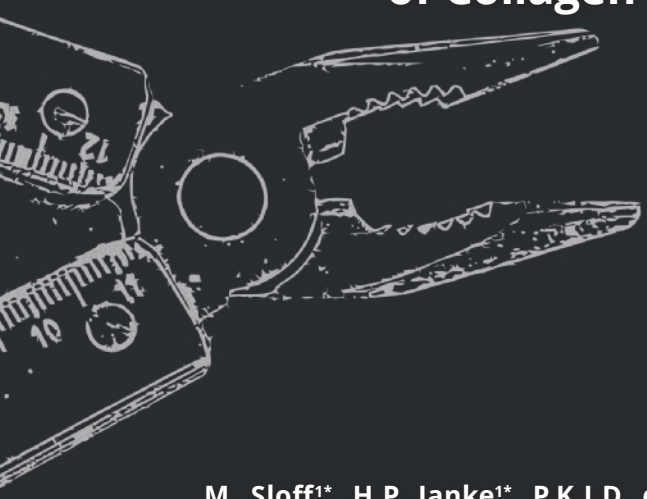

M. Sloff[1*], H.P. Janke[1*], P.K.J.D. de Jonge[1], D.M. Tiemessen[1], B.B.M. Kortmann[1,2], S.M. Mihaila[1], P.J. Geutjes[1], W.F.J. Feitz[1,2] and Egbert Oosterwijk[1]

[1]: Department of Urology – Experimental Urology, Radboud Institute for Molecular Life Science Radboud University Medical Center, Geert Grooteplein 28, 6525 GE Nijmegen, The Netherlands

[2]: Radboudumc Amalia Children's Hospital, Geert Grooteplein-Zuid 10, 6525GA Nijmegen, The Netherlands

ACS Biomater Sci Eng. 2018 Sep 10;4(9):3282-3290
DOI: 10.1021/acsbiomaterials.8b00369

ABSTRACT

Clinical implementation of novel products for tissue engineering and regenerative medicine requires a validated sterilization method. In this study, we investigated the effect of γ-irradiation and EtO degassing, on material characteristics *in vitro* and the effect on template remodeling of hybrid tubular constructs in a large animal model. Hybrid tubular templates were prepared from type I collagen and Vicryl® polymers and sterilized by 25 kGray of γ-irradiation or EtO degassing. The *in vitro* characteristics were extensively studied, including tensile strength analysis and degradation studies. For *in vivo* evaluation, constructs were subcutaneously implanted in goats for 1 month to form vascularized neo-tissue. Macroscopic and microscopic appearances of the γ- and EtO-sterilized constructs slightly differed due to additional processing required for the COL-Vicryl®-EtO constructs. Regardless of the sterilization method, incubation in urine resulted in fast degradation of the Vicryl® polymer and decreased strength (<7 days). Incubation in SBF was less invasive and strength was maintained for at least 14 days. The difference between the two sterilization methods was otherwise limited. In contrast, subcutaneous implantation showed that the effect of sterilization was considerable. A well-vascularized tube was formed in both cases, but the γ-irradiated construct showed an organized architecture of vasculature and was mechanically more comparable to the native ureter. Moreover, the γ-irradiated construct showed advanced tissue remodeling as shown by enhanced ECM production. This study shows that the effect of sterilization on tissue remodeling cannot be predicted by *in vitro* analyses alone. Thus, validated sterilization methods should be incorporated early in the development of tissue engineered products and this requires both *in vitro* and *in vivo* analyses.

1 INTRODUCTION

Recent advances in the field of tissue engineering and regenerative medicine have led to the application of advanced tissue engineered products (skin grafts, tracheas, cartilage, bladder augmentations) in different patient groups, albeit that patient numbers were limited [1–4]. The majority of research within this field is still at the pre-clinical stage and novel biomaterials are still being developed for a variety of indications. Evaluation of novel biomaterials varies from mechanical characterization and degradation studies to cyto- and biocompatibility assays [5,6]. In general, the first step in *in vivo* evaluation is limited to subcutaneous implantation in small animals [7,8]. For evaluation in larger animals, and in particular for successful clinical translation and implementation, standardized production with medical grade materials is required. One of the essential steps in this process is sterilization of constructs using a validated sterilization procedure [9]. The choice of sterilization method may affect the mechanical and biological features, for instance due to the aggressiveness of the sterilization procedure [10]. It is therefore important to evaluate the final sterilized medical grade products *in vitro* and *in vivo* [11,12].

For pre-clinical application of biomaterials, gamma(γ)-irradiation and ethylene oxide degassing (EtO) are the most frequently used sterilization methods [13]. With γ-irradiation wet materials can be sterilized, which eliminates additional processing. Materials can therefore be packaged in ethanol, which is necessary for long-term sterility and storage at -80°C. However, during γ-irradiation of wet materials free radicals are formed, leading to altered material properties [9]. Ethylene oxide (EtO) is a highly diffusive alkylating agent and adequate degassing is needed to permit diffusion of remaining toxic derivatives, like chlorohydrin and ethylene glycol [14]. Compared to γ-irradiation, EtO degassing is a less invasive sterilization technique and this may result in a material with prolonged strength and support. It may therefore be a preferred technique for polymeric materials [15,16].

Collagen-based templates have been used for various reconstructive purposes, including in preclinical studies for urological tissue engineering to reconstruct parts of the urological tract [17–19]. In a previous study, a γ-irradiated hybrid tubular construct from type I collagen and a biodegradable Vicryl® polymer mesh was used to create an artificial urinary conduit in a porcine model [20]. Interestingly, a functional conduit with urinary flow could be created after subcutaneous pre-implantation, although severe shrinkage of the graft and skin contraction was observed. The implanted material was completely remodeled and did not provide sufficient

structural integrity to prevent contraction. This could have been the consequence of several important aspects. It is possible that urine can contribute to the tissue remodeling as it creates an aberrant (micro)environment which may ultimately lead to deposition of more fibroblasts leading to graft shrinkage. Secondly, young (porcine) animals were used, known for their fast growth, specific skin properties and regeneration [21]. This may also cause excessive wound contraction. Thirdly, the choice of sterilization technique may have extensively influenced the final outcome since γ-sterilization enhances Vicryl® biodegradability from 2 months to less than 1 month [22].

We hypothesized that using a less invasive sterilization technique, i.e. EtO-degassing would result in prolonged template stability and improved remodeling. In this study we therefore compared two validated sterilization techniques, i.e. γ-irradiation and EtO degassing, in terms of mechanical properties, degradation and template remodeling in an adult animal model (goat) mimicking tissue regeneration in the adult patient population.

2 MATERIALS AND METHODS

2.1 Tubular Hybrid Template Preparation

Tubular hybrid templates (l = 10 cm, Ø = ± 15 mm) were prepared in a cleanroom facility (EMCM B.V., Nijmegen, The Netherlands), using a previously described protocol [23]. In brief, a 0.7% (w/v) collagen type I suspension prepared from bovine achilles tendon (Collagen Solutions, Eden Praire, USA) was combined with a tailor-made tubularized Vicryl® polymer mesh (VM74, Ethicon, Somerville, NJ, USA) in a silicon mold. A stainless steel mandrel (Ø = 15 mm) was inserted to create a lumen in the tubular construct. After freezing and freeze-drying, scaffolds were strengthened by chemical cross-linking using EDC/NHS [24]. Subsequently, constructs were either packaged in blisters with 70% ethanol for sterilization by a standard dose of 25 kGray of gamma (γ)-irradiation (Synergy Health, Etten-Leur, The Netherlands), or further processed for sterilization by ethylene oxide degassing (EtO, Synergy Health, Venlo, The Netherlands). This required additional freezing and freeze-drying and subsequent packaging in blisters. Cross-linking efficiency was determined by trinitrobenzene sulfonic acid assay [24] and construct morphology was assessed by scanning electron microscopy (SEM, JEOL 6310) and histology by hematoxylin (Klinipath, Duiven, The Netherlands) and eosin (Boom, Meppel, The Netherlands) (HE).

2.2 Tensile Strength Analysis

The mechanical characteristics of the wetted tubular constructs were evaluated using a tensile tester with a 2.5 kN load cell (Z2.5 TN, Zwick/Roell, Ulm, Germany). A circular ring test was performed on ring pieces of the constructs (width (w): 6.4 ± 0.7 mm, thickness (t): 3.1 ± 0.4 mm, n = 14 from 2 COL-Vicryl®-EtO constructs and l: 6.1 ± 0.6 mm, t: 2.9 ± 0.4 mm, n = 11 from 2 COL-Vicryl®-γ constructs). The hooks of the apparatus were placed in contact with the upper and lower areas opposite each other (hook-to-hook distance), spaced 18.45 mm apart for the COL-Vicryl®-EtO and 22.53 mm for the COL-Vicryl®-γ avoiding any 'pre-stretch'. The upper hook was then moved upwards with a crosshead speed of 50 mm/min until rupture. Samples were compared to native goat ureters, the primary anastomosis site for the artificial urostomy, which acts as an extended ureter. Ureters from two different goats were similarly analyzed, spaced 1.27 mm apart (n=12). Data generation were performed as previously described [25,26]. In brief, recorded force-displacement data were normalized to the test specimen dimensions to compute a stress-strain curve. The stress was expressed as the recorded force F [N] which reacted on the

cross-sectional area A [mm2] of the test specimen (thickness (t) x width (w) x 2), while the strain was expressed as the change in length delta L [mm] divided by its original length (hook-to-hook distance) L0 [mm]. As an indicator for construct stiffness, the Young´s modulus was calculated from the slope (upswing region) of the computed stress-strain curve. Ultimate tensile strength (UTS) and failure strain were defined as the maximum stress and maximum strain, respectively in the stress-strain curve before failure of the construct.

2.3 Degradation Assay

A degradation assay was performed in goat urine as well as in simulated body fluid (SBF) during 28 days. The goat urine was centrifuged at 2000 g for 10 min at 4°C and filter sterilized to avoid cellular contaminants and ensure sterility. Urine was kept at 4°C until use. SBF was created as described [27]. In brief, SBF was made in a plastic beaker with 700 mL demi-water and the consecutive addition of the following: 9.23 mM NaCl (Merck, Darmstadt, Germany), 0.56 nM $NaHCO_3$ (Sigma-Aldrich, St. Louis, MO, USA), 0.41 mM Na_2CO_3 (Boom, Meppel, The Netherlands), 0.30 mM KCl (Sigma-Aldrich, St. Louis, MO, USA), 0.10 mM $K_2HPO_4 \cdot 3H_20$ (Merck, Darmstadt, Germany), 0.15 mM $MgCl_2 \cdot 6H_20$ (Merck, Darmstadt, Germany), 200 mL 0.2 M NaOH (Merck, Darmstadt, Germany), 7.51 mM HEPES (Invitrogen, Thermo Scientific, Waltham, MA, USA), 0.26 mM $CaCl_2$ (Sigma-Aldrich, St. Louis, MO, USA), 0.05 mM Na_2SO_4 (Sigma-Aldrich, St. Louis, MO, USA). The mixture was then warmed until 36.5°C and adjusted to pH 7.4 with 1.0 M NaOH (Merck, Darmstadt, Germany). The precipitation potential of the SBF was checked on broken glass at 37°C. In contrast, the mixture should not precipitate at 4°C on plastic. Ring pieces of COL-Vicryl®-EtO (w: 6.2 ± 0.8 mm, t: 2.8 ± 0.5 mm, n = 36 from 3 constructs) and COL-Vicryl®-γ (w: 5.2 ± 0.6 mm, t: 3.2 ± 0.4 mm, n= 36 from 3 constructs) and incubated in 6-well plates (Corning, Corning, New York, USA) at 37°C. N = 3 was used for each time point (day 0, 3, 7, 14 and 28) for 3 different conditions (goat urine and SBF). The constructs were evaluated by histology and tensile strength analysis using circular ring tests as described above. COL-Vicryl®-EtO and COL-Vicryl®-γ rings in urine were spaced 'hook-to-hook' 21.05 ± 1.75 mm and 21.81 ± 0.40 mm apart, respectively. COL-Vicryl®-EtO and COL-Vicryl®-γ rings in SBF were spaced 24.84 ± 1.50 mm and 21.63 ± 1.27 mm apart, respectively.

2.4 Subcutaneous Implantation

The animal experiment was approved by the Ethical Committee on Animal Research of the Radboud University Medical Center, Nijmegen, The Netherlands (RU-DEC 2014

233). We included nine adult Saane goats (2-3 years, ± 60 kg), receiving restricted diet and water ad libitum. Animals were transported with a 'buddy' goat, but were individually housed with nose contact after surgery and placed in groups when possible at the animal farm. Randomization and blinding was not possible due to clear differences in physical appearances. Subcutaneous implantation was performed to form vascularized neo-tissue as previously described.20 Under general anesthesia subcutaneous pockets were created on the right flank below the muscle layer of the skin, through a 5 cm incision above the shoulder of the right hind leg. In 3 animals one COL-Vicryl®-EtO construct was implanted and in 3 other animals both the COL-Vicryl®-EtO and COL-Vicryl®-γ were implanted in different pockets on the same flank. The pockets were spatially apart to avoid interference of regeneration and/or inflammation. Constructs were extensively washed in PBS, slid over a silicon mandrel and attached to the mandrel using CT-1 Vicryl® sutures (Ethicon, Somerville, NJ, USA). The construct was then inserted into the pocket and attached to the fascia with CT-1 Vicryl® sutures (Ethicon). The skin incision was subsequently closed with 2-0 Vicryl® (Ethicon) for the subcutaneous fat and the skin. Goats received Albipen LA (ampicillin) 15 mg/kg I.M. during surgery and Albipen LA 15 mg/kg S.C. every 48h after surgery.

2.4.1 Evaluation of Implants

One month later, the remodeled tubes were harvested and evaluated. Ring pieces (w: 7.0 ± 2.1 mm, t: 3.1 ± 0.1 mm, n = 7 for COL-Vicryl®-EtO from 2 goats and w: 7.0 ± 1.5 mm, t: 3.4 ± 1.0 mm; n = 11 for COL-Vicryl®-γ from 3 goats) were transferred to PBS and immediately measured by tensile strength analysis by circular ring tests as described above. The hook spacing was 12.7 ± 1.9 mm for COL-Vicryl®-EtO and 15.5 ± 0.6 mm for COL-Vicryl®-γ, respectively. Ring pieces were transferred to 4% (v/v) formaldehyde (Sigma-Aldrich, St. Louis, MO, USA) in PBS for fixation and subsequent embedding in paraffin for microscopic analysis. HE slides were scored by three independent observers (MS, PG, PdJ) for collagen and Vicryl® degradation, inflammation, tissue integration and vascularity. Averages of the independent scorings were calculated and combined into a scoring profile. Representative slides were used for confirmation by Masson's Trichrome and immunohistochemistry.

2.4.2 Immunohistochemistry

Expression of type IV Collagen (COLIV) and HIF1α was analyzed on paraffin-embedded material (5 µm thickness), mounted on Silane-coated slides (New Silane

III, Muto Pure Chemicals Co., Ltd., Tokyo, Japan). After deparaffinization and PBS washings, endogenous peroxidase activity was blocked by incubation in 1% (v/v) H2O2 in PBS for 20 min.

For COLIV, antigen retrieval was performed using 0.05% (v/v) proteinase in PBS (20 min, 37°C, Merck, Darmstadt, Germany). Slides were then washed with PBS/Tween and incubated with 10% (v/v) swine serum (30 min) followed by incubation with the primary antibody (1h, rabbit-α-human COLIV, 1:250, Abcam, Cambridge, UK). After washings, the sections were incubated with peroxidase-labelled swine-α-rabbit secondary antibody (30 min, SWARPO, 1:100, DakoCytomation, Glostrup, Denmark) followed by washings.

For HIF1α, heat-induced antigen retrieval was performed using sodium citrate (pH 6) followed by TBS/0.1%Tween20 washings. Blocking of endogenous biotin (and receptors) and avidin receptors (10 min, Vector Laboratories, Burlingame, California, USA) was performed with washing in between. After additional washing, endogenous proteins were blocked with 2% BSA (5 min), directly followed by incubation with the primary antibody (45 min, mouse-α-human HIF1α, 1:500, BD Biosciences, San Jose, CA, USA). After washings, sections were incubated with a biotin-labeled secondary antibody (15 min, donkey-α-mouse, 1:500, Jackson ImmunoResearch, West Grove, PA, USA). Slides were then washed and 15 min incubated with peroxidase-labeled streptavidin/biotin complex (1:100 Avidin solution and 1:100 Biotin solution, 30 min pre-incubation, Vector Laboratories, Burlingame, California, USA). An amplification step was performed after washings using biotinyl tyramide (15 min, DAKO, Heverle, Belgium). After washings, slides were incubated with peroxidase-labelled streptavidin (15 min, 1:250, Thermoscientific, Rockford, IL, USA) followed by washings.

For both COLIV and HIF1α, sections were developed with Bright-DAB (ImmunoLogic, Duiven, The Netherlands) and counterstained with hematoxylin (Klinipath, Duiven, The Netherlands). For negative controls the primary antibody was omitted, and no staining was observed in these samples. Native tissue was used for a positive control, showing staining in expected tissue components.

2.5 Statistics

Data is presented as mean with standard deviation and analyzed with Prism software (Version 5.03, Graphpad Software Inc, La Jolla, CA, USA). A one-way ANOVA with Bonferroni post-hoc test was performed for statistical analysis of differences between COL-Vicryl®-EtO, COL-Vicyl®-γ and native goat ureter.

3 RESULTS

3.1 Construct Analysis

The macroscopic appearance of the COL-Vicryl®-EtO and COL-Vicryl®-γ constructs can be seen in **Figure 1A-B**. The luminal diameter (13.1 ± 1.1 mm for COL-Vicryl®-EtO and 14.6 ± 1.4 mm COL-Vicryl®-γ, respectively) slightly differed due to additional processing (freezing and freeze-drying) required for COL-Vicryl®-EtO constructs. Microscopic analysis by scanning electron microscopy and histology showed integration of the Vicryl® polymer as indicated by visible collagen-Vicryl® connections and a typical honeycomb structure (**Figure 1C-D**). For the COL-Vicryl®-EtO constructs, that required additional processing (freezing and freeze-drying), a thinner and compressed wall with smaller pores was observed (**Figure 1E-F**). Cross-linking was successful as indicated by the decrease in free amine groups and was comparable for both groups: 35% for the COL-Vicryl-γ (reduced to 109 ± 15 nmol/mg) and 37% for the COL-Vicryl®-EtO (reduced to 202 ± 5 nmol/mg). The mechanical characteristics of the construct were compared to native goat ureter, the primary anastomosis site for the construct in an artificial urostomy and conform the animal model (**Figure 1G-H**). The COL-Vicryl®-γ Young's modulus (2.31 ± 0.67 MPa) was approximately twice as high as the ureter (0.95 ± 0.39 MPa) whilst the COL-Vicryl®-EtO showed a Young's modulus only 1.5x as high (1.57 ± 0.75 MPa). The ultimate tensile strength (UTS) and failure strain of the ureter and both constructs was similar (ureter: 0.83 ± 0.26 MPa at 2.6 ± 1.1 mm/mm strain, COL-Vicryl®-EtO: 0.66 ± 0.39 MPa at 1.22 ± 0.31 mm/mm strain, COL-Vicryl®-γ: 0.74 ± 0.28 MPa at 0.85 ± 0.10 mm/mm strain).

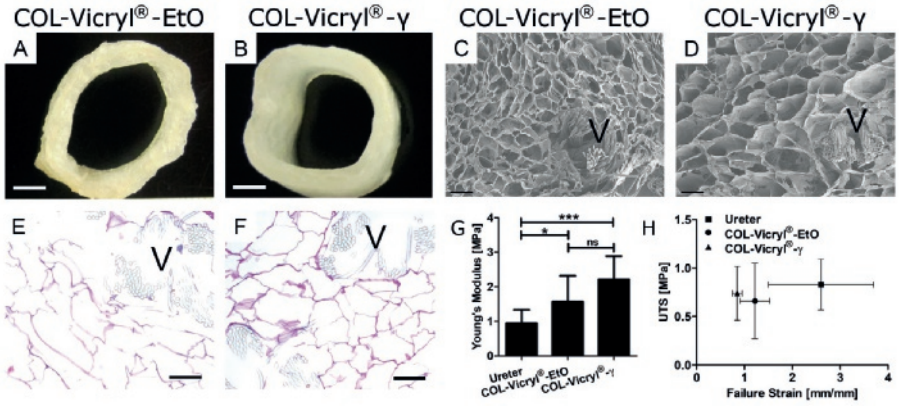

Figure 1. Construct analysis. A-B) show the macroscopic overview of the COL-Vicryl®-EtO and COL-Vicryl®-γ, scale bar = 0.5 cm. C-D) show the SEM images, scale bar = 250 µm, pore size for COL-Vicryl®-EtO is approximately 150-250 µm and for COL-Vicryl®-γ 200-300 µm, and E-F) show the histological overview of the construct, scale bar = 250 µm. G-H) represents the mechanical characteristics of the constructs. V = Vicryl® polymer, * $p < 0.05$, *** $p < 0.0001$, ns = non-significant.

3.2 Degradation Assay

Incubation in goat urine resulted in fast degradation (<7 days) of the Vicryl® polymer in both constructs (**Figure 2A**). Microscopic analysis revealed negative imprints of the multi-filamented Vicryl® in the scaffold after 3 days. The collagen structure was barely affected in the COL-Vicryl®-γ constructs. In contrast, swelling of collagen lamellae was seen in the urine-incubated COL-Vicryl®-EtO constructs at day 28 (**Figure 2A**). Tensile strength analysis of the ring pieces showed a strongly diminished UTS and Young's modulus, already after 3 days (**Figure 2B**), regardless of the sterilization method.

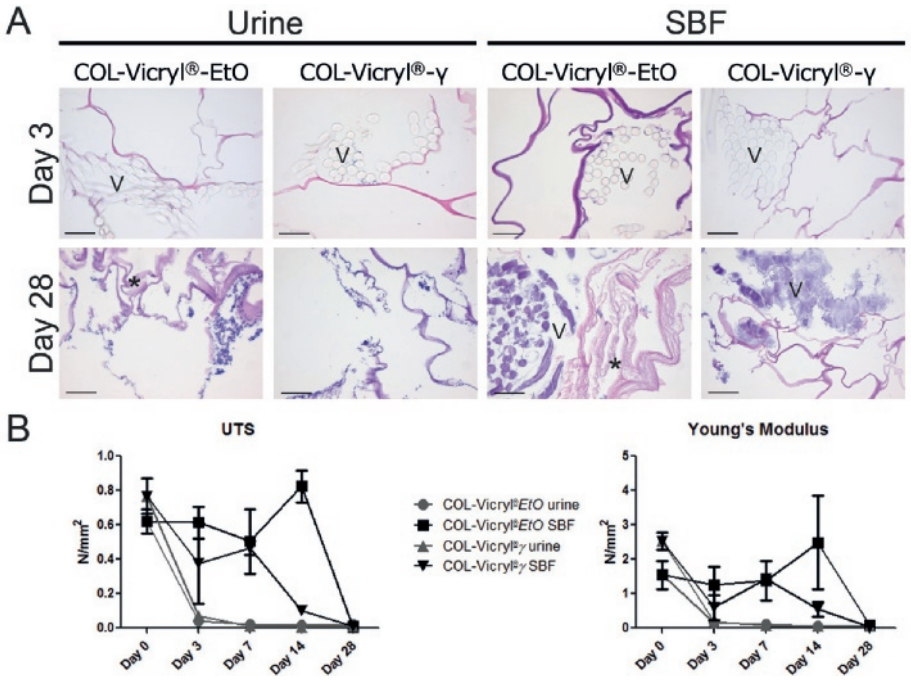

Figure 2. Degradation assay. A) shows the microscopic overview by HE of the degradation assay in urine and SBF, scale bar = 100 µm, V = Vicryl® polymer, * = collagen degradation. Images presented at for urine day 28 are representable for day 14 and 7. Images presented for SBF day 3 are representable for day 7 and 14. B) Mechanical characteristics of the degraded constructs. Urine exposure resulted in immediate diminished mechanical properties of both construct types at day 3, although the Vicryl® was still morphologically visible. In SBF prolonged mechanical stability was observed until day 14 for both constructs. At day 28 the mechanical properties were lost and the polymer showed signs of severe degradation.

The effect of SBF was less extensive, and Vicryl® remnants were still present at 28 days in both constructs, although their original multi-filamented structure was lost. Only in the COL-Vicryl®-EtO construct the collagen was substantially affected by SBF and showed swelling of collagen lamellae at 14 and 28 days. The UTS and Young's modulus

of the constructs in SBF were maintained for at least 14 days. At this evaluation point, COL-Vicryl®-EtO showed a higher UTS and Young's modulus then COL-Vicryl®-γ, but after 28 days UTS and Young's modulus of both constructs were similar.

3.3 Subcutaneous Implantation

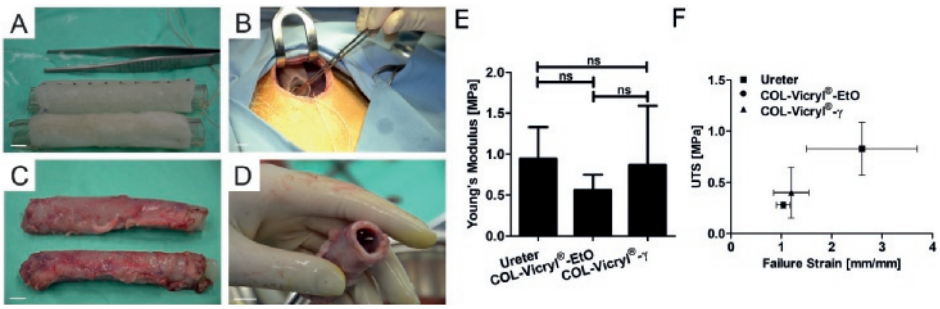

Figure 3. Subcutaneous implantation. A) shows the overview of the washed constructs with the inserted mandrel, all scale bars – 1 cm. COL-Vicryl®-γ is the upper construct, COL-Vicryl®-EtO is the lower construct, B) shows the subcutaneous pocket, C) shows the autologous tissue tubes one month after implantation (same formation as in A) and D) shows the open lumen after removal of the mandrel. E-F) shows the mechanical characteristics of the implanted constructs compared to native goat ureter. ns = non-significant.

Subcutaneous implantation was successful in all goats and for all constructs. After one month, a remodeled neo-tissue tube was formed regardless of the sterilization method. The neo-tissue tube was encapsulated but easy to harvest from the subcutaneous pocket (**Figure 3A-D**). The rims of the neo-tissue, where scaffold material was absent, were fragile and ruptured easily and were therefore eliminated from analysis. After removal of the mandrel, the firm tissue was able to maintain an open lumen and was suitable for translocation to serve as an artificial urostomy. No clear macroscopic differences between the construct types were observed.

Ring pieces of both implants were analyzed by tensile strength analysis and compared to the native goat ureter (**Figure 3E-F**). After subcutaneous implantation, the UTS of the COL-Vicryl®-EtO was 0.28 ± 0.03 MPa at 1.04 ± 0.14 mm/mm strain and 0.40 ± 0.25 MPa at 1.26 ± 0.33 mm/mm strain for the COL-Vicryl®-γ. This was significantly lower than the UTS for the native goat ureter (0.83 ± 0.26 MPa at 2.6 ± 1.1 mm/mm strain). The Young's modulus was similar for all groups (ureter: 0.95 ± 0.39 MPa, COL-Vicryl®-EtO: 0.56 ± 0.19 MPa and COL-Vicryl®-γ 0.87 ± 0.72 MPa). The UTS and Young's modulus of the COL-Vicryl®-γ implant approximated the native ureter (the tissue to be mimicked in the urostomy) more closely than the COL-Vicryl®-EtO.

3.4 (Immuno)histological Analysis of Implants

Table 1. Scoring profile. Hematoxyline and eosin (HE) slides of implanted COL-Vicryl®-EtO and COL-Vicryl®-γ constructs were independently scored for relative comparison to one another to create a representative profile for each implanted construct. No reference material was used. Items were scored – (not present), +/- (sporadically present), + (moderately present), ++ (abundantly present) or +++ (excessively present).

	COL-Vicryl®-EtO	COL-Vicryl®- γ
Collagen degradation	+	++
Vicryl® degradation	+/-	+
Inflammation	+	+
Tissue integration	+	++
Vascularity	+	+

Detailed microscopic evaluation showed a clear difference between the COL-Vicryl®-EtO and the COL-Vicryl®-γ implants (**Figure 4** and **Table 1**). The implanted COL-Vicryl®-γ constructs were well integrated in the surrounding tissue and both collagen and the Vicryl® polymer were partially degraded. Ingrowing fibroblast-like cells from the surrounding tissue were present within the honeycomb structures of the collagen and between the Vicryl® filaments. In contrast, the COL-Vicryl®-EtO constructs did not successfully integrate in the surrounding tissue, resulting in a clear boundary between the construct and surrounding tissue in some areas (**Figure 4D**). Degradation of collagen and Vicryl® was substantially less in the COL-Vicryl®-EtO constructs. In these less degraded areas of the COL-Vicryl®-EtO constructs and increased expression of HIF1α+ was observed, indicating hypoxia.

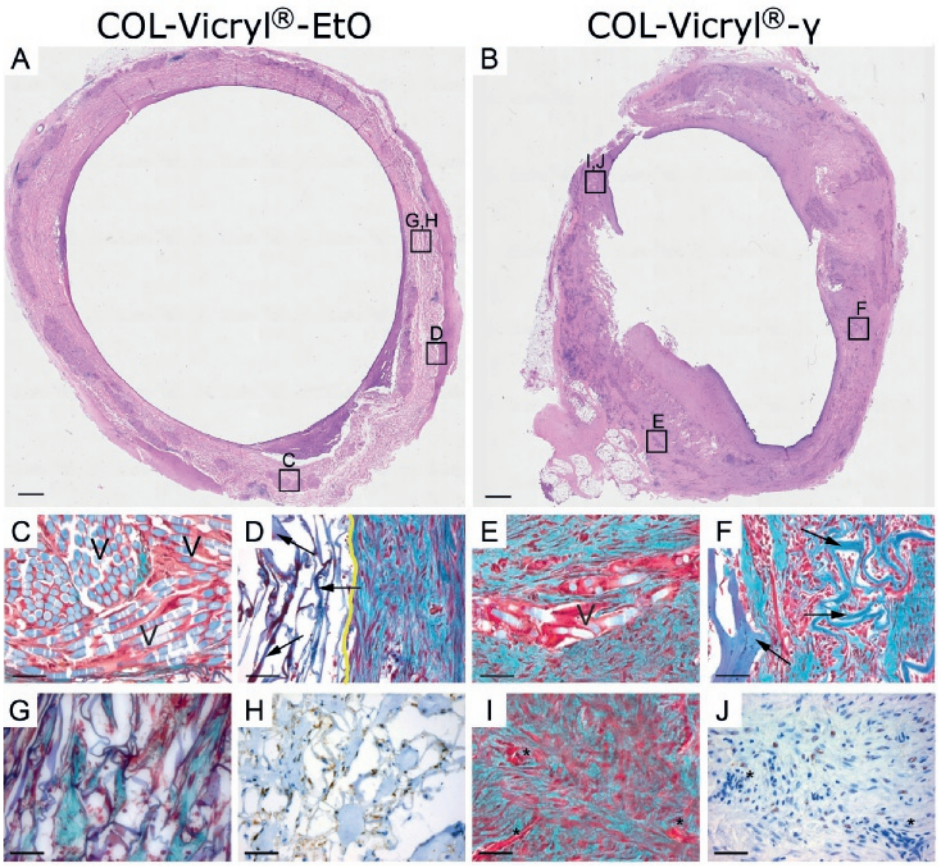

Figure 4: Histological and immunohistochemical analysis of the implants. A-B) Macroscopic overview of ring pieces of COL-Vicryl®-EtO and COL-Vicryl®-γ by HE, scale bar = 1 mm. C-G, I) Masson's Trichrome staining from indicated boxes in A and B, blue/green = collagen, collagen from constructs is indicated by arrows, light blue (V) = Vicryl® polymer, red/brown = cell nuclei, yellow line = construct/tissue boundary, scale bar = 100 µm. G-H) contruct material showing limited regeneration, without vascular structures, but high expression of HIFαα. I-J) construct material showing progressive regeneration with presence of vascular structures (*) and limited HIF1α expression. Scale bar = 200 µm.

Although the amount of vascularity was comparable between groups, a different vascular architecture was observed in the luminal area (**Table 1** and **Figure 5**). In the COL-Vicryl®-γ an organized layer of COLIV+ vasculature was formed, whilst in the COL-Vicryl®-EtO group an aberrant architecture of vasculature was observed when compared to the vascular bed in normal tissue. Since COL IV staining completely coincided with capillaries, COL IV staining was judged to be an appropriate surrogate marker for the capillary network.

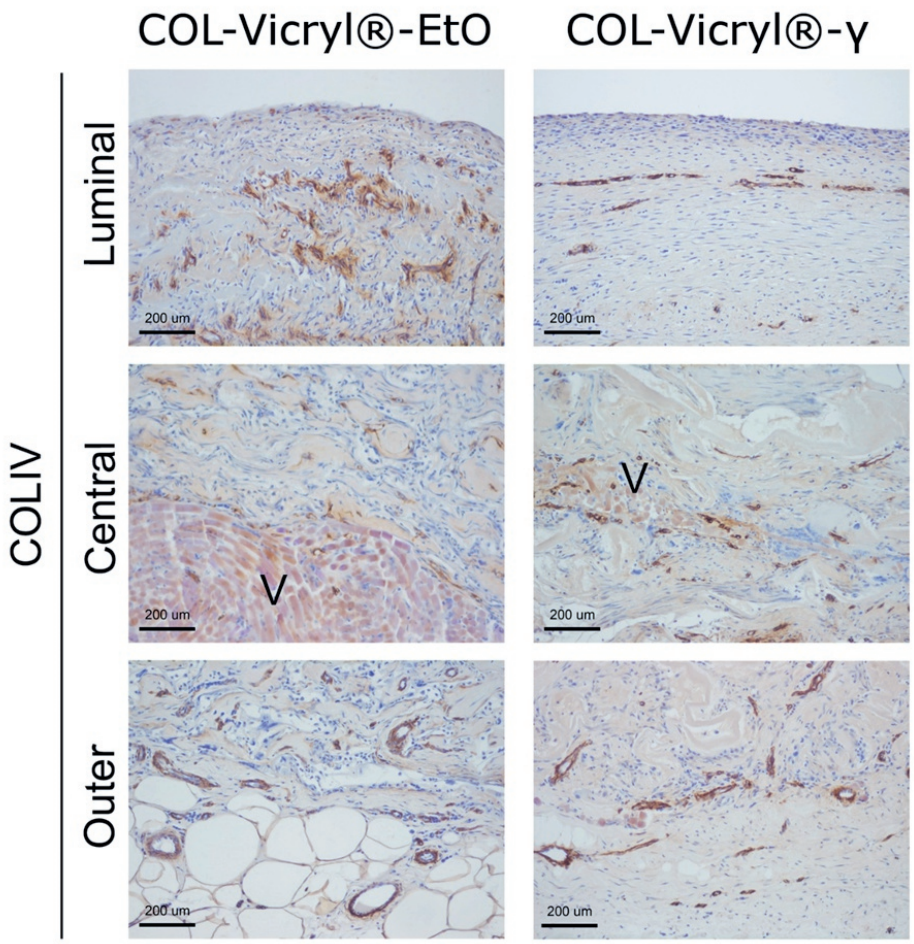

Figure 5. Evaluation of vascularization in COL-Vicryl®-EtO and COL-Vicryl®-γ implant. Luminal, middle and outer area of implants were stained with COLIV to visualize the vasculature. Outer and central areas are comparable between construct types. However, the luminal area showed a thin organized architecture of vasculature in the COL-Vicryl®-γ, which is comparable to native urinary tissue. The COL-Vicryl®-EtO shows an aberrant vasculature in the luminal area. V = Vicryl®, scale bar = 200 µm.

4 DISCUSSION

Clinical implementation of biomaterials requires sterilization with EMA- (European Medicines Agency) and FDA- (United States Food and Drug Administration) approved techniques, like γ-irradiation or EtO-degassing. In the pre-clinical phase materials are generally tested *in vitro* and *in vivo* with non-validated, in-house disinfection or sterilization methods, to evaluate strength, cyto- and biocompatibility. This study shows that sterilization procedures are a crucial aspect in template design as it significantly influences tissue remodeling upon implantation. Therefore, evaluation of the effects of the sterilization procedures should become standard in early biomaterial development. Moreover, we demonstrate that *in vitro* data cannot be solely used as predictive factors for material behavior *in vivo*: whereas remodeling of EtO-sterilized constructs –the initial method of choice- was limited, enhanced tissue remodeling was observed after γ-sterilization. I.e., the *in vivo* behavior of templates is heavily dependent on the sterilization methods used. Biomaterial evaluation, preferably in a large animal, is required to facilitate clinical translation and registration as a medical device.

In the *in vitro* part of this study, we evaluated the mechanical and morphological characteristics of the hybrid tubular constructs. For urological tissue engineering and specifically the artificial urinary conduit, the addition of a reinforcing polymer to the collagen, e.g. Vicryl®, is desired to provide additional strength for template functionality and surgical handling [25,28]. Terminal sterilization of this hybrid tubular construct by EtO-degassing or γ-irradiation did not lead to major differences between constructs with respect to the morphological and mechanical characteristics, similar to earlier studies for collagen alone [29]. Other studies already showed that γ-sterilization of collagen results in enhanced enzymatic degradation and reduced integrity and stability due to chain disintegration in collagen molecules in comparison to non-sterilized construct. In contrast, the structure and stability of EtO-sterilized collagen is reported to remain unaltered and comparable to unsterilized scaffolds [29,30]. The enhanced tissue remodeling of the γ-irradiated constructs, when placed in a subcutaneous pocket in our study, may well be explained by the γ-irradiation induced alterations of the collagen.

Furthermore, we assessed the influence of a wet environment using either urine, mimicking direct implantation e.g. when used as an artificial urinary conduit, or Simulated Body Fluid (SBF), mimicking subcutaneous implantation. Interestingly, exposure of both constructs to urine resulted in immediate loss of Vicryl® polymer

integrity (3 days). This suggests that direct implantation of the construct in the urinary tract will lead to material collapse before sufficient tissue regeneration can occur and may therefore not be advisable. Pre-implantation to form neo-tissue may solve this by creating a (semi-)autologous construct.

The biomechanical properties of absorbable multifilament sutures, like Vicryl®, have been previously evaluated in equine urine and similarly showed total loss of Vicryl® integrity albeit after 21 days [31]. The absence of any buffering capacity of both goat and equine urine may have influenced Vicryl® degradation by enhancing pH-dependent hydrolysis. The higher degradation rate of the Vicryl® mesh observed in our study was probably the consequence of additional γ-sterilization of the commercially available and already sterilized Vicryl® polymer mesh [32].

Exposing the construct to SBF instead of urine prolonged Vicryl® polymer stability up to two weeks. At this time, the strength and Young's Modulus of the COL-Vicryl®-EtO was significantly higher than the COL-Vicryl®-γ. After 28 days, signs of collagen degradation (swelling) were observed in the EtO-sterilized construct and not in the γ-sterilized constructs. The swelling may have been the consequence of the thinner and compressed wall in the COL-Vicryl®-EtO. The γ-sterilization results in additional crosslinking and strengthening of collagen which may explain this difference [33]. In contrast, it is well established that sterilization of Vicryl® by γ-irradiation results in enhanced degradability due to chain fragmentation [34]. Although this explains the lower Young's modulus of the COL-Vicryl®-γ over time, this *in vitro* assay only evaluated material degradation, whilst the creation of an autologous tissue tube is a balance between material degradation and tissue regeneration. Adequate assessment of this balance requires *in vivo* analysis.

Besides the slightly prolonged stability of the COL-Vicryl®-EtO in a wet environment, neither of the constructs was superior in the *in vitro* analyses. Both constructs were therefore tested in a subcutaneous implantation model. Interestingly, when the implanted constructs were harvested, tissue ingrowth of pre-implanted COL-Vicryl®-γ was much further developed compared to EtO-degassed constructs. In accordance with the *in vitro* data, the Vicryl® polymer in the EtO-sterilized constructs was less susceptible to degradation *in vivo* and contributed to prolonged strength over time. This is in agreement with a previous study showing that γ-irradiation enhanced Vicryl® degradation when implanted in the lumbar muscle of rats [22,33]. It is likely that the enhanced degradation rate of Vicryl® facilitates the ingrowth of surrounding tissue and the formation of an organized subluminal vasculature in the pre-implanted COL-Vicryl®-γ. The aberrant vascular

architecture in the COL-Vicryl®-EtO pre-implant may have been the consequence of prolonged and increased levels of hypoxia. Full comprehension of the sterilization effect required functional analysis *in vivo*. Our earlier studies suggested that perhaps prolongation of template stability to achieve sustained mechanical stability might be important in the formation of the artificial conduit [17]. Indeed, our *in vitro* analyses showed that prolonged stability in a fluid could be accomplished by applying EtO-sterilization to the hybrid tubular construct. However, the COL-Vicryl®-EtO was not superior *in vivo*. Clearly, other aspects like cellular ingrowth and vascularization are equally or even more important. Furthermore, mechanical analysis after implantation did not indicate a difference in strength or elasticity, suggesting that the loss of construct integrity is compensated by tissue ingrowth, with no net loss of strength as a result.

Absorption of urine by collagen scaffolds may cause aberrant remodeling. Previously, cell seeded constructs have been tested as urostomy constructs, but this was not very successful, although urine exposure of the collagen graft was limited [20]. In an ongoing pilot experiment, we noticed that creation of an artificial conduit with pre-implanted COL-Vicryl®-EtO tubes was not successful due to disconnection from the ureter and poor integration to the surrounding tissue. In contrast, when the completely remodeled COL-Vicryl®-γ construct was used, this ultimately resulted in a functional conduit (results not shown, manuscript in preparation), showing that urine did not influence the outcome of constructs aligned with cells, but that the outcome is more dependent on the sterilization method used.

EtO and γ-irradiation are two of the most commonly used and FDA-approved sterilization techniques and were therefore chosen as comparators. Recently, novel sterilization techniques, like supercritical carbon dioxide (scCO2), have come available and this may provide a valuable alternative [35]. In combination with an altered collagen component and/or bioreactor conditioning in combination with cells this may ultimately lead to superior constructs for *in vivo* use. Our study shows that for full comprehension of the effect of a novel sterilization method on *in vivo* biomaterial behavior a complete panel of analyses ranging from mechanical characterization to implantation in a functional setting in a large animal model is essential.

5 CONCLUSION

Thorough analysis of the *in vitro* and *in vivo* behavior of sterilized collagen-Vicryl® tubular templates shows that the effect of final sterilization is considerable. Subcutaneous implantation of a γ-sterilized hybrid template resulted in better tissue remodeling compared to EtO-sterilized constructs. This study shows that sterilization affects tissue remodeling upon implantation. Clinical translation of tissue engineered biomaterials can only be achieved when EMA-FDA-approved sterilization methods are included in a full panel of *in vitro* and *in vivo* analyses.

6 ACKNOWLEDGEMENTS

C. Van den Broek, T. Wijga, A.E.J. Hanssen, and M.M.A. School (Radboudumc, Nijmegen, The Netherlands) are greatly acknowledged for their participation and assistance during the animal experiments.

This work was financially supported by Fonds NutsOhra (FNO), Kunststoma 1102-56 (www.stichtingnutsohra.nl) and PIDON, Novio Tissue, PID 101020. Additionally, the research leading to these results has received funding from the People Programme (Marie Curie Actions) of the European Union's Seventh Framework Programme FP7/2007-2013/ under REA grant agreement No. 607868 (iTERM).

7 REFERENCES

[1] N. Morimoto, N. Kakudo, M. Matsui, T. Ogura, T. Hara, K. Suzuki, M. Yamamoto, Y. Tabata, K. Kusumoto, Exploratory clinical trial of combination wound therapy with a gelatin sheet and platelet-rich plasma in patients with chronic skin ulcers: study protocol, BMJ Open. 5 (2015) e007733. DOI:10.1136/bmjopen-2015-007733.

[2] K. Omori, T. Nakamura, S. Kanemaru, R. Asato, M. Yamashita, S. Tanaka, A. Magrufov, J. Ito, Y. Shimizu, Regenerative medicine of the trachea: the first human case, Ann Otol Rhinol Laryngol. 114 (2005) 429–433. DOI: 10.1177/000348940511400603.

[3] D.C. Crawford, T.M. DeBerardino, R.J. Williams 3rd, NeoCart, an autologous cartilage tissue implant, compared with microfracture for treatment of distal femoral cartilage lesions: an FDA phase-II prospective, randomized clinical trial after two years, J Bone Jt. Surg Am. 94 (2012) 979–989. DOI:10.2106/jbjs.k.00533.

[4] D.B. Joseph, J.G. Borer, R.E. De Filippo, S.J. Hodges, G.A. McLorie, Autologous cell seeded biodegradable scaffold for augmentation cystoplasty: phase II study in children and adolescents with spina bifida, J Urol. 191 (2014) 1389–1395. DOI:10.1016/j.juro.2013.10.103.

[5] M. Grimes, J.T. Pembroke, T. McGloughlin, The effect of choice of sterilisation method on the biocompatibility and biodegradability of SIS (small intestinal submucosa), Biomed Mater Eng. 15 (2005) 65–71. ISSN: 0959-2989.

[6] J. Rnjak-Kovacina, T.M. DesRochers, K.A. Burke, D.L. Kaplan, The effect of sterilization on silk fibroin biomaterial properties, Macromol Biosci. 15 (2015) 861–874. DOI:10.1002/mabi.201500013.

[7] T. Watanabe, K. Kanda, M. Yamanami, H. Ishibashi-Ueda, H. Yaku, Y. Nakayama, Long-term animal implantation study of biotube-autologous small-caliber vascular graft fabricated by in-body tissue architecture, J Biomed Mater Res B Appl Biomater. 98 (2011) 120–126. DOI:10.1002/jbm.b.31841.

[8] Z. Wang, C. Roberge, L.H. Dao, Y. Wan, G. Shi, M. Rouabhia, R. Guidoin, Z. Zhang, *In vivo* evaluation of a novel electrically conductive polypyrrole/poly(D,L-lactide) composite and polypyrrole-coated poly(D,L-lactide-co-glycolide) membranes, J Biomed Mater Res A. 70 (2004) 28–38. DOI:10.1002/jbm.a.30047.

[9] H. Nguyen, D.A. Morgan, M.R. Forwood, Sterilization of allograft bone: effects of gamma irradiation on allograft biology and biomechanics, Cell Tissue Bank. 8 (2007) 93–105. DOI:10.1007/s10561-006-9020-1.

[10] L.M. Delgado, A. Pandit, D.I. Zeugolis, Influence of sterilisation methods on collagen-based devices stability and properties, Expert Rev Med Devices. 11 (2014) 305–314. DOI:10.1586/17434440.2014.900436.

[11] M. Sloff, R. de Vries, P. Geutjes, J. IntHout, M. Ritskes-Hoitinga, E. Oosterwijk, W. Feitz, Tissue Engineering in Animal Models for Urinary Diversion: A Systematic Review, PLoS One. 9 (2014) e98734. DOI:10.1371/journal.pone.0098734.

[12] M. Sloff, V. Simaioforidis, R. de Vries, E. Oosterwijk, W. Feitz, Tissue Engineering of the Bladder—Reality or Myth? A Systematic Review, J. Urol. 192 (2014) 1035–1042. DOI:10.1016/j.juro.2014.03.116.

[13] C.L. Dearth, T.J. Keane, C.A. Carruthers, J.E. Reing, L. Huleihel, C.A. Ranallo, E.W. Kollar, S.F. Badylak, The effect of terminal sterilization on the material properties and *in vivo* remodeling of a porcine dermal biologic scaffold, Acta Biomater. 33 (2016) 78–87. DOI:10.1016/j.actbio.2016.01.038.

[14] A.M. Matuska, P.S. McFetridge, The effect of terminal sterilization on structural and biophysical properties of a decellularized collagen-based scaffold; implications for stem cell adhesion, J Biomed Mater Res B Appl Biomater. 103 (2015) 397–406. DOI:10.1002/jbm.b.33213.

[15] G.C. Mendes, T.R. Brandao, C.L. Silva, Ethylene oxide sterilization of medical devices: a review, Am J Infect Control. 35 (2007) 574–581. DOI:10.1016/j.ajic.2006.10.014.

[16] E. Phillip Jr., N.S. Murthy, D. Bolikal, P. Narayanan, J. Kohn, L. Lavelle, S. Bodnar, K. Pricer, Ethylene oxide's role as a reactive agent during sterilization: effects of polymer composition and device architecture, J Biomed Mater Res B Appl Biomater. 101 (2013) 532–540. DOI:10.1002/jbm.b.32853.

[17] P. Geutjes, L. Roelofs, H. Hoogenkamp, M. Walraven, B. Kortmann, R. de Gier, F. Farag, D. Tiemessen, M. Sloff, E. Oosterwijk, T. van Kuppevelt, W. Daamen, W. Feitz, Tissue engineered tubular construct for urinary diversion in a preclinical porcine model, J Urol. 188 (2012) 653–660. DOI:10.1016/j.juro.2012.03.119.

[18] G.A. Abraham, J. Murray, K. Billiar, S.J. Sullivan, Evaluation of the porcine intestinal collagen layer as a biomaterial, J Biomed Mater Res. 51 (2000) 442–452. DOI: 10.1002/1097-4636(20000905)51:33.3.CO;2-W.

[19] A. Rahmanian-Schwarz, M. Held, T. Knoeller, S. Stachon, T. Schmidt, H.E. Schaller, L. Just, *In vivo* biocompatibility and biodegradation of a novel thin and mechanically stable collagen scaffold, J Biomed Mater Res A. 102 (2014) 1173–1179. DOI:10.1002/jbm.a.34793.

[20] M. Sloff, V. Simaioforidis, D.M. Tiemessen, H.P. Janke, B.B.M. Kortmann, L.A.J. Roelofs, P.J. Geutjes, E. Oosterwijk, W.F.J. Feitz Prof, Tubular constructs as artificial urinary conduits., J. Urol. (2016). DOI:10.1016/j.juro.2016.04.092.

[21] D. Leonhäuser, M. Vogt, R.H. Tolba, J.O. Grosse, Potential in two types of collagen scaffolds for urological tissue engineering applications - Are there differences in growth behaviour of juvenile and adult vesical cells?, J. Biomater. Appl. 30 (2016) 961–73. DOI:10.1177/0885328215610824.

[22] I.N. Bird, I.A. Silver, S.D. Gorham, D.A. French, *In vivo* degradation of collagen-vicryl materials in rabbit ear chambers, J. Mater. Sci. Mater. Med. 2 (1991) 36–42. DOI:10.1007/BF00701685.

[23] M. Sloff, V. Simaioforidis, P.J. Geutjes, H.R. Hoogenkamp, T.H. van Kuppevelt, W.F. Daamen, E. Oosterwijk, W.F. Feitz, Novel tubular constructs for urinary diversion: a biocompatibility study in pigs., J. Tissue Eng. Regen. Med. (2016). DOI:10.1002/term.2122.

[24] L.H. Olde Damink, P.J. Dijkstra, M.J. van Luyn, P.B. van Wachem, P. Nieuwenhuis, J. Feijen, Cross-linking of dermal sheep collagen using a water-soluble carbodiimide, Biomaterials. 17 (1996) 765–773. DOI: 10.1016/0142-9612(96)81413-X.

[25] H.P. Janke, J. Bohlin, R.M.L.M. Lomme, S.M. Mihaila, J. Hilborn, W.F.J. Feitz, E. Oosterwijk, Bioinspired coupled helical coils for soft tissue engineering of tubular structures – Improved mechanical behavior of tubular collagen type I templates, Acta Biomater. 59 (2017) 234–242. DOI:10.1016/j.actbio.2017.06.038.

[26] C.-H. Lin, Y.-C. Kao, Y.-H. Lin, H. Ma, R.-Y. Tsay, A fiber-progressive-engagement model to evaluate the composition, microstructure, and nonlinear pseudoelastic behavior of porcine arteries and decellularized derivatives, Acta Biomater. 46 (2016) 101–111. DOI:10.1016/j.actbio.2016.09.025.

[27] A. Oyane, H.M. Kim, T. Furuya, T. Kokubo, T. Miyazaki, T. Nakamura, Preparation and assessment of revised simulated body fluids, J Biomed Mater Res A. 65 (2003) 188–195. DOI:10.1002/jbm.a.10482.

[28] H.R. Hoogenkamp, M.J.W. Koens, P.J. Geutjes, H. Ainoedhofer, G. Wanten, D.M. Tiemessen, J. Hilborn, B. Gupta, W.F.J. Feitz, W.F. Daamen, A.K. Saxena, E. Oosterwijk, T.H. van Kuppevelt, Seamless vascularized large-diameter tubular collagen scaffolds reinforced with polymer knittings for esophageal regenerative medicine., Tissue Eng. Part C. Methods. 20 (2014) 423–30. DOI:10.1089/ten.TEC.2013.0485.

[29] K.A. Faraj, K.M. Brouwer, P.J. Geutjes, E.M. Versteeg, R.G. Wismans, J.A. Deprest, H. Chajra, D.M. Tiemessen, W.F.J. Feitz, E. Oosterwijk, The effect of ethylene oxide sterilisation, beta irradiation and gamma irradiation on collagen fibril-based scaffolds, Tissue Eng. Regen. Med. 8 (2011) 460–470. ISSN: 1932-6254.

[30] E.M. Noah, J. Chen, X. Jiao, I. Heschel, N. Pallua, Impact of sterilization on the porous design and cell behavior in collagen sponges prepared for tissue engineering, Biomaterials. 23 (2002) 2855–2861. DOI: 10.1016/S0142-9612(01)00412-4.

[31] C.M. Kearney, C.T. Buckley, F. Jenner, P. Moissonnier, P.A. Brama, Elasticity and breaking strength of synthetic suture materials incubated in various equine physiological and pathological solutions, Equine Vet J. 46 (2014) 494–498. DOI:10.1111/evj.12181.

[32] R.L. Kerstein, T. Sedaghati, A.M. Seifalian, N. Kang, Effect of human urine on the tensile strength of sutures used for hypospadias surgery, J Plast Reconstr Aesthet Surg. 66 (2013) 835–838. DOI:10.1016/j.bjps.2013.02.006.

[33] S.D. Gorham, S. Srivastava, D.A. French, R. Scott, The effect of gamma-ray and ethylene oxide sterilization on collagen-based wound-repair materials, J. Mater. Sci. Mater. Med. 4 (1993) 40–49.

[34] C.C. Chu, D.F. Williams, The effect of gamma irradiation on the enzymatic degradation of polyglycolic acid absorbable sutures., J. Biomed. Mater. Res. 17 (1983) 1029–40. DOI:10.1002/jbm.820170612.

[35] J.L. Balestrini, A. Liu, A.L. Gard, J. Huie, K.M. Blatt, J. Schwan, L. Zhao, T.J. Broekelmann, R.P. Mecham, E.C. Wilcox, L.E. Niklason, Sterilization of Lung Matrices by Supercritical Carbon Dioxide, Tissue Eng Part C Methods. (2016). DOI:10.1089/ten.TEC.2015.0449.

CHAPTER 7

Summary
Discussion
Future Perspectives

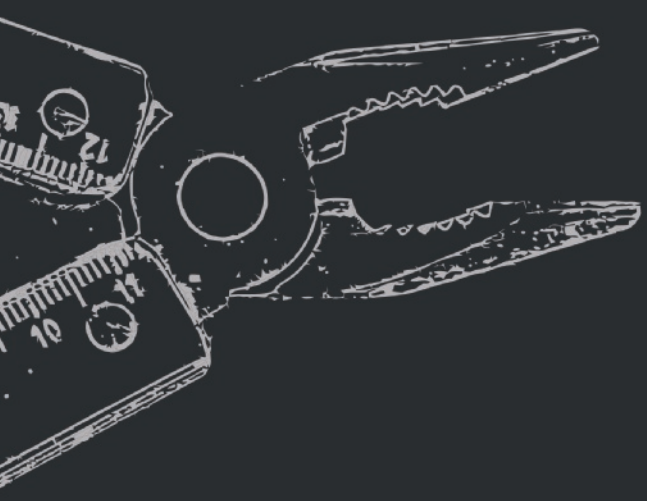

Samenvatting
Discussie
Toekomstvisie

1 SUMMARY AND DISCUSSION

1.1 Clinical Challenge and Aim of this Thesis

Long-segment ureter reconstruction (e.g. after trauma) or forming an urinary diversion (e.g. after radical cystectomy) can be a challenge for most urologists. The standard treatment is the creation of neotissue by using autologous bowel segments. However, this source of tissue is associated with multiple side effects [1–5]. Alternative graft (bio)materials are highly desirable and may circumvent standard-treatment related complications and graft shortage. The field of Tissue Engineering (TE) aims to replace or repair damaged organs and tissues [6]. The backbone of tissue-engineered grafts is the so-called scaffold which can be composed of natural biomaterials, synthetic biomaterials or combining both to create smart hybrid scaffolds. The scaffold acts as a starter matrix to fill the defect and carries various (bio)mechanical loads until it is remodeled by host tissue [7]. Since the ultimate goal of ureter reconstruction and urinary diversion is the safe transport of urine, implanted graft (bio)materials should actively contribute to this safe transport and protect surrounding tissue. Furthermore, the patient's own cells may be seeded on the scaffold to generate functional tissue substitutes [8]. Upon implantation, noninvasive imaging techniques are of utmost importance to access graft patency and tissue remodeling in real-time [9].

The aim of this thesis was to develop innovative imageable tissue-engineered tools which can be used for ureteral reconstruction and/or creation of an artificial urostomy.

1.2 State-of-the-Art Ureter Reconstruction and Urinary Diversion using Tissue Engineering Approaches

In **chapter 2**, the state-of-the-art TE approaches for ureter reconstruction and urinary diversion with emphasis on biomaterials and scaffold design was reviewed. Studies were further categorized based on whether scaffolds were directly implanted, seeded with cells prior to implantation, or preimplanted (with or without cells) before functional implantation.

The collective evidence showed that regeneration of ureteral tissue and the formation of a urinary diversion using TE approaches is possible, albeit that it is complex to achieve well-developed and functional neotissue. Preclinical studies showed that cell-free functional implantation of scaffolds is problematic: it leads to fibrosis, graft-shrinkage, stricture formation and hydronephrosis despite the

generation of a urothelial lining. The addition of autologous smooth muscle cells (SMCs) and urothelial cells (UCs) to achieve contractile yet functional neotissue prior to implantation does not significantly improve the functional outcome. In contrary, results with stem cells sources are promising.

Preimplantation to improve vascularization of scaffolds alone or in combination with cell seeding has shown encouraging results, but these procedures are extraordinary time consuming and they can only be used for individual patients. Faster regeneration approaches with defined scaffolds are desirable.

1.3 Hybrid Scaffolds

Thus far the proper biomaterial and scaffold design have not been identified for genitourinary reconstruction. Scaffolds designed from different (bio)materials may be advantageous, because strength, tunability, and controllability of synthetic polymers can be combined with overall biocompatibility derived from natural biomaterials such as collagen.

Besides being the main structural protein of most hard and soft tissues in mammals, collagen is a promising naturally-derived biomaterial due to its biocompatibility, biodegradability, bioactivity and low antigenicity [10,11]. However, highly porous scaffolds produced from collagen are too weak to withstand the (bio) mechanical demands of native tissue, hence collagen scaffolds have been reinforced with synthetic polymers to create stronger hybrid tubular scaffolds [12,13]. Indeed, reinforcement with a tubularized biodegradable synthetic polymer mesh increased the overall strength and greatly improved the surgical handling which was much better compared to collagen-alone scaffolds [14].

When hybrid scaffolds such as COL-Vicryl® were used for ureter reconstruction or urinary diversion in preclinical models, tissue regeneration with urothelial lining was possible. However, graft shrinkage, stricture formation, and ultimately hydronephrosis occurred [15–17]. This suggests that new hybrid scaffold designs are needed. In a first approach the (bio)mechanical performance, hence the synthetic component of the hybrid scaffold may be further optimized. In **chapter 3**, coupled helical coils (CHCs) were manufactured to mimic collagen fiber orientation as found in nature. Monofilaments of different commercially available biodegradable polymers were wound and subsequently fused, resulting in right-handed and left-handed polymer helices fused together in joints where the filaments cross. Subsequently, seamless and stable hybrid constructs were embedded in porous collagen type scaffolds which showed similar (bio)mechanical properties as native (ureteral)

tissue. Importantly, these stent-like hybrid templates can resist compressive loads which may be beneficial to prevent strictures or graft occlusion [18]. Furthermore, these CHCs are very versatile as the overall (bio)mechanical performance of CHCs can be modified by simply changing the diameter of fiber filaments, the filament arrangement and the filament intersection points. The overall degradation profile can be adjusted by changing the polymer.

1.4 Noninvasive Magnetic Resonance Imaging of Tissue-Engineered Grafts

Since the failure rate of implanted scaffolds for ureter reconstruction and urinary diversion are relatively high, real-time monitoring of tissue-engineered constructs is of tremendous importance to assess their integrity, remodeling, and degradation upon implantation *in vivo*. Magnetic resonance imaging (MRI) is an attractive multifunctional and noninvasive imaging modality that does not use ionizing radiation and MRI has been used to image tissue engineered collagen based scaffolds [19,20]. However, monitoring of these grafts is challenging because their contrast with neighboring tissues is low, necessitating labeling with contrast agents (CAs). But current CAs have limitations such as toxicity, negative contrast, label instability.

Therefore, a naturally derived hemin-L-lysine (HL) complex was used as a potential CA to label collagen-based scaffolds for MRI (**chapter 4)**. Labeling through chemical conjugation of HL to collagen did not change the basic characteristics of the collagen scaffolds. When hybrid scaffolds composed of collagen type I reinforced with degradable polymers were subcutaneously implanted in a mouse model, longitudinal visualization by MRI was possible with good contrast and contrast change correlated with scaffold remodeling. On the contrary, unlabeled collagen templates were hardly visible, and the fate of these templates could not be monitored by MRI. Interestingly, tissue remodeling and vascularization were enhanced within HL-labeled templates. Taken together, HL labeling was introduced as a promising universal imaging marker to label tissue-engineered implants for MRI, which additionally seems to accelerate tissue regeneration.

Alternatively, hydrogels are versatile tools for TE applications. For example, injectable hydrogels offer the advantage to be applied in a minimal invasive manner. Once injected, they can form a stable 3D environment which can mimic the extracellular matrix of native tissues, hence hydrogels are ideal candidates for cell- and drug delivery [21,22]. In **chapter 5**, fully synthetic imageable hydrogels

composed of polyisocyanopeptide (PIC) were produced. this material has unique properties: PIC gels remain liquid below 15°C and form a stable 3D network at 37°C, and, more importantly, closely resemble the native extracellular matrix including stiffening response at high strains [23]. Through chemical conjugation by "copper-free" click chemistry, soft (G' ~ 200 Pa) PIC hydrogels were further functionalized with cell binding motifs (PIC-GRGDS) and a gadolinium-based contrast agent (PIC-GdDO3A). Subsequently, mixtures of both gels were prepared to create hybrid gels allowing both cellular outgrowth and visualization via MRI (PIC hybrid). Upon injection in a mouse model, PIC-GdDO3A- and PIC hybrids were monitored by MR imaging. Longitudinal follow up provided a fundamental insight on hydrogel patency over time: soft PIC hydrogels lost approximately 50 % of its volume within 7 days after injection. R_1 relaxometry and the contrast-to-noise ratio confirmed densification of the injected material due to fluid loss rather than bulk degradation. Furthermore, MRI signal remained stable till the end of the experiment (28 days). Conventional histology correlated well with MR images. The findings of this study may help to further develop smart PIC hydrogels which can be used for a wide variety of purposes such as drug- and cell delivery for ureter regeneration or urinary diversion.

1.5 Sterilization of Collagen-based Hybrid Scaffolds

Clinical implementation of tissue-engineered hybrid constructs, which is governed by Advance Therapies Medical Products (ATMP) regulation of EMA and FDA, requires a validated FDA- and EMA approved sterilization method. Since the choice of the sterilization method may affect the scaffold performance of both synthetic [24]- and natural polymers [25,26], the effect of γ-irradiation (25 kGray) and EtO degassing on hybrid scaffolds *in vitro* and the effect on scaffold remodeling in a large animal model was studied (**chapter 6**). In this chapter, collagen scaffolds were reinforced with a biodegradable surgical mesh (Vicryl®) to form a hybrid scaffold (COL-Vicryl®). The *in vitro* characteristics were extensively studied, including tensile strength analysis and degradation studies. For *in vivo* evaluation, constructs were subcutaneously implanted in goats for 1 month to form vascularized neo-tissue. Macroscopic and microscopic appearances of the γ- and EtO-sterilized constructs slightly differed due to additional processing required for the COL-Vicryl®-EtO constructs. Regardless of the sterilization method, incubation in urine resulted in fast degradation of the Vicryl® polymer and decreased strength. The difference between the two sterilization methods was otherwise limited. In contrast, subcutaneous implantation

showed that the effect of sterilization was considerable. A well-vascularized tube was formed in both cases, but the γ-irradiated construct showed an organized architecture of vasculature and was mechanically more comparable to the native ureter. Moreover, the γ-irradiated construct showed advanced tissue remodeling as shown by enhanced ECM production of invading cells.

This study showed that the effect of sterilization on tissue remodeling cannot be predicted by *in vitro* analyses alone. Thus, validated sterilization methods should be carefully considered when designing hybrid scaffolds. As shown in this chapter, γ-sterilization enhanced tissue remodeling by changing its degradation profile, but γ-sterilization also enhanced the degradation rate of the supportive polymer. This suggests that polymers with a low degradation profile such as polycaprolactone (PCL) should be used to ensure long-term support of the hybrid [27]. In view of ureter regeneration and urinary diversion, the supportive structure should be at least longer than 1 month when considered to be used after preimplantation. Subsequently, when EtO is chosen as the sterilization method of choice, the degradation rate of the supportive structure and collagen remains unaffected [24–26,28,29].

2 FUTURE PERSPECTIVES

2.1 Animal Models and Clinical Translation

This thesis describes multiple components of scaffold design which may aid in development of personalized functional grafts for ureter reconstruction and urinary diversion. To foster clinical translation, these tools need to be evaluated in preclinical studies to reconstruct a ureter or forming an artificial urinary conduit. Choosing a proper animal model is a critical step. Large animal models are preferred as they allow a better translation to the human situation, within respect to surgical techniques, scaffold dimensions and anatomy [30]. Nevertheless, remodeling kinetics of tissue-engineered constructs may vary: for example, Göttingen minipigs and juvenile German Landrace pigs differ in (cell) growth, and show different regeneration kinetics [31]. In view of clinical translation, the overall scaffold design should be adjusted to specific patient dimensions since the diameter of the ureter, its wall thickness, and its (bio)mechanical properties differ between the defect area and these are also unique for a particular species [32,33]. Therefore, it may worthwhile to derive specific ureter dimensions from CT- and/or MRI scans to be able to develop custom made grafts.

To fully assess the benefit of a (personalized) tissue-engineered construct, future animal studies should include the standard clinical treatment such as reconstruction with autologous bowel tissue to permit adequate comparison with the chosen scaffold biomaterial and reconstruction strategy. This may ultimately aid the translation of TE approaches to the clinic as alternative reconstruction procedures.

Furthermore, the time-frame to generate functional graft material is of utmost importance in clinical settings when complex reconstruction procedures, including cell-seeding and preimplantation, are considered. For urinary diversion (e.g. after radical cystectomy) there is a time-window of up to 3 months between diagnosis and surgical intervention [4]. In contrary, ureter reconstruction (e.g. due to trauma) is usually acute and requires urgent surgical interaction. A percutaneous nephrostomy catheter could be used to drain urine in a first step before a long segment ureter reconstruction can follow [34]. Taken together, there may be a time-window which would allow for a complex reconstruction procedure albeit formation of functional neotissue by means of SMCs and UCs formation should be as fast as possible.

2.2 Generation of Functional Neotissue

In general, collagen scaffolds are chemically crosslinked e.g. by N-ethyl-3-(3-dimethylaminopropyl)-carbodiimide (EDC) / N-hydroxysuccinimide (NHS) to enhance strength and resistance against enzymatic degradation. However, this crosslinking strategy may diminish the availability of essential cell binding motifs, hence has a strong impact on cell spreading, apoptosis and proliferation within scaffolds [35]. Since the CHC component dictates strength and faster regeneration strategies are desired for ureter reconstruction and urinary diversion, it may worthwhile to neglect crosslinking and use collagen in its native fashion. Indeed, when hybrid scaffolds were not crosslinked more cells attached to collagen and cellular outgrowth was enhanced in ongoing experiments (manuscript in preparation). Furthermore, when primary human bladder smooth muscle cells (hbSMCs) were seeded on non-crosslinked hybrid scaffolds and conditioned in a bioreactor functional neotissue could be generated most likely because the dynamic stimulation in combination with native collagen triggered hbSMCs to a more mature contractile phenotype.

In healthy conditions, the urine flow is actively guided by smooth muscle cells (SMCs) within the ureter wall. Thus, addition of SMCs to (hybrid) scaffolds to achieve functional neotissue may reduce the complication rate for ureter reconstruction and urinary diversion. As described in **chapter2**, stem cells such as adipose derived stem cells (ADSCs) are of interest for genitourinary TE applications. In future studies, the so-called adipose stromal vascular fraction (SVF) may be an appropriate cell source: it can be isolated from easily from accessible fat tissue and seeded to (hybrid) scaffolds. The SVF contains a heterogeneous cell population comprised of endothelial cells, macrophages, pericytes, and various stem cell populations [36] and when these cells are stimulated in a bioreactor system, smooth muscle tissue can be generated [37]. Indeed when cells are added to scaffolds, bioreactor stimulation should be implemented in the study design, as they provide mechanical cues which can differentiate cells to a more matured contractile phenotype and align cells similar to native tissue [37,38]. Furthermore, generated functional muscular tubes showed a high patency when used for urethra reconstruction in a preclinical setting [39].

2.3 Noninvasive Monitoring of Functional Grafts and Cells

In view of imaging hybrid scaffolds as described in this thesis, there is need to adequately image both the supportive component and the cellular stratum. Since supportive structures such as the CHC gives a negative contrast in ^{1}H-MR imaging,

the collagen component needs to give a positive contrast. When cells are seeded to these imageable hybrids, cells may also be labeled with a contrast agent for visualization. ^{19}F-MRI have been established as a proper tool to track and quantify therapeutic cells upon injection *in vivo* [40]. For TE applications, cells can be simply labeled with an ^{19}F-MRI contrast agent such as PERFECTA [41] for localization of their fate upon seeding to (hybrid) scaffolds. This strategy can give valuable qualitative and quantitative information of cell distribution within the scaffold. ^{19}F-MR images can be simply overlaid with ^{1}H-MR images; it would permit efficient visualization of all 3 distinct structures: cells, collagen labeled with HL and CHC by ^{1}H-MR imaging. However, labelling of cells allows only short-term monitoring as the contrast decreases e.g. due to dilution of the label during cell division and this should be carefully considered.

Other non-invasive monitoring strategies such as ultrasound imaging (US) can be implemented during maturation of tissue-engineered scaffold in a bioreactor. It has been shown that the grey values of US images correlated well with the newly synthetized collagen content within fibrin-based constructs [42]. Furthermore, US can be used to assess the mechanical behavior of tissue-engineered constructs when stimulated in bioreactor [43]. How this translates to *in vivo* remains to be established.

3 REFERENCES

[1] F.N. Burks, R.A. Santucci, Management of iatrogenic ureteral injury., Ther. Adv. Urol. 6 (2014) 115–24. DOI:10.1177/1756287214526767.

[2] A. Martini, D. Villari, G. Nicita, Long-term complications arising from bowel interposition in the urinary tract, Int. J. Surg. 44 (2017) 278–280. DOI:10.1016/j.ijsu.2017.07.030.

[3] T.W. Pike, S. Pandanaboyana, T. Hope-Johnson, L. Hostert, N. Ahmad, Ureteric reconstruction for the management of transplant ureteric stricture: a decade of experience from a single centre., Transpl. Int. 28 (2015) 529–534. DOI:10.1111/tri.12508.

[4] J. Alfred Witjes, T. Lebret, E.M. Compérat, N.C. Cowan, M. De Santis, H.M. Bruins, V. Hernández, E.L. Espinós, J. Dunn, M. Rouanne, Y. Neuzillet, E. Veskimäe, A.G. van der Heijden, G. Gakis, M.J. Ribal, Updated 2016 EAU Guidelines on Muscle-invasive and Metastatic Bladder Cancer, Eur. Urol. 71 (2017) 462–475. DOI:10.1016/j.eururo.2016.06.020.

[5] R.E. Hautmann, S.H. Hautmann, O. Hautmann, Complications associated with urinary diversion, Nat. Rev. Urol. 8 (2011) 667–77. DOI:10.1038/nrurol.2011.147.

[6] R. Langer, J.P. Vacanti, Tissue engineering., Science. 260 (1993) 920–6. DOI: 10.1126/science.8493529.

[7] S.J. Hollister, Scaffold design and manufacturing: from concept to clinic., Adv. Mater. 21 (2009) 3330–42. DOI:10.1002/adma.200802977.

[8] J.P. Vacanti, R. Langer, Tissue engineering: the design and fabrication of living replacement devices for surgical reconstruction and transplantation., Lancet (London, England). 354 Suppl 1 (1999) SI32-4. DOI: 10.1016/s0140-6736(99)90247-7.

[9] A.A. Appel, M.A. Anastasio, J.C. Larson, E.M. Brey, Imaging challenges in biomaterials and tissue engineering., Biomaterials. 34 (2013) 6615–30. DOI:10.1016/j.biomaterials.2013.05.033.

[10] F.J. O'Brien, Biomaterials & scaffolds for tissue engineering, Mater. Today. 14 (2011) 88–95. DOI:10.1016/S1369-7021(11)70058-X.

[11] C. Dong, Y. Lv, Application of Collagen Scaffold in Tissue Engineering: Recent Advances and New Perspectives, Polymers (Basel). 8 (2016) 42. DOI:10.3390/polym8020042.

[12] H.R. Hoogenkamp, M.J.W. Koens, P.J. Geutjes, H. Ainoedhofer, G. Wanten, D.M. Tiemessen, J. Hilborn, B. Gupta, W.F.J. Feitz, W.F. Daamen, A.K. Saxena, E. Oosterwijk, T.H. van Kuppevelt, Seamless vascularized large-diameter tubular collagen scaffolds reinforced with polymer knittings for esophageal regenerative medicine., Tissue Eng. Part C. Methods. 20 (2014) 423–30. DOI:10.1089/ten.TEC.2013.0485.

[13] P. Geutjes, L. Roelofs, H. Hoogenkamp, M. Walraven, B. Kortmann, R. de Gier, F. Farag, D. Tiemessen, M. Sloff, E. Oosterwijk, T. van Kuppevelt, W. Daamen, W. Feitz, Tissue engineered tubular construct for urinary diversion in a preclinical porcine model, J Urol. 188 (2012) 653–660. DOI:10.1016/j.juro.2012.03.119.

[14] M. Sloff, V. Simaioforidis, P.J. Geutjes, H.R. Hoogenkamp, T.H. van Kuppevelt, W.F. Daamen, E. Oosterwijk, W.F. Feitz, Novel tubular constructs for urinary diversion: a biocompatibility study in pigs., J. Tissue Eng. Regen. Med. (2016). DOI:10.1002/term.2122.

[15] M. Sloff, V. Simaioforidis, D.M. Tiemessen, H.P. Janke, B.B.M. Kortmann, L.A.J. Roelofs, P.J. Geutjes, E. Oosterwijk, W.F.J. Feitz Prof, Tubular constructs as artificial urinary conduits., J. Urol. (2016). DOI:10.1016/j.juro.2016.04.092.

[16] P. de Jonge, V. Simaioforidis, P. Geutjes, E. Oosterwijk, W. Feitz, Ureteral reconstruction with reinforced collagen scaffolds in a porcine model., J. Tissue Eng. Regen. Med. (2016). DOI:10.1002/term.2366.

[17] P.K.J.D. de Jonge, M. Sloff, H.-P. Janke, L.R.M. Versteegden, B.B.M. Kortmann, R.P.E. de Gier, P.J. Geutjes, E. Oosterwijk, W.F.J. Feitz, Ureteral Reconstruction in Goats Using Tissue-Engineered Templates and Subcutaneous Preimplantation., Tissue Eng. Part A. 24 (2018) 863–872. DOI:10.1089/ten.TEA.2017.0347.

[18] Y. Ikada, Challenges in tissue engineering, J. R. Soc. Interface. 3 (2006). DOI: 10.1098/rsif.2006.0124

[19] M.E. Mertens, A. Hermann, A. Buhren, L. Olde-Damink, D. Mockel, F. Gremse, J. Ehling, F. Kiessling, T. Lammers, Iron Oxide-labeled Collagen Scaffolds for Non-invasive MR Imaging in Tissue Engineering, Adv Funct Mater. 24 (2014) 754–762. DOI:10.1002/adfm.201301275.

[20] H.R. Hoogenkamp, M.W. Pot, T.G. Hafmans, D.M. Tiemessen, Y. Sun, E. Oosterwijk, W.F. Feitz, W.F. Daamen, T.H. van Kuppevelt, Scaffolds for whole organ tissue engineering: Construction and *in vitro* evaluation of a seamless, spherical and hollow collagen bladder construct with appendices, Acta Biomater. (2016). DOI:10.1016/j.actbio.2016.07.022.

[21] A. Sivashanmugam, R. Arun Kumar, M. Vishnu Priya, S. V. Nair, R. Jayakumar, An overview of injectable polymeric hydrogels for tissue engineering, Eur. Polym. J. 72 (2015) 543–565. DOI:10.1016/J.EURPOLYMJ.2015.05.014.

[22] M. Norouzi, B. Nazari, D.W. Miller, Injectable hydrogel-based drug delivery systems for local cancer therapy, Drug Discov. Today. 21 (2016) 1835–1849. DOI:10.1016/J.DRUDIS.2016.07.006.

[23] P.H.J. Kouwer, M. Koepf, V.A.A. Le Sage, M. Jaspers, A.M. van Buul, Z.H. Eksteen-Akeroyd, T. Woltinge, E. Schwartz, H.J. Kitto, R. Hoogenboom, S.J. Picken, R.J.M. Nolte, E. Mendes, A.E. Rowan, Responsive biomimetic networks from polyisocyanopeptide hydrogels., Nature. 493 (2013) 651–5. DOI:10.1038/nature11839.

[24] C.E. Holy, C. Cheng, J.E. Davies, M.S. Shoichet, Optimizing the sterilization of PLGA scaffolds for use in tissue engineering, Biomaterials. 22 (2001) 25–31. DOI: 10.1016/S0142-9612(00)00136-8

[25] J. Rnjak-Kovacina, T.M. DesRochers, K.A. Burke, D.L. Kaplan, The effect of sterilization on silk fibroin biomaterial properties, Macromol Biosci. 15 (2015) 861–874. DOI:10.1002/mabi.201500013.

[26] S.D. Gorham, S. Srivastava, D.A. French, R. Scott, The effect of gamma-ray and ethylene oxide sterilization on collagen-based wound-repair materials, J. Mater. Sci. Mater. Med. 4 (1993) 40–49.

[27] M.A. Woodruff, D.W. Hutmacher, The return of a forgotten polymer—Polycaprolactone in the 21st century, Prog. Polym. Sci. 35 (2010) 1217–1256. DOI:10.1016/J.PROGPOLYMSCI.2010.04.002.

[28] K.A. Faraj, K.M. Brouwer, P.J. Geutjes, E.M. Versteeg, R.G. Wismans, J.A. Deprest, H. Chajra, D.M. Tiemessen, W.F.J. Feitz, E. Oosterwijk, The effect of ethylene oxide sterilisation, beta irradiation and gamma irradiation on collagen fibril-based scaffolds, Tissue Eng. Regen. Med. 8 (2011) 460–470. ISSN: 1932-6254.

[29] E.M. Noah, J. Chen, X. Jiao, I. Heschel, N. Pallua, Impact of sterilization on the porous design and cell behavior in collagen sponges prepared for tissue engineering, Biomaterials. 23 (2002) 2855–2861. DOI: 10.1016/S0142-9612(01)00412-4.

[30] M. Sloff, R. de Vries, P. Geutjes, J. IntHout, M. Ritskes-Hoitinga, E. Oosterwijk, W. Feitz, Tissue Engineering in Animal Models for Urinary Diversion: A Systematic Review, PLoS One. 9 (2014) e98734. DOI:10.1371/journal.pone.0098734.

[31] D. Leonhauser, M. Vogt, R.H. Tolba, J.O. Grosse, Potential in two types of collagen scaffolds for urological tissue engineering applications - Are there differences in growth behaviour of juvenile and adult vesical cells?, J Biomater Appl. 30 (2016) 961–973. DOI:10.1177/0885328215610824.

[32] D.P. Sokolis, D.C. Petsepe, S.A. Papadodima, S.K. Kourkoulis, Age- and region-related changes in the biomechanical properties and composition of the human ureter, J. Biomech. (2016). DOI:10.1016/j.jbiomech.2016.11.067.

[33] D.C. Petsepe, S.K. Kourkoulis, S.A. Papadodima, D.P. Sokolis, Regional and age-dependent residual strains, curvature, and dimensions of the human ureter, Proc. Inst. Mech. Eng. Part H J. Eng. Med. 232 (2018) 149–162. DOI:10.1177/0954411917750192.

[34] C.S. Ogg, H.M. Saxton, J.S. Cameron, Percutaneous needle nephrostomy., Br. Med. J. 4 (1969) 657–60. DOI: 10.1136/bmj.4.5684.657.

[35] D. V. Bax, N. Davidenko, D. Gullberg, S.W. Hamaia, R.W. Farndale, S.M. Best, R.E. Cameron, Fundamental insight into the effect of carbodiimide crosslinking on cellular recognition of collagen-based scaffolds, Acta Biomater. 49 (2017) 218–234. DOI:10.1016/j.actbio.2016.11.059.

[36] V.M. Ramakrishnan, N.L. Boyd, The Adipose Stromal Vascular Fraction as a Complex Cellular Source for Tissue Engineering Applications, Tissue Eng. Part B Rev. 24 (2018) 289–299. DOI:10.1089/ten.teb.2017.0061.

[37] M. Parvizi, L.A.M. Bolhuis-Versteeg, A.A. Poot, M.C. Harmsen, Efficient generation of smooth muscle cells from adipose-derived stromal cells by 3D mechanical stimulation can substitute the use of growth factors in vascular tissue engineering, Biotechnol. J. 11 (2016) 932–944. DOI:10.1002/biot.201500519.

[38] E. Vardar, E.-M. Engelhardt, H.M. Larsson, E. Mouloungui, K. Pinnagoda, J.A. Hubbell, P. Frey, Tubular Compressed Collagen Scaffolds for Ureteral Tissue Engineering in a Flow Bioreactor System., Tissue Eng. Part A. 21 (2015) 2334–45. DOI:10.1089/ten.TEA.2015.0048.

[39] Q. Fu, C.-L. Deng, R.-Y. Zhao, Y. Wang, Y. Cao, The effect of mechanical extension stimulation combined with epithelial cell sorting on outcomes of implanted tissue-engineered muscular urethras., Biomaterials. 35 (2014) 105–12. DOI:10.1016/j.biomaterials.2013.09.067.

[40] M. Srinivas, A. Heerschap, E.T. Ahrens, C.G. Figdor, I.J.M. de Vries, (19)F MRI for quantitative *in vivo* cell tracking., Trends Biotechnol. 28 (2010) 363–70. DOI:10.1016/j.tibtech.2010.04.002.

[41] I. Tirotta, A. Mastropietro, C. Cordiglieri, L. Gazzera, F. Baggi, G. Baselli, M.G. Bruzzone, I. Zucca, G. Cavallo, G. Terraneo, F. Baldelli Bombelli, P. Metrangolo, G. Resnati, A Superfluorinated Molecular Probe for Highly Sensitive *in Vivo* ^{19}F-MRI, J. Am. Chem. Soc. 136 (2014) 8524–8527. DOI:10.1021/ja503270n.

[42] S. Kreitz, G. Dohmen, S. Hasken, T. Schmitz-rode, P. Mela, S. Jockenhoevel, Nondestructive Method to Evaluate the Collagen Content of Fibrin-Based Tissue Engineered Structures Via Ultrasound, 17 (2011). DOI:10.1089/ten.tec.2010.0669.

[43] D. Dutta, K.-W. Lee, R. a Allen, Y. Wang, J.C. Brigham, K. Kim, Non-invasive assessment of elastic modulus of arterial constructs during cell culture using ultrasound elasticity imaging., Ultrasound Med. Biol. 39 (2013) 2103–15. DOI:10.1016/j.ultrasmedbio.2013.04.023.

1 SAMENVATTING EN DISCUSSIE

1.1 Klinische Uitdaging en Doel van dit Proefschrift

Reconstructie van lange ureter-segmenten (bijv. na een trauma) of het vormen van een urineafleiding door een urostoma (bijv. na radicale cystectomie) kan voor urologen een uitdaging zijn. De standaardbehandeling bestaat uit het creëren van nieuw weefsel van autologe darmsegmenten. Dit is geassocieerd met meerdere bijwerkingen [1-5]. Alternatieve (bio)materialen zijn daarom zeer wenselijk en kunnen standaard behandelingsgerelateerde complicaties en weefseltekorten mogelijk oplossen indien goed toepasbaar. Het doel van Tissue Engineering (TE) is het vervangen of herstellen van beschadigde organen en weefsels [6]. De basis van TE is een zogenaamde scaffold die kan worden samengesteld uit natuurlijke biomaterialen, synthetische biomaterialen of een combinatie van beide om hybride scaffolds te creëren. De scaffold fungeert als startmatrix om het defect op te vullen en de verschillende (bio)mechanische belastingen te dragen tot het door eigen weefsel wordt vervangen [7]. Aangezien het uiteindelijke doel van ureterreconstructie en urineafleiding het veilig transporteren van urine is, moet een geïmplanteerd (bio)materiaal hier actief aan bijdragen en het omringende weefsel beschermen. Verder is het mogelijk om cellen van de patiënt op de scaffold te laten groeien om de vorming van functioneel weefsel te stimuleren [8]. Bij de implantatie zijn niet-invasieve beeldvormingstechnieken belangrijk om real-time de doorgankelijkheid en weefselhermodellering te kunnen volgen [9].

Het doel van dit proefschrift was de ontwikkeling van innovatieve hybride TE constructen die gebruikt kunnen worden bij ureter reconstructie en/of het creëren van een kunst-urostoma voor urineafleiding.

1.2 State-of-the-art van Reconstructie van de Ureter Reconstructie en Urineafleiding met Behulp van Tissue Engineering

Een overzicht van state-of-the-art TE-benaderingen voor ureter reconstructie en urineafleiding door een urostoma met de nadruk op biomaterialen en scaffolds is beschreven In **hoofdstuk 2**. De studies werden verder gecategoriseerd op basis van de vraag of de scaffolds direct werden geïmplanteerd, werden ingezaaid met cellen voorafgaand aan de implantatie, of vooraf werden geïmplanteerd (met of zonder cellen) voorafgaand aan de functionele implantatie.

Deze studies toonden samen aan dat regeneratie van ureteraal weefsel en de vorming van een urineafleiding met behulp van TE-benaderingen mogelijk is, hoewel het

complex is om goed ontwikkeld en functioneel weefsel te creëren. Preklinische studies hebben aangetoond dat de celvrije functionele implantatie van scaffolds problematisch is: het leidt tot fibrose, krimpen van het construct, vernauwing en hydronefrose ondanks de vorming van urotheel cellen. Het toevoegen van autologe gladde spiercellen (engels: smooth muscle cells, SMCs) en urotheliale cellen (UCs) om vóór de implantatie contractiel, functioneel weefsel te verkrijgen, verbetert het functionele resultaat niet significant. Daarentegen zijn de resultaten met stamcellen veelbelovend.

Preimplantatie ter verbetering van de vascularisatie van scaffolds, alleen of in combinatie met het zaaien van cellen, heeft veelbelovende resultaten opgeleverd, maar deze procedures zijn zeer tijdrovend en kunnen alleen voor individuele patiënten worden gebruikt. Snellere benaderingen met gedefinieerde scaffolds zijn wenselijk.

1.3 Hybride Scaffolds

Tot nu toe zijn het juiste biomateriaal en scaffold design nog niet geïdentificeerd voor genitourinaire reconstructie. Scaffolds samengesteld uit meerdere verschillende (bio)materialen kunnen van voordeel zijn, omdat de sterkte en controleerbaarheid van synthetische polymeren gecombineerd kunnen worden met natuurlijke biomaterialen zoals collageen.

Naast het feit dat collageen het belangrijkste structurele eiwit is van de meeste harde en zachte weefsels in zoogdieren, is collageen een veelbelovend natuurlijk biomateriaal vanwege zijn biocompatibiliteit, biologische afbreekbaarheid, bio-activiteit en lage antigeengehalte [10,11]. Hoogporeuze scaffolds geproduceerd uit collageen zijn echter te zwak om de (bio)mechanische eisen van normaal weefsel te weerstaan, vandaar dat collageen-scaffolds zijn versterkt met synthetische polymeren om sterkere hybride buisvormige scaffolds te creëren [12,13]. Versterking met een buisvormig, biologisch afbreekbaar synthetisch polymeernetwerk verhoogde de totale sterkte en verbeterde de chirurgische hanteerbaarheid aanzienlijk ten opzichte van scaffolds die alleen uit collageen bestonden [14].

Wanneer hybride scaffolds zoals COL-Vicryl® werden gebruikt voor ureter reconstructie of een urostoma in preklinische modellen, was weefselregeneratie met urotheliale bekleding mogelijk. Er was echter sprake van krimpen van het construct, vernauwing en uiteindelijk hydronefrose [15-17]. Dit suggereert dat er nieuwe hybride scaffold ontwikkelt moeten worden. In een eerste stap moeten de (bio)mechanische eigenschapen van het synthetische component van de hybride scaffold verder geoptimaliseerd worden. In **hoofdstuk 3** werden coupled helical coils (CHCs) gemaakt die de natuurlijke collageenvezel oriëntatie nabootst.

Monofilamenten van verschillende commercieel verkrijgbare biologisch afbreekbare polymeren werden gewikkeld en vervolgens samengesmolten. Dit resulteerde in rechtshandige en linkshandige polymeer helices die samensmelten in kruisende verbindingen. Vervolgens werden deze naadloze en stabiele hybride constructies ingebed in poreuze collageen scaffolds die dezelfde (bio)mechanische eigenschappen vertoonden als natuurlijk ureteraal weefsel. Belangrijk is dat deze stent-achtige hybride scaffolds drukbelastingen kunnen weerstaan die nodig kunnen zijn om vernauwingen of occlusie van het construct te voorkomen [18]. Bovendien zijn deze CHCs zeer veelzijdig doordat de algemene (bio)mechanische eigenschappen van CHC's kan worden gewijzigd door bijvoorbeeld het veranderen van de diameter van de vezeldraden, de filament indeling en de filament snijpunten. Het afbraakprofiel kan worden aangepast door het veranderen van de polymeer compositie.

1.4 Niet-invasieve Magnetic Resonance Imaging van Tissue-engineered Weefsel

Aangezien de kans op problemen met geïmplanteerde scaffolds voor ureter reconstructie en urineafleiding door een urostoma relatief hoog is, is real-time monitoring van tissue-engineered constructies van groot belang om hun integriteit, weefselingroei en degradatie na implantatie *in vivo* te beoordelen. Magnetic Resonance Imaging (MRI) is een aantrekkelijke multifunctionele en niet-invasieve beeldvormingsmodaliteit die geen gebruik maakt van ioniserende straling en gebruikt kan worden voor beeldvorming van collageen scaffolds [19,20]. Echter, beeldvorming van deze scaffolds is uitdagend omdat hun contrast met naburige weefsels laag is, waardoor labeling met contrastmiddelen (CAs) nodig is. Huidige CA's hebben echter beperkingen zoals toxiciteit, negatief contrast en instabiliteit van het labeling.

Daarom werd een natuurlijk hemin-L-lysine (HL) complex gebruikt als een potentieel CA om scaffolds op basis van collageen voor MRI te labelen (**hoofdstuk 4**). Labeling door middel van chemische conjugatie van HL met collageen veranderde de basiskenmerken van de collageen scaffolds niet. Wanneer hybride scaffolds bestaande uit collageen type I versterkt met afbreekbare polymeren subcutaan werden geïmplanteerd in een muismodel, was longitudinale visualisatie door MRI mogelijk met een goed contrast.Verder gecorreleerde contrastveranderingen aan hermodellering van de scaffolds. Daarentegen waren ongelabelde collageen scaffolds nauwelijks zichtbaar en konden deze scaffolds niet worden vervolgd met MRI. Interessant is de betere weefselhermodellering en vascularisatie van HL-gelabelde scaffolds. Samenvattend werd HL-labeling geïntroduceerd als een veelbelovende

universele beeldvormingsmarker voor het labelen van van tissue-engineered constructen voor MRI, waarbij bovendien de weefselregeneratie lijkt te versnellen.

In aanvulling op scaffolds zijn hydrogelen veelzijdige hulpmiddelen voor TE-toepassingen. Injecteerbare hydrogelen bieden bijvoorbeeld het voordeel dat ze op een minimale invasieve manier kunnen worden toegepast. Eenmaal geïnjecteerd, kunnen ze een stabiele 3D-omgeving vormen die de extracellulaire matrix van natuurlijke weefsels kan nabootsen, vandaar dat hydrogelen ideale kandidaten zijn voor cel- en medicijnafgifte [21,22]. In **hoofdstuk 5** werden volledig synthetische afbeeldbare hydrogelen geproduceerd die bestaan uit polyisocyanopeptide (PIC). Dit materiaal heeft unieke eigenschappen: PIC-gels blijven vloeibaar onder de 15°C en vormen een stabiel 3D-netwerk bij 37°C en de structuur lijkt sterk op de natuurlijke extracellulaire matrix met een vergelijkbare verstijvingsreactie bij hoge spanningen [23]. Door chemische conjugatie door "kopervrije" klikchemie, werden zachte (G'~200 Pa) PIC hydrogels verder gefunctionaliseerd met celbindende petiden (PIC-GRGDS) en met een MRI contrast contrastmiddel (PIC-GdDO3A). Vervolgens werden mengsels van beide gelen (PIC hybride) bereid om gels te creëren waardoor zowel cellulaire uitgroei en visualisatie via MRI mogelijk was. Na injectie in een muismodel werden PIC-GdDO3A- en PIC hybriden geevalueerd met behulp van MR beeldvorming. Longitudinale follow-up zorgde voor een fundamenteel inzicht in het gedrag van de hydrogel in de tijd: zachte PIC hydrogels verloren ongeveer 50% van het volume binnen 7 dagen na injectie. R_1 relaxometrie en evaluatie van de contrast-to-noise-ratio bevestigde de verdichting van het geïnjecteerde materiaal als gevolg van vochtverlies in plaats van bulkdegradatie. Bovendien bleef het MRI-signaal stabiel tot het einde van het experiment (28 dagen). Conventionele histologie correleerde goed met de MR beelden. De bevindingen van deze studie kunnen helpen bij de verdere ontwikkeling van PIC hydrogels die kunnen worden gebruikt voor een breed scala van doeleinden, zoals medicijn-en celtoevoer voor ureter regeneratie of urine afleiding door een kunststoma.

1.5 Sterilisatie van Collageen-gebaseerde Hybride Scaffolds

Voor de klinische implementatie van tissue-engineered hybride constructen, die wordt gereguleerd door de Advance Therapies Medical Products (ATMP)-regeling van het EMA, en de FDA, is een gevalideerde FDA- en EMA-goedgekeurde sterilisatiemethode vereist. Aangezien de keuze van de sterilisatiemethode de prestaties van zowel synthetische [24]- als natuurlijke polymeren [25,26] kan beïnvloeden, werd het effect van γ-straling (25 kGray) en EtO-ontgassing op hybride scaffolds *in vitro* en

het effect op het remodelleren van de scaffolds in een groot diermodel bestudeerd (**hoofdstuk 6**). In dit hoofdstuk werden de collageen scaffolds versterkt met een biologisch afbreekbaar chirurgisch gaas (Vicryl®) om hybride scaffolds te vormen (COL-Vicryl®). De *in vitro* eigenschappen werden uitgebreid bestudeerd, met behulp van treksterkteanalyses en degradatiestudies. Voor *in vivo* evaluatie werden de constructen gedurende 1 maand subcutaan geïmplanteerd in geiten om gevasculariseerd weefsel te vormen. Macroscopisch en microscopisch verschilden de γ- en EtO-gesteriliseerde constructen licht van elkaar door de extra bewerking die nodig is voor de COL-Vicryl®-EtO-constructen. Ongeacht de sterilisatiemethode leidde incubatie in urine tot een snelle afbraak van het Vicryl® -polymeer en een verminderde sterkte. Het verschil tussen de twee sterilisatiemethoden was verder beperkt. Subcutane implantatie daarentegen toonde aan dat het effect van de sterilisatie aanzienlijk was. In beide gevallen werd een goed gevasculariseerde buis gevormd, maar de γ-bestraalde constructen toonde een georganiseerde bloedvat architectuur en deze was mechanisch beter vergelijkbaar met een natuurlijke ureter. Bovendien vertoonde het γ-bestraalde construct een betere weefselhermodellering, blijkend uit verhoogde ECM-productie van ingroeiende cellen.

Deze studie toonde aan dat het effect van sterilisatie op weefselhermodellering niet alleen kan worden voorspeld door *in vitro* analyses. Daarom moeten gevalideerde sterilisatiemethoden zorgvuldig worden overwogen bij het ontwerpen van hybride scaffolds. Zoals in dit hoofdstuk wordt aangetoond, verbeterd γ-sterilisatie de weefselhermodellering door het degradatieprofiel te veranderen, maar leidt γ-sterilisatie ook tot een versnelde degradatie van het ondersteunende polymeer. Dit suggereert dat polymeren met een langzaam afbraakprofiel zoals polycaprolacton (PCL) moeten worden gebruikt om de constructen ook op lange termijn te kunnen ondersteunen [27]. Met het oog op ureterregeneratie en urineafleiding moet de ondersteunende structuur ten minste 1 maand intact blijven als deze na de preimplantatie gebruikt moet kunnen worden. Wanneer vervolgens EtO wordt gekozen als de gewenste sterilisatiemethode, blijft de afbraaksnelheid van de ondersteunende structuur en het collageen onaangetast [24-26,28,29].

2 TOEKOMSTVISIE

2.1 Diermodellen en Klinische Translatie

Dit proefschrift beschrijft meerdere onderdelen van het ontwerpen van scaffolds voor het ontwikkelen van gepersonaliseerde functionele weefsels voor ureter reconstructie en urineafleiding. Om klinische translatie te bevorderen moeten deze hulpmiddelen worden geëvalueerd in preklinische studies. Het kiezen van een goed diermodel is hierbij een kritische stap. Grote diermodellen hebben de voorkeur omdat ze een betere vertaling naar de menselijke situatie mogelijk maken met betrekking tot de chirurgische technieken, dimensies van de scaffold en anatomie [30]. Toch kan de kinetiek van tissue-engineered constructen variëren: zo verschillen bijvoorbeeld Göttingen minivarkens van landrasvarkens in(cel)ingroei en vertonen ze verschillende regeneratiekinetiek [31]. Met het oog op de klinische translatie moet het totale scaffold design worden aangepast aan de specifieke afmetingen van de patiënt: De diameter, wanddikte en de (bio)mechanische eigenschappen van de ureter kunnen verschillen [32,33]. Daarom kan het de moeite waard zijn om specifieke ureterafmetingen af te leiden uit CT- en/of MRI-scans om vervolgens op maat gemaakte constructen te kunnen produceren.

Om het nut van een (gepersonaliseerd) tissue-engineered construct volledig te kunnen beoordelen, moeten toekomstige dierstudies rekening houden met de standaard klinische behandeling, zoals reconstructie met autoloog darmweefsel. Alleen met een dergelijke controle kan een adequate vergelijking met het gekozen biomateriaal en de reconstructiestrategie gemaakt worden. Dit kan uiteindelijk helpen bij de vertaling van TE-benaderingen naar de kliniek als alternatieve behandeloptie.

Bovendien is het tijdsbestek voor het genereren van functioneel kunstmateriaal belangrijk in de klinische setting wanneer complexe reconstructieprocedures, inclusief cel-zaaien en preimplantatie, worden overwogen. Voor urineafleiding (bijvoorbeeld na radicale cystectomie) is er maximaal 3 maanden tussen diagnose en chirurgische ingreep beschikbaar [4]. Aan de andere kant is ureterreconstructie (bijv. door een trauma) meestal acuut en is de beschikbare tijd veel korter. Een percutane nefrostomiekatheter kan worden gebruikt om de urine in een eerste stap af te voeren voordat een lange segmentaire ureterreconstructie volgt [34]. Door deze combinatie kan tijdwinst geboekt worden zodat een complexe reconstructieprocedure mogelijk wordt, hoewel de vorming van functioneel weefsel door middel van SMCs en UCs zo snel mogelijk dient te gebeuren.

2.2 Functioneel Weefsel

In het algemeen worden collageen in scaffolds chemisch aan elkaar gekoppeld door bijvoorbeeld N-ethyl-3-(3-dimethylaminopropyl)-carbodiimide (EDC)-carbodiimide (N-hydroxysuccinimide (NHS) om de sterkte en weerstand tegen enzymatische afbraak te verhogen. Deze crosslinking strategie kan echter de beschikbaarheid van essentiële celbindende eigenschappen verminderen, en heeft dus een sterke invloed op celmigratie, apoptose en proliferatie binnen de scaffolds [35]. Bij het gebruik van CHC zullen deze de sterkte bepalen en aangezien snellere regeneratiestrategieën gewenst zijn voor ureterreconstructie en urinereproductie, kan het de moeite waard zijn om collageen crosslinking achterwege te laten. Wanneer hybride scaffolds niet werden gecrosslinked konden er meer cellen aan collageen hechten en was de cellulaire uitgroei verbeterd (manuscript in voorbereiding). Conditionering van niet-gecrosslinkte hybride scaffolds bezaaid met primaire menselijke blaas gladde spiercellen (hbSMCs) in een bioreactor, genereerde functioneel weefsel waarschijnlijk omdat de dynamische stimulatie in combinatie met collageen de hbSMCs induceerde tot een meer volwassen, contractiel fenotype.

Onder normale omstandigheden wordt de urinestroom actief geregeld door gladde spiercellen (SMCs) in de ureterwand. Zo kan toevoeging van SMCs aan (hybride) scaffolds helpen om functioneel weefsel te verkrijgen en complicaties te verminderen. Zoals beschreven in hoofdstuk 2, zijn stamcellen zoals ADSCs (vet afgeleide stamcellen) van belang voor genitourinaire TE-toepassingen. In toekomstige studies kan de zogenaamde adipose stromal vascular fraction (SVF) een geschikte celbron zijn. Deze kan worden geïsoleerd uit gemakkelijk toegankelijk vetweefsel en gezaaid worden op (hybride) scaffolds. De SVF bevat een heterogene celpopulatie bestaande uit endotheelcellen, macrofagen, pericyten en verschillende stamcelpopulaties [36] en wanneer deze cellen worden gestimuleerd in een bioreactorsysteem, kan glad spierweefsel worden gegenereerd [37]. Waneer cellen worden toegevoegd aan een scaffold is bioreactorstimulatie aan te raden. De mechanische stimulatie kan cellen stimularen te differentiëren naar een meer contractiel fenotype en cellen kunnen zich orientieren analoog aan natuurlijk weefsel [37,38]. In een preklinsche studie is aangetoond dat gecreerd functioneel spierbuisweefsel goed toepasbaar is bij urethra-reconstructies [39].

2.3 Niet-invasive Monitoring van Functioneel Weefsel en Cellen

Met het oog op de beeldvorming van hybride scaffolds zoals beschreven in dit proefschrift, is er behoefte aan het in beeld brengen van zowel de ondersteunende component als de cellulaire laag. Aangezien ondersteunende structuren zoals de hier beschreven CHC een negatief contrast geeft in ^{1}H-MR beeldvorming, moet de collageencomponent een positief contrast geven. Wanneer cellen worden gezaaid op deze constructen, kunnen cellen ook worden gelabeld met een contrastmiddel voor visualisatie. ^{19}F-MRI kan worden gebruikt als instrument om cellen na injectie in vivo te volgen en te kwantificeren [40]. Voor TE toepassingen kunnen cellen eenvoudig worden gelabeld met een ^{19}F-MRI contrastmiddel zoals PERFECTA [41] om ze te volgen. Deze strategie kan waardevolle kwalitatieve en kwantitatieve informatie geven over de celverdeling binnen de scaffolds. ^{19}F-MR beelden kunnen eenvoudig over 1H-MR beelden worden gelegd en zo een efficiënte visualisatie van de 3 verschillende structuren mogelijk maken: cellen, collageen gelabeld met HL en CHC door ^{1}H-MR imaging. Echter, het labelen van de cellen is tijdelijk en het contrast neemt af in de tijd, bijvoorbeeld door verdunning van het label tijdens de celdeling.

Andere niet-invasieve monitoring strategieën zoals echografie kunnen ook worden gebruikt tijdens de kweek in een bioreactor. Het is aangetoond dat de grijswaarden van de beelden goed correleren met nieuw gevormd collageen in fibrine gebaseerde constructen [42]. Bovendien kan deze techniek worden gebruikt om het mechanische gedrag van TE constructen te beoordelen tijdens stimulatie in een bioreactor [43]. Hoe dit zich vertaalt naar de *in vivo* omgeving moet nog worden vastgesteld.

3 REFERENTIES

[1] F.N. Burks, R.A. Santucci, Management of iatrogenic ureteral injury., Ther. Adv. Urol. 6 (2014) 115–24. DOI:10.1177/1756287214526767.

[2] A. Martini, D. Villari, G. Nicita, Long-term complications arising from bowel interposition in the urinary tract, Int. J. Surg. 44 (2017) 278–280. DOI:10.1016/j.ijsu.2017.07.030.

[3] T.W. Pike, S. Pandanaboyana, T. Hope-Johnson, L. Hostert, N. Ahmad, Ureteric reconstruction for the management of transplant ureteric stricture: a decade of experience from a single centre., Transpl. Int. 28 (2015) 529–534. DOI:10.1111/tri.12508.

[4] J. Alfred Witjes, T. Lebret, E.M. Compérat, N.C. Cowan, M. De Santis, H.M. Bruins, V. Hernández, E.L. Espinós, J. Dunn, M. Rouanne, Y. Neuzillet, E. Veskimäe, A.G. van der Heijden, G. Gakis, M.J. Ribal, Updated 2016 EAU Guidelines on Muscle-invasive and Metastatic Bladder Cancer, Eur. Urol. 71 (2017) 462–475. DOI:10.1016/j.eururo.2016.06.020.

[5] R.E. Hautmann, S.H. Hautmann, O. Hautmann, Complications associated with urinary diversion, Nat. Rev. Urol. 8 (2011) 667–77. DOI:10.1038/nrurol.2011.147.

[6] R. Langer, J.P. Vacanti, Tissue engineering., Science. 260 (1993) 920–6. http://www.ncbi.nlm.nih.gov/pubmed/8493529 (accessed November 11, 2014).

[7] S.J. Hollister, Scaffold design and manufacturing: from concept to clinic., Adv. Mater. 21 (2009) 3330–42. DOI:10.1002/adma.200802977.

[8] J.P. Vacanti, R. Langer, Tissue engineering: the design and fabrication of living replacement devices for surgical reconstruction and transplantation., Lancet (London, England). 354 Suppl 1 (1999) SI32-4. http://www.ncbi.nlm.nih.gov/pubmed/10437854.

[9] A.A. Appel, M.A. Anastasio, J.C. Larson, E.M. Brey, Imaging challenges in biomaterials and tissue engineering., Biomaterials. 34 (2013) 6615–30. DOI:10.1016/j.biomaterials.2013.05.033.

[10] F.J. O'Brien, Biomaterials & scaffolds for tissue engineering, Mater. Today. 14 (2011) 88–95. DOI:10.1016/S1369-7021(11)70058-X.

[11] C. Dong, Y. Lv, Application of Collagen Scaffold in Tissue Engineering: Recent Advances and New Perspectives, Polymers (Basel). 8 (2016) 42. DOI:10.3390/polym8020042.

[12] H.R. Hoogenkamp, M.J.W. Koens, P.J. Geutjes, H. Ainoedhofer, G. Wanten, D.M. Tiemessen, J. Hilborn, B. Gupta, W.F.J. Feitz, W.F. Daamen, A.K. Saxena, E. Oosterwijk, T.H. van Kuppevelt, Seamless vascularized large-diameter tubular collagen scaffolds reinforced with polymer knittings for esophageal regenerative medicine., Tissue Eng. Part C. Methods. 20 (2014) 423–30. DOI:10.1089/ten.TEC.2013.0485.

[13] P. Geutjes, L. Roelofs, H. Hoogenkamp, M. Walraven, B. Kortmann, R. de Gier, F. Farag, D. Tiemessen, M. Sloff, E. Oosterwijk, T. van Kuppevelt, W. Daamen, W. Feitz, Tissue engineered tubular construct for urinary diversion in a preclinical porcine model, J Urol. 188 (2012) 653–660. DOI:10.1016/j.juro.2012.03.119.

[14] M. Sloff, V. Simaioforidis, P.J. Geutjes, H.R. Hoogenkamp, T.H. van Kuppevelt, W.F. Daamen, E. Oosterwijk, W.F. Feitz, Novel tubular constructs for urinary diversion: a biocompatibility study in pigs., J. Tissue Eng. Regen. Med. (2016). DOI:10.1002/term.2122.

[15] M. Sloff, V. Simaioforidis, D.M. Tiemessen, H.P. Janke, B.B.M. Kortmann, L.A.J. Roelofs, P.J. Geutjes, E. Oosterwijk, W.F.J. Feitz Prof, Tubular constructs as artificial urinary conduits., J. Urol. (2016). DOI:10.1016/j.juro.2016.04.092.

[16] P. de Jonge, V. Simaioforidis, P. Geutjes, E. Oosterwijk, W. Feitz, Ureteral reconstruction with reinforced collagen scaffolds in a porcine model., J. Tissue Eng. Regen. Med. (2016). DOI:10.1002/term.2366.

[17] P.K.J.D. de Jonge, M. Sloff, H.-P. Janke, L.R.M. Versteegden, B.B.M. Kortmann, R.P.E. de Gier, P.J. Geutjes, E. Oosterwijk, W.F.J. Feitz, Ureteral Reconstruction in Goats Using Tissue-Engineered Templates and Subcutaneous Preimplantation., Tissue Eng. Part A. 24 (2018) 863–872. DOI:10.1089/ten.TEA.2017.0347.

[18] Y. Ikada, Challenges in tissue engineering, J. R. Soc. Interface. 3 (2006).

[19] M.E. Mertens, A. Hermann, A. Buhren, L. Olde-Damink, D. Mockel, F. Gremse, J. Ehling, F. Kiessling, T. Lammers, Iron Oxide-labeled Collagen Scaffolds for Non-invasive MR Imaging in Tissue Engineering, Adv Funct Mater. 24 (2014) 754–762. DOI:10.1002/adfm.201301275.

[20] H.R. Hoogenkamp, M.W. Pot, T.G. Hafmans, D.M. Tiemessen, Y. Sun, E. Oosterwijk, W.F. Feitz, W.F. Daamen, T.H. van Kuppevelt, Scaffolds for whole organ tissue engineering: Construction and in vitro evaluation of a seamless, spherical and hollow collagen bladder construct with appendices, Acta Biomater. (2016). DOI:10.1016/j.actbio.2016.07.022.

[21] A. Sivashanmugam, R. Arun Kumar, M. Vishnu Priya, S. V. Nair, R. Jayakumar, An overview of injectable polymeric hydrogels for tissue engineering, Eur. Polym. J. 72 (2015) 543–565. DOI:10.1016/J.EURPOLYMJ.2015.05.014.

[22] M. Norouzi, B. Nazari, D.W. Miller, Injectable hydrogel-based drug delivery systems for local cancer therapy, Drug Discov. Today. 21 (2016) 1835–1849. DOI:10.1016/J.DRUDIS.2016.07.006.

[23] P.H.J. Kouwer, M. Koepf, V.A.A. Le Sage, M. Jaspers, A.M. van Buul, Z.H. Eksteen-Akeroyd, T. Woltinge, E. Schwartz, H.J. Kitto, R. Hoogenboom, S.J. Picken, R.J.M. Nolte, E. Mendes, A.E. Rowan, Responsive biomimetic networks from polyisocyanopeptide hydrogels., Nature. 493 (2013) 651–5. DOI:10.1038/nature11839.

[24] C.E. Holy, C. Cheng, J.E. Davies, M.S. Shoichet, Optimizing the sterilization of PLGA scaffolds for use in tissue engineering, Biomaterials. 22 (2001) 25–31.

[25] J. Rnjak-Kovacina, T.M. DesRochers, K.A. Burke, D.L. Kaplan, The effect of sterilization on silk fibroin biomaterial properties, Macromol Biosci. 15 (2015) 861–874. DOI:10.1002/mabi.201500013.

[26] S.D. Gorham, S. Srivastava, D.A. French, R. Scott, The effect of gamma-ray and ethylene oxide sterilization on collagen-based wound-repair materials, J. Mater. Sci. Mater. Med. 4 (1993) 40–49.

[27] M.A. Woodruff, D.W. Hutmacher, The return of a forgotten polymer—Polycaprolactone in the 21st century, Prog. Polym. Sci. 35 (2010) 1217–1256. DOI:10.1016/J.PROGPOLYMSCI.2010.04.002.

[28] K.A. Faraj, K.M. Brouwer, P.J. Geutjes, E.M. Versteeg, R.G. Wismans, J.A. Deprest, H. Chajra, D.M. Tiemessen, W.F.J. Feitz, E. Oosterwijk, The effect of ethylene oxide sterilisation, beta irradiation and gamma irradiation on collagen fibril-based scaffolds, Tissue Eng. Regen. Med. 8 (2011) 460–470.

[29] E.M. Noah, J. Chen, X. Jiao, I. Heschel, N. Pallua, Impact of sterilization on the porous design and cell behavior in collagen sponges prepared for tissue engineering, Biomaterials. 23 (2002) 2855–2861.

[30] M. Sloff, R. de Vries, P. Geutjes, J. IntHout, M. Ritskes-Hoitinga, E. Oosterwijk, W. Feitz, Tissue Engineering in Animal Models for Urinary Diversion: A Systematic Review, PLoS One. 9 (2014) e98734. DOI:10.1371/journal.pone.0098734.

[31] D. Leonhauser, M. Vogt, R.H. Tolba, J.O. Grosse, Potential in two types of collagen scaffolds for urological tissue engineering applications - Are there differences in growth behaviour of juvenile and adult vesical cells?, J Biomater Appl. 30 (2016) 961–973. DOI:10.1177/0885328215610824.

[32] D.P. Sokolis, D.C. Petsepe, S.A. Papadodima, S.K. Kourkoulis, Age- and region-related changes in the biomechanical properties and composition of the human ureter, J. Biomech. (2016). DOI:10.1016/j.jbiomech.2016.11.067.

[33] D.C. Petsepe, S.K. Kourkoulis, S.A. Papadodima, D.P. Sokolis, Regional and age-dependent residual strains, curvature, and dimensions of the human ureter, Proc. Inst. Mech. Eng. Part H J. Eng. Med. 232 (2018) 149–162. DOI:10.1177/0954411917750192.

[34] C.S. Ogg, H.M. Saxton, J.S. Cameron, Percutaneous needle nephrostomy., Br. Med. J. 4 (1969) 657–60. http://www.ncbi.nlm.nih.gov/pubmed/5359921.

[35] D. V. Bax, N. Davidenko, D. Gullberg, S.W. Hamaia, R.W. Farndale, S.M. Best, R.E. Cameron, Fundamental insight into the effect of carbodiimide crosslinking on cellular recognition of collagen-based scaffolds, Acta Biomater. 49 (2017) 218–234. DOI:10.1016/j.actbio.2016.11.059.

[36] V.M. Ramakrishnan, N.L. Boyd, The Adipose Stromal Vascular Fraction as a Complex Cellular Source for Tissue Engineering Applications, Tissue Eng. Part B Rev. 24 (2018) 289–299. DOI:10.1089/ten.teb.2017.0061.

[37] M. Parvizi, L.A.M. Bolhuis-Versteeg, A.A. Poot, M.C. Harmsen, Efficient generation of smooth muscle cells from adipose-derived stromal cells by 3D mechanical stimulation can substitute the use of growth factors in vascular tissue engineering, Biotechnol. J. 11 (2016) 932–944. DOI:10.1002/biot.201500519.

[38] E. Vardar, E.-M. Engelhardt, H.M. Larsson, E. Mouloungui, K. Pinnagoda, J.A. Hubbell, P. Frey, Tubular Compressed Collagen Scaffolds for Ureteral Tissue Engineering in a Flow Bioreactor System., Tissue Eng. Part A. 21 (2015) 2334–45. DOI:10.1089/ten.TEA.2015.0048.

[39] Q. Fu, C.-L. Deng, R.-Y. Zhao, Y. Wang, Y. Cao, The effect of mechanical extension stimulation combined with epithelial cell sorting on outcomes of implanted tissue-engineered muscular urethras., Biomaterials. 35 (2014) 105–12. DOI:10.1016/j.biomaterials.2013.09.067.

[40] M. Srinivas, A. Heerschap, E.T. Ahrens, C.G. Figdor, I.J.M. de Vries, (19)F MRI for quantitative in vivo cell tracking., Trends Biotechnol. 28 (2010) 363–70. DOI:10.1016/j.tibtech.2010.04.002.

[41] I. Tirotta, A. Mastropietro, C. Cordiglieri, L. Gazzera, F. Baggi, G. Baselli, M.G. Bruzzone, I. Zucca, G. Cavallo, G. Terraneo, F. Baldelli Bombelli, P. Metrangolo, G. Resnati, A Superfluorinated Molecular Probe for Highly Sensitive *in Vivo* ^{19}F-MRI, J. Am. Chem. Soc. 136 (2014) 8524–8527. DOI:10.1021/ja503270n.

[42] S. Kreitz, G. Dohmen, S. Hasken, T. Schmitz-rode, P. Mela, S. Jockenhoevel, Nondestructive Method to Evaluate the Collagen Content of Fibrin-Based Tissue Engineered Structures Via Ultrasound, 17 (2011). DOI:10.1089/ten.tec.2010.0669.

[43] D. Dutta, K.-W. Lee, R. a Allen, Y. Wang, J.C. Brigham, K. Kim, Non-invasive assessment of elastic modulus of arterial constructs during cell culture using ultrasound elasticity imaging., Ultrasound Med. Biol. 39 (2013) 2103–15. DOI:10.1016/j.ultrasmedbio.2013.04.023.

CHAPTER 8

Acknowledgements

List of Publications

PhD Portfolio

Research Data Management using FAIR Principles

Curriculum Vitae

ACKNOWLEDGEMENTS

„ Art is I; Science is we. “
-Claude Bernard-

So, there it is: the last chapter of my thesis. After years of hard work, my adventure „PhD“ has come to an (happy)end. Although, this thesis consumed a lot of energy and time, there are a lot of wonderful memories associated during my time as a PhD student and Marie Curie fellow in the Netherlands. I really feel nostalgic during writing this chapter and I would like to thank everybody who supported me during this unforgettable journey.

First, I would like to express my deepest gratitude to my promotor Prof. Dr. Wout Feitz. Dear Wout, thank you very much for your fundamental support. Despite your busy schedule, you were always available and took your time when I had burning questions. You always trusted in my projects, and equally important, you acted as a strong motivator. I will never forget your quotes such as „typen, typen, typen!“, or „hoe moelijk kan het zijn!?“, meaning that manuscript writing, experiments or administrative stuff aren't that difficult as they seem. I am still impressed of your positive energy which you showed me all the time.

Truly, this thesis was not possible without the extensive support of Dr. Egbert Oosterwijk, my co-promotor, daily supervisor, experienced scientists and mastermind of my projects. Dear Egbert, your mission is accomplished: you made a researcher! I am deeply thankful that I had you as a supervisor. I appreciate that you gave me the freedom to operate when I had some ideas especially about the “ideal” scaffold design. If necessary, you brought me back on track, and when I was in a lag-phase (or we better call it “not focused”) you had the best strategies to motivate me (e.g. the whatsapp from you standing next to my poster at the ESUR meeting 2015 in Nijmegen). I needed a supervisor like you, otherwise I would be still performing experiments for my first manuscript. Based on your experience and patience, I could tremendously improve my writing skills, design of experiments and the way to look at results. Thanks for everything Egbert! Furthermore, many thanks for being the coordinator of the iTERM project.

The next person I would like to thank is Dr. Nicoline Geverink, the project manager of the iTERM project and actually, the best EU project manager I ever had! Dear Nicoline, I still remember when you wrote me the mail that Egbert had chosen me for the job (in this context, many thanks for being the “good cop” at the job interview).

Furthermore, I am so thankful that you arranged all the administrative things to ensure a smooth start in Nijmegen. You were always a very good person to talk with. Many thanks for the many (non)scientific talks and for your encouragement. Furthermore, without you the iTERM project would not have been that organized and successful as it was! You took care that, we the fellows, were aware on reaching deliverables, milestones and secondments.

By the way, the iTERM project. I am proud that I was a part of this awesome Marie Curie ITN. Many thanks to all the fellows (Maruthi, Daniel, Alicja, Simone, Ulrich, Joan, Alexander, Kuba, Penny, Nehar, Nihan and Weiqiang) and all the supervisors. There were legendary moments when I look back at our inspiring consortium meetings in Nijmegen, Uppsala, Hull, Zürich and Warsaw. Every meeting had his special character, but all meetings combined science (the main part), action, drama and comedy. Subsequently, I will never forget the summer school in Riva del Garda or the toxicity course in Maastricht.

As a reference for the big scientific success of this project, fruitful collaborations were initiated which resulted in publications and finally in this thesis. First, I would like to thank Prof. Dr. Jöns Hilborn, Janne Bohlin and Dr. Daniel Bermeijo from the Uppsala group. Dear Jöns and Janne, thank you very much for showing me the basics on creating coupled helical coils -the backbone of my project-! I don't know on how many coils I made, and on how many times I failed during the secondment. However, you encouraged me to stay on the topic and provided me with smart ideas. "Danielito", thanks for the good time in Uppsala and for your friendship.

Another example for a fruitful collaboration within iTERM was the work with MRI contrast agents. Dear Joan, thank you so much for your help on synthesizing various PIC hydrogels and for the good times we had spent together inside- and outside the lab. I wish you all the best for the future. Furthermore, my deepest gratitude goes to Dr. Paul Kouwer for enlightening discussions, proofreading sessions and his encouragement.

Furthermore, I will never forget the good memories associated with the awesome MRI contrast agent called Hemin-Lysinate. Many thanks to Nihan Güvener and Dr. Sjef Cremers for providing me this contrast agent. Dear Nihan and Sjef, furthermore I would like to thank both of you for your help in the lab and on finalizing the manuscript, and the many good talks we had after work in the "cultuur café" or the "Tangente"! Nihan, I wish you all the best for finalizing your PhD thesis. Don't worry,

you will rock it! Furthermore, I appreciate the comments and suggestions of Prof. Dr. Paul Borm and Prof. Dr. Fabian Kiessling to improve the "hemin story".

After having prepared (hybrid) scaffolds it was time for MR imaging. Without the help of the following people I would still sit at PRIME and cry. My deepest gratitude goes to Prof. Dr Arend Heerschap. Dear Arend, many thanks for giving me the opportunity to work with the 11.7T preclinical MR scanner and to perform my experiments with animal models. You were always highly interested in my work and very curious in testing TE-constructs in the MRI. Your help and MRI knowledge were of utmost importance especially during finalizing the manuscripts. Regarding the MRI scanner itself, I would like to thank Andor Veltien and Sjaak van Asten for technical support. Dear Andor and Sjaak, you were also there to help especially when there were technical problems. Just one call, you came within 15 minutes, and solved the problem! I owe you many drinks! Last but not least, special thanks to Dr. Weiqiang (Chris) Dou. Dear Weiqiang, I am still very happy that I met you. Without your huge help and knowledge especially on optimizing the MR scanning protocols, several projects weren't that successful. We spend uncountable hours at PRIME. However, and more important, besides all the experiments you became a good friend!

Now it's time to acknowledge Dr. Simone Mastrogiacomo! Dear Simone, we started together in Nijmegen as iTERM fellows and PhD students, albeit in different labs. However, we always had a strong connection. You were a good friend since the beginning. When I was frustrated or just in doubt about PhD-related issues, you were the best person to talk with. After long discussions with you -preferably at the bar- and Pizza at your place, everything was fine again! Together we managed the ups and downs in the tough life of a PhD student. You also introduced me to all the smart- and amazing people of the Biomaterials Department. Together we had a lot of fun at the PhD retreat or just at the "Casa Mastrogiacomo". Thank you very much for everything my brother! It was an honour to be your paranymph at your defence. I wish you and Giuliana all the best in the US!

All the animal studies that performed during my PhD would have been very challenging without the support from the staff of the central animal laboratory (CDL) and Preclinical Imaging Center (PRIME). Thanks to Michael, Kitty, Karin, Iris, Wilma and Bianca. With your help, the animal experiments were performed much easier. Furthermore, I would like to thank Dr. Rob de Vries et al. from SYRCLE (SYstematic Review Centre for Laboratory animal Experimentation) for the hands-on training in synthesis of evidence in animal experimentation which inspired and still inspires a lot of (young) researcher.

When I recall all the experiments to characterize the (bio)mechanical of my constructs, I am deeply thankful that I had the support of two persons: Roger Lomme and Edwin Rozen, or better called the "Nijmegen super-centre for testing (bio)mechanical properties of soft tissue". Dear Roger and Edwin, I will never forget your help with the "Zwick" and its equipment. We had many fruitful discussions about the different (bio)mechanical testing methods and there were uncountable nice testing sessions we have spent in your lab. Thanks a lot!

There was always a strong collaboration between the matrix biochemistry group and the Tissue Engineering group within the Lab of Experimental Urology. I would like to express my deepest gratitude to Dr. Toin van Kuppevelt for his broad expertise in using collagen as a smart biomaterial for Tissue Engineering applications. Subsequently, I would to thank Dr. Willeke Daamen for being my mentor within the RIMLS PhD programme and for the discussions we had during our regular meetings. Dear Willeke, many thanks for your advice and encouragement. Additionally, many thanks to Elly Versteeg. Dear Elly, I appreciate your help at the microscope, the homogenizer, and the freeze-dryer. Furthermore, thank you very much for performing some trial/feasibility stainings for me and my student.

In general, great memories are associated with the matrixbiochemistry group. Many thanks to Danique, Lars, Henk, René, Corien, Luuk and Michiel for integrating in your group and many thanks for the unforgettable moments in- and outside the lab! We did a lot of activities together (e.g. NBTE meetings, after work meetings at the SQL, pizza at Romana, whiskey tasting, 4 daagse and the legendary "Frinkandelleneetwedstrijd 2014"). I will never forget my first Party in Nijmegen: "Apres-Ski Party" @ SQL + "Aftershow Party" @ Rene' ☺.

Now let's write about the famous "Collagen Mansion" at the "Via Gladiola"! Dear Luuk and Michiel, I am so thankful and proud that you asked me to join the mansion when Paul left. I really enjoyed the time there and it became a second home for me. Many thanks for the good times in- and outside the mansion. For me, the mansion was always the "place-to-be" not only during 4 daagse! Dear Michiel, thanks for being a good friend at any time. I wish you, Lies and Mieke all the best for the future! Dear Luuk, thanks for all the legendary discussions we had, especially those about football and our villages! I still have the "Lierop-Song" in my ears!

I would also like to thank the other housemates Ruud, Daniek and Dianne for being a part and enrichment of the mansion.

Truly, this thesis was not possible without the people from the Lab of Experimental Urology: MY FAMILY! My time in the Netherlands would never been so pleasant and enjoyable without my wonderful colleagues which made me feel home since the first day! I am so thankful that I ever met Gerald, Onno, Cindy, Mirjam, Egbert, Tilly, Dorien, Kees, Jeannette, Elze, Marion and Renate. All smart people, open-minded, true saviors and friends! I learned a lot from each of you and all truly contributed to this thesis! Thanks for the pleasant time and unforgettable moments (there are far too many to list) in the lab. Furthermore, I would like to thank all the other PhD students and residents for their friendship and good vibrations. Levi, Vicky, Ola, Sabrina, Anglita, Caroline, Allert, Siebren, Boy, Dick, Hans, Rianne, Ruben, Max, Tom, Elle, Maarten, Sebastian, Cindy and Jasmijn. Really the URL was like a family! We respected each other, laughed together and had much fun… but we also stayed together and took care of each other in (very) dark times.

Many thanks to Boy Rozenberg for being my personal medical doctor during the time in Nijmegen. Dear Boy, you diagnosed me often with "Aanstelleritis" especially when I was too pessimistic and even scared of future experiments. The best treatment for this kind of illness were drinks @ SQL, eating "Kapsalon" and watching STAR WARS with you. May the force be with you, Marcella and James! Dear Allert, thanks for the many "wordgrapjes" which made my day in the lab. Will never forget our weekly Pubquiz activities together with Gabriel. Dear Kees, many thanks for organizing the famous Lab Pubquiz, for arranging all the lab equipment I needed, and your friendship. Dear Caroline, you became my U-mate 2.0 and a good colleague to talk with. Our analyses over the recent Game of Thrones episodes together with Paul and Sebastian were just EPIC! Dear Anglita, many thanks for your support regarding scoring of the histological stainings. Furthermore, many thanks for the great Indonesian dishes you prepared for lunchbreak. Herr Professor(!), Dear Jack, you can be proud of this people. It was an honour to have performed this thesis in your lab. Jack, thanks for all the nice scientific- and non-scientific discussions, interest in my work and your encouragement. I wish you and Anja all the best for the future.

And Egbert you can be proud of the Tissue Engineering group in our lab. For me it was an honour to work with Alejandra, Silvia, Kaizheng (Max), Rayna, Bronte, Wouter, Peter L., Tamar, Linde, Bronte, Paul, Marije and Dorien. Furthermore, I would like to thank my students Sanne, Dounia and Leonie for their contribution to several projects.

Dear Alejandra, I still remember your direct and warm-hearted personality. Thanks for all the nice moments in the lab or after work at Sint Anneke. I wish you and Alan all the best for the future.

Dear Silvia, what would I do without you? I guess still sitting in the corner and thinking about the best experimental set-ups. Thank you very much for all the discussions and brilliant ideas you had. I still have your voice in my ears when you started the discussion with "PETERRRRR JANKE". You were truly an enrichment for the whole TE group. I am still impressed about your broad knowledge about TE. You are a real tissue-engineer! I wish you, Dennis, Amy, Noah and Jason all the best for the future.

Dear Kaizheng, thanks for helping me with handling the PIC hydrogels and for your good explanations. Dear Rayna, I really enjoyed your company especially during cell culturing.

Dear Bronte, many thanks for your help especially in the beginning of my adventure in Nijmegen. I will never forget all the amazing conversations we had.

I would also like to thank Dr. Martin Koens and Dr. Paul Geutjes, the pioneers of designing tubular collagen-based scaffolds! Dear Martin and Paul, thank you very much for all the priceless discussions and advices you gave especially at the beginning of my PhD.

To be a successful PhD candidate you need to learn, to be patient, to focus... and you need to have Dorien Tiemessen! Dear Dorien, some experiments would have been very challenging without your fundamental help. When you were around, everything was fine! Thank you very much for your support in the cell culture room, at the SEM and for helping me with all the histochemistry. There was always a positive atmosphere when we worked together. Truly, I really learned a lot from you, and I am so thankful for this. Besides that, you became a good mentor and a friend in- and outside the lab.

This section is dedicated to my paranymphs. It's an honour to have Dr. Marije Sloff on my side. Dear Marije, you were my U-mate and colleague, but more important you became a true friend! You were always there when help was needed. Since the beginning, you are good partner to talk with. You were listening to all my issues and gave the right feedback. If needed, in a sensitive, yet direct way. In the beginning, I was a bit afraid of that directness ;-). Seriously, I really enjoyed your company in the lab and when we went to symposia or congresses. Also, outside the scientific world, we had legendary moments. I will never forget our trips together with your husband Derk und the "Milsbeek / Jaarclub" crew to the Oktoberfest in Munich. I am very glad that you will be on my side during the defence. Thanks for everything Malije! Actually, I am so thankful that you were sitting right between Paul and me in lab, so you could act as a referee or as a "slapmaster" when I was in trouble with that guy.

This brings us to the next paranymph: Dr. Paul, Kees, Jan, Dick de Jonge. I am so sorry for you that you cannot be one of the opponents during my defence. I wanted you to be at my side! “Junge”, you are like a brother for me. During the past 6 years we had lot of hilarious/legendary/awesome moments together. You were a good partner in crime in the lab, @ SQL, or elsewhere in the world. Additionally, many thanks for being my personal coach in the gym, during next-level-outdoor exercises and during boxing sessions. I will never forget that I showed you a kick you will never forget. Bro! Thanks for being a very good friend!

Ein guter Gegenpol zu dem anstrengenden Leben als Doktorand bilden Freunde und Familie. Ein herzlicher Dank gilt meinen „Jungs“ in der Heimat, die mich teilweise seit dem Kindergarten begleiten. Benni, Peterchen, Thomas, Christoph, Nils, Martin B., Lucas, Gregor, Andreas, Hermann-Josef, Dominik, Martin S., Jörn, Christian und Volker. In besonderer Erinnerung bleibt mein Junggesellenabschied während 4 daagse in Nijmegen! Aber auch an den „normalen“ Wochenenden wart ihr in besonderer Weise für mich da. Ihr wart Therapeuten, gute Zuhörer, und ziemlich beste Freunde! Danke für alles!

Zum guten Schluss möchte ich meiner Familie danken. Ihr wart wahrhaftig immer für mich da!

Zunächst gilt ein besonderer Dank meiner (Schwieger)-Familie in Niederkrüchten Karin, Klaus, Janina und Theo. Danke für Eure Unterstützung und das Interesse an meiner Doktorarbeit während all den langen Jahren.

Ich danke meinem Zwillingsbruder Heinz Bert. Berti, mein kleiner Bruder, du hast dich schon seit frühester Kindheit um mich gekümmert. So hat es mich nicht gewundert, dass Du deine Passion im Pflegebereich gefunden hast. Ich habe großen Respekt vor deiner Tätigkeit in der Intensivpflege. Du bist jeden Tag für deine Patienten und Mitmenschen da! Der Patient steht bei dir im Vordergrund; ein hohes Ideal welches leider nicht mehr selbstverständlich ist. Lass dich nicht entmutigen. Auch bin ich froh, dass du deinen Weg gefunden hast. Ich wünsche dir und Sebastian alles Gute für die Zukunft.

Ein weiterer Dank gilt meiner großen Schwester Beate. Liebes Schwesterherz, nie werde ich deine Unterstützung vergessen! Seit ich denken kann, warst du immer für mich und die ganze Familie da. Oft warst du Taxifahrer, Zuhörer, Ratgeber, Betreuer und Führsprecher in einer Person. Wer dich an seiner Seite hat, kann sich Wahrhaft glücklich schätzen. Danke für alles liebste Schwester!

Ein großer Dank gilt meiner lieben Mutter. Liebe Mama, du hast mich, Beate und Berti allein großgezogen und dabei noch eine Metzgerei (+ Partyservice + Wirtschaft) geführt. Du warst und bist ein großes Vorbild für mich. Du hast mir vieles beigebracht und oft gezeigt was richtig und was falsch ist. Weiter hast du mir vieles ermöglicht. Natürlich habe ich dir so manche Bauchschmerzen bereitet und oft warst du skeptisch über manchen eingeschlagenen Weg. Aber du bist den Weg mitgegangen und warst mit gutem Rat an meiner Seite. Den Weg Doktorarbeit konnte ich meistern. Mama, ich hoffe du bist stolz auf mich.

Zum Schluss möchte ich mich bei meiner geliebten Frau bedanken. Mein Leben einschließlich dieser Doktorarbeit wäre sicherlich nicht so wie jetzt verlaufen, hätte ich dich, liebe Alena, nicht kennengelernt. Du hast mich ermutigt Biomedical Engineering zu studieren und mich weiterzuentwickeln. Als ich das Angebot bekam nach Nijmegen zu gehen, hast du nicht lange überlegt und dein volles Einverständnis gegeben. Während dieser Zeit warst du die tragende Säule in meinem Leben. Du warst immer an meiner Seite und dein Support kannte keine Grenzen. Du hast mir den Rücken freigehalten, so dass ich mich voll auf diese Arbeit konzentrieren konnte. Oft war ich sehr angespannt und unsicher. Doch du hast alles ertragen und konntest mich immer wieder aufs Neue motivieren.

Während dieser Zeit gab es viele Höhen und Tiefen, die wir durchlebten. Doch wir sind immer wieder aufgestanden und speziell du hast dafür gesorgt, dass es weiter geht! Dafür bin ich dir unendlich dankbar. Daher ist diese Doktorarbeit Dir gewidmet. Wahrhaftig hast Du sehr großen Anteil an dieser Arbeit!

Du bist eine großartige Ehefrau und eine herzensgute Mutter. Ich bin unsagbar stolz auf dich und auf unseren Sohn Mares! Lieber Mares, du hast das Leben von Mama und mir grundlegend verändert. Du hast uns gezeigt, was im Leben wirklich wichtig ist. Danke für jedes Lächeln und die nötige Ablenkung während der Endphase dieser Doktorarbeit. Ich verspreche dir ein guter Vater zu sein!

Danke für alles ihr 2! Ich liebe Euch!... Immer!

Garzweiler im August 2019

LIST OF PUBLICATIONS

Related to this Thesis

H.P. Janke*, J. Simo Padial*, W. Dou, D.M. Tiemessen, K. Liu, W.F.J. Feitz, A. Rowan, A. Heerschap, P.H.J. Kouwer and E. Oosterwijk; ***Noninvasive Magnetic Resonance Imaging Demonstrates Structural Changes of Gd-functionalized Polyisocyanopeptide Hydrogels upon Injection***; Submitted. *: Contributed equally.

H.P.Janke, P.K.J.D. de Jonge, W.F.J. Feitz, E. Oosterwijk; ***Reconstruction Strategies of the Ureter and Urinary Diversion using Tissue Engineering Approaches***; Tissue Eng Part B Rev. 2019 Jun;25(3):237-248. DOI: 10.1089/ten.TEB.2018.0345.

M. Sloff*, **H.P. Janke***, P.K.J.D. de Jonge, D.M. Tiemessen, B.B.M. Kortmann, S.M. Mihaila, P.J. Geutjes, W.F.J. Feitz, E. Oosterwijk; ***The Impact of y-Irradiation and EtO Degassing on Tissue Remodeling of Collagen-based Hybrid Tubular Templates***; ACS Biomater. Sci. Eng. 4 (2018) 3282-3290. DOI:10.1021/acsbiomaterials.8b00369. *: Contributed equally.

H.P. Janke*, N. Güvener*, W. Dou, D.M. Tiemessen, A. YantiSetiasti, J.G.O. Cremers, P.J.A. Borm, W.F.J. Feitz, A. Heerschap, F. Kiessling, E. Oosterwijk*; **Labeling of Collagen Type I Templates with a Naturally Derived Contrast Agent for Noninvasive MR Imaging in Soft Tissue Engineering***; Adv. Healthc. Mater. 18 (2018) 1800605. DOI:10.1002/adhm.201800605. *: Contributed equally.

H.P. Janke, J. Bohlin, R.M.L.M. Lomme, S.M. Mihaila, J. Hilborn, W.F.J. Feitz, E. Oosterwijk; ***Bioinspired Coupled Helical Coils for Soft Tissue Engineering of Tubular Structures – Improved Mechanical Behavior of Tubular Collagen Type I Templates***; Acta Biomater. 59 (2017) 234–242. DOI:10.1016/j.actbio.2017.06.038.

Other

P.K.J.D. de Jonge, M. Sloff, **H.P. Janke**, L.R.M. Versteegden, B.B.M. Kortmann, R.P.E. de Gier, P.J. Geutjes, E. Oosterwijk, W.F.J. Feitz; ***Ureteral Reconstruction in Goats Using Tissue-Engineered Templates and Subcutaneous Preimplantation***; Tissue Eng. Part A. 24 (2018) 863–872. DOI:10.1089/ten.TEA.2017.0347.

P.K.J.D. de Jonge, M. Sloff, **H.P. Janke**, B.B.M. Kortmann, R.P.E. de Gier, P.J. Geutjes, E. Oosterwijk, W.F.J. Feitz, ***Clinical Protocol Levels are Required in Laboratory Animal Surgery when using Medical Devices: Experiences with Ureteral Replacement Surgery in Goats***; Lab. Anim. 51 (2017) 538–541. DOI:10.1177/0023677217696520.

L.R. Versteegden, K.A. van Kampen, **H.P. Janke**, D.M. Tiemessen, T.G. Hafmans, E.A. Roozen, R.M. Lomme, H. van Goor, E. Oosterwijk, W.F. Feitz, T.H. van Kuppevelt, W.F. Daamen, ***Tubular Collagen Scaffolds with Radial Elasticity for Hollow Organ Regeneration;*** Acta Biomater. 52 (2017) 1-8. DOI:10.1016/j.actbio.2017.02.005.

V. Seifarth, J.O. Grosse, M. Gossmann, **H.P. Janke**, P. Arndt, S. Koch, M. Epple, G.M. Artmann, A.T. Artmann, ***Mechanical Induction of Bi-directional Orientation of Primary Porcine Bladder Smooth Muscle Cells in Tubular Fibrin-Poly(vinylidene fluoride) Scaffolds for Ureteral and Urethral Repair Using Cyclic and Focal Balloon Catheter Stimulation***; J. Biomater. Appl. 32 (2017) 321–330. DOI:10.1177/0885328217723178.

M. Sloff, V. Simaioforidis, D.M. Tiemessen, **H.P. Janke**, B.B.M. Kortmann, L.A.J. Roelofs, P.J. Geutjes, E. Oosterwijk, W.F.J. Feitz Prof; ***Tubular Constructs as Artificial Urinary Conduits***; J. Urol. 196 (2016) 1279-1286. DOI:10.1016/j.juro.2016.04.092.

V. Seifarth, M. Gossmann, **H.P. Janke**, J.O. Grosse, C. Becker, I. Heschel, G.M. Artmann, A. Temiz Artmann, ***Development of a Bioreactor to Culture Tissue Engineered Ureters Based on the Application of Tubular OPTIMAIX 3D Scaffolds***; Urol. Int. 95 (2015) 106–113. DOI:10.1159/000368419.

Institute for Molecular Life Sciences
Radboudumc

PhD Portfolio

Name PhD candidate: H.P. Janke	**PhD period:**
Department: Urology	***01-11-2013 – 31-10-2017***
Graduate School: Radboud Institute for Molecular Life Sciences (RIMLS)	***Promotor: Prof. W.F.J Feitz***
	Co-promotor: Dr. E. Oosterwijk

		Year(s)	ECTS
	TRAINING ACTIVITIES		
a)	***Courses & Workshops***		
-	iTERM Marie Curie ITN Research Training and Courses (5x)	2014-2017	6.0
-	Graduate Course	2014	2.0
-	Course on Laboratory Animal Science	2014	5.25
-	Hands-on Training Systematic Reviews of Animal Studies	2014	0.2
-	Dutch language Course MENTAAL (A1)	2014-2015	2.0
-	Scientific Writing	2015	0.2
-	Summer School on Biomaterials and Regenerative Medicine	2015	1.75
-	MIC Coure ImageJ / Fiji	2015	0.8
-	Course Scientific Integrity	2015	1.0
-	Course Bioreactor Keele University	2016	1.75
-	Nano4Imaging: Nanomedicine and Contrast Agents	2016	1.75
-	The Art of Presenting Science	2017	0.8
b)	***Seminars & lectures***		
-	Technical Fora (4x)	2014-2017	0.4
-	Seminars (4x)	2014-2017	0.4
-	Radboud Research Rounds (8x)	2014-2017	0.8
c)	***Symposia & congresses (*: oral; #: poster)***		
-	iTERM Marie Curie ITN Consortium Meetings (6x *)	2014-2017	5.5
-	NBTE Annual Conference #,#,#	2014-2016	2.25
-	RIMLS PhD Retreat #,#,#,*	2014-2017	4.0
-	KNAW StemCell Forum	2014	0.25
-	ESUR-SBUR Annual Conference #,#	2015	2.0
-	TERMIS World Conference #	2015	1.75
-	TERMIS EU Chapter Conference #,#	2016	2.0
-	ISMRM Annual Meeting #	2017	1.5
d)	***Other***		
-	Reviewing a Scientific Article	2014	0.1
-	Journal Club (8x)	2014-2017	2.0
-	Organization Technical Forum (Lab-on-a-Chip)	2016	0.5
-	Organization iTERM-TERMIS Satellite Symposium	2016	2.0
-	TERMIS SYIS Co-Chair	2016	1.0
-	TERMIS Volunteer Organization Commitee	2016	1.0
	TEACHING ACTIVITIES		
e)	***Lecturing***	na	
f)	***Supervision of internships***		
-	Bachelor Internship HLO, HAN	2016	1.0
-	Graduation / Master Internship Biomedical Science, Radboud University (6 month)	2017	2.0
-	Master Internship Bioengineering EPFL Lausanne	2017	1.0
TOTAL			**54.95**

Research Data Management using FAIR Principles

The research data management of this thesis was performed according to the FAIR principles to ensure **f**indability, **a**ccessibility, **i**nteroperability, and **r**eusability [1]:
For **findability** purposes, raw- and processed data produced in this thesis were recorded on paper in traditional laboratory notebooks as well as digitally on a local server (H drive) within the Laboratory of Experimental Urology, Department of Urology, Radboud Institute for Molecular Life Sciences (RIMLS), Radboudumc Nijmegen (NL). In the end-period of this thesis, data were also recorded and stored on a digital laboratory notebook (Labguru) within the department. Back-up of the local server and Labguru were performed by the Information and Communications Technology (ICT) Radboudumc. Furthermore, published data and references used in this thesis were assigned to a unique digital object identifier (DOI) which allows for exact findability.

For **accessibility**, data files on the local server and Labguru are accessible by assigned laboratory members of the Laboratory of Experimental Urology. After the end of the experiment, data were locked and can only be viewed but not edited. Furthermore, the standard communication protocol for already published data and references were in general http(s)-based which are open, free and universally implementable. For example, data and references are accessible via the homepage of the journal on which the data and references have been published. Subsequently, published data and references are accessible e.g. via PubMed and ResearchGate as well as all data files can be requested by the author of this thesis.

The data used for this thesis were saved in widely used file formats (e.g. doc(x), xls(x), pzf(x), pdf, tif, jpg) ensuring **interoperability**. The language used in this thesis is English to reach a broad audience and data are presented in a detailed, formal and objective way. Furthermore, the vocabulary, keywords and chapter titles mainly include MeSH (medical subject headings) terms and sub headings for standardization.

In this thesis, the Materials and Methods section in every chapter are described as detailed as possible to ensure **reusability** of generated data.

REFERENCE

[1] M.D. Wilkinson, M. Dumontier, Ij.J. Aalbersberg, G. Appleton, M. Axton, A. Baak, N. Blomberg, J.-W. Boiten, L.B. da Silva Santos, P.E. Bourne, J. Bouwman, A.J. Brookes, T. Clark, M. Crosas, I. Dillo, O. Dumon, S. Edmunds, C.T. Evelo, R. Finkers, A. Gonzalez-Beltran, A.J.G. Gray, P. Groth, C. Goble, J.S. Grethe, J. Heringa, P.A.. 't Hoen, R. Hooft, T. Kuhn, R. Kok, J. Kok, S.J. Lusher, M.E. Martone, A. Mons, A.L. Packer, B. Persson, P. Rocca-Serra, M. Roos, R. van Schaik, S.-A. Sansone, E. Schultes, T. Sengstag, T. Slater, G. Strawn, M.A. Swertz, M. Thompson, J. van der Lei, E. van Mulligen, J. Velterop, A. Waagmeester, P. Wittenburg, K. Wolstencroft, J. Zhao, B. Mons, The FAIR Guiding Principles for scientific data management and stewardship, Sci. Data. 3 (2016) 160018. DOI:10.1038/sdata.2016.18.

CURRICULUM VITAE (CV)

Heinz Peter Janke was born on 30th September 1984 in Neuss, North Rhine-Westphalia, Germany. After vocational training to become a hearing aid audiologist between 2001 and 2004, he gained work experience in the field of active medical devices until 2007.

In 2007, he started studying Biomedical Engineering at the FH Aachen University of Applied Sciences. He received his Bachelor of Engineering (BEng) degree in August 2010 and his Master of Science (MSc) degree in February 2013. In his master internship, Heinz Peter joined the URPLACE project which focused on the development of a bioreactor system for generating tissue-engineered tubular constructs for ureter reconstruction. This master internship was performed at the Laboratory of Medical- and Molecular Biology, FH Aachen University of Applied Sciences (DE) under supervision of Dr. Volker Seifarth and Prof. Dr. Dr. Aysegul Temiz-Artmann in collaboration with the Department of Urology within the RWTH University Medical Center Aachen (DE) under supervision of OA Dr. med. Joachim Grosse. In his master thesis, smooth muscle- and urothelial cells were isolated from porcine bladder biopsies and seeded to collagen scaffolds to study cell-matrix interactions. After his graduation, he continued to work for the UREPLACE project as a Research Assistant.

In Autumn 2013, Heinz Peter gained the opportunity to work as an Early Stage Researcher at the Department of Urology within the Radboudumc Nijmegen (NL) under supervision of Dr. Egbert Oosterwijk and Prof. Dr. Wout Feitz. Here he focused on the development of smart devices which can be used for soft tissue repair of tubular structures. This project was part of the Marie Curie Initial Training Network (iTN) on training scientists to develop and image materials for Tissue Engineering and Regenerative Medicine (iTERM) funded by the European Union. During this project, he was a visiting researcher at the Department of Chemistry, Polymer Chemistry, University of Uppsala (SE) and initiated collaborations with Nano4Imaging Aachen (DE), the Institute for Experimental Molecular Imaging (ExMi) at the RWTH University Medical Center Aachen (DE), the Institute for Molecules and Materials within the Radboud University Nijmegen (NL) and the Department of Radiology, Radboudumc Nijmegen (NL). The results of this training and research activities are described in this PhD thesis. Furthermore, these results were presented on (inter)national conferences and published in several international journals.

After his PhD and the iTERM project, Heinz Peter underwent training at the mibeg-Institute Medicine in Cologne (DE) and became a Clinical Research Associate (CRA). Thereafter, he worked at JOTEC GmbH, a fully owned subsidiary of CryoLife Inc., as a product specialist for individual vascular implants.

Since July 2019, Heinz Peter is working for the Police Department Neuss, North Rhine-Westphalia as a crime scene investigator.

Institute for Molecular Life Sciences

Radboudumc